AIX-MARSEILLE UNIVERSITY

THESIS

Submitted with the view to obtaining the degree of

DOCTOR OF AIX-MARSEILLE UNIVERSITY

Discipline: Material Science

Doctoral school: Physics and Material Science

By

Ahmad BAHRAMIAN

Thesis defense: 14th December 2018

Enhanced protection of electronic modules: metallic film synthesis and corrosion study

Supervisors: Dr. Marielle EYRAUD

Prof. Philippe KNAUTH

JURY

Prof. François Xavier PERRIN, University of Toulon	Reviewer
Prof. Stefano ROSSI, University of Trento	Reviewer
Prof. Philippe MARCUS, ParisTech	Examiner
Prof. Ahmed CHARAI, Aix-Marseille University	Examiner
Prof. Philippe KNAUTH, Aix-Marseille University	Supervisor
Dr. Marielle EYRAUD, Aix-Marseille University	Supervisor
Mme. Line DÉGEILH, GEMALTO	Invited

Acknowledgments

At the very beginning, I would like to express my sincere gratitude to my supervisors Dr. Marielle EYRAUD and Prof. Philippe KNAUTH from MADIREL (ELMA team) for giving me the opportunity to work with them and their encouragement, assistance, and motivation. They have been very supportive throughout my Ph.D. journey and there is no way to thank them enough. I would also like to thank GEMALTO, where we had casual technical meetings and fruitful conversations with Ms. Line DÉGEILH, Mr. Jean-Marie BOSC, and Ms. Lucile DOSSETTO.

I would like to thank the jury members of my thesis, Prof. François Xavier PERRIN from University of Toulon (reviewer), Prof. Stefano ROSSI from University of Trento (reviewer), Prof. Philippe MARCUS from ParisTech (examiner), Prof. Ahmed CHARAI from Aix-Marseille University (examiner), and Ms. Line DÉGEILH from GEMALTO (invited), for graciously accepting to judge this work.

I would like to thank the collaboration of Prof. Thierry DJENIZIAN (the department of Flexible Electronics, CMP, Gardanne) and Dr. Sebastien MARIA (Institute de Chimie Radicalaire), Dr. Florence VACANDIO (MADIREL, ELMA), Dr. Florence BLOCH'E (MADIREL, ELMA), and Dr. Virginie HORNBECQ (MADIREL, ELMA). It would have been impossible to finish this work without their help. I also appreciate the help of Mr. Paolo MUSARDO (GEMALTO) and Ms. Carine CHASSIGNEUX (MADIREL) that helped me by preparing the cross-section of my samples and doing the XRD measurements on my samples, respectively. I would like to specifically thank Mr. Alain TONETTO, for his help and collaboration regarding SEM imaging of my samples.

I would like to thank Dr. Pascal BOULET (current director of MADIREL) and Dr. Renaud DENOYEL (former of MADIREL) for their support and advice. I would like to thank the other members of the ELMA team; Dr. Luca PASQUINI, Dr. Chrystelle LEBOUIN, and Ms. Amelie DEMOULIN (research engineer) for their help and support during my research activities. I would like also to thank Dr. Vanessa COULET (MADIREl, S2G team) for of her help and motivational conversations we had. I thank Dr. Renaud DENOYEL, Dr. Veronique WERNERT, and Dr. Yves ZEREGA for kindly presiding over the thesis committee to evaluate my work every year. I would also thank Ms. Marilyne BARBAROUX, Ms. Joelle FORESTIER, and Ms. Zainaba KASSIM for helping me out with all the administrative work at MADIREL.

I am immensely grateful to all my fellow researchers and colleagues at MADIREL for their constant friendship and all the fun we had during the last three years, and now I have so many joyful memories about my stay in Marseille. I would like to specifically thank Dr. Michele BRAGLIA, and Dr. Girish SALIAN for not just being my closest friends but dearest brothers.

I am unbelievably grateful to my family, especially my mother, for all their support and help. They have always put my needs first and were there whenever I needed them; there is no way I can ever thank them enough. My sincere gratitude to my beautiful wife Zahra, this journey was impossible without you.

Finally, I would like to acknowledge the financial support from:

Abstract

Cu/Ni(Ni-P)/Au systems are used as electrical contacts due to their combination of electrical conductivity, corrosion resistance, and mechanical behavior. Cu has a unique electrical conductivity that made it the most used metal in electronics. However, protective coatings must be applied on Cu due to its poor corrosion resistance. Au films are used to secure a proper lifetime of electrical contacts. Ni films are essential to avoid the diffusion of Cu into Au. Electrodeposition is the method of choice to form these multi-layer systems. The Au top-coat is notably thin and hence porous. The corrosive media penetrate through these pores, hence electrical contacts are suffering from a galvanic coupling. This work is dedicated to identify and test the strategies to enhance the lifetime of electrical contacts and electronic modules.

Three strategies were detected, (1) improve the properties of the Ni barrier layer, (2) replacing the Au film with a thicker but cheaper alternative metal, and (3) seal the pores of Au top-coat using a post-treatment process. The reliability of these strategies was tested by forming various samples that were characterized by several techniques including scanning electron microscopy, energy dispersive spectroscopy, X-ray diffraction, electrochemical impedance spectroscopy, and potentiodynamic polarization.

To improve the properties of Ni-P films, the effects of various additives including saccharine, glycine, pyridinium propyl sulfonate, coumarin, sodium citrate, and cerium sulfate were investigated. It was found that an optimized concentration of these additives, except saccharine, noticeably improved the corrosion resistance, especially at high potentials (about 25% increase in instantaneous corrosion efficiency and about 300% in corrosion efficiency at high potentials). All the additives, except Saccharine, enhanced the P content of Ni-P films. Saccharine highly suppressed the incorporation of P inside the Ni lattice and a mixed amorphous-crystalline structure was stabilized. Therefore, it led to a fast dissolution of Ni

deposits at high potentials, and therefore, the use of saccharine for Ni-P barriers should be avoided. The use of other additives, on the other hand, is recommended since they would be beneficiary for electrical contacts.

The effect of Ag, Sn, Zn, and Mo as alloying elements was studied on the corrosion properties of Ni deposits. The corrosion resistance of films increased with Zn and Sn (about 160-230%), but it decreased in the presence of Mo and Ag (about 50-320%). These results were attributed to the formation of a stable nanometric oxide film, suppression of hydrogen evolution reaction, and inducing the galvanic coupling for Sn, Zn, and Ag and Mo, respectively. To investigate composite films, Ni deposits were formed in the presence of nanoparticles (TiO_2, Carbon nanotubes, and Cu), and a monomer (Allyl Phenyl Ether or APhE). It was found out that APhE enhanced the corrosion resistance (about 240%) due to the formation of a thicker and compacter film, but the particles decreased the corrosion resistance due to the formation of a highly porous surface (about 180%).

NiAg and NiPd noble top-coats were investigated as alternatives to Au thin films. Although highly adhesive films were formed using the pulse deposition, the films were porous and thus did not offer a proper corrosion behavior.

And finally, to investigate the effect of a post-treatment, a cathodic electropolymerization was employed. It was found out that the pores of Au top-coat can be sealed by the electrodeposition of polymethyl methacrylate that decreased the porosity index (about 97%) and increased about 10 times the corrosion resistance (even at long-term exposures) of electrical contacts after 10 cycles of electropolymerization. A non-uniform polymeric film, however, was formed at a higher number of polymerization cycles (> 50) that decreased the corrosion resistance.

Résumé

Les systèmes Cu / Ni (Ni-P) / Au sont utilisés comme contacts électriques car ils présentent une conductivité électrique élevée, alliée à un bon comportement mécanique et une résistance à la corrosion. L'électrodéposition est la méthode de choix pour former ces systèmes multicouches. Le Cu possède une conductivité électrique unique qui en a fait le métal le plus utilisé en électronique. Cependant, sa faible résistance à la corrosion nécessite l'application de revêtements protecteurs. Les sous couches de Ni (généralement Ni-P) permettent essentiellement d'éviter la diffusion entre Cu et Au. Enfin, la couche de finition en Au est utilisée pour garantir la durée de vie des contacts électriques. Pour des raisons économiques, ce film de faible épaisseur est poreux, entrainant ainsi un couplage galvanique entre l'Au et le Ni au détriment du nickel. Ainsi ce travail est dédié à l'identification et la mise en œuvre des stratégies visant à améliorer la durée de vie des contacts électriques et plus globalement des modules électroniques.

Lors de cette thèse, nous avons développé 3 stratégies : (1) améliorer les propriétés de la couche barrière de Ni, (2) remplacer l'or par un métal moins onereux, (3) sceller les pores de la couche d'Au. La fiabilité de chaque stratégie a été testée et nous avons réalisé de nombreux dépôts ainsi que leur caractérisation structurale, l'étude de leur morphologie, de leur composition chimique et de leur résistance à la corrosion.

Pour améliorer les propriétés des films de Ni-P, nous avons étudié les effets de divers additifs, (saccharine, glycine, propyl sulfonate de pyridinium, coumarine, citrate de sodium, sulfate de cérium). Il a été constaté qu'une concentration optimisée de ces additifs, à l'exception de la saccharine, améliorait notablement la résistance à la corrosion des dépôts, en particulier aux potentiels élevés (augmentation d'environ 25% de l'efficacité de la corrosion instantanée et d'environ 300% de l'efficacité de la corrosion à des potentiels élevés). L'ajout d'additifs, sauf

la saccharine, augmente la teneur en P des films ce qui rend la structure amorphe et est bénéfique d'un point de vue anti-corrosion.

L'effet de l'ajout dans la couche de Ni-P d'Ag, Sn, Zn et Mo en tant qu'éléments d'alliage a été étudié. La résistance à la corrosion des films a augmenté avec Zn et Sn (environ 160-230%), mais elle a diminué en présence de Mo et d'Ag (environ 50-320%). Ces résultats ont été attribués à la formation d'un film d'oxyde nanométrique stable, à la suppression de la réaction de dégagement d'hydrogène et à une protection galvanique par Sn et Zn. Des films composites de Ni ont été réalisés en présence de nanoparticules (TiO_2, Nanotubes de carbone et Cu) ou d'un monomère (Allyl Phenyl Ether ou APhE). Nous avons montré que si APhE augmentait la résistance à la corrosion (environ 240%) en raison de la formation d'un film plus épais et compact, les nanoparticules elles, diminuaient cette résistance en raison de la formation d'une surface hautement poreuse.

D'autres couches de finition nobles NiAg et NiPd ont été étudiées. Bien que des films hautement adhésifs aient été formés par potentiel pulsé, ces films poreux n'offraient pas un comportement correct à la corrosion.

Enfin, nous avons étudié l'effet d'une électropolymérisation de polyméthacrylate de méthyle sur des couches poreuses d'or d'échantillons industriels. Après 10 cycles d'électropolymérisation, les pores de la couche de finition ont pu être colmatés à environ 97% permettant d'augmenter nettement la résistance à la corrosion lors d'expositions prolongées au brouillard salin. Pour un nombre de cycles plus important (>50) le film de polymère est non uniforme, ce qui ne permet pas d'augmenter la résistance à la corrosion.

Table of Contents

MAJOR ABBREVIATIONS

AFM	Atomic Force Microscopy
APhE	Allyl Phenyl Ether
CMC	Critical micelle concentration
CPE	Constant Phase Element
CTAB	Cetyltrimethylammonium Bromide
CV	Cyclic Voltammetry
DESs	Deep Eutectic Solvents
DMF	Dimethylformamide
DMH	5,5-dimethylhydantoin
DMSO	Dimethyl Sulfoxide
ED	Electrodeposition
EDS	Energy Dispersive Spectroscopy
EIS	Electrochemical Impedance Spectroscopy
EL	Electroless deposition
EDS	Energy Dispersive Spectroscopy
FCBs	Flexible Circuit Boards
HER	Hydrogen Evolution Reaction
HPMC	Hydroxypropyl Methylcellulose
HTAB	Hexadecyltrimethylammonium Bromide
ILs	Ionic Liquids
IR	Infrared Spectroscopy
MD	Molecular Dynamic
MMA	Methyl Methacrylate

NA	Nicotinic Acid
OCP	Open Circuit Potential
PEG	Polyethylene Glycol
PMMA	Poly(methyl methacrylate)
R	Resistor
SAMs	Self-Assembled Monolayers
SEM	Scanning Electron Microscopy
SDBS	Sodium Dodecyl Benzene Sulfonate
SDS	Sodium Dodecyl Sulfate
SLS	Sodium Lauryl Sulfate
THF	Tetrahydrofuran
TU	Thiourea
U	Ultrasonic
W	Warburg
WCA	Water Contact Measurements
XRD	X-Ray Diffraction
XRF	X-Ray Florescence

Chapter 1

Introduction

1.1. Background

Cu/Ni (Ni alloys)/Au (noble metals) are the most used multi-layer films in electronics and microelectronics. They are implemented in applications such as switches, relays, circuit breakers, and contactors and are also typically employed as an electrical contact due to an optimal combination of high electrical conductivity, corrosion resistance, and wear resistance [1–3]. Cu/Ni/Au is especially employed in contact smart cards, like identity cards, SIM cards, and so on. A smart card is a device that contains an embedded integrated circuit, which can be either a secure microcontroller or equivalent intelligence with internal memory or a memory chip alone. The processors, the readers, and the background systems are the essential parts of a typical smart card. The reader is connected to the processor either with a physical contact or with a remote contactless radio frequency interface [4]. This paper is focused on the electrical contacts and the purpose and characteristics of each part are explained in the following.

Copper (Cu) and its alloys are base materials in electronics. Cu alloys are popular due to their high electrical and thermal conductivity, mechanical workability, and low chemical reactivity. Their main purpose, however, is to provide the required electrical conductivity [5–11]. Nowadays, Cu can be even electrodeposited on plastics and polymers given the development of conductive polymers and doped plastics. This possibility made Cu a suitable target for electronics, microelectronics, solar cells, transistors, and IT gadgets (cellular phones or chips) as flexible interconnections that are known as flexible circuit boards (FCBs) [12–16]. However, the poor corrosion and oxidation resistance of Cu alloys, especially in the presence of aggressive ions like chlorides, are their main drawbacks. Corrosion products are usually

electrically insulators, thus they increase the contact resistance and terminate the functionality of the electric contacts. Therefore, the corrosion process limits the usage of Cu alloys and makes the presence of protective coatings necessary [5–11].

There are two groups of metals that could be used as protective coatings; firstly noble metals (like gold (Au), silver (Ag) and palladium (Pd)), and secondly so-called passive metals (such as nickel (Ni) and tin (Sn)). Noble metals are chemically almost inert in all environments, while passive metals owe their corrosion resistance to the ability to form a nanometric oxide layer that hinders deeper corrosion. However, not all passive metals can be employed since the conductivity can be lost if the passive layer is too thick (like aluminum (Al)) [17].

The primary function of electrical contacts is to pass the electrical currents across the contact interface with no interruption. Hence, the electrical connectors can read information from and write back on the chip when the smart card is inserted into a reader. Figure 1- 1 shows a typical standard contact, with a description of the purpose of its different parts[1]. A thin layer of a noble metal is typically used to secure a stable contact resistance during the lifetime of the device [2,18,19].

Contact	Designation	Function
C1	VCC	Supply voltage
C2	RST	Reset input
C3	CLK	Clock input
C4	AUX1	Auxiliary contact 1
C5	GND	Ground
C6	VPP	Programming voltage (no longer used)
C7	I/O	Input/output
C8	AUX2	Auxiliary contact 2

Figure 1- 1 contacts of a typical contact smart card and a brief description of each part [4].

[1] Before 1990s, applying an external voltage was necessary to keep the smart cards functional, and thus the purpose of the part c6 (VPP). Later, a charge pump was employed to apply this voltage directly on the chip, and therefore, made the c6 part useless. However, to avoid any conflicts with the ISO standard, the c6 part could not be eliminated [4].

Au, Pd, and Ag are considered as noble metals due to their high standard electrode potentials; 1.38 V, 0.92 V, and 0.8 V, respectively. Au is the most used top-coat [6]; over 300 tons of Au [20] is annually used in electronic components. The production of Au causes environmental problems. Therefore, reducing the consumption of Au is a vital issue from both the economic and the ecological point of view [17]. Many studies were dedicated to improve the wear resistance of Au that reduces its consumption or develop cheaper and more reliable plating materials [17,18].

Noble metals are expensive, and thus their thickness should be kept as low as possible. Au films with a thickness above 2 µm are known to be pore-free and corrosion-resistant. The porosity of thin films, however, drastically increases with decreasing thickness. Therefore, films on top of electronic contacts are porous because they are usually thinner than 0.8 µm [21]. These pores induce the galvanic corrosion of the sublayer [18]. As a result, the thickness of noble metal coatings is their most important characteristic: it should be thick enough to offer a good corrosion and wear resistance, and be as thin as possible due to its cost [17].

Au top-coats on Cu are not recommended due to the Cu diffusion into Au, which happens during high-temperature processes, i.e. wire bonding and encapsulation. Loss of conductivity, loss in bondability, and weakening in bond strength are the known effects of the diffusion of Cu into Au.

Ni or Ni alloys can be applied as barrier layers [5,22] between Cu and Au. Ni could be simply deposited on Cu because of their similar fcc structure with only 2.5 % lattice mismatch [3]. Ni coatings are known to have anti-corrosion properties, and they can act as sacrificial anodes due to a more cathodic potential than Cu [23,24]. More importantly, the required thickness of the Au top-coat is reported to decrease drastically when Ni barrier layers are used (hence Ni films are economically desirable) [5,25]. Unfortunately, however, Ni ions cause dermatitis and nickel

allergy (Figure 1- 2). Therefore, the use of Ni surfaces that can release more than 0.5 µg/cm^2/week of Ni is forbidden for applications that are in a direct contact with the human body [22]. Note that 0.5 µg/cm^2/week corresponds to a very low corrosion rate of Ni about two atomic layers per week [26].

Figure 1- 2. Ni dermatitis or skin allergy caused by Ni in a cell phone [26].

Other alternatives, such as Co [22] and Sn-Zn [27], have been investigated to replace Ni. However, Co, compared to Ni, has a higher cost and a lower corrosion resistance, and both Sn and Zn are reactive elements that can form intermetallic compounds with Au and Cu. As a result, Ni seems to be inevitable, which makes it necessary to use more resistant Ni films, i.e. Ni alloys or Ni composites.

Nonetheless, the protection of Cu/Ni/Au systems against corrosion is highly challenging [1]. The following mechanism has been proposed for Cu/Ni/Au systems [5]:

The porous Au layer and the Ni under it undergo a galvanic corrosion, where Au and Ni are the cathode and anode, respectively. As a result, an intensified corrosion of Ni occurs due to the large cathode-small anode phenomenon. Meanwhile, Cu is using the defects of the Ni layer (such as grain boundaries) to diffuse to the top surface, and it will be eventually oxidized there. Therefore, localized corrosion with pitting, as depicted in Figure 1- 3, is the main form of corrosion in Au/Ni/Cu systems. Moreover, the oxidation of Ni increases the electrical resistance that can terminate the lifetime of electrical contacts [18].

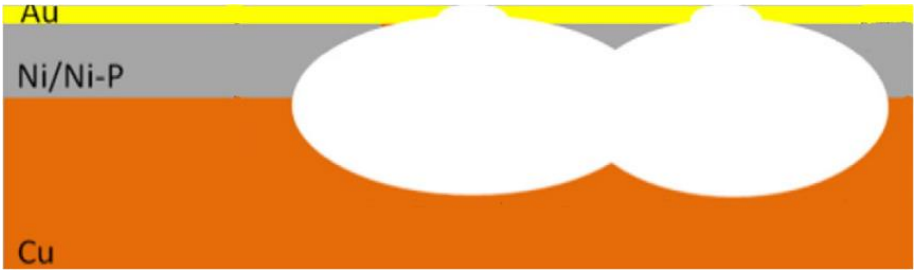

Figure 1- 3. Schematics of localized corrosion in the form of pitting in Cu/Ni(Ni-P)/Au systems [5].

The electronic waste (e-waste) is estimated to be around 500000 tons per year [28]. Therefore, extending the lifetime of electronics is a vital issue. The lifetime of Au/Ni/Cu films will increase by decreasing their porosity. As a result, many studies have been dedicated to the use of post-treatment methods (e.g. Self-Assembled Monolayers (SAMs) [17,29]) to modify or control the porosity of thin films.

High corrosion resistance is, obviously, the main criterion for choosing a protective coating. However, there are motions between electrical contacts, and therefore, the lifetime of electronics is also limited by mechanical phenomena, like wear and fretting [17]. As a result, protective coatings should simultaneously present a good mechanical properties and a proper corrosion resistance [6]. Moreover, the roughness of the surface is another vital criterion for electrical contacts. The contact resistance R_c can be calculated using the Holm equation [7]: it is proportional to the specific electrical resistance (ρ) and the inverse of the radius of the contact area (a):

$$R_c = \frac{\rho}{2a} \qquad (1\text{- }1)$$

Therefore, coatings with lower roughness present a higher electrical conductivity. Lower roughness is an especially important factor for Ni barrier layers since the quality and properties of the applied top-coat, especially the porosity content, is directly related to their roughness [30–32]. Furthermore, films with spherical surface morphology (Figure 1- 4) are known to be superior regarding electrical contact purposes [6].

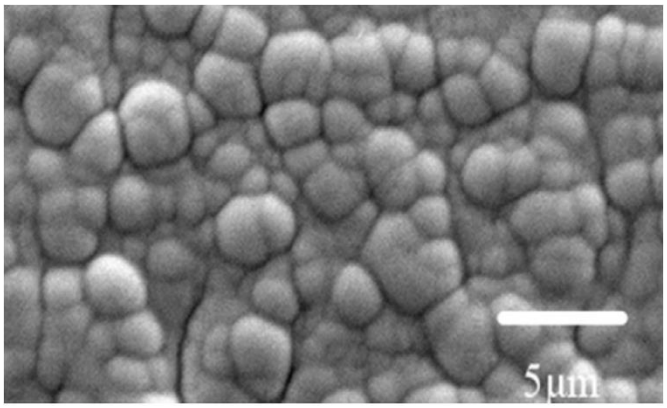

Figure 1- 4. A typical surface with spherical features [33].

In summary, high and stable electrical conductivity, high corrosion and wear resistance, low roughness, and spherical surface morphology can be considered as the main criteria for a good protective coating for electronic and microelectronic applications.

1.2. Objectives

The outline of this study is described as the following:

- Recent studies about modifying Ni and noble metal deposits and post-treatment processes are checked to identify the strategies to improve the lifetime of electrical contacts by finding the best candidates in each part of the mentioned multi-layer system (i.e. Ni barrier layer and noble metallic top-coat).
- Study the aqueous and non-aqueous electrodeposition of Ni barrier films with the aim of improving the corrosion resistance and stability of the barrier film.
- Investigate the electrodeposition of other noble metallic thin films as alternatives to Au top-coats.
- Study the effects of a post-treatment process on the lifetime of an available industrial sample.

Therefore, the following chapters are dedicated to the literature review (chapter 2), experimental procedure (chapter 3), aqueous electrodeposition (chapter 4), non-aqueous electrodeposition (chapter 5), and conclusions and perspectives (chapter 6).

References

[1] Z.H. Huang, Y.J. Zhou, W. He, Surface and Coatings Technology 320 (2017) 126–131.
[2] M. Uysal, H. Akbulut, M. Tokur, H. Algül, T. Çetinkaya, Journal of Alloys and Compounds 654 (2016) 185–195.
[3] J. Lamovec, V. Jović, I. Mladenović, M. Sarajlić, V. Radojević, in: 2014 29th International Conference on Microelectronics Proceedings - MIEL 2014, 2014, pp. 183–186.
[4] X. Leng, Information Security Technical Report 14 (2009) 36–45.
[5] V.K. Murugan, Z. Jia, G.J. Syaranamual, C.L. Gan, Y. Huang, Z. Chen, Microelectronics Reliability 60 (2016) 84–92.
[6] J. Song, C. Koch, L. Wang, Advances in Tribology 2012 (2012) 1–9.
[7] J. Song, V. Schinow, Wear 330–331 (2015) 400–405.
[8] E.-S.M. Sherif, Applied Surface Science 252 (2006) 8615–8623.
[9] S. Adhami, M. Atapour, A.R. Allafchian, Journal of Sol-Gel Science and Technology 74 (2015) 800–809.
[10] E.M. Sherif, S.-M. Park, Journal of The Electrochemical Society 152 (2005) B428.
[11] S. Kologo, M. Eyraud, L. Bonou, F. Vacandio, Y. Massiani, Electrochimica Acta 52 (2007) 3105–3113.
[12] W. Gui-xiang, L. Ning, H. Hui-li, Y. Yuan-chun, Applied Surface Science 253 (2006) 480–484.
[13] A. Islam, H.N. Hansen, P.T. Tang, CIRP Annals 66 (2017) 209–212.
[14] D.K. Yfantis, S.I. Kakos, S. Lamprakopoulos, S. Depountis, C.D. Yfantis, WSEAS Transactions on Environment and Development 2 (2006) 1105–1109.
[15] F. Touyeras, J.-Y. Hihn, M.-L. Doche, X. Roizard, Ultrasonics Sonochemistry 8 (2001) 285–290.
[16] Y. Lu, Applied Surface Science 256 (2010) 3554–3558.
[17] J. Song, L. Wang, A. Zibart, C. Koch, Metals 2 (2012) 450–477.
[18] K. Meyyappan, G. Murtagian, A. Kurella, B. Pathangey, A. McAllister, S. Parupalli, IEEE Transactions on Device and Materials Reliability 14 (2014) 869–877.
[19] M. Grandin, U. Wiklund, Wear 302 (2013) 1481–1491.
[20] Y. Wang, Y. Ju, S. Wei, W. Lu, B. Yan, W. Gao, Materials Characterization 102 (2015) 189–194.
[21] V.K. Murugan, Z. Jia, G.J. Syaranamual, C.L. Gan, Y. Huang, Z. Chen, Surface and Coatings Technology 300 (2016) 95–103.
[22] C.L. Siu, H.C. Man, C.H. Yeung, Surface and Coatings Technology 200 (2005) 2223–2227.
[23] A.P. Abbott, A. Ballantyne, R.C. Harris, J.A. Juma, K.S. Ryder, G. Forrest, Electrochimica Acta 176 (2015) 718–726.
[24] G. Liu, Z. Huang, L. Wang, W. Sun, S. Wang, X. Deng, Surface and Coatings Technology 222 (2013) 25–30.
[25] A.M. Pillai, A. Rajendra, A.K. Sharma, Journal of Coatings Technology and Research 9 (2012) 785–797.
[26] P. Møller, J.B. Rasmussen, S. Köhler, NASF SURFACE TECHNOLOGY WHITE PAPERS 78 (2013) 15–24.
[27] Y.-W. Yen, C.-Y. Lin, G.N. Hermana, P.-Y. Chen, Y.-P. Wu, Journal of Alloys and Compounds 710 (2017) 479–490.
[28] S. Yedla, Waste Management & Research 34 (2016) 81–86.
[29] S. Nineva, S. Berger, F. Talgner, Jahrbuch Oberflächentechnik 72 (2016) 52-59.
[30] S.-H. Jeon, W.-I. Choi, G.-D. Song, Y.-H. Son, D.H. Hur, Coatings 6 (2016) 62.
[31] S. Lin, K. Zhou, M. Dai, F. Hu, Q. Shi, H. Hou, C. Wei, F. Li, X. Tong, Transactions of Nonferrous Metals Society of China 25 (2015) 451–456.
[32] M. Braunovic, N.K. Myshkin, V.V. Konchits, Electrical Contacts: Fundamentals, Applications and Technology, CRC Press, 2006.
[33] W. Wang, W. Zhang, Y. Wang, N. Mitsuzak, Z. Chen, Applied Surface Science 367 (2016) 528–532.

Chapter 2

Literature Review

2.1 . Ni barrier layers

Electrochemical deposition of Ni is over a century old and several studies have been dedicated to its optimization. The mechanism of the deposition of Ni, which traditionally occurs in aqueous solutions, is well known and has been described in many reviews and books [1–3]. As a result, we deliberately skip the publications that are older than a decade and just focus on the most recent ones. To summarize, a combination of Ni salts is employed as Ni source inside the electrolyte, i.e. sulfates (majority) due to better metal distribution and conductivity, and chlorides (minority) to enhance the throwing power, thickness uniformity, and refining grains. Chloride salts can promote dendritic growth, hence its concentration should be kept as low as possible. Boric acid is also usually added as buffering agent [3]. This bath, generally known as Watts bath, was developed by O.P. Watts and is the most popular aqueous based solution to deposit Ni [4].

The following three reactions are generally accepted as the mechanism of Ni deposition:

$$Ni^{2+} + X^{-} \rightarrow NiX^{+} \quad (2\text{-}1)$$

$$NiX^{+} + e^{-} \rightarrow NiX_{ads} \quad (2\text{-}2)$$

$$NiX_{ads} + e^{-} \rightarrow Ni + X^{-} \quad (2\text{-}3)$$

While anions are usually assumed to perform as X^{-}, the electron itself also could act as X^{-} in acidic solutions with pH values less than 4 [1]. Note that hydrogen evolution occurs at the same time, which is the biggest disadvantage of Ni deposition in aqueous solutions [5]. Hydrogen

formation decreases the current efficiency and the incorporation of H inside the deposits leads to hydrogen embrittlement [1,6].

The electrodeposition of metals from ionic liquids (ILs) and deep eutectic solvents (DESs) are specifically developed to overcome the problem of the evolution of hydrogen. ILs and DESs (that is a eutectic mixture obtained by mixing quaternary ammonium halides with hydrogen bond donors, such as amides, carboxylic acids or alcohols) are alternative baths to traditional aqueous ones. These baths offer interesting properties like low vapor pressure and wide electrochemical window. DESs were particularly developed due to their lower cost and greater stability. The importance of coating parameters and the bath composition on the quality of the obtained films is well known. This is especially true in DESs, where the addition of complexing agents and additives have a huge impact on the obtained layers [7].

The nucleation and growth processes of metals from organic media are completely different from aqueous ones due to their fundamental differences, i.e molecule structure, polarity, viscosity, and so on. For example, the viscosity of DES is much higher than Watts bath (16.80 vs. 0.84 cP at 80 ºC). Therefore, higher temperatures should be employed since the viscosity and resistivity of DESs and generally all deposition baths decrease with increasing the operating temperature. Moreover, the dissolved Ni ions inside a DES have thermochromic behavior, i.e. there are octahedral and tetrahedral ion coordination at low and high temperatures, respectively. A proper deposition of Ni from DESs can happen only from its tetrahedral ion state, and this is another reason to apply high operating temperatures [6].

Abbott et al. [6] compared the deposition of Ni from Watts and DES baths and reported the same deposition rate at high temperatures, even though the conductivity of DES was remarkably lower than Watts. They found out that the deposition is not controlled by mass transport at high temperatures and high concentrations of Ni. A similar thickness from both

DES and Watts was obtained. DES coatings had a nano-crystalline morphology, with a smoother and brighter surface, and a higher hardness (up to 100 HV) compared to the Watts coatings that presented a micro-crystalline morphology and a mate and rough surface.

Dimethyl sulfoxide (DMSO) is an organic solution that recently has been used to deposit thin films [8–10]. DMSO has a strong polarity, high stability, and a wide electrochemical window. Temperature found to be an important parameter affecting the properties of deposited thin films from DMSO (since it affects the complexing yield [11]). 50-60º C is reported the best temperature range for this purpose [12]. The Gutmann's donor number of DMSO is 29.8 that makes it able to easily form stable complexes with Ni ions. Moreover, dissolution of Ni in DMSO is an exothermic reaction, and Ni ions have a higher freedom in DMSO than other organic solvents [13]. Therefore, DMSO is a suitable electrolyte for the deposition of Ni and its alloys.

Ni deposits with nano-crystalline structures are denser, and thus they offer better oxidation and corrosion resistance, hardness, elastic modulus, and catalytic capability. Zhou et al. [14] developed a novel method using an ultrasonic-assisted pulse current deposition and successfully formed coatings with superior corrosion resistance, smoother surface, and higher hardness. However, a crystalline Ni layer still presents defects like grain boundaries, voids, and dislocations that makes it vulnerable to corrosion attacks. Moreover, such defects enhance the diffusion of copper inside thin films [15]. Therefore, Ni alloys or composites that are known to offer better wear resistance, hardness, and corrosion behavior, are usually recommended to be used as a barrier.

2.2 . Deposition of Ni alloys

In general, Ni Alloys offer superior properties, e.g. corrosion and wear resistance. They can be deposited by adding the source of alloying elements to the electrolyte. The obtained properties

of a deposited alloy depend on the atomic radius, the position in the periodic table, the cohesive energy (melting temperature), electronegativity and density of valence electrons in the elementary cell [16]. The deposition of alloys is a more challenging process compared to the individual metals. Alloy electrodeposition needs a precise control and monitoring of electrolyte composition and coating parameters. Moreover, an overlapping potential window of each component is necessary for the alloy deposition. The electrochemical standard potential for most of the metals may differ by 1 V that limits the number of metals that can be simultaneously deposited. As a result, complexing agents should be employed to shift the potential of elements towards each other. Note that the deposition of alloys can occur at potentials more anodic than the Nernst potential, called under-potential deposition [17].

Ni alloy deposits can be categorized based on the type of the alloying element, i.e. those that can be deposited individually and those that can be only co-deposited. The former group consists of metals that are much nobler than Ni, like Ag [18–21] and Cu [22–32]; metals that have similar standard potentials, such as Co [33–40] and Sn [41–49]; and metals that are more cathodic, like Cr [50,51], Zn [52–64] and Mn [65–67]. Refractory metals, such as W [68–79] and Mo [80–92] and non-metallic elements, i.e. B [93–99] and P [100–104], can be only co-deposited.

2.2.1. Ni alloys with alloying elements that can be individually deposited

2.2.1.1. Ni-Ag

Ag and Ni are thermodynamically immiscible in any state (liquid or solid), i.e. the solubility of Ni in Ag is about 0.02 at. % at 400ºC. However, the formation of a metastable supersaturated solid solution of Ni-Ag thin films has been reported to be possible by electrodeposition. Ni-Ag alloys can be considered as a proper low-cost barrier layer in electrical contacts. Ag and Ni

have a huge difference in their redox potentials (0.799 V_{SHE} vs. -0.257 V_{SHE} for Ag and Ni, respectively). Because of this gap, Ag tends to be deposited under diffusion control that makes the final surface morphology rough and porous (which is highly undesired). Therefore, a proper complexing agent should be employed to reduce the potential gap for a successful deposition of a Ni-Ag film.

A complexing agent for Ni-Ag deposits is considered proper when it makes stronger complexes with Ag than Ni. Citrate and thiourea (TU) are two most known complexing agents that were widely used as levelers and brighteners. Citrate complexes with Ni are notably stronger than those with Ag, and thus citrate complexes led to a high gap between the Ag and Ni redox potentials (about 1100 mV). Instead, TU had the required properties as a proper complexing agent since it decreased the gap down to less than 330 mV. In the presence of TU, the co-deposition of Ni occurs at more positive potentials than expected from the Nernst equation. S will be also incorporated into the Ag-Ni deposits [18].

The co-deposition amount of Ag depends on the concentration of the used complexing agent; a higher concentration of complexing agent increases the Ag content of Ni-Ag films. Despite their granular morphology, Ag-Ni films showed a superior corrosion resistance to pure Ni. It was reported that incorporation of Ag in small contents (up to 7 at. %) highly increases the corrosion potential and enhances the corrosion resistance due to the formation of a supersaturated solution. At higher Ag contents, however, Ni-rich and Ag-rich phases are formed that decrease the corrosion resistance due to the galvanic corrosion between them [21].

Eom et al. [19] employed the galvanostatic method to generate Ni-Ag thin layers with citrate ions as complexing agents and investigated the effect of the applied current density, the concentration of Ag ions, and pH of electrolyte on the surface morphology and composition of the obtained films. A minimum concentration of Ag ions (0.005 M) found necessary for Ag deposition. The applied current density was found to be the most important factor in the

deposition of Ag and Ni. Deposition of Ag is favored at low current densities, while Ni deposition is higher at high current densities. The obtained coatings at low current densities showed a highly dendritic structure that is undesired for contact materials. The higher deposition rate of Ni was observed in acidic media. However, increasing the pH increased the Ag content. This observation was attributed to the role of citrates that made stronger complexes of Ag at higher pH values. The surface morphology of Ni-Ag deposits consists of granular features, while pure Ag and Ni present bean-like and sheet-like morphologies, respectively [20].

2.2.1.2. Ni-Cu

During the deposition of Ni-Cu coatings, Cu will be deposited first due to its nobler potential. This results in a non-uniform distribution of current density, and the deposited Cu acts as a nucleation site for the reduction of Ni ions. In such conditions, the deposition of Cu is controlled by diffusion, and it is incorporated into the film during the prominent deposition of Ni. At high concentration, however, the high applied overpotential leads to the formation of dendritic structures that is highly undesired [105]. As a result, the addition of a small amount of Cu could highly affect the nucleation and growth mechanism of the coatings and subsequently the surface morphology and other properties [31].

Cu is one of the most investigated alloying elements of Ni deposits, and a comprehensive literature review about it can be found in Ref. [1]. To summarize, complexing agents, like citrates, are necessary to obtain proper Ni-Cu coatings. Otherwise unsatisfactory coatings with nonhomogeneous dendritic structures will be formed. The employed current density also can determine the structure of Ni-Cu coatings; i.e. higher current densities increased the amount of Ni but the obtained coatings were greyish with a black powdery nature. The coatings, however,

were uniform, bright, smooth, and copper colored at low current densities. Stirring the electrolyte during the process also affects the properties of coatings, because it increases the mass transfer. Stirring changes the appearance of coatings from a black, powdery, and not shiny aspect to a reddish brown metallic look. The electrolyte composition also plays an important role in the formation of the coating. While a slight change of Ni salt concentration has no noticeable effect on the coating properties, the same change for Cu salt concentration, or complexing agent, i.e. citrate ions, noticeably affects the Cu content of the coating. Moreover, higher pH values apparently favor the deposition of Cu, and thus the obtained coatings are Cu richer compared to lower pH values. Such behavior was observed with Ag as well, meaning that it can be expected for all metals much nobler than Ni.

2.2.1.3. Ni-Co

Ni and Co form a solid solution over the whole concentration range. Ni-Co films are known to offer better adhesion, mechanical properties, higher hardness, corrosion resistance, thermal stability, magnetic properties, and composite ability than pure Ni [33]. The deposition of Ni-Co coatings occurs by preferential deposition of the less noble metal (here Co) [106]. The anomalous deposition happens due to kinetic factors, i.e Co(II), reaches mass transfer limitation at less cathodic potentials compared to Ni(II). This condition, however, is only for short coating times; thus the anomalous deposition diminishes at longer process times [39]. The mechanism of the anomalous deposition of Ni-Co coatings can be found in Ref. [1].

Pellicer et al. [107] investigated the effects of the used salt: the coatings obtained from sulfate baths present a finer structure and smaller grain size, and thus lower roughness, shinier surface, and higher hardness. Moreover, the coatings obtained from sulfate and chloride baths have an fcc and hcp structure, respectively. The anomalous deposition was more evident for chloride

baths. Increasing pH and Co/Ni ion ratio induced the deposition of Co. Films with low Co contents were solid solutions with fcc structure, while those with high Co content presented an extra hcp Co phase as well [40]. The deposited Co acts as nucleation site for Ni ions, therefore, films with finer grains are formed [33]. As a result, electrodeposition of these alloys usually leads to the formation of rough surfaces that is interesting for their superhydrophobic capabilities [35], but will have a negative effect on the porosity of the applied noble top-coats.

Nowadays Co is considered a toxic metal, due to its effects on hearing and visual impairment, and cardiovascular and endocrine deficits [108]. Co salts have been recently categorized as substances of very high concern, and thus, its electroplating is likely to face strict regulations soon [109]. Therefore, Co, even though it promotes the properties of Ni deposits, cannot be considered as a proper alloying element.

2.2.1.4. Ni-Sn

Ni-Sn alloys have a dense and less porous surface compared to the unevenly nodular surface of the individual deposits. More compact and finer grain films formed when Sn is co-deposited alongside Ni atoms. Ni-Sn films form a dense $NiSnO_3$ oxide during corrosion that gives them a unique passivation up to 1200 mV (vs. SHE) even in the presence of Cl ions [110]. These films also own a bright appearance, a high tarnish resistance, and a high hardness (6-7 GPa) [111]. Ni-Sn coatings have no known health concern; they present a corrosion rate of 0.1 $\mu g/cm^2$/week in artificial sweat that proves their immunity against promoting Ni allergy [110]. The use of Ni-Sn films as the barrier layer is reported to improve the wear resistance of electrical contacts [112]. As a result, these alloys are especially interesting for electronic industries [46].

Sn forms an insoluble basic salt when it is added to large amounts of water with neutral or slightly acidic pH values [113]. Therefore, a high concentration of complexing agents and various additives, such as gelatin or cresol, should be used to deposit a proper Ni-Sn films [43,111]. The deposition electrolyte of Ni-Sn coatings is, therefore, very complicated. This complexity is their main disadvantage since the composition of the bath and the deposition parameters need to be closely controlled.

A chloride-fluoride aqueous electrolyte, that is highly toxic, is normally used to form Ni-Sn films. A pyrophosphate bath is an alternative with lower toxicity [114]. However, the quality of the coatings obtained from a pyrophosphate bath is not as appealing as those obtained from chloride-fluoride electrolytes [111]. Therefore, chloride-fluoride baths are still the most used electrolyte to form Ni-Sn coatings [115]. Shekhanov et al. [116] used an oxalate-sulfate bath as an alternative. They found that the oxalate-sulfate bath offers a higher throwing power, a finer crystalline structure, and a better corrosion behavior. Rudnik [115] studied the effect of sulfate ions on the properties of Ni-Sn electrodeposited alloys. The sulfate ions were found to inhibit the deposition of Ni ions due to the formation of complexes that reduce the cathodic reaction rate. This inhibition leads to an improved surface morphology of Ni-Sn films. It was also found that the deposition of Sn occurs under limiting current and the growth of the Ni-Sn alloy is controlled by an instantaneous nucleation mechanism. The use of ILs, as an alternative to aqueous electrolytes, to form superior Ni-Sn films has also been investigated [112].

The phase composition of Ni-Sn films depends on the used electrolyte. NiSn [111,115] is the main reported phase for the common chloride-fluoride baths. However, the formation of other intermetallic compounds such as Ni_3Sn_2 [114,117], Ni_4Sn [115], $NiSn_3$ [115], and $NiSn_9$ [115] have also been reported for other electrolytes. Note that NiSn, Ni_3Sn_4 and Ni_3Sn_2 phases present very similar diffraction patterns [115].

Intermetallic compounds form in the solid state during simultaneous deposition of Sn and Ni. NiSn intermetallic compounds are deposited at potentials higher than the deposition of Sn and Ni due to the interaction of the atoms. Therefore, the deposition of intermetallic compounds is thermodynamically favored. Note that kinetic factors also play an important role in the deposition of intermetallic compounds. For example, $NiSnF_6$ complexes are found to be responsible for the deposition of the NiSn intermetallic compound from the common chloride-fluoride baths [115]. The mentioned intermetallic compounds can be obtained only through electrodeposition [110].

The deposition current density and the concentration of the Sn source are the most important determining factors for Ni-Sn films. For example, the surface of Ni-Sn films changes from a smooth and fine grain morphology at low current densities to a nodular appearance with particles about 15 μm at high current densities [111]. Increasing the deposition current density increases the Ni content, thus decreases the Sn content of Ni-Sn films [117]. Shetty et al. [114] prepared Ni-Sn films from an alkaline electrolyte at different current densities (1-4 Adm^{-2}) and studied their corrosion behavior. They found that films obtained at lower current densities offer a better corrosion resistance due to their higher Sn content and smoother morphology. The phase structure of their films, regardless to their deposition current density, was a homogenous intermetallic compound, i.e. Ni_3Sn_2.

Sn, noting the above information, seems to be a very good candidate for alloying Ni barriers in electrical contacts.

2.2.1.5. Ni-Cr

Cr is known for its corrosion and wear resistance. However, it is also famous as a highly toxic metal and its usage is internationally restricted [118–121]. Moreover, Ni-Cr films are prone to

the formation of surface cracks [50,51]. Therefore, Cr is not a proper alloying element for Ni barrier layers, even though very appealing properties have been reported for Ni-Cr films [50,51,122].

2.2.1.6. Ni-Zn

Alloying Ni with Zn is expected to improve the corrosion performance [63]. The individual deposition of Zn is possible only from basic solutions due to the well-known inhibiting effect of Zn on the autocatalytic deposition [52]. Metallic ions form stable complexes in highly alkaline baths that can precipitate. The precipitation of these complexes decreases the reduction ability of ions and the stability of the bath. To avoid this precipitation, sodium citrate and ammonium chloride are usually added to the deposition bath [54]. Deposition of Ni-Zn alloys is possible in both acidic [55–57,60] and basic [53,54] baths. The anomalous deposition of Zn and Ni ions is reported to happen in baths with pH below 9 [54]. The addition of Zn into the Ni bath hinders the reduction of Ni and its co-deposition (more than 7 wt.%) in the fcc structure of Ni highly decreases the coating's grain size [56].

The pH of the bath has important effects on the composite and morphology of the deposits. For example, increasing the pH from 8 to 11 increased the deposition of Ni, hence decreased the co-deposition content of Zn, changed the dark deposits to shiny ones, shifted the corrosion potential to more anodic values, and decreased the corrosion current density [54]. Moreover, flower-like morphology, spherical morphology, and dendritic morphologies are obtained depending on the pH of the deposition bath [58]. However, Ni-Zn coatings usually present a cracked surface due to the inclusion of the hcp Zn into the fcc Ni [54,55]. They have also a lower corrosion resistance compared to Ni films due to the formation of corrosion cells between Zn and Ni [61]. As a result, Zn cannot be considered as a good alloying element for Ni barriers.

2.2.1.7. Ni-Mn

The co-deposition of Mn improves the mechanical properties, temperature resistance, and plasticity of Ni deposits. However, Mn is generally the least noble metal that can be electrodeposited from aqueous solutions. The co-deposition of Mn with Ni is highly challenging due to the high difference between their standard electrode potentials (-0.257 V and -1.185 V vs. SHE for $E_{Ni^{2+}/Ni}$ and $E_{Mn^{2+}/Mn}$, respectively). The high cathodic potential of Mn causes an intensified hydrogen evolution that subsequently decreases the current efficiency and adhesion of the obtained coatings. As a result, non-aqueous solutions should be employed to form proper Ni-Mn coatings [65].

The presence of Mn in the Ni-Mn film can strongly inhibit the dissolution of Ni. In contrary, the use of glycine as complexing agent enhanced the dissolution of both Ni and Mn. Glycine forms a strong complex with Ni that decreases the deposition of Ni, but it increases the adsorption of Mn ions at the surface and thus increases the Mn content inside the layer. As a result, the co-deposition of Mn depends on the concentration of the complexing agent [65].

The use of glycine affects the nucleation and growth mechanism of Ni-Mn films; it can weaken the mode of island growth (Volmer-Weber type) and gradually changes it into the mixed mode of layer-plus-island growth (Stranski-Krastanov type). The formation of more uniform and compact films was reported in the presence of glycine. Coatings with a small content of Mn (3.1 at. %) had the highest corrosion resistance. However, coatings with higher Mn contents were found to have a lower corrosion resistance [65]. Note that the incorporation of more Mn occurred in the presence of a higher concentration of glycine.

The applied current density is another determining factor that affects the chemical composition and surface morphology of Ni-Mn films; only Ni will be deposited at low current densities

(less than 3 mA/cm^2), and the co-deposition of Mn happens at higher current densities. The surface morphology changes from “pyramid” shapes (1 mA/cm^2) to “cauliflower-like” shapes with several leaves (3 mA/cm^2) and finally to “tumor-like” shapes (more than 6 mA/cm^2). A solid solution with an fcc structure was formed by the co-deposition of Mn due to the absence of any intermetallic compounds [65].

Increasing the Mn salt concentration, and employing higher current densities lead to more incorporation of Mn inside Ni-Mn films, however, cracked surfaces appeared at high Mn contents due to increasing internal stress [66]. Therefore, it seems that alloying Ni with highly cathodic elements leads to cracked surfaces, and thus, alloys with a low content of alloying elements should be employed since they offer finer structures and better properties.

Nonetheless, all of these alloys have crystalline structures. They have crystalline defects like grain boundaries that act as short-circuit diffusion paths [92,123]. Therefore, amorphous films that are considered as better diffusion barriers made the second type of Ni alloys more interesting.

2.2.2. Ni alloys with alloying elements that can be only co-deposited

2.2.2.1. Ni-refractory metals

The refractory elements, such as W and Mo, are known to be corrosion resistant elements due to their ability to form a passive layer in aqueous media [84]. The formation of Ni-Mo (Ni-W) alloys with thermal techniques is not economically justified due to the high melting temperature of refractory metals [83]. For example, there is a huge difference between the melting points of Ni and Mo (1455 and 2620 ºC for Ni and Mo, respectively) and they have a limited mutual solubility [88]. Therefore, the electrochemical deposition of Ni-refractory metal alloys has

gained a lot of interest. Note that refractory metals cannot be deposited individually. They can be only incorporated inside the growing Ni films, which is known as induced co-deposition [92].

Sodium tungstate (for Ni-W) or sodium molybdate (for Ni-Mo) are usually added instead of sulfate or chloride salts as source of refractory metals. Given the fundamental similarities of refractory metals, this part is focused only on Ni-Mo films.

The co-deposition of refractory metals with Ni increases the hardness, tensile strength, wear resistance, thermal stability, physical and electrical properties, and corrosion resistance. As an example, Ni-Mo coatings are found to be a supersaturated solid solution with a relatively high residual stress (400-600 MPa), a nano-crystalline structure (2-15 nm), a high hardness (close to 800 HV), and a good corrosion resistance [88]. These films are usually formed in an alkaline citric acid- ammonia bath with sodium citrate as a complexing agent. Increasing the content of the refractory metal decreases the grain size and can lead to the formation of an amorphous coating. However, coatings with high contents of refractory metals become brittle and cracked due to an increase in their internal stress [76,79,83,91].

The mechanism of the incorporation of refractory metals is not fully understood. The following multi-step mechanism is suggested to explain the co-deposition of Mo from its anionic form MoO_4^{2-} [82]. The first step is the reduction of MoO_4^{2-} to an intermediate $[NiCitMoO_2]^{2+}$ in the presence of a complexing agent (here citrate ions):

$$MoO_4^{2-} + [NiCit]^{2+} + 2H_2O + 2e^- \rightarrow [NiCitMoO_2]^{2+} + 4OH^- \qquad (2\text{-}4)$$

This intermediate compound then acts as a catalyzer for the reduction of Mo in the metallic state.

$$[NiCitMoO_2]^{2+} + 2H_2O + 4e^- \rightarrow Mo + [NiCit]^{2+} + 4OH^- \qquad (2\text{-}5)$$

Lehman et al. [88] showed that the formation of homogenous, smooth, and compact Ni-Mo films with high adhesion, high hardness, and high wear resistance is possible using DC plating. The applied current density was found to be the most important operating factor; it determines the chemical composition, surface morphology, crystallite size, electrical conductivity, hardness, and corrosion resistance of electrodeposited Ni-Mo films [84]. Low current densities in alkaline baths at slightly higher temperatures (40 ºC) are the best conditions to form dense Ni-Mo coatings [83].

Haung et al. [91] used the pulse electroplating method to form Ni-Mo coatings. They found that the coating with around 30% Mo had the best hardness and corrosion resistance. However, while the Ni-30Mo coating had a better corrosion resistance than pure Ni (around 10 times better), it did not have the common passivation behavior of Ni. Therefore, Ni-30Mo would have a fast dissolution at high potentials. Ni-30Mo had also a more negative corrosion potential. As a result, films with a high content of refractory alloying elements should be avoided for a barrier layer purpose.

2.2.2.2. Ni-B

Incorporation of a small amount of B or P inside the iron group coatings increases the resistivity value of these coatings and transforms their structure to an amorphous state with improved magnetic properties, ductility, and corrosion resistance [124]. Ni-B coatings are well known due to their high wear and abrasion resistance, low porosity, high adhesion, thickness uniformity, fine solderability, good conductivity, and cost-effectiveness [5,97,98].

The incorporation of B inside the Ni lattice decreases the grain size and changes the morphology from a faceted to a dome-like one. The mechanism of incorporation of B inside Ni lattice is not yet completely understood, but it is assumed that the B source is adsorbed on

the surface of the deposited Ni and then decomposes to the elemental B. The amount of B co-deposition, therefore, depends on the concentration of its source and the thickness of the diffusion layer. It is assumed that the applied current density (or potential) has no effect on the content of B. However, the effects of B depends on its source inside the electrolyte, i.e. boric acid, boron hydrides, boron carboranes, trimethylamine borane, and dimethylamine borane [5,93].

Generally, coatings with 4 wt.% or more B content are known to be amorphous. However, in the case of using sodium decahydridodecaborane ($Na_2B_{10}H_{10}$), coatings with B content less than 6 at.% had a polycrystalline structure, the ones with B content between 6 to 20 at.% had a mixed crystalline and amorphous structure, and those with more than 20 at.% B content were completely amorphous. Coatings from a trimethylamine borane source kept a significant crystallinity even with more than 20 at.% B content [5,93].

Ni-B coatings have a superior hardness, wear resistance, and a slightly better oxidation resistance than Ni-P coatings, however, they do not offer a high corrosion resistance [94–96]. Moreover, Ni-B coatings have a more cathodic potential than Ni-P ones [104]. Choi et al. [125] compared Ni-B and Ni-P coatings as diffusion barriers on Cu and reported that Ni-P is more effective due to the higher decomposition temperature of Ni_3P than Ni_3B. Therefore, Ni-P coatings can be considered to generally offer better barrier properties.

2.2.2.3. Ni-P

Ni-P coatings are important engineering alloys because they present an interesting combination of properties, i.e. good corrosion and wear resistance, good solderability, high electrical conductivity, smooth and uniform surface morphology and low friction coefficient [126–130]. Ni-P films also own a proper adhesion to their substrate that secures the electron transfer [103].

Compared to Ni coatings, Ni-P films present a bright, shiny, and smooth look [129], and are less susceptible to oxidation [100].

P can be only co-deposited with iron group metals. Ni^{2+} ions are reduced on active surface sites of the cathode and then they diffuse to a proper site of the fcc lattice. P ions are co-deposited in the octahedral interstitial sites due to a strong atomic interaction between Ni and P ions [129]. The following mechanism has been suggested for deposition of Ni-P films [100]:

The reduction and deposition of Ni ions occur as:

$$Ni^{2+} + 2e^- \rightleftharpoons Ni(s), \qquad E^o\ (V) = -0.25 \qquad (2\text{-}6)$$

The co-deposition of P ions happens as:

$$H_3PO_3(aq) + 3H^+ + 3e^- \rightleftharpoons P(red) + 3\ H_2O, \quad E^o\ (V) = -0.454 \qquad (2\text{-}7)$$

The co-deposited P atoms hinder the Ni diffusion that impedes crystallite growth. A colony like morphology will be formed in the presence of a certain content of P. As the P content increases, the number and size of grains increase and decrease, respectively. This means that the surface morphology will be refined from course micrometer grains to smooth nanometric ones.

The amount of P in the alloy affects its crystallographic structure, and increasing the P content will change the structure from crystalline to nano-crystalline and finally to an amorphous state. There is not a known specific amount but a range of P content where the crystalline to amorphous transition of Ni-P coatings occurs [129]. However, coatings with P contents higher than 8% present usually an amorphous structure [126].

The electrochemical reactions occurring during deposition depend on the electrolyte type. Therefore, the composition of the bath affects the properties of the deposited coatings. These effects are related to the formation of metal complexes; e.g. sulfates make more stable

complexes with metallic cations compared to chlorides [107]. Sknar et al. [130] have investigated the effects of the type of used Ni salt. They have compared the composition and hardness of Ni-P films obtained from methanesulfonate and sulfate electrolytes. The films obtained from the former group showed higher hardness and lower P content. This was attributed to the incorporation of nickel hydroxide that occurred due to the lower buffering properties of the methanesulfonate bath. The pH of the bath is another important factor for the P content of the films. It was found that decreasing the pH leads to a notable decrease in the internal stress of the coatings [128].

The good corrosion resistance of Ni-P coatings comes from their enriched P surface that is formed by the dissolution of Ni occurring in the early stages of corrosion. The surface of Ni-P films can be passivated by the formation of a layer of adsorbed hypophosphite anions. This passivated surface hinders more dissolution of Ni and thus improves the corrosion resistance [36,131]. Ni-P films found to have a higher hardness and lower elastic modulus compared to Ni coatings. However, a peak for hardness as a function of P content was observed, i.e. a nano-structured coating with 4-7% P was harder than an amorphous one with higher P contents [129].

It is well known that introducing even a small amount of certain compounds as additives to the electrolyte significantly affects the properties and appearance of deposits [132]. The refinement of the microstructure, with a decrease of the internal stress and the surface roughness, an increase of the brightness , and the improvement of the corrosion resistance and mechanical properties of the coatings are some of the reported benefits of additives [127,128,133–139]. Organic compounds are the most commonly used additives, and they are called carriers, brighteners, complexing agents, leveling agents, and so on, based on their purpose; carriers are those that are added to refine the grain size and increase the luster [135]. There are several studies regarding the effects of using saccharine [134], glycine [136], coumarin [139], sodium citrate [140] as organic additives. Moreover, similar benefits have been also reported by adding

rare metal salts to the deposition electrolyte [141]. Based on these studies, utilizing even small quantities of these compounds can highly enhance the properties of the obtained coatings, and thus, their usage is highly recommended.

When P is co-deposited with Ni ions, it affects the dissolution equilibrium of Ni during the corrosion process by forming a partial covalent bond [37]. Therefore, a pseudo-passivation region in the anodic branch of the obtained Ni-P coatings can be usually seen in their Tafel plots, meaning they have a higher Ni stability at higher potentials [15]. Therefore, Ni-P films are suitable candidates for barrier purposes in electrical contacts.

Murugan et al. [142] characterized the corrosion performance of Ni/Au, Ni-P/Au, Ni-P/Ni/Au, Ni/Ni-P/Au, and Ni-P/Ni/Ni-P/Au multi-layer electronic contacts. They found out that all of these systems suffer from a localized pitting corrosion due to the large cathode (Au) – small anode (Ni or Ni-P) phenomenon. They have also reported that eliminating the Ni/Ni-P interface improves the corrosion performance because Ni and Ni-P layers form a galvanic couple (Figure 2- 1). They reported that the pit propagation in Ni-P/Ni and Ni/Ni-P layers are horizontally and vertically, respectively. As a result, individual amorphous Ni-P films should be used, however, their properties still can be improved.

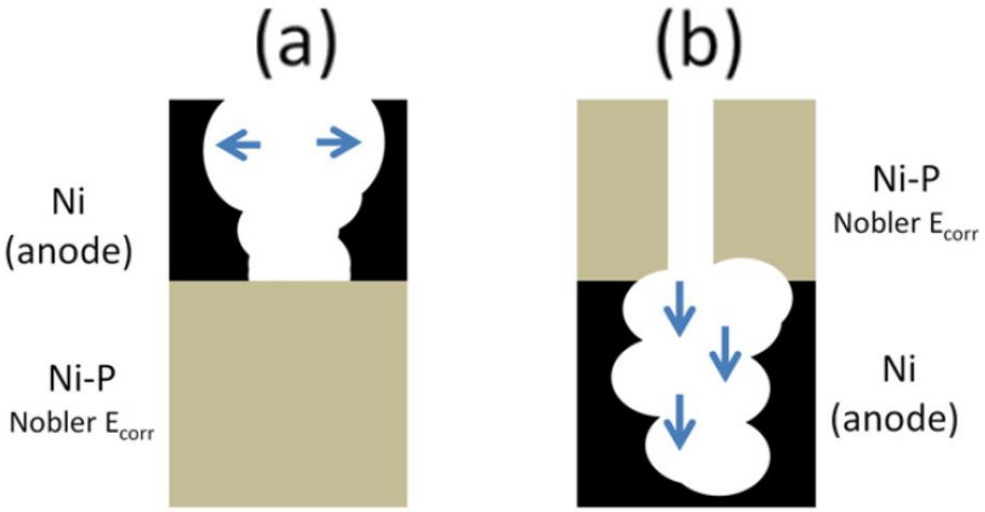

Figure 2- 1. The corrosion mechanism in (a) Ni-P/Ni, and (b) Ni/Ni-P barrier films [142].

To summarize, the chemical composition, surface morphology, and crystalline structure of some of the Ni alloy deposits are presented in Table 2- 1. It can be seen that Ni-P is the only alloy that can provide the desired properties of a proper barrier layer (spherical morphology with amorphous structure) at a low content of the alloying element. This alloy is therefore further investigated in the following.

Table 2- 1. Chemical composition, surface morphology, and crystalline structure of Ni-alloy deposits

Coating	Chemical Composition	Surface Morphology	Crystalline Structure	Ref.
Ni-Ag	Ni-20 Ag (at.%)	Dendritic	Crystalline (fcc)	[18]
Ni-Ag	Ni-5 Ag (at.%)	Spherical	Crystalline (fcc)	[19]
Ni-Co	Ni-8 Co (wt.%)	Pyramidal-shaped	Crystalline (fcc)	[33]
Ni-Sn	Ni-60 Sn (wt.%)	Pyramidal-shaped	Intermetallic	[46]
Ni-Cr	Ni- 20 Cr (wt.%)	Spherical	Crystalline	[50]
Ni-Zn	Ni- 4 Zn (wt.%)	Pyramidal-shaped	Crystalline (fcc)	[56]
Ni-Zn	Ni- 50 Zn (wt.%)	Spherical	Amorphous	[56]
Ni-Mn	Ni-9 Mn (at.%)	Spherical	Crystalline (fcc)	[65]
Ni-W	Ni-30 W (wt.%)	Pyramidal-shaped	Crystalline (fcc)	[79]
Ni-Mo	Ni-5 Mo (wt.%)	Spherical	Crystalline (fcc)	[88]
Ni-Mo	Ni-22 Mo (wt.%)	Spherical	Amorphous	[88]
Ni-B	Ni-5 B (wt.%)	Spherical	Crystalline	[93]
Ni-P	Ni-8 P (wt.%)	Spherical	Amorphous	[102]

2.2.2.3.1. Heat treatment of Ni-P films

Heat treatment is a commonly used method to improve Ni-P films. It leads to the precipitation of Ni_xP_y intermetallic compounds (mainly Ni_3P) and formation of an oxide layer that highly increases the hardness of the films. The precipitated phases, due to their inhomogeneous nature, could decrease the corrosion resistance by creating active-passive cells. The heat treatment also grows the grains and transits the amorphous structure to a crystalline one [126,129,131]. Obtaining a nano-crystalline structure is usually the goal of designing a heat treatment process since the corrosion resistance of coatings follows this trend: nano-crystalline> amorphous > crystalline [143]. Zhao *et al.* [101] have investigated the effect of heat treatments of amorphous Ni-P films under their crystallization temperature and reported that the corrosion resistance improved by doing a heat treatment at 250 ºC up to 12 h and then decreased at longer times.

Unfortunately, however, the typical heat treatment methods use a furnace (that is restrict the size of samples) and require heating up the entire sample to high temperatures. This is obviously a disadvantage for thermally sensitive and unstable substrates (like electronic modules stacked to plastics) [144]. Laser annealing could be employed as an alternative to common furnace annealing in order to eliminate or reduce the diffusion of elements at the interface of multilayer coatings due to its rapid heating process [104]. However, the formation of the oxide layer could lead to a loss of electron conductivity and thus heat treatment may be destructive for electrical applications.

2.3. Ternary Ni alloys

Ternary Ni alloys also could be employed as barrier films in electronic contacts. Ni-P ternary alloys are presented in this part since they can enhance the desirable properties of Ni-P coatings. As an example, noble metals act as nucleation sites and thus alloying Ni-P with a small amount of nobler metals, such as Cu, leads to coatings with a finer microstructure. The properties of some ternary Ni-P films with different alloying elements are listed in Table 2- 2.The following equation is used to measure the improvement by alloying elements of the Ni-P films:

$$(Q.I\%) = \left(1 - \left(\frac{Q_A}{Q_B}\right)\right) * 100 \qquad (2\text{- }8)$$

Q corresponds to C, F, R, and H for corrosion resistance, friction coefficient, roughness, and hardness. When an increase means an improvement, for example corrosion resistance and hardness, Q_A and Q_B are related to Ni-P and modified Ni-P, respectively. When a decrease means an improvement, for example corrosion current density, roughness, friction coefficient, Q_A and Q_B are representing modified Ni-P and Ni-P, respectively.

Table 2- 2. The effect of alloying element on the properties of Ni-P films; deposition method (DM; Electroless: EL, and Electrodeposition: ED), corrosion resistance improvement (C.I), corrosion potential variation (ΔE), corrosive media (CM), friction coefficient improvement (F.I), roughness improvement (R.I), and hardness improvement (H.I)

System	DM	Corrosion Properties			Mechanical Properties			Ref.
		C.I %	ΔE (mV)	CM	F.I %	R.I %	H.I %	
Ni-8.6P-6.2Cu/Cu	EL	97.2	-82	Flue gas	-	-	-	[22]
Ni-4.0P-7.0Cu/Mg	EL	73.9	60	NaCl	-	-	-	[25]
Ni-12.3P-4.3Cu/Fe	EL	12.9	75	NaCl	-	-	-	[26]
Ni-6.8P-0.1Cu/C	EL	99.5	15	KOH	-	-	-	[29]
Ni-8.5P-0.3Cu/Fe	EL	-	-	-	28.6	33.3	-	[30]
Ni-14.0P-6.3Cu/Fe	EL	27.8	46	NaCl	-	-	-	[32]
Ni-11.3P-2.6Cu/Al	EL	97.1 88.9	520 390	NaCl H_2SO_4	-	-	-	[49]
Ni-10.6P-9.3Cu/Fe	EL	-15.0 -284.0	20 -85	NaCl HCl	-	-166.7	3.8	[145]
Ni-P-Co/Al	EL	22.4	60	NaCl	-	-	-	[36]
Ni-2.2P-45.0Co/Fe	EL	-	-	-	-5.8	-207.1	20.9	[38]
Ni-9.2P-10.1Sn/Fe	EL	51.1	322	NaCl	15.1	-	-	[42]
Ni-15.6P-4.0Sn/Cu	EL	24.6	90	H_2SO_4	-	-	-	[45]
Ni-8.5P-2.5Sn/Mg	EL	70.3 90.6	136 109	NaCl HCl	-	-	13.4	[48]
Ni-11.3P-0.5Sn/Al	EL	73.7 60.7	61 265	NaCl H_2SO_4	-	-	-	[49]
Ni-P-Zn/Fe	EL	-4914.3	-198	NaCl	-	2.5	-	[59]
Ni-11.0P-9.9Zn/Al	EL	-1907.4	13	NaCl	-	-	-	[61]
Ni-2.8P-29.9W/Fe	ED	84.1	-	NaCl	-	-	13.8	[68]
Ni-4.9P-4.5W/Mg	EL	-	-	-	-	-	12.1	[73]
Ni-5.9P-4.5W/Fe	EL	5.0 -276.0	-30 -200	NaCl HCl	-	-400.0	26.4	[145]
Ni-12.4P-4.6Mo/Fe	EL	61.9	38	H_2SO_4	-	-237.9	-	[80]

As mentioned, Ni-P films owe their corrosion resistance to the formation of a P-rich surface. The incorporation of nobler metals accelerates the formation of the P-rich film and thus improves the passivation behavior. They also shift the corrosion to more anodic regions. Noble metals inside the coatings can reduce the free energy of the alloy and suppress the cathodic reactions by increasing the over-potential of hydrogen evolution [22,25,131]. Low Cu content Ni-Cu-P films found to have a lower friction coefficient, and a lower roughness [30]. High Cu content ones, however, had slightly higher hardness but rougher surface and notably lower corrosion resistance [145]. Therefore, noble metals, in small contents, are very proper alloying candidates for Ni-P barrier films. Cu, on the other hand, is not a suitable candidate since it

defies one of the most important purposes of barrier films; i.e. avoiding the diffusion of Cu to the noble top-coat.

Sn promotes the formation of amorphous Ni-P films, and highly improves the corrosion resistance by enhancing the passivation behavior [43]. The incorporation of Sn found to shift the corrosion potential to more anodic regions, increase the corrosion resistance, increase the hardness, and decrease the friction coefficient [45,48,49]. Therefore, Sn is a proper alloying element with a similar standard potential to Ni for Ni-P films.

The incorporation of more cathodic elements, like Zn, was found to highly decrease the corrosion resistance (especially localized corrosion), and slightly decrease the roughness of Ni-P films [59,61,62]. The incorporation of Zn hinders the co-deposition of P, i.e. coatings with more Zn content own lower P [58,61]. The presence of at least 4 wt.% P is necessary to obtain a crack-free surface [55]. Therefore, more cathodic elements, especially Zn, are not suitable for barrier goals.

The co-deposition of refractory metals; i.e. Mo or W; could enhance the barrier properties of Ni-P films since these metals accumulate at the grain boundary and obstruct the diffusion. Hamid *et al.* [82] investigated the effects of coating conditions on the properties of Ni-Mo-P coatings on Cu for diffusion barrier purposes. They successfully formed highly conductive Ni-Mo-P films with a solid solution fcc structure. The incorporation of more Mo was reported at higher deposition current densities. However, high Mo content films were highly prone to cracking.

A higher Mo content increases the corrosion resistance only when the crystallite size of Ni-Mo-P films is above 8 nm. The corrosion behavior is determined by grain boundaries and triple junctions in crystallite size lower than 8 nm. The applied current density found to have no effect

on the chemical composition of Ni-Mo-P films, while it had a notable effect on their surface morphology [84].

The incorporation of refractory metals hinders the co-deposition of P, however, Ni-Mo-P films keep their amorphous structure. Therefore, Ni-Mo-P films have higher electrical conductivity since Mo is a better electrical conducive material and P has an electrical scattering effect [85,92]. Such coatings offer an interesting combination of high corrosion resistance [68,77,80,145], and high hardness and wear resistance [68,72,73,75,145]. However, the incorporation of refractory metals usually increases the roughness of Ni-P films [80,145]. As a result, refractory metals, only in low contents, could be considered as good alloying elements for Ni-P barriers.

2.4. **Deposition of Ni composites**

Composite films offer a superior corrosion resistance, wear resistance, hardness, and chemical compatibility [146–148]. The incorporation of particles inside the film leads to more compact coatings with less defects. Moreover, composite films were found to have a higher resistance against the diffusion of Cu [149]. The particles could be categorized based on their type and properties as metallic particles (such as Ag [148,150–152], Al [153,154], Bi [155], and Ti [156]), hard particles including oxides, nitrides, and carbides (like Al_2O_3 [157–162], TiO_2 [149,163–169], SiO_2 [170–172], ZrO_2 [87,173], CeO_2 [174], TiN [143,175], Si_3N_4 [176–178], TiCN [179], TiC [147,180], WC [181,182], SiC [183–191], B_4C [192], and hBN [98,193,194] diamonds [195–197]), and solid lubricants (such as MoS_2 [109,198–200], WS_2 [201]). hBN [98,193,194], carbon nano-tubes (CNTs) [164,190,202–204], graphite [205,206], and PTFE [200,207–210]).

Gugliemi's model is often employed to explain the incorporation of particles inside the deposited coatings [5,79,153,170]. Based on this model, Ni ions adsorb on the surface of particles at the first step. Then these particles with their ionic cloud will diffuse toward the cathode surface and loosely adsorb there. Finally, the reduction of Ni ions encapsulate these particles inside the coating's matrix. The incorporated particles induce a non-uniform distribution of current around themselves and act as nucleation sites (Figure 2- 2.a). As a result, the incorporated particles can highly affect the obtained properties, i.e. the morphology, hardness, and corrosion resistance (Figure 2- 2.b).

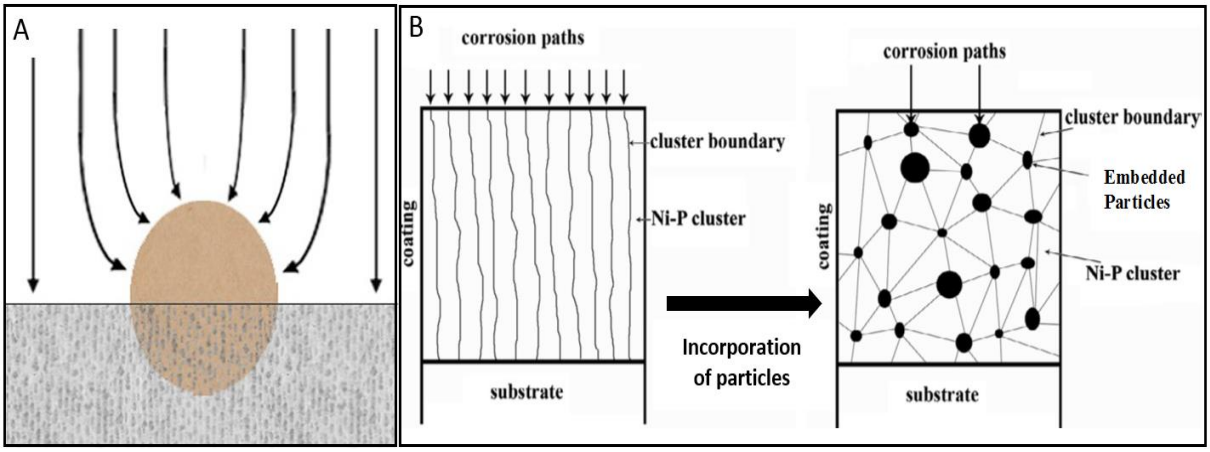

Figure 2- 2.(A) a schematic of a non-uniform distribution of current around an embedded particle in the growing deposit that could act as nucleation site [109], and (B) schematics of the effects of the incorporated particles on the structure and corrosion behavior of deposited coatings [197].

The effect of particles depends on their properties; i.e. size, conductivity, density, zeta potential, and etc. [148]. Table 2- 3 presents the effects of some particles (using equation 2-8) on Ni-P films.

Table 2- 3. The effect of embedded particles on the properties of Ni-P films; deposition method (DM; Electroless: EL, and Electrodeposition: ED), Dispersion method (Mechanical stirring: M, Ultrasonic assisted: U, Surfactants: S (anionic surfactant: AS, cationic surfactant: CS, and non-ionic surfactant: NS), corrosion resistance improvement (C.I), corrosion potential variation (ΔE), corrosive media (CM), friction coefficient improvement (F.I), roughness improvement (R.I), and hardness improvement (H.I)

Particle	DM	Dispersion method	Corrosion Properties			Mechanical Properties			Ref.
			C.I %	ΔE (mV)	CM	F.I %	R.I %	H.I %	
Ag, 2-7 µm	EL	CS:CTAB + M	-	-	-	-13.2	-	-12.0	[148]
Ag, 20 nm	EL	AS:O7501 + M	-	-	-	-	-	24.4	[151]
Al_2O_3, 80 nm	EL	CS:CTAB + M	-	-	-	76.3	-	27.3	[148]
Al_2O_3, nm	EL	AS:SDS + M	68.2	160	NaCl	-55.0	-	19.8	[157]
Al_2O_3, 30 nm	EL	M AS: SDBS + M AS: SDS + M AS: SLS + M CS:CTAB + M	47.8 50.2-69.0 18.0 -31.5 -9.2	15 -21 5 47 9	NaCl	-	-	-	[159]
Al_2O_3, 74 nm	EL	M	67.4	54	-	-	-	19.6	[160]
Al_2O_3, 30-50 nm	EL	AS:SDS + M	-	-	-	-	-185.7	6.3	[161]
Al_2O_3, nm	EL	M	25.4	50	-	71.4	-	33.0	[162]
TiO_2, nm	ED	Sol + M	-	-	-	-	-	26.8	[163]
TiO_2, 15 nm	EL	M	23.4	184	NaCl	-	-	-	[164]
TiO_2, 250 nm	EL	M	63.0	74	NaCl	-	-	-	[165]
TiO_2, 25 nm	EL	M AS:SDS + M CS:DTAB + M	50.5 69.3 76.8	-	NaCl	-	-	-	[166]
TiO_2, 21 nm	EL	M	-	-	-	-	-41.6	-	[149]
TiO_2, nm	EL	Sol + M	23.3	30	NaCl	-	-	11.2	[167]
TiO_2, 200-300 nm	EL	Sol + M AS:SDS + M AS:SDBS + M NS:HPMC + M	-	-	-	-	-32.2 -15.9 -16.4 -12.6	11.3	[168]
TiO_2, nm	EL	M	-	-	-	28.6	-	26.3	[169]
SiO_2, 20 nm	EL	M	26.0	43	NaCl	-	-	-	[170]
SiO_2, nm	EL	Sol + M	-	-	-	27.7	-	29.6	[171]
SiO_2, 10-20 nm	EL	M	99.7	154	NaCl	-	96.5	59.8	[172]
CeO_2, 20-50 nm	ED	U	-	-	-	-	-	20.9	[174]
TiN, 20 nm	EL	NS:PEG +M	-566.7	-	NaCl	-	-	14.9	[175]
Si_3N_4, µm	EL	M	22.5	23	NaCl	-	-	-	[176]
Si_3N_4, 0.73 µm	EL	M	-	-	-	-	-	21.9	[177]
Si_3N_4, nm	EL	AS:SDS + M	-	-	-	83.3	-	15.8	[178]
TiCN, 3.4 µm	EL	M	71.4 71.1	399 46	NaCl H_2SO_4	-	-	57.7	[179]
WC, nm	EL	AS:SDS + M	75.0	64	NaCl	-	-	36.2	[181]
WC, 80 nm	EL	S + M	-	-	-	39.3	-	25.9	[182]
SiC, 40 nm	EL	CS:HTAB + M	77.9	189	NaCl	-	-	26.8	[185]
SiC, 40 nm	EL	CS:CTAB + M	60.9	70	NaCl	-24.6	-150.0	9.6	[186]
SiC, 40 nm	EL	M	-33.0	-	NaCl	-	-	34.8	[187]
SiC, 20 nm SiC, 50 nm SiC, 200 nm	EL	CS:CTAB + M	15.8 50.7 24.4	-	NaCl	-	-	-	[188]
SiC, nm	EL	CS:CTAB + M	77.8	150	NaCl	-	-	-	[189]
SiC, 40 nm	EL	AS:SDS + M	1.4	23	NaCl	-	-	-	[190]
SiC, 0.5-0.7 µm	EL	AS:SDS + M	26.6	1	NaCl	-	-	9.7	[191]
B_4C, µm	EL	M	-1100.0	-223	NaCl	-	-	41.7	[192]
DNP, 20 nm	EL	M	63.5	40	NaCl	-	-	36.5	[196]
DNP, 4 nm	EL	U	59.2	275	NaCl	-	-	-	[197]
MoS_2, 80-100 nm	EL	M	-311.1	40	NaCl	-	-	-	[198]
MoS_2, µm	EL	CS:CTAB + M	-226.6 -246.8	-55 -33	NaCl H_2SO_4	50.0	-	-	[200]

Table 2- 3.

Particle	DM	Dispersion method	Corrosion Properties			Mechanical Properties			Ref.
			C.I %	ΔE (mV)	CM	F.I %	R.I %	H.I %	
WS_2, 2 µm	EL	S + M	35.5	-	NaCl	26.3	65.8	51.5	[201]
hBN, 0.5-0.7 µm	EL	CS:CTAB + M	9.2	80	NaCl	-	-56.1	-10.6	[193]
hBN, 0.5 µm	EL	CS:CTAB + M	-	-	-	31.8	-7.2	-10.2	[194]
CNT, 5 nm	EL	M	53.6	324	NaCl	-	-	-	[164]
CNT, nm	EL	AS:SDS + M	43.8	40	NaCl	-	-	-	[190]
CNT, nm	EL	M	97.5	205	NaCl	-	-	5.6	[202]
CNT, 40-60 nm	EL	AS:SDS + M	32.7	30	NaCl	-	-	24.7	[203]
CNT, nm	EL	CS:CTAB + M	54.7	120	NaCl	50.0	32.8	27.5	[204]
Graphite, 40 nm	ED	M	-	-	-	54.0	-	16.7	[205]
PTFE, µm	EL	CS:CTAB + M	53.2 92.1	116 452	NaCl H_2SO_4	-	-	-	[200]
PTFE, nm	EL	CS:FC-4 + M	45.4	158	NaCl	-	-	-	[207]
PTFE, 0.2 µm	EL	AS:SDS + M CS:CTAB + M NS:PVP + M	0.0 93.8 75.0	-	NaCl	-	-	-	[209]
PTFE, 0.3 µm	EL	NS:CO-890 + M	35.0	0	NaCl	50.0	-	-56.6	[210]

Micrometer and sub-micrometer particles could induce cracks and pores in the surface and decrease the surface uniformity. The removal of loosely embedded particles leaves holes behind that make the coatings vulnerable to corrosion [153,192,200]. Therefore, nanometer particles are superior to micrometer ones. However, it was found [188] that very small particles (< 20 nm) have a high tendency of agglomeration, and very big particles (> 200 nm) are reported to not be able to impose a notable effect on deposits.

An optimum concentration of particles is usually reported [97,98,109,156,157,178,182,202]. Agglomeration occurs at higher concentrations that diminishes their influence. Note that the incorporation of particles inside Ni-P films impedes the deposition of P [147,165]. The corrosion resistance of composite films may be decreased at low concentrations of particles.

The particles conductivity is another determining factor that affects the properties of composite films. Inert particles (like Al_2O_3 [153]) will be uniformly distributed inside deposits and enhance their properties. However, high conductive particles (such as TiN [175] and MoS_2 [198]) lead to the formation of a rough surface with nodular morphology, a porous structure, and a low corrosion resistance. The incorporation of inert hard secondary particles, based on Table 2- *3*, improves the corrosion resistance and hardness of films, however, increases the

roughness of the surface as well. Solid lubricating particles, except CNTs, decrease the hardness of films. CNTs, on the other hand, improve all desired properties and thus could be considered the best candidate for forming Ni-P barrier films.

Nonetheless, the key to improve the properties is to obtain well-dispersed structures. The major challenge is to keep the particles in a stable suspension since they have a high tendency of agglomeration due to their high surface activity [146,163]. Mechanical stirring [165,202,211], ultrasonic agitation [63,174,196], surfactants [139,158,159], and sol-enhanced electroplating [97,152,163] are the main employed methods to enhance the dispersion of particles.

2.4.1. Particle dispersion by mechanical stirring

The bath is usually stirred mechanically to keep the particles in suspension during the deposition of composite coatings. The stirring speed has been shown to have an important impact on the incorporation of nanoparticles into the deposited metals. The incorporation rate has been reported to increase with increasing the stirring rate up to a certain speed and then decrease again in faster rotations [146].

2.4.2. Ultrasonic assisted particle dispersion

The ultrasonic assisted method is commonly used to disperse particles. Ultrasonic waves form cavitation bubbles inside the bath. These bubbles then will implode in an asymmetric way while they are moving at a high speed. This unique stirring is called the cavitation phenomenon. It will agitate the bath, especially near the electrode surface, in a much greater extent than could be achieved by mechanical stirring. Such turbulence found to also impose catalytic effects on the occurring chemical reactions and ease the detachment of the formed hydrogen bubbles (degassing) during the deposition process. As a result, using ultrasonic waves not just stabilizes

the particles suspension, but leads to the formation of denser coatings with superior properties including higher adhesion to the substrate, and higher electrical conductivity [212–214].

2.4.3. Particle dispersion using surfactants

Surfactants, as the most used method of dispersing particles, are organic amphiphilic compounds, i.e. they have both hydrophobic (tail) and hydrophilic (head) groups in their structure. They adsorb on the surface of particles and decrease their agglomeration tendency. Moreover, surfactants act as wetting agents and thus can ease the gas escapement [100,158]. These compounds can be categorized based on their hydrophilic groups. Anionic surfactants such as sodium dodecyl sulfate (SDS) [157,161,178], sodium lauryl sulfate (SLS) [159], and sodium dodecyl benzene sulfonate (SDBS) [159,168] have anionic functional groups. Cationic surfactants like cetyltrimethylammonium bromide (CTAB) [139,146,183], dodecyl trimethyl ammonium bromide (DTAB) [166,173,215], and hexadecyltrimethylammonium bromide (HTAB) [185,203] present cationic functional groups. Non-ionic surfactants, such as hydroxypropyl methylcellulose (HPMC) [168], polyethylene glycol (PEG) [180], and tetraethyleneglycol dodecyl ether (Brij30) [173], have covalently bonded oxygen groups.

The critical micelle concentration (CMC) defines the behavior of surfactants inside the electrolytes [215]. The concentration of surfactants should be determined regarding their CMC. The adsorption mechanism of surfactants on particles depends on their concentration. An electrostatic mechanism (i.e. ion exchange/and ion pairing) occurs at low concentrations. At high concentration, however, a hydrophobic bonding mechanism happens [183]. While surfactants are efficient in low contents, high concentrations were found to impose negative effects on the coatings properties [215–217].

Considering that the substrate is negatively charged during the deposition process, cationic surfactants are usually assumed to efficiently incorporate the particles inside the growing

matrix. Cationic surfactants increase the zeta potential of particles and induce their movement toward the cathode [146]. However, anionic surfactants were found to be superior [159,168,203] as it is explained in the following [195].

A Helmholtz layer is formed on the metal surface when they are submerged in the deposition bath. The first layer is a compact layer of adsorbed metallic cations and other complex cations at the surface of the electrode. Therefore, negatively charged particles are more capable to diffuse through the Helmholtz layer and reach the surface. Moreover, cationic surfactants and metallic ions compete over winning electrons during the deposition procedure. This competition suppresses the cationic reactions, which can degrade the coating's qualities. For example, the adhesion of coatings decreases due to weakening the bonding strength between the substrate and the film [1,158,175,183].

Although anionic surfactants are generally superior, some exceptional behavior is reported for DTAB (as a cationic surfactant). SDS and CTAB are the most used surfactants, however, they are not as effective as SDBS or DTAB, and some negative effects of their usage is reported [159,166,168,173,209,215].

Dispersing the particles in deposition electrolytes is more complicated than in distilled water due to the interactions of ions and particles. Jiang et al. [158] have tried to disperse nano- Al_2O_3 particles in Watt's bath using a combination of SDS and HPB (hexadecylpyridinium bromide) surfactants. While surfactants had no notable impact on the dispersion, they changed the particles agglomeration from hard to soft state. Stirring the electrolyte breaks the soft agglomerated particles and keep them in suspension. The migration of the particles to the cathode surface found to occur mechanically during the stirring; the electrophoretic motion was too weak to be taken into account. Noted that ILs and DESs have higher viscosity and

lower surface energy than water that is beneficial for wetting and dispersing the particles. Therefore, employing ILs or DESs could completely eliminate the use of surfactants [218].

2.4.4. Sol-enhanced electroplating

The recent development of the sol-enhanced technique made it possible to obtain perfectly stable nano-fluids (Figure 2- 3). They are successfully used to obtain a uniform distribution of nanoparticles [97,152,163,171]. The sol could be formed by mixing the salt of the goal material (such as Ag) with a reduction agent (like sodium borohydride) and a capping agent (like glycerol). No agglomeration happens when the formed sol is added to the deposition bath.

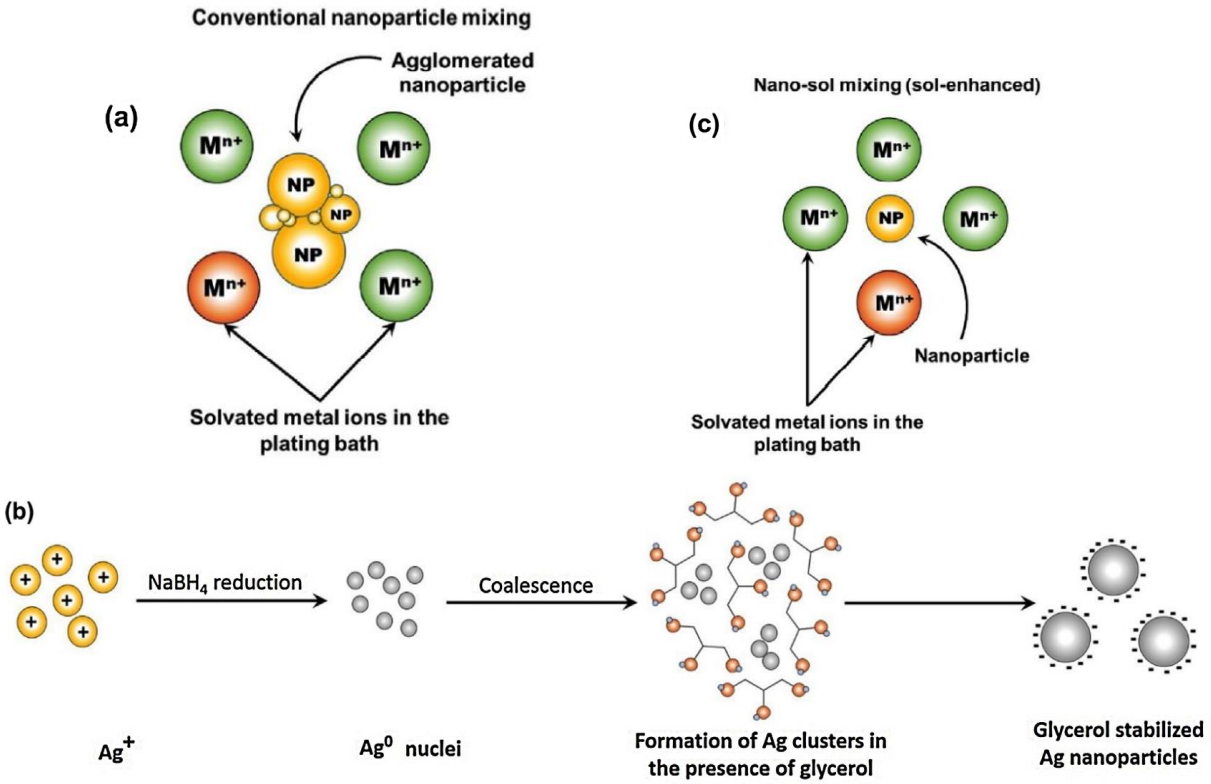

Figure 2- 3. (a) Agglomeration of nanoparticles when they are added in the conventional mixing method, (b) the formation of nano-particles sol, and (c) the stable suspension of nanoparticles inside the deposition bath using the sol-enhanced method [152].

The importance of the used dispersion method, especially ultrasound and surfactants, on the properties of deposited coatings is now well-known. Unfortunately, however, this fact is sometimes ignored unintentionally or deliberately. For example, Ni-P-PTFE films are obtained by using a cationic surfactant to disperse PTFE particles [207,208]. The films were superior in low concentrations of particles emulsion, i.e. 0.2 mL/L. At high concentrations, however, the properties of the films were drastically diminished. It was concluded the incorporation of high PTFE content increases the porosity and thus diminishes the corrosion properties. However, the effects of the used surfactant were ignored. As a result, a lower corrosion resistance could be due to increasing the concentration of the used cationic surfactant rather than high contents of PTFE.

In conclusion (based on Table 2- 3), Ni-P composite films, specifically with CNTs, seem to fulfill the requirements of a proper barrier layer, and ultrasonic, sol-enhanced electroplating, and SDBS and DTAB surfactants could be considered the best techniques to obtain them.

2.5. Noble top-coats

2.5.1. Au top-coats

Au is the most used noble top-coat for an electrical contact due to having a combination of good corrosion resistance and high electrical conductivity. Au films were traditionally obtained from a cyanide electrolyte. However, cyanide electrolytes suffer from a high toxicity and a low long-term stability. This limitation led to several studies about finding new alternative electrolytes. Thiosulphate-sulphite mixed bath, thiourea bath, and mercaptotriazole bath are a few examples of such developed non-cyanide electrolytes. The stability of Au inside the electrolyte increases by increasing the pH of electrolyte, i.e. the highest concentration of free Au ions will be found at pH below 2 [219].

Organic solvents were recently investigated as an alternative to common cyanide electrolytes. Dimethylformamide (DMF) and dimethyl sulfoxide (DMSO) are well-known organic solvents that are stable at elevated temperatures. They can be considered as the base of electrolytes to deposit thin metallic films over a large range of potentials without decomposition, but elevated temperatures may need to be applied [220,221].

The following mechanism was proposed for the deposition of Au in aqueous and organic solutions [220]. A single three-electron process of reduction of $AuCl_4^-$ to metallic Au occurs in aqueous media.

$$AuCl_{4(aq)}^- + 3e^- \rightarrow Au_{(s)} + 4Cl_{(aq)}^- \qquad E^0 = 1.002\ V\ vs.NHE \qquad (2\text{-}9)$$

In organic solutions, however, the reduction happens in two consecutive electrochemical steps, possibly due to the poor solvation of Cl^- ions in such solvents.

$$AuCl_{4(o)}^- + 2e^- \rightarrow AuCl_{2(o)}^- + 2Cl^- \qquad E_1 \qquad (2\text{-}10)$$

$$AuCl_{2(o)}^- + e^- \rightarrow Au_{(s)} + 2Cl^- \qquad E_2 \qquad (2\text{-}11)$$

The electroreduction of $AuCl_2^-$ ions highly depends on the material of the working electrode and its surface morphology. Superior films are formed on smoother surfaces. The employed complex has an important impact on the quality and properties of the Au deposits as well. For example, a non-uniform deposit was reported for the reduction of $AuCl_4^-$ ions, while uniform deposits were obtained from the reduction of $Au(CN)_2^-$ ions [220].

The surface morphology of the top-Au is a dominant factor for electrical contacts. It could be either hemispherical or faceted features; the former is always preferred since the latter results in a substantial increase of the contact resistance [222]. Thickness is another determining factor; it varies from 0.1 to 5 µm depending on the purpose of the conductive surface. A non-porous layer is necessary to secure a good corrosion resistance; coatings thinner than 0.5 µm

are highly porous, while those that are thicker than 0.8 µm had almost no porosity. Therefore, 0.8 µm is reported as the optimized thickness for Au protective coatings [223].

The microstructure of the deposits and the hydrogen evolution during the deposition process was reported to determine the porosity of these thin films [224]. The formed pores during the electrodeposition process can be classified into two types. The pores are called through-pores if they are extended from the sublayer to the surface, otherwise, they are known as the masked pores. Through-pores (and their size) are important due to their negative effects on the corrosion performance of electrical contacts. This type of pores is usually found around grain boundaries. They have a uniform round shape that suggests they were formed by hydrogen bubbles during the electrodeposition process. Thickening of the deposited layer is known to dramatically decrease the porosity content of Au layers [222].

The applied current density is an important factor regarding the formation of pores. The applied current density determines the nucleation and growth mechanisms. At low current densities, crystal growth is preferred over nucleation that leads to the formation of large grains. High current densities, however, favors nucleation over growth and leads to finer grains. The hydrogen reduction, as a side reaction, occurs alongside the reduction of Au. This reaction is more important at high current density [222], it may consume more than 40% of the current during the electrodeposition [224]. A reverse relationship between the porosity content of deposits and their current efficiency was reported, i.e. more compact coatings were formed when they had higher current efficiencies [222].

Fewer pores are known to be generated in pulse plating rather than DC. Hydrogen bubbles tend to be formed at the junctions of grains in DC coatings. There is enough time for bubbles to grow and reach the stable phase. These bubbles could be finally trapped inside the growing layer and form pores. In a pulse mode, the formed bubbles have less time to grow during the

on-pulse and they can be detached from the surface during the off-pulse. It was also found that there is a direct relationship between the pulse frequency and the current efficiency. More compact coatings with smaller pore sizes were formed using pulse plating at high frequencies (>100 Hz) [222]. As a result, finer and smoother coatings with round grains and less porosity are formed by using the pulse plating method.

Sus *et al.* [221] have investigated the mechanism of Au deposition from DMF using pulse electrolysis. A wide range of Au deposits, from Au nanoparticles to compact thin films, can be obtained by controlling the pulse deposition parameters (deposition cycles, voltage range, and pulse and pause times). For example, Au nanoparticles were formed when a voltage range of 0.1-1.6 V, a pulse time of 6 ms, and a 300 ms pause time were used. Increasing the number of pulse cycles (to more than 1000 cycles) led to the formation of a compact thin layer with spherical features. Chen *et al.* [225] used the pulse electrodeposition technique and successfully formed a thin layer of Au from a non-toxic sulfite-based bath. The obtained coating had a notably smaller grain size (10.5 nm vs. 22.8 nm), lower roughness (117 nm vs. 200-250 nm), higher hardness, and denser texture compared to DC samples.

Coatings with even lower porosity content were formed using on-off pulse and pulse-reverse plating techniques by Liu et *al.* [224]. The anodic cycle in the reversed pulse partially dissolves the deposited film and oxidizes the formed hydrogen bubbles. Smoother and more compact coatings were formed when a reverse current density above 5 $mA.cm^{-2}$ was applied [226].

Wear resistance and material costs are the only limits of Au coatings. Au alloys or Au composite coatings offer a notably higher hardness and thus they can be used to overcome the softness. Forming such coatings, however, should be done with high precision since the contact resistance could be remarkably increased [227].

Hard Au, i.e. an Au alloy with Ni, Fe, or Co, has been developed as an electrical contact material due to its mechanical and electrical properties. Alloying Au with Ni, Fe, or Co can increase its hardness from 70 HV to about 170 HV. The type of alloying element and its concentration have a huge impact on the hardness, ductility, brittleness, wear resistance, and corrosion behavior of Au alloys [224].

Au nano-composites are reported to have a high hardness of 2100 HV [223]. Several nano-particles, including aluminum oxide, titanium oxide, titanium nitride, silicon carbide, silicon oxide, silicon nitride, diamonds, and zirconium oxide were investigated. Aluminum oxide and titanium oxides were reported the most applicable particles to enhance the lifetime of electrical contacts [223]. PTFE nano-particles were also reported to improve the lifetime of electrical contacts. PTFE particles reduced the friction and thus enhanced the wear resistance [228].

The uniform distribution of particles inside the matrix is the main challenge to improve the properties of composite films. A well dispersed and stable suspension of particles in the bath is the vital key for this purpose. An increase of hardness was observed when TiO_2 particles were added to the bath (2.55 and 2.91 GPa for hard Au and composite hard Au, respectively). However, the agglomeration of particles limited their effect and introduced some anomalies in the final surface morphology. The composite coatings obtained from the sol-enhanced deposition had the highest hardness (3.20 GPa) with highly dispersed particles and a uniform morphology [229].

Song *et al.* [227] employed fretting corrosion tests to compare the lifetime of different top coats. They used contact resistance to define two different stages of the lifetime of electrical contacts. Lifetime I is assigned when a 300% increase in the contact resistance is observed and lifetime II is defined when the contact resistance reached 300 mΩ. The lifetime I usually happens when the top coat wears off. After lifetime I the contact is damaged but still works

properly. However, a normal electrically functional contact could not be expected after lifetime II. A further increase in lifetime of Au top-coats can be expected by forming hard Au and Au nano-composite coatings. Modifying the Au layer with alloying elements or nano-sized particles increased the wear resistance of the contacts and thus noticeably improved the lifetime. However, a huge range of lifetimes (from extraordinary short lifetimes to very long ones) was observed for the composite coatings. They concluded that nanoparticles have a high potential to improve the lifetime. However, the concentration, size, stability, and distribution of particles are key factors that determine the general lifetime.

2.5.2. Ag top-coats

Ag is known for its good corrosion resistance, high electrical conductivity, esthetical appearance, and immunity to fretting corrosion. It is extensively considered as an economical alternative to Au-top coats. However, Ni and Ag cannot form bonds [230] and thus deposition of a smooth, compact, and adhesive Ag layer on Ni is highly challenging. Ag also suffers from its softness (hence low wear resistance) and getting tarnished. As a result, a thick Ag coating (> 3 µm) is usually necessary for satisfying properties. The tarnished film that usually forms in sulfite environment is very soft and can be easily broken by the contact force. Even though this film can in some extent transfer the electrical current, its brown color suggests a change in the surface and thus it is often considered a failure [223,231–233].

Ag is traditionally deposited from cyanide baths. Numerous studies are dedicated to finding more environment-friendly non-cyanide baths for Ag deposition. Thiosulfate bath was reported to form smooth, compact and thick silver deposits. However, its low stability made it impractical for commercial uses. The obtained Ag films had also a low tarnishing resistance.

Another approach is to introduce complexing agents to non-cyanide stable baths. Uracil, ammonia, and thiourea are some proposed examples. Liu *et al.* [233] used quantum chemical calculations and molecular dynamic (MD) simulations to investigate different complexing agents. It was found that 5,5-dimethylhydantoin (DMH) and nicotinic acid (NA) are promising agents for Ag deposits. Mirror bright Ag deposits with excellent leveling capability, smooth and compact morphologies, high purity, high conductivity, high weldability, and hardness were formed. Moreover, the solution was reported to be stable up to at least one year. Such properties are promising to replace the commonly used cyanide baths.

Ag tends to electrodeposit in a highly dendritic way. However, the formation of smooth, homogeneous, finer-grained Ag deposits was reported with thiourea. TU moves the reduction potential of Ag closer to other transition metals (deposition of Ag alloys) and makes it possible to deposit Ag from a more environment-friendly electrolyte. A dendritic structure will form at high current densities, and thus the electrodeposition should be done at low current densities [234].

Electrodeposition of Ag from ILs is another alternative. Ispas *et al.* [235] obtained proper Ag deposits from 1-ethyl-3 methylimidazolium trifluoromethanesulfonate ([EMIm][TfO]) bath. The microstructure and morphology of deposits could be controlled by parameters like the temperature and ion concentration. Sebastian *et al.* [7] investigated the differences between Ag deposits obtained from DES and aqueous baths. An elevated temperature (70ºC) was necessary for plating Ag from DES due to its low conductivity and high viscosity (increasing temperature slightly decreases the viscosity and enhances the conductivity up to 10 times). A higher concentration of Ag was needed in deep eutectic solvents (0.02 M) than aqueous (0.001 M) baths to deposit Ag.

Shanthi *et al.* [236] studied the effect of pulse plating on Ag films. The highest quality was obtained by using a low peak current density (3 Adm^{-2}) and a high duty cycle (60%). Increasing the frequency from 10 to 100 Hz decreased the thickness and current efficiency but increased the hardness of deposits.

Alloying Ag with hard metals, similar to Au, could improve its hardness and thus enhance its wear resistance. However, Ag is incapable to form solid solutions with hard metals, particularly Ni, that confines this option. Ag-Ni deposits with low Ni content have a bright and smooth appearance. However, increasing the Ni concentration roughen and blacken the surface. This was attributed to the diffusion limited conditions for Ag reduction. The Ni inside the deposit increased with increasing the deposition time (and thus thickening the layer). The incorporation of Ni inside Ag seemed to happen due to kinetic trapping of Ni within the growing Ag; however, this process highly depends on the Ni:Ag ions ratio in the electrolyte [18].

Composite films could be considered the best solution to the softness of Ag deposits. WC and graphene were simultaneously used, as the reinforcing phase and lubricating particles, to improve the wear resistance of Ag films. The composite coatings had a lower friction coefficient but a rougher surface, a porous structure, and a dendritic morphology. The finer grains with similar morphology, however, were obtained by the addition of sole WC particles [237]. The co-deposition of fine diamond particles also highly improved the wear resistance of Ag films [232].

2.5.3. Other top-coats

Sn is extensively used as an inexpensive passive top-coat. Sn has a slow growth of oxide layer that remains thin and can be mechanically broken by a low contact force. Their thickness, however, should be kept low, because of their ductility not their cost. It is not as effective as

Au or Ag; Sn has comparably a low lifetime in intense environments. Hence, Sn should be reserved only for applications where a severe corrosive media is absent [223].

Iridium (Ir) is mainly famous due to its biological and medical applications. However, its good electrical conductivity, high hardness, and proper corrosion resistance could make it a suitable candidate for electrical contacts. Unfortunately, no commercial electrolyte has been developed for its deposition. In an attempt to electrodeposit Ir, Nather *et al*. [238] investigated different electrolytes and deposition parameters. They found out that Ir could be deposited only from its tetravalent state at high temperatures and low pH values. They have successfully deposited crack-free, adherent and bright layers up to 2µm of Ir and IrNi films with a hardness of 600 HV and 900 HV, respectively, from a hexabromoiridate electrolyte. Such characteristics are promising enough to consider Ir layers as a proper top-coat in electrical contacts.

Palladium (Pd) is another interesting metal that could be considered as an economical alternative top-coat. Pd is not normally prone to corrosion but could be subjected to fretting corrosion. PdNi alloys are common protective coatings for conductive surfaces due to their proper wear resistance. However, their brittleness could lead to the formation of cracks, which affects the corrosion resistance [223]. Meyyappan *et al*. [239] investigated an alternative Ni-Pd-Au multi-layer coating with an 85% reduction in Au thickness. They found out that Pd layer acted as a barrier against diffusion of Ni and Cu into Au and thus improved the corrosion resistance and lifetime.

2.6. Post-treatment processes

Passivation can improve the lifetime of electronic contacts. A passive layer can be formed by oxidizing the surface of the metal itself or through the assembly of a non-reactive layer. Self-organized nano-particles or self-assembled monolayers (called SAM) can be used to passivate

the electrical contacts. SAMs can decrease the porosity density of the top layer and thus improve the corrosion resistance. A huge decrease in the porosity index of an Au layer with 0.4 µm thickness was reported by employing AUTRONEX^{TM} Nano 104S [223]. A more stable SAM forms on the pores of the gold nano-porous layer rather than the flat parts. The size of pores was found to be irrelevant on the obtained properties [240]. This could be especially interesting for electrical contacts. However, the electrical conductivity of nanoporous gold layers decreased up to 22% when SAMs were applied [241]. The successful use of SAMs as anti-tarnishing agent for Ag deposits has been also reported. It was found that the modified Ag coatings present a better wear resistance, a more stable contact resistance during their lifetime, and a higher corrosion resistance [242].

SAMs are bi-functional or multi-functional molecules that have two (or more) termination groups with dissimilar functionality (Figure 2- 4). While one end of such molecules attach to the surface, the other one provides a specific functionality. The part of SAMs that will be attached to the metal surface is called the head group. The head group is a ligand (like thiols, silanes, and phosphonates) with a specific affinity for a surface and forms a chemical bond with it. The tail group attaches the head group to the functional end. The organization of the tail group occurs slowly after the chemisorption of the head group. An ordered 2D “lying down phase” forms at first stages that will be transmitted to a 3D crystalline or semicrystalline structure over periods of minutes or hours [243]. Thiol compounds are the most used materials as SAMs [244], and a more homogeneous film of them was reported to be formed from an organic phase rather than an aqueous one [245].

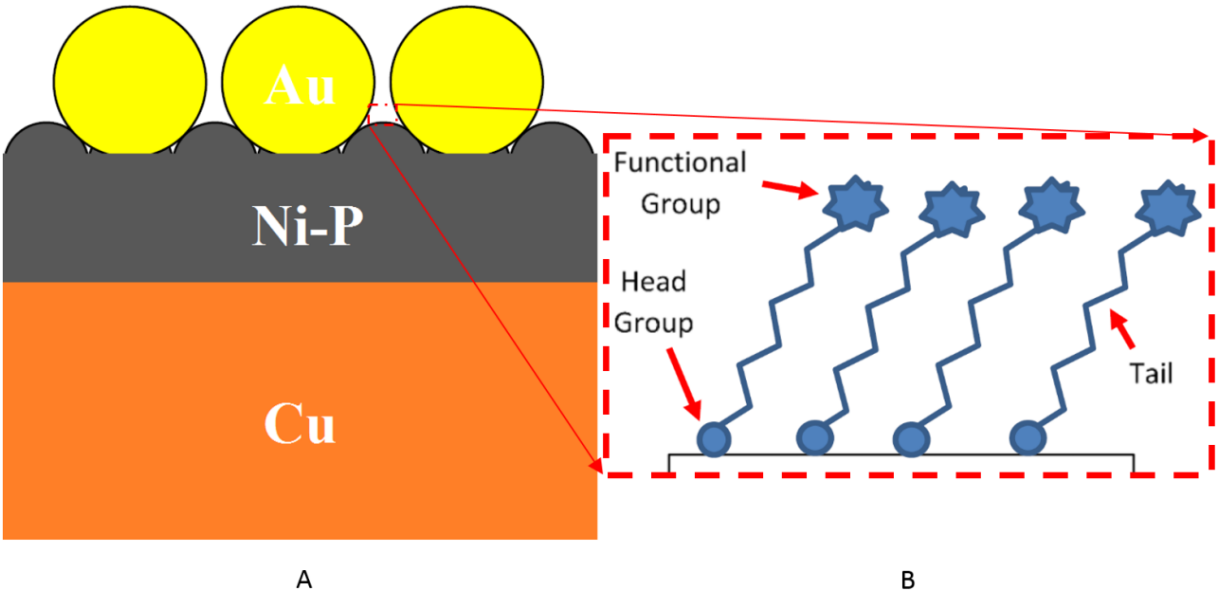

Figure 2- 4. Schematic presentation of a Cu/Ni-P/Au system (A), and its modification with a SAM structure [243].

These molecules can be applied to metals through different methods, like ultrasonic assisted immersion, photocatalytic, electrochemical or gas phase evaporation. They form a thin layer on their surface that enhances the corrosion and wear resistance by filling the pores [223]. Forming SAMs by immersing the gold-coated samples inside their bath is simple and efficient. However, it requires almost high concentrations of SAMs (>1 mM) that is not cost effective. It also suffers from reproducibility issues. The electro-assisted method, however, found to be able to form reproducible densely packed SAMs in micromolar range concentrations [246].

Employing polymers is a well-known strategy to enhance the corrosion resistance [247–250]. Surface anomalies and irregularities, such as pores or surface roughness, have a different surface energy and thus they can act as polymerization centers [251,252]. It was found that pores have a strong free-energy minimum. The monomer, therefore, can be adsorbed (partially or completely) inside the pore and polymerize there [253]. Moreover, pores provide a confined place and thus facilitate the combination of the monomer molecules [254]. As a result, it is theoretically possible to fill the pores of thin Au top-coats with polymers. However, most organic coatings suffer from a poor adhesion to their metallic substrate. Poly(methyl

methacrylate) or PMMA, on the other hand, can be strongly chemisorbed (electrografted) on metals due to its carbonyl functionality [255,256]. PMMA is a transparent colorless polymer with a light weight, and high corrosion and chemical resistance [257]. Interestingly, it is possible to etch PMMA using UV [258–260] to remove the possible polymeric growth outside the pores that partially covers the gold surface and thus increases the electrical resistivity. As a result, PMMA seems to be a potential candidate to improve the corrosion behavior of electrical contacts.

Electropolymerization is a simple economical technique that initiates, controls, and terminates the polymerization by the electron transfer [261]. The cathodic electropolymerization of MMA can then be employed to avoid the oxidation of the metallic electrode during the process [256]. A good solvent for electropolymerization should be able to dissolve the monomer and supporting salt in order to provide sufficient conductivity. DMSO is reported to be an excellent solvent for MMA [261].

As a result, the application of a post treatment technique remarkably decreases the optimized thickness of noble top-coats by modifying their porosity content and thus bring many economic and ecologic benefits.

Summary

Cu/Ni/Au multi-layer films are commonly used in electronics and microelectronics to serve as electrical contacts, due to their combination of mechanical properties, corrosion resistance, and electrical conductivity. Cu is the most used material in electronics due to its relatively low price and exceptional electrical conductivity. The low corrosion resistance of Cu, however, requires to apply protective coatings. Noble metal films, such as Au, Ag, Pd, present a combination of high electrical conductivity and corrosion resistance. Therefore, they are extensively employed

in electronics to serve as electric contacts. The desirable properties of noble metals will be deteriorated if Cu diffuses into them. As a result, Ni films are applied as a diffusion barrier. The applied noble top-coat is thin (and thus porous), because of its price. The pores are the biggest disadvantage of these systems. They worsen the corrosion behavior by imposing a galvanic corrosion and a rapid dissolution of the under-layer. Therefore, the properties of the Ni barrier layer and the noble top-coat mainly determine the lifetime of Cu/Ni/Au films.

Ni films with superior properties can be obtained by pulse deposition, specifically in a DES bath. However, Ni alloys or Ni composite films are more practical to meet the requirements of a good barrier. Two types of metals can be added into the deposition bath to form Ni alloys. Firstly, metals that could be individually deposited, i.e. metals such as Cu, Co, Sn, Zn. Secondly, elements that can only be co-deposited, i.e. refractory metals, B, and P. The first group presents promising improvements in corrosion and mechanical behavior, except for Ni alloys with more cathodic elements, such as Zn. However, they have crystalline structures and thus suffer from crystalline defects. Amorphous Ni alloys, i.e. the second group, are superior for barrier purposes due to their lack of crystalline defects. Ni-P films are the most promising one, since they are inexpensive and offer a combination of good mechanical and corrosion behavior as well as a low surface roughness. Further improvement of Ni-P films can be achieved by adding a small amount of Ag, or Sn, or refractory metals to their deposition electrolytes.

Ni-P films are well-known because of their amorphous structure. Although they are free of crystalline defects such as grain boundaries, their structure consists of several clusters and the cluster boundaries. These defects are prone to corrosion and diffusion. Making composites with Ni-P films, particularly with CNTs, modifies their structure and enhances their corrosion, wear, and diffusion resistance. Highly conductive particles, however, can increase the roughness of the surface and diminish the corrosion resistance by forming localized corrosion cells.

Nonetheless, the most vital parameter in forming proper composite films is the used dispersion method. Surfactants are extensively used to disperse particles in electrolytes. However, they might interact with deposition reactions and compete with metallic ions over winning electrons, specifically cationic surfactants. This fact could decrease the growth rate of films or deteriorate their properties. Anionic surfactants were found to be superior in general. SDBS and DTAB were the most promising used anionic and cationic surfactants, respectively. Meanwhile, surfactants cannot completely eliminate the agglomeration problem. They form soft agglomerated particles that can be kept in suspension by stirring the electrolyte. Sol-enhanced electroplating was recently developed, i.e. particles are added to the bath in their colloidal state. They can be expected to form composite films with superior properties.

Au and Ag are the most used noble top-coats and Ir and Pd were recently investigated as their alternatives. They are, however, very soft and suffer from low wear resistance. Alloying them with hard metals, i.e. Ni, Co, or Fe, and making composites with hard secondary phases can highly improve their hardness and wear behavior. Employing high content of alloying elements, however, diminishes the desired properties, i.e. corrosion resistance and surface roughness. Therefore, composite films are superior for electrical contacts, but the employed particles should not decrease the electrical conductivity. Al_2O_3 and TiO_2 nanoparticles were found to be the best candidates to form composite noble metal films. Moreover, well-distributed particles are the main key to improve the wear resistance of composite films. This is pointing out yet again to the importance of the used dispersion method.

Applying a post-treatment process can modify the pores of the thin noble films. They can compensate the negative effects of pores on the corrosion properties. Therefore, they can be used to assure a successful and secure performance of electrical contacts, particularly for crucial applications in severe corrosive environments.

References

[1] R. Oriňáková, A. Turoňová, D. Kladeková, M. Gálová, R.M. Smith, Journal of Applied Electrochemistry 36 (2006) 957–972.
[2] C.A. Loto, Silicon 8 (2016) 177–186.
[3] G.A. Di Bari, Modern Electroplating 5 (2000) 79–114.
[4] J. Wojciechowski, M. Baraniak, J. Pernak, G. Lota, International Journal of Electrochemical Science (2017) 3350–3360.
[5] R.A. Shakoor, R. Kahraman, U. Waware, Y. Wang, W. Gao, Materials & Design 64 (2014) 127–135.
[6] A.P. Abbott, A. Ballantyne, R.C. Harris, J.A. Juma, K.S. Ryder, G. Forrest, Electrochimica Acta 176 (2015) 718–726.
[7] P. Sebastián, E. Vallés, E. Gómez, Electrochimica Acta 112 (2013) 149–158.
[8] L.M.A. Monzon, F. Byrne, J.M.D. Coey, Journal of Electroanalytical Chemistry 657 (2011) 54–60.
[9] F.-H. Li, W. Wang, Electrochimica Acta 55 (2010) 5000–5005.
[10] S. Koussi-Daoud, A. Planchat, A. Renaud, Y. Pellegrin, F. Odobel, T. Pauporté, ChemElectroChem 4 (2017) 2618–2625.
[11] G.L. Peres, D.C. Leite, N.P. da Silveira, Starch - Stärke 68 (2016) 1129–1138.
[12] W. Le, K. Du, L. Zhang, J. Xiao, C. Zhang, Y. Zhang, L. Zhou, Q. Yin, Electrochimica Acta 95 (2013) 179–184.
[13] Y. Kawazu, H. Hoke, Y. Yamada, T. Umecky, K. Ozutsumi, T. Takamuku, Phys. Chem. Chem. Phys. 19 (2017) 31335–31344.
[14] X. Zhou, Y. Shen, Applied Surface Science 324 (2015) 677–690.
[15] V.K. Murugan, Z. Jia, G.J. Syaranamual, C.L. Gan, Y. Huang, Z. Chen, Microelectronics Reliability 60 (2016) 84–92.
[16] W. Plieth, Surface and Coatings Technology 169 (2003) 96–99.
[17] Y.D. Gamburg, G. Zangari, in: Theory and Practice of Metal Electrodeposition, Springer New York, New York, NY, 2011, pp. 205–232.
[18] D. Liang, Z. Liu, R.D. Hilty, G. Zangari, Electrochimica Acta 82 (2012) 82–89.
[19] H. Eom, B. Jeon, D. Kim, B. Yoo, Materials Transactions 51 (2010) 1842–1846.
[20] K. Santhi, S.N. Karthick, H.-J. Kim, M. Nidhin, V. Narayanan, A. Stephen, Applied Surface Science 258 (2012) 3126–3132.
[21] Y. Raghupathy, K.A. Natarajan, C. Srivastava, Materials Science and Engineering: B 206 (2016) 1–8.
[22] G. Liu, L. Yang, L. Wang, S. Wang, L. Chongyang, J. Wang, Surface and Coatings Technology 204 (2010) 3382–3386.
[23] E. Valova, J. Georgieva, S. Armyanov, I. Avramova, J. Dille, O. Kubova, M.-P. Delplancke-Ogletree, Surface and Coatings Technology 204 (2010) 2775–2781.
[24] X. Fang, H. Zhou, Y. Xue, Transactions of Nonferrous Metals Society of China 25 (2015) 2594–2600.
[25] J. Liu, X. Wang, Z. Tian, M. Yuan, X. Ma, Applied Surface Science 356 (2015) 289–293.
[26] J. Chen, Y. Zou, K. Matsuda, G. Zhao, Materials Letters 191 (2017) 214–217.
[27] S. Roy, P. Sahoo, Procedia Technology 14 (2014) 320–327.
[28] M. Cissé, M. Abouchane, T. Anik, K. Himm, R.A. Belakhmima, M. Ebn Touhami, R. Touir, A. Amiar, International Journal of Corrosion 2010 (2010) 1–9.
[29] R.M. Abdel Hameed, A.M. Fekry, Electrochimica Acta 55 (2010) 5922–5929.
[30] Y. Xu, X. Zheng, X. Hu, Y. Yin, T. Lei, Surface and Coatings Technology 258 (2014) 790–796.

[31] Q. Yu, Z. Zeng, W. Zhao, M. Li, X. Wu, Q. Xue, Colloids and Surfaces A: Physicochemical and Engineering Aspects 427 (2013) 1–6.
[32] Y. Gan, T. Zhao, Z. Kang, J. Sang, Surface and Interface Analysis 49 (2017) 190–196.
[33] Y. Li, H. Jiang, D. Wang, H. Ge, Surface and Coatings Technology 202 (2008) 4952–4956.
[34] X. Wang, B. Lv, Z. Hu, B. Xu, Physics Procedia 50 (2013) 191–198.
[35] Z. She, Q. Li, Z. Wang, C. Tan, J. Zhou, L. Li, Surface and Coatings Technology 251 (2014) 7–14.
[36] A.A. Aal, A. Shaaban, Z.A. Hamid, Applied Surface Science 254 (2008) 1966–1971.
[37] A.E. Fetohi, R.M. Abdel Hameed, K.M. El-Khatib, E.R. Souaya, International Journal of Hydrogen Energy 37 (2012) 7677–7688.
[38] K. Theeratatpong, S. Danchaivijit, Y. Boonyongmaneerat, Surface and Interface Analysis 46 (2014) 276–282.
[39] J. Vazquez-Arenas, M. Pritzker, Electrochimica Acta 66 (2012) 139–150.
[40] L. Tian, J. Xu, S. Xiao, Vacuum 86 (2011) 27–33.
[41] V.S. Kublanovsky, V.M. Nikitenko, N.I. Globa, Materials Science 52 (2017) 687–693.
[42] A.P.I. Popoola, C.A. Loto, C.O. Osifuye, V.S. Aigbodion, O.M. Popoola, Alexandria Engineering Journal 55 (2016) 2901–2908.
[43] H.Z. Wang, Y. Song, Z.X. Zhang, S.W. Yao, W.G. Zhang, Surface Engineering 29 (2013) 6–10.
[44] J. Yu, T. Jing, J. Yang, Q. Li, Journal of Materials Processing Technology 209 (2009) 14–17.
[45] H. Wang, X. Lei, S. Yao, W. Zhang, Surface Engineering (2017) 1–7.
[46] L. Anicai, A. Petica, S. Costovici, P. Prioteasa, T. Visan, Electrochimica Acta 114 (2013) 868–877.
[47] J.-H. Bae, H.-B. Kang, J. Ryu, C.-W. Yang, Surface and Interface Analysis 44 (2012) 1503–1506.
[48] W.X. Zhang, Z.H. Jiang, G.Y. Li, Q. Jiang, J.S. Lian, Surface and Coatings Technology 202 (2008) 2570–2576.
[49] J. Georgieva, S. Armyanov, Journal of Solid State Electrochemistry 11 (2007) 869–876.
[50] A. Sheibani Aghdam, S.R. Allahkaram, S. Mahdavi, Surface and Coatings Technology 281 (2015) 144–149.
[51] P. de Lima-Neto, A.N. Correia, G.P. da Silva, Journal of the Brazilian Chemical Society 17 (2006) 1419–1427.
[52] E. Valova, S. Armyanov, Russian Journal of Electrochemistry 44 (2008) 709–715.
[53] J. Kubisztal, J. Niedbała, A. Budniok, Surface and Interface Analysis 42 (2010) 1222–1225.
[54] C. Srivastava, S.K. Ghosh, S. Rajak, A.K. Sahu, R. Tewari, V. Kain, G.K. Dey, Surface and Coatings Technology 313 (2017) 8–16.
[55] S. Pouladi, M.H. Shariat, M.E. Bahrololoom, Surface and Coatings Technology 213 (2012) 33–40.
[56] G. Roventi, R. Cecchini, A. Fabrizi, T. Bellezze, Surface and Coatings Technology 276 (2015) 1–7.
[57] A.C. Hegde, K. Venkatakrishna, N. Eliaz, Surface and Coatings Technology 205 (2010) 2031–2041.
[58] V. Bachvarov, M. Peshova, S. Vitkova, N. Boshkov, Materials Chemistry and Physics 136 (2012) 999–1007.
[59] Y. Li, P. Kumar, X. Shi, T.A. Nguyen, Z. Xiao, J. Wu, International Journal of Electrochemical Science 7 (2012) 8151–8169.

[60] G.A.G. Pedroza, C.A.C. de Souza, M.D. de Jesus, L.R.P. de Andrade Lima, D.V. Ribeiro, Surface and Coatings Technology 258 (2014) 232–239.
[61] K. Chouchane, A. Levesque, O. Aaboubi, S. Crequy, N. Mesrati, J.P. Chopart, International Journal of Materials Research 106 (2015) 52–59.
[62] I. Constantin, Journal of Metallurgy 2014 (2014) 1–6.
[63] H.-Y. Zheng, M.-Z. An, Journal of Alloys and Compounds 459 (2008) 548–552.
[64] S. Ranganatha, T.V. Venkatesha, K. Vathsala, Applied Surface Science 256 (2010) 7377–7383.
[65] J. Guo, X. Guo, S. Wang, Z. Zhang, J. Dong, L. Peng, W. Ding, Applied Surface Science 365 (2016) 31–37.
[66] K.-H. Cheng, F.-J. Chen, C.-Y. Lee, C.-S. Lin, J.-T. Huang, C.-C. Lan, P.-H. Tsou, T.-I. Ho, Advances in Materials Science and Engineering (2014).
[67] A. Stephen, M.V. Ananth, V. Ravichandran, Anti-Corrosion Meth & Material 46 (1999) 117–121.
[68] F.J. He, Y.Z. Fang, S.J. Jin, Wear 311 (2014) 14–20.
[69] J.N. Balaraju, S. Millath Jahan, C. Anandan, K.S. Rajam, Surface and Coatings Technology 200 (2006) 4885–4890.
[70] X. Shu, Y. Wang, X. Lu, C. Liu, W. Gao, Surface and Coatings Technology 276 (2015) 195–201.
[71] H. Liu, F. Viejo, R.X. Guo, S. Glenday, Z. Liu, Surface and Coatings Technology 204 (2010) 1549–1555.
[72] M. Palaniappa, S.K. Seshadri, Wear 265 (2008) 735–740.
[73] W.X. Zhang, N. Huang, J.G. He, Z.H. Jiang, Q. Jiang, J.S. Lian, Applied Surface Science 253 (2007) 5116–5121.
[74] L. Elias, A. Chitharanjan Hegde, Surface and Coatings Technology 283 (2015) 61–69.
[75] H. Liu, R.X. Guo, Z. Liu, Surface and Coatings Technology 219 (2013) 31–41.
[76] K.R. Sriraman, S. Ganesh Sundara Raman, S.K. Seshadri, Materials Science and Engineering: A 460–461 (2007) 39–45.
[77] H.B. Lee, M.Y. Wu, Metallurgical and Materials Transactions A 48 (2017) 4667–4680.
[78] Y. Liao, S.T. Zhang, R. Dryfe, Materialwissenschaft Und Werkstofftechnik 42 (2011) 833–837.
[79] S. Sangeetha, G.P. Kalaignan, J.T. Anthuvan, Applied Surface Science 359 (2015) 412–419.
[80] H. Liu, P. Wang, Z. Liu, G. Harrison, G.E. Thompson, Transactions of the IMF 94 (2016) 76–85.
[81] A.E. Fetohi, R.M. Abdel Hameed, K.M. El-Khatib, Journal of Power Sources 240 (2013) 589–597.
[82] Z. Abdel Hamid, H.B. Hassan, Surface and Coatings Technology 212 (2012) 37–45.
[83] R. Mousavi, M.E. Bahrololoom, F. Deflorian, L. Ecco, Applied Surface Science 364 (2016) 9–14.
[84] H. Rashtchi, K. Raeissi, M. Shamanian, Y. Acevedo Gomez, C. Lagergren, R. Wreland Lindström, V. Rajaei, Fuel Cells 16 (2016) 784–800.
[85] D. Liu, Z. Yang, C. Zhang, Materials Science and Engineering: B 166 (2010) 67–75.
[86] N. Krstajic, V. Jovic, L. Gajickrstajic, B. Jovic, A. Antozzi, G. Martelli, International Journal of Hydrogen Energy 33 (2008) 3676–3687.
[87] A. Laszczyńska, J. Winiarski, B. Szczygieł, I. Szczygieł, Applied Surface Science 369 (2016) 224–231.
[88] E. Beltowska-Lehman, A. Bigos, P. Indyka, M. Kot, Surface and Coatings Technology 211 (2012) 67–71.

[89] I.G. Serin, A. Göksenli, B. Yüksel, R.A. Yildiz, Journal of Materials Engineering and Performance 24 (2015) 3032–3037.
[90] I.G. Serin, A. GöKsenli, Surface Review and Letters 22 (2015) 1550058.
[91] P.-C. Huang, K.-H. Hou, G.-L. Wang, M.-L. Chen, J.-R. Wang, International Journal of Electrochemical Science 10 (2015) 4972–4984.
[92] Y.-H. Chou, Y. Sung, Y.-M. Liu, N.-W. Pu, M.D. Ger, Surface and Coatings Technology 203 (2009) 1020–1026.
[93] O.R. Monteiro, S. Murugesan, V. Khabashesku, Surface and Coatings Technology 272 (2015) 291–297.
[94] F. Madah, A.A. Amadeh, C. Dehghanian, Journal of Alloys and Compounds 658 (2016) 272–279.
[95] V. Niksefat, M. Ghorbani, Journal of Alloys and Compounds 633 (2015) 127–136.
[96] S. Eraslan, M. Ürgen, Surface and Coatings Technology 265 (2015) 46–52.
[97] Y. Wang, S.-J. Wang, X. Shu, W. Gao, W. Lu, B. Yan, Journal of Alloys and Compounds 617 (2014) 472–478.
[98] E. Ünal, I.H. Karahan, Surface and Coatings Technology 333 (2018) 125–137.
[99] Y. Liang, Y.-S. Li, Q.-Y. Yu, Y.-X. Zhang, W. Zhao, Z.-X. Zeng, Surface and Coatings Technology 264 (2015) 80–86.
[100] Z.H. Fang, CAS OpenIR (1997).
[101] G. Zhao, Y. Zou, H. Zhang, Z. Zou, Materials Letters 132 (2014) 221–223.
[102] W. Wang, W. Zhang, Y. Wang, N. Mitsuzak, Z. Chen, Applied Surface Science 367 (2016) 528–532.
[103] J.-D. Lin, C.-T. Chou, Surface and Coatings Technology 325 (2017) 360–369.
[104] H. Liu, Z. Liu, Surface and Coatings Technology 330 (2017) 270–276.
[105] J.M. Lee, K.M. Bae, K.K. Jung, J.H. Jeong, J.S. Ko, Applied Surface Science 289 (2014) 14–20.
[106] K. Ignatova, S. Kozhukharov, L. Vladimirov, M. Milanes, НАУЧНИ ТРУДОВЕ НА РУСЕНСКИЯ УНИВЕРСИТЕТ 54 (2015) 81–85.
[107] E. Pellicer, S. Pané, K.M. Sivaraman, O. Ergeneman, S. Suriñach, M.D. Baró, B.J. Nelson, J. Sort, Materials Chemistry and Physics 130 (2011) 1380–1386.
[108] L. Leyssens, B. Vinck, C. Van Der Straeten, F. Wuyts, L. Maes, Toxicology 387 (2017) 43–56.
[109] Y. He, S.C. Wang, F.C. Walsh, Y.-L. Chiu, P.A.S. Reed, Surface and Coatings Technology 307 (2016) 926–934.
[110] P. Møller, J.B. Rasmussen, S. Köhler, NASF SURFACE TECHNOLOGY WHITE PAPERS 78 (2013) 15–24.
[111] U. Lačnjevac, B.M. Jović, V.D. Jović, Journal of The Electrochemical Society 159 (2012) D310.
[112] L. Anicai, A. Petica, S. Costovici, P. Prioteasa, T. Visan, Electrochimica Acta 114 (2013) 868–877.
[113] In: Kirk-Othmer Encyclopedia of Chemical Technology, John Wiley & Sons, Inc., 2000.
[114] S. Shetty, A.C. Hegde, Materials Science Forum 830–831 (2015) 655–658.
[115] E. Rudnik, Journal of Electroanalytical Chemistry 726 (2014) 97–106.
[116] R.F. Shekhanov, S.N. Gridchin, A.V. Balmasov, Surface Engineering and Applied Electrochemistry 52 (2016) 152–156.
[117] Y. Zhu, X. Zhang, J. Song, W. Wang, F. Yue, Q. Ma, Applied Catalysis A: General 500 (2015) 51–57.
[118] Q. Li, H. Lu, J. Cui, M. An, D.Y. Li, Surface and Coatings Technology 324 (2017) 146–152.

[119] R. Giovanardi, G. Orlando, Surface and Coatings Technology 205 (2011) 3947–3955.
[120] W. Jin, K. Yan, RSC Adv. 5 (2015) 37440–37450.
[121] W. Jin, H. Du, S. Zheng, Y. Zhang, Electrochimica Acta 191 (2016) 1044–1055.
[122] M. Moniruzzaman, M.M. Rakib, F.T. Matin, International Journal of Automotive and Mechanical Engineering 6 (2012) 692–700.
[123] C.L. Siu, H.C. Man, C.H. Yeung, Surface and Coatings Technology 200 (2005) 2223–2227.
[124] G.-F. Huang, W.-Q. Huang, L.-L. Wang, B.-S. Zou, D.-P. Chen, D.-Y. Li, J.-M. Wei, J.-H. Zhang, Int. J. Electrochem. Sci 2 (2007) 321–328.
[125] J.W. Choi, G.H. Hwang, W.K. Han, S.G. Kang, Applied Surface Science 253 (2006) 2171–2178.
[126] A.R. Madram, H. Pourfarzad, H.R. Zare, Electrochimica Acta 85 (2012) 263–267.
[127] M.S. Nur Ariffah, M.S. Nurulakmal, A.S. Anasyida, E.K. Shiu, Materials Science Forum 819 (2015) 97–102.
[128] L. Chang, C.-H. Chen, H. Fang, Journal of The Electrochemical Society 155 (2008) D57.
[129] A.M. Pillai, A. Rajendra, A.K. Sharma, Journal of Coatings Technology and Research 9 (2012) 785–797.
[130] Y.E. Sknar, O.O. Savchuk, I.V. Sknar, Applied Surface Science 423 (2017) 340–348.
[131] G. Liu, Z. Huang, L. Wang, W. Sun, S. Wang, X. Deng, Surface and Coatings Technology 222 (2013) 25–30.
[132] L. Bonou, M. Eyraud, R. Denoyel, Y. Massiani, Electrochimica Acta 47 (2002) 4139–4148.
[133] R. Oriňáková, A. Turoňová, D. Kladeková, M. Gálová, R.M. Smith, Journal of Applied Electrochemistry 36 (2006) 957–972.
[134] Z.H. Fang, CAS OpenIR (1997).
[135] G.A. Di Bari, in: Modern Electroplating, John Wiley & Sons, Inc., 2010, pp. 79–114.
[136] C.D. Grill, I. Pötzelberger, J.P. Kollender, A.W. Hassel, Physica Status Solidi (A) 213 (2016) 1417–1426.
[137] İ.H. Karahan, The Scientific World Journal 2013 (2013) 1–7.
[138] Y. Li, H. Jiang, D. Wang, H. Ge, Surface and Coatings Technology 202 (2008) 4952–4956.
[139] S.T. Aruna, P.G. Lashmi, H.M. Seema, RSC Adv. 6 (2016) 11185–11192.
[140] X.-C. Wang, W.-B. Cai, W.-J. Wang, H.-T. Liu, Z.-Z. Yu, Surface and Coatings Technology 168 (2003) 300–306.
[141] G. Liu, Z. Huang, L. Wang, W. Sun, S. Wang, X. Deng, Surface and Coatings Technology 222 (2013) 25–30.
[142] V.K. Murugan, Z. Jia, G.J. Syaranamual, C.L. Gan, Y. Huang, Z. Chen, Surface and Coatings Technology 300 (2016) 95–103.
[143] C. Ma, X. Guo, J. Leang, F. Xia, Ceramics International 42 (2016) 10428–10432.
[144] S.H. Hashemi, R. Shoja-Razavi, Optics & Laser Technology 85 (2016) 1–6.
[145] J.N. Balaraju, K.S. Rajam, Surface and Coatings Technology 195 (2005) 154–161.
[146] F. Kılıç, H. Gül, S. Aslan, A. Alp, H. Akbulut, Colloids and Surfaces A: Physicochemical and Engineering Aspects 419 (2013) 53–60.
[147] S. Afroukhteh, C. Dehghanian, M. Emamy, Applied Surface Science 258 (2012) 2597–2601.
[148] S. Alirezaei, S.M. Monirvaghefi, A. Saatchi, M. Ürgen, K. Kazmanlı, Tribology International 62 (2013) 110–116.
[149] X. Hu, S. Xu, Y. Yang, Z. Chen, Y.C. Chan, Materials Science and Engineering: A 600 (2014) 67–75.

[150] S. Alirezaei, S.M.M. Vaghefi, M. Ürgen, A. Saatchi, K. Kazmanli, Applied Surface Science 261 (2012) 155–158.
[151] H. Ma, F. Tian, D. Li, Q. Guo, Journal of Alloys and Compounds 474 (2009) 264–267.
[152] L. Elias, A.C. Hegde, Electrochimica Acta 219 (2016) 377–385.
[153] X. Cui, W. Wei, H. Liu, W. Chen, Electrochimica Acta 54 (2008) 415–420.
[154] M. Adabi, A.A. Amadeh, Transactions of Nonferrous Metals Society of China 24 (2014) 3189–3195.
[155] S.L. Tay, C. Yao, X. Wei, W. Chen, W. Gao, Surface and Coatings Technology 260 (2014) 279–283.
[156] Y. Zhao, C. Jiang, Z. Xu, F. Cai, Z. Zhang, P. Fu, Materials & Design 85 (2015) 39–46.
[157] P. Gadhari, P. Sahoo, Silicon 9 (2017) 761–774.
[158] S.W. Jiang, L. Yang, J.N. Pang, H. Lin, Z.Q. Wang, Surface and Coatings Technology 286 (2016) 197–205.
[159] Y. Chen, Y. Hao, W. Huang, Y. Ji, W. Yang, X. Yin, Y. Liu, X. Ling, Surface and Coatings Technology 310 (2017) 122–128.
[160] A.R. Rahimi, H. Modarress, S. Amjad Iranagh, Surface Engineering 27 (2011) 26–31.
[161] S. Karthikeyan, B. Ramamoorthy, Applied Surface Science 307 (2014) 654–660.
[162] P. Makkar, R.C. Agarwala, V. Agarwala, Journal of Materials Science 50 (2015) 2813–2823.
[163] Y. Wang, W. Chen, A. Shakoor, R. Kahraman, W. Lu, B. Yan, W. Gao, Int. J. Electrochem. Sci 9 (2014) 4384–4393.
[164] C.-K. Lee, Int. J. Electrochem. Sci 7 (2012) 12941–12954.
[165] M.A. Shoeib, M.M. Kamel, S.M. Rashwan, O.M. Hafez, Surface and Interface Analysis 47 (2015) 672–680.
[166] T.R. Tamilarasan, R. Rajendran, G. Rajagopal, J. Sudagar, Surface and Coatings Technology 276 (2015) 320–326.
[167] X. Wu, J. Mao, Z. Zhang, Y. Che, Surface and Coatings Technology 270 (2015) 170–174.
[168] I. Subakova, I. Petukhov, N. Medvedeva, Materials & Manufacturing Processes 30 (2015) 766–770.
[169] P. Makkar, R.C. Agarwala, V. Agarwala, Advanced Powder Technology 25 (2014) 1653–1660.
[170] T. Rabizadeh, S.R. Allahkaram, Materials & Design 32 (2011) 133–138.
[171] A. Sadeghzadeh-Attar, G. AyubiKia, M. Ehteshamzadeh, Surface and Coatings Technology 307 (2016) 837–848.
[172] M. Islam, M.R. Azhar, N. Fredj, T.D. Burleigh, O.R. Oloyede, A.A. Almajid, S. Ismat Shah, Surface and Coatings Technology 261 (2015) 141–148.
[173] K. Zielińska, A. Stankiewicz, I. Szczygieł, Journal of Colloid and Interface Science 377 (2012) 362–367.
[174] X. Zhou, Y. Shen, H. Jin, Y. Zheng, Transactions of Nonferrous Metals Society of China 22 (2012) 1981–1988.
[175] I.R. Mafi, C. Dehghanian, Applied Surface Science 258 (2011) 1876–1880.
[176] J.N. Balaraju, V.E. Selvi, K.S. Rajam, Transactions of the IMF 88 (2010) 311–316.
[177] U. Matik, Surface and Coatings Technology 302 (2016) 528–534.
[178] S. Wang, X. Huang, M. Gong, W. Huang, Applied Surface Science 357 (2015) 328–332.
[179] H.B. Hassan, Z. Abdel Hamid, M. Hassan, Surface and Interface Analysis 46 (2014) 512–520.

[180] S. Afroukhteh, C. Dehghanian, M. Emamy, Progress in Natural Science: Materials International 22 (2012) 480–487.
[181] H. Luo, M. Leitch, Y. Behnamian, Y. Ma, H. Zeng, J.-L. Luo, Surface and Coatings Technology 277 (2015) 99–106.
[182] C. Zhao, Y. Yao, Journal of Materials Engineering and Performance 23 (2014) 193–197.
[183] E. Rudnik, L. Burzyńska, Ł. Dolasiński, M. Misiak, Applied Surface Science 256 (2010) 7414–7420.
[184] P. Gyftou, E.A. Pavlatou, N. Spyrellis, Applied Surface Science 254 (2008) 5910–5916.
[185] F. Bigdeli, S.R. Allahkaram, Materials & Design 30 (2009) 4450–4453.
[186] R. Soleimani, F. Mahboubi, M. Kazemi, S.Y. Arman, Surface Engineering 31 (2015) 714–721.
[187] A. Zarebidaki, S.R. Allahkaram, Micro & Nano Letters 6 (2011) 937.
[188] A. Farzaneh, M. Ehteshamzadeh, M. Can, O. Mermer, S. Okur, Protection of Metals and Physical Chemistry of Surfaces 52 (2016) 632–636.
[189] A. Farzaneh, M. Mohammadi, M. Ehteshamzadeh, F. Mohammadi, Applied Surface Science 276 (2013) 697–704.
[190] A. Zarebidaki, S.-R. Allahkaram, Surface Engineering 28 (2012) 400–405.
[191] H.-L. Wang, L.-Y. Liu, Y. Dou, W.-Z. Zhang, W.-F. Jiang, Applied Surface Science 286 (2013) 319–327.
[192] A. Araghi, M.H. Paydar, Materials & Design 31 (2010) 3095–3099.
[193] International Journal of Electrochemical Science (2016) 4352–4361.
[194] C.-I. Hsu, K.-H. Hou, M.-D. Ger, G.-L. Wang, Applied Surface Science 357 (2015) 1727–1735.
[195] M. Abdoli, A. Sabour Rouhaghdam, Diamond and Related Materials 31 (2013) 30–37.
[196] H. Mazaheri, S.R. Allahkaram, Applied Surface Science 258 (2012) 4574–4580.
[197] H. Ashassi-Sorkhabi, M. Es′haghi, Corrosion Science 77 (2013) 185–193.
[198] X.G. Hu, W.J. Cai, Y.F. Xu, J.C. Wan, X.J. Sun, Surface Engineering 25 (2009) 361–366.
[199] X. Hu, P. Jiang, J. Wan, Y. Xu, X. Sun, Journal of Coatings Technology and Research 6 (2009) 275–281.
[200] M. Mohammadi, M. Ghorbani, Journal of Coatings Technology and Research 8 (2011) 527–533.
[201] S. Karthikeyan, P.A. Jeeva, N. Arivazhagan, V. Umasankar, K.N. Srinivasan, M. Paramasivam, Procedia Engineering 64 (2013) 720–726.
[202] Z. Gao, S. Zhao, Y. Wang, X. Wang, L. Wen, Int. J. Electrochem. Sci 10 (2015) 637–648.
[203] A. Zarebidaki, S.-R. Allahkaram, Journal of Alloys and Compounds 509 (2011) 1836–1840.
[204] M. Alishahi, S.M. Monirvaghefi, A. Saatchi, S.M. Hosseini, Applied Surface Science 258 (2012) 2439–2446.
[205] Y. Suzuki, S. Arai, M. Endo, Applied Surface Science 256 (2010) 6914–6917.
[206] J. Lapinski, D. Pletcher, F.C. Walsh, Surface and Coatings Technology 205 (2011) 5205–5209.
[207] J. Wang, J. Tian, X. Liu, Y. Yin, X. Wang, Thin Solid Films 519 (2011) 5905–5911.
[208] J. Tian, X. Liu, J. Wang, X. Wang, Y. Yin, Materials Chemistry and Physics 124 (2010) 751–759.
[209] I.R. Mafi, C. Dehghanian, Applied Surface Science 257 (2011) 8653–8658.

[210] H.-H. Sheu, S.-Y. Jian, M.-H. Lin, C.-I. Hsu, K.-H. Hou, M.-D. Ger, International Journal of Electrochemical Science (2017) 5464–5482.
[211] R.G. Wang, H. Sawada, M. Kido, Materials Science Forum 654–656 (2010) 2767–2770.
[212] Y. Lu, Applied Surface Science 256 (2010) 3554–3558.
[213] F. Touyeras, J.-Y. Hihn, M.-L. Doche, X. Roizard, Ultrasonics Sonochemistry 8 (2001) 285–290.
[214] N.H. Ince, G. Tezcanli, R.K. Belen, I.G. Apikyan, Applied Catalysis B: Environmental 29 (2001) 167–176.
[215] T.R. Tamilarasan, R. Rajendran, M. Siva shankar, U. Sanjith, G. Rajagopal, J. Sudagar, Wear 346–347 (2016) 148–157.
[216] D. Liu, Y. Yan, K. Lee, J. Yu, Materials and Corrosion 60 (2009) 690–694.
[217] F. El-Taib Heakal, M.A. Maanoum, International Journal of Electrochemical Science (2016) 7198–7215.
[218] Y.-H. You, C.-D. Gu, X.-L. Wang, J.-P. Tu, Int. J. Electrochem. Sci 7 (2012) 12440–12455.
[219] S. Dimitrijević, M. Rajčić-Vujasinović, S. Alagić, V. Grekulović, V. Trujić, Electrochimica Acta 104 (2013) 330–336.
[220] L.M.A. Monzon, F. Byrne, J.M.D. Coey, Journal of Electroanalytical Chemistry 657 (2011) 54–60.
[221] L. Sus, Y. Okhremchuk, I. Saldan, O. Kuntyi, O. Reshetnyak, S. Korniy, Materials Letters 139 (2015) 296–299.
[222] Z. Liu, M. Zheng, R.D. Hilty, A.C. West, Journal of The Electrochemical Society 157 (2010) D411.
[223] J. Song, L. Wang, A. Zibart, C. Koch, Metals 2 (2012) 450–477.
[224] Z. Liu, A.C. West, Electrochimica Acta 56 (2011) 3328–3333.
[225] C.-Y. Chen, M. Yoshiba, T. Nagoshi, T.-F.M. Chang, D. Yamane, K. Machida, K. Masu, M. Sone, Electrochemistry Communications 67 (2016) 51–54.
[226] Z. Liu, M. Zheng, R.D. Hilty, A.C. West, Electrochimica Acta 56 (2011) 2546–2551.
[227] J. Song, C. Koch, L. Wang, Advances in Tribology 2012 (2012) 1–9.
[228] S.-Y. Tsai, C.-H. Lin, Y.-J. Jian, K.-H. Hou, M.-D. Ger, Surface and Coatings Technology 313 (2017) 151–157.
[229] Y. Wang, Y. Ju, S. Wei, W. Lu, B. Yan, W. Gao, Materials Characterization 102 (2015) 189–194.
[230] N. Okamoto, F. Wang, T. Watanabe, MATERIALS TRANSACTIONS 45 (2004) 3330–3333.
[231] J. Song, V. Schinow, Wear 330–331 (2015) 400–405.
[232] V.I. Rigou, G. Marginean, D. Frunzăverde, C.V. Câmpian, Wear 290–291 (2012) 61–65.
[233] A. Liu, X. Ren, B. Wang, J. Zhang, P. Yang, J. Zhang, M. An, RSC Adv. 4 (2014) 40930–40940.
[234] A. Kola, X. Geng, E.J. Podlaha, Journal of Electroanalytical Chemistry 761 (2016) 125–130.
[235] A. Ispas, M. Pölleth, K.H.T. Ba, A. Bund, J. Janek, Electrochimica Acta 56 (2011) 10332–10339.
[236] C. Shanthi, S. Barathan, R. Jaiswal, R.M. Arunachalam, S. Mohan, Materials Letters 62 (2008) 4519–4521.
[237] M. Uysal, H. Akbulut, M. Tokur, H. Algül, T. Çetinkaya, Journal of Alloys and Compounds 654 (2016) 185–195.

[238] J. Näther, F. Köster, R. Freudenberger, C. Schöberl, T. Lampke, IOP Conference Series: Materials Science and Engineering 181 (2017) 012041.
[239] K. Meyyappan, G. Murtagian, A. Kurella, B. Pathangey, A. McAllister, S. Parupalli, IEEE Transactions on Device and Materials Reliability 14 (2014) 869–877.
[240] D.A. Patel, A.M. Weller, R.B. Chevalier, C.A. Karos, E.C. Landis, Applied Surface Science 387 (2016) 503–512.
[241] M. Hakamada, N. Kato, M. Mabuchi, Applied Surface Science 387 (2016) 1088–1092.
[228] S. Nineva, S. Berger, F. Talgner, Jahrbuch Oberflächentechnik 72 (2016) 52-59.
[243] Z.H. Huang, Y.J. Zhou, W. He, Surface and Coatings Technology 320 (2017) 126–131.
[244] V. Vasumathi, M.N.D.S. Cordeiro, Chemical Physics Letters 600 (2014) 79–86.
[245] H. Tian, L. Qi, D. Xiang, H. Shao, H.-Z. Yu, Electrochimica Acta 170 (2015) 369–375.
[246] D. Capitao, B. Limoges, C. Fave, B. Schöllhorn, Electrochimica Acta 257 (2017) 165–171.
[247] A.M. Fenelon, C.B. Breslin, Corrosion Science 45 (2003) 2837–2850.
[248] D. Kowalski, M. Ueda, T. Ohtsuka, Corrosion Science 50 (2008) 286–291.
[249] Z. Grubač, I.Š. Rončević, M. Metikoš-Huković, Corrosion Science 102 (2016) 310–316.
[250] İ. Çakmakcı, B. Duran, M. Duran, G. Bereket, Corrosion Science 69 (2013) 252–261.
[251] A. Baumgärtner, M. Muthukumar, The Journal of Chemical Physics 94 (1991) 4062–4070.
[252] J.F. Douglas, Macromolecules 22 (1989) 3707–3716.
[253] G.F. Hermsen, N.F.A. van der Vegt, M. Wessling, Soft Materials 1 (2003) 295–312.
[254] G. Pistoia, O. Bagnarelli, M. Maiocco, Journal of Applied Electrochemistry 9 (1979) 343–349.
[255] N. Baute, L. Martinot, R. Jérôme, Journal of Electroanalytical Chemistry 472 (1999) 83–90.
[256] S.L. Cram, G.M. Spinks, G.G. Wallace, H.R. Brown, Journal of Applied Polymer Science 87 (2003) 765–773.
[257] G. Lu, Y.-M. Li, C.-H. Lu, Z.-Z. Xu, Colloid and Polymer Science 288 (2010) 1445–1455.
[258] B. Braren, D. Seeger, Journal of Polymer Science Part C: Polymer Letters 24 (1986) 371–376.
[259] R.W. Johnstone, I.G. Foulds, M. Parameswaran, Journal of Vacuum Science & Technology B: Microelectronics and Nanometer Structures 26 (2008) 682.
[260] N. Yufa, S. Fronk, S.B. Darling, R. Divan, W. Lopes, S.J. Sibener, Soft Matter 5 (2009) 1683.
[261] B.L. Funt, K.C. Yu, Journal of Polymer Science 62 (1962) 359–367.

Chapter 3

Experimental Procedure

This chapter is dedicated to the methods and procedures used to improve the lifetime of electrical contacts. The first part deals with the synthesis of the barrier films (Ni alloys) and noble top-coats, and post-treatments on electrical contacts. The second part focuses on the methods used to characterize the obtained samples. Note that the chemical products used are introduced in the respective parts in the next chapter (results and discussions); all of them are provided by Sigma-Aldrich at high purity.

3.1. Coating and synthesis

3.1.1. Electrochemical deposition

Electrochemical deposition is a popular method to obtain thin films. Simplicity, opportunity to work generally at ambient temperature, uniform, and controllable deposition rate, ability to coat large surfaces in almost any shape and geometry, low cost, and the possibility to form multilayers, alloys and composites are some of the known advantages of electrochemical deposition [1–5]. Figure 3- 1 depicts the elements that can be electrochemically deposited.

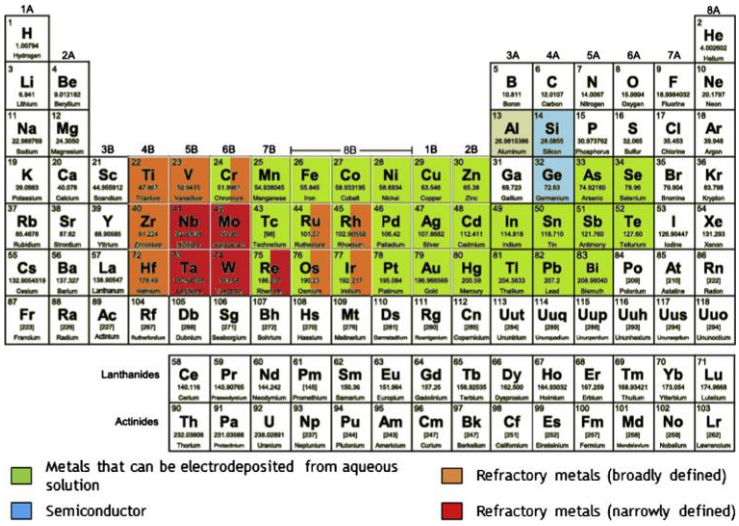

Figure 3- 1. The periodic table of elements that can be electrodeposited [6].

Electroless deposition (EL) and electrodeposition (ED) methods are two major coating preparation methods. Their difference comes from the source of the electron transfer, an external power source or a reducing agent in the bath are providing the required electrons in ED and EL (Figure 3- 2), respectively [6]. The EL method offers a more uniform thickness, higher hardness, and better barrier properties. However, it suffers from disadvantages like a restricted choice of elements (namely only the nobler metal a Co, Ni, Cu, Pd, Ag, Pt and Au), an expensive electrolyte, huge electrolyte waste due to the weak stability of the baths, high working temperature, and low deposition rate (10 µm/h). ED, on the other hand, is able to deposit thick coatings in a relatively short time. ED offers also lower porosity, higher purity, larger production rate, and easier and more controllable procedure. ED also decreases the costs of the process by reducing the waste of electrolyte. Furthermore, ED does not need an after cleaning procedure and its electrolyte is more stable due to the lack of reducing agents. As a result, ED is usually the preferred method even though EL is also used extensively [7–10].

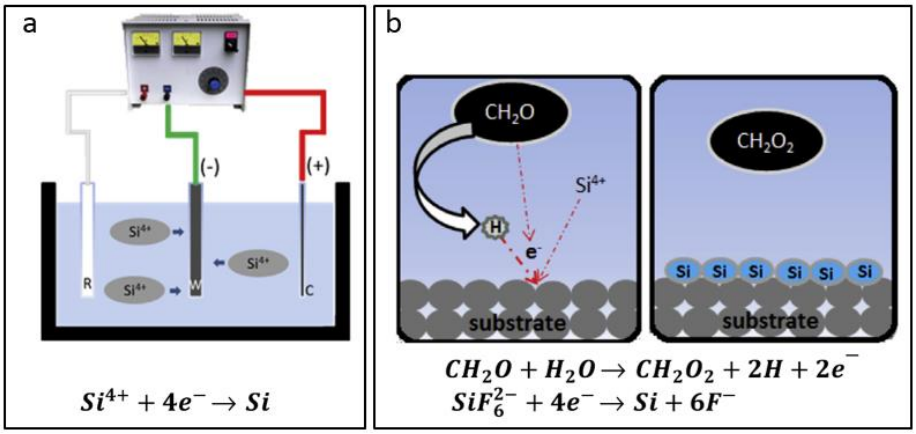

Figure 3- 2. Electrochemical deposition methods: (a) Electrodeposition, and (b) Electroless deposition [6].

Potentiostatic and galvanostatic methods are two types of ED. The potentiostatic technique is favored when a precise composition is needed (the applied potential can be adjusted regarding the redox potential of the deposited elements). However, the deposition rate and coating thickness are easier to control in galvanostatic method [11]. Pulsed plating offers coatings with better qualities, mainly because there are more parameters, i.e. duty cycle, pulse duration, and

pulse current, which can be modified [12]. For the same reason, however, pulsed deposition is more expensive than simple DC techniques. In this thesis, potentiostatic ED was used to form the metallic films (Ni barriers and noble metal top-coats).

3.1.2. Electropolymerization as the post-treatment method

Cyclic voltammetry (CV) is a potentiodynamic electrochemical technique, where the applied potential on the working electrode is swept between two potentials at a given scan rate (in mVs^{-1}) for a definite number of cycles [13]. CV has been extensively used to form polymeric films on the surface of metals [14–18]. It is also a powerful method to determine the best potential or current windows to electrodeposit coating. In this thesis, CV was used to do the cathodic electrodeposition of MMA as a post-treatment on the industrial electrical contacts.

CV tests are carried out in a three-electrode setup containing the sample as the working electrode, a Pt plate as the counter electrode, and an Ag/AgCl (KCl saturated) reference electrode (Figure 3- 3). All the tests are conducted by a BioLogic VP300 potentiostat/galvanostat.

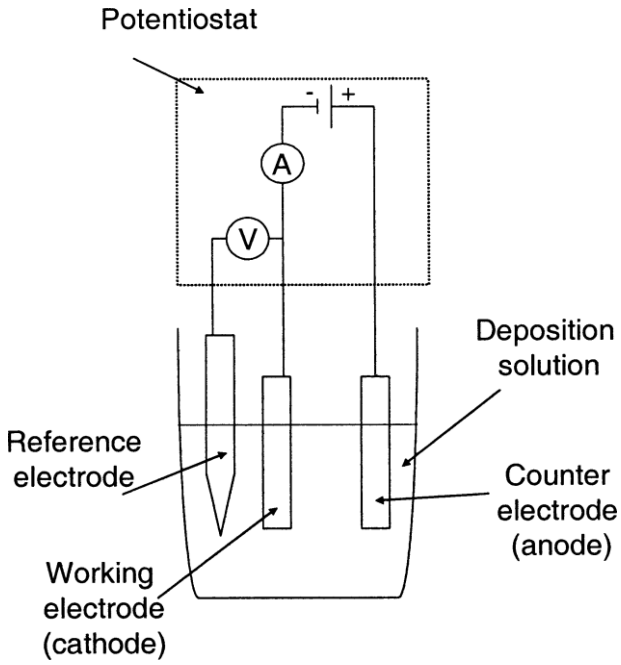

Figure 3- 3. A schematic view of the three-electrode setup used in the electrochemical tests [19].

3.2. Characterization techniques

3.2.1. Corrosion behavior

Corrosion is a determining factor regarding the lifetime of materials. There are non-electrochemical and electrochemical methods to assess the corrosion behavior. Salt spray [as a non-electrochemical test], Electrochemical Impedance Spectroscopy (EIS), and Potentiodynamic Polarization [as electrochemical tests] are used to evaluate the corrosion resistance of the synthesized samples.

3.2.1.1. Salt Spray

Salt Spray is aimed to simulate the atmospheric corrosion behavior of materials by exposing samples to a fog of salt mist in a confined chamber at a slightly elevated temperature (35 ºC) [20]. An Ascott S450 Salt Spray apparatus was employed to do the salt spray tests. The tests were carried out in accordance with the B 117 ASTM standard, where the samples were periodically exposed to a 5% NaCl fog at 35 ºC for 24 hours. The surface of the samples was evaluated after each round of the test by an optical microscope (ARISTOMET) at 100x magnification. The obtained images were analyzed by ImageJ software.

3.2.1.2. EIS

EIS is a powerful non-destructive electrochemical technique that can help to understand the reactions occurring at the interface of the materials and hence their corrosion mechanism. In EIS experiments, the current is read while a small amplitude sinusoidal potential signal is applied to the working electrode over a range of frequency. The impedance value depends on the frequency and is calculated by dividing the potential by the current as in the following equations.

$$Z(\omega) = \frac{E(\omega)}{i(\omega)} \qquad (3\text{- }1)$$

Where Z(ω) is the impedance, E(ω) is the applied AC potential ($E(\omega) = E_0\sin(\omega t)$), i(ω) is the read current ($i(\omega) = i_0\sin(\omega t + \theta)$) , and ω is the angular frequency ($\omega = 2\pi f$). Z(ω) can also be presented as:

$$Z(\omega) = Z'(\omega) + iZ''(\omega) \qquad (3\text{-}2)$$

Where Z′(ω) is called the real component of impedance; $Z'(\omega) = |Z(\omega)|\cos(\theta)$; Z″(ω) is the imaginary component of impedance; $Z''(\omega) = |Z(\omega)|\sin(\theta)$, and i is the imaginary number; $i^2 = -1$.

The EIS spectra can be presented as Nyquist and Bode plots. In Nyquist diagrams, the real impedance part; Z′(ω); is plotted on the X-axis while the imaginary part of impedance; Z″(ω); is plotted along the Y-axis. The Bode plots are presenting the impedance magnitude; $|Z(\omega)| = (Z'(\omega)^2 + Z''(\omega)^2)^{0.5}$; (i.e. Bode Z), and phase angle; $\theta = \tan^{-1}(\frac{Z''(\omega)}{Z'(\omega)})$; (i.e. Bode phase) as a function of the frequency. The experimental EIS results then can be fitted by equivalent circuits composed of electrical elements; i.e. resistors ($Z_R = R$), capacitors ($Z_C = \frac{-1}{i\omega C}$), and inductors ($Z_L = \omega L$) [21]. Note that the impedance value (|Z(ω)|) at low frequencies (e.g. 0.01 Hz) is a criteria of the corrosion resistance [22].

In this thesis, all the EIS measurements were carried out after 60 minutes of immersion in a 3% NaCl solution (as a common corrosive media to simulate the marine corrosion) at Open Circuit Potential (OCP) from 10 kHz to 10 mHz (frequency range) with 10 mV voltage amplitude (peak-to-peak).

3.2.1.3. Potentiodynamic polarization

Potentiodynamic polarization is certainly the most used electrochemical technique to evaluate the corrosion resistance of materials. In this test, the potential is swept from a more cathodic to a more anodic potential than the OCP value of the material while the current is recorded. As a

result, the behavior of the material can be assessed in cathodic and anodic branches. The Tafel extrapolation method, as it is depicted in Figure 3- 4, can be employed to obtain the corrosion current density (i_{corr}), the corrosion potential (E_{corr}), and the anodic (β_a) and cathodic (β_c) slopes from the experimental results. The extrapolated lines should be applied ± 50 mV away of E_{corr} to achieve an acceptable accuracy. However, it should be noted that the experimental results may not always present a Tafel behavior due to some factors such as the diffusion of reducing agent, the presence of multiple reducing agents, and so on. Therefore, the Tafel extrapolation method is only applicable when the experimental curves have at least one linear branch over at least one decade of current density [21].

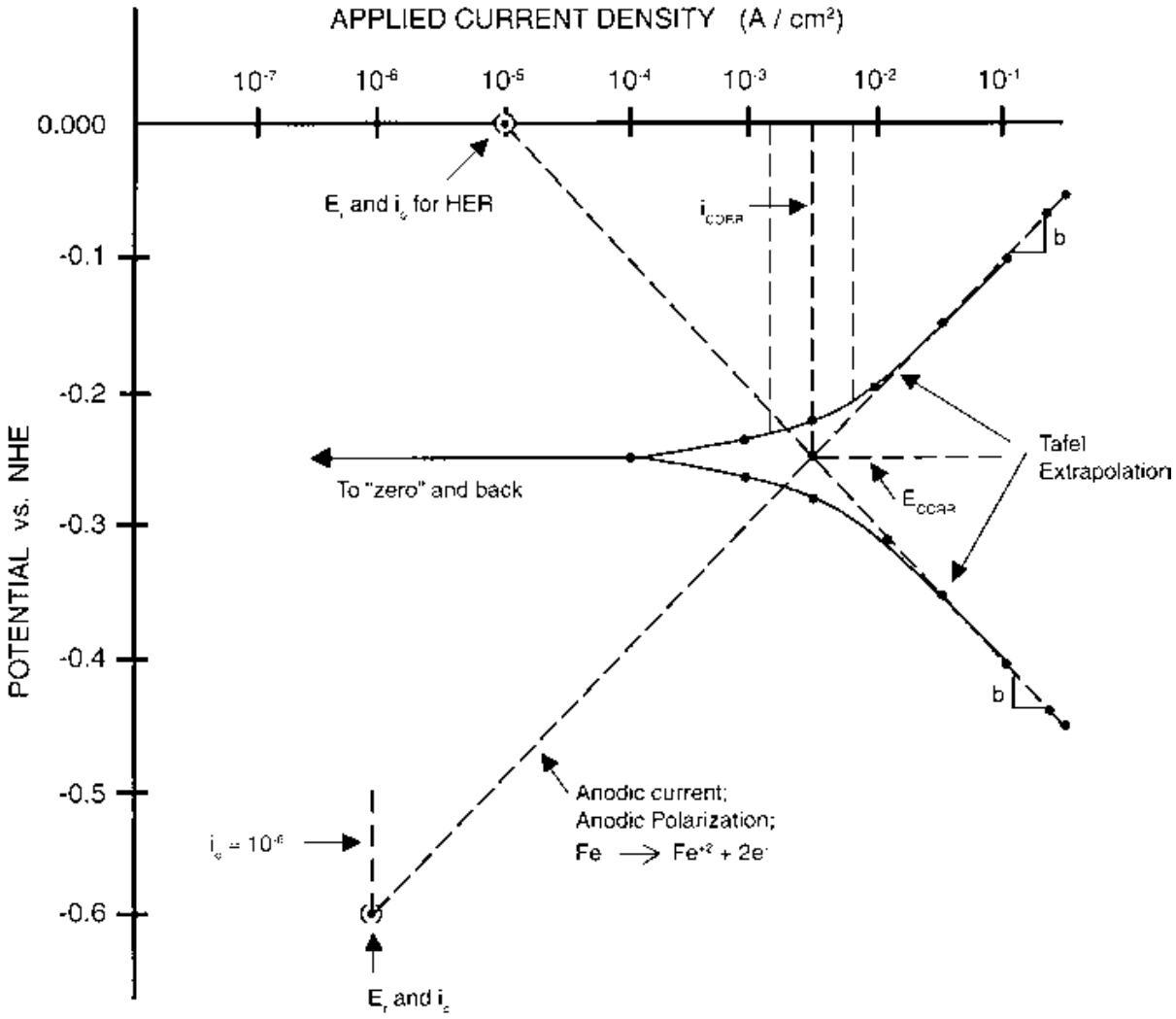

Figure 3- 4. A schematic of the potentiodynamic polarization curves of Fe and the application of the Tafel extrapolation method [21].

In this thesis, all the potentiodynamic experiments were done after an EIS test at a scan rate of 0.5 mV/s from -300 mV (vs. OCP) as the starting point to 500 mV (vs. reference electrode) as the finishing point. A similar three-electrode setup as in the deposition process (Figure 3- 3) was used to perform the electrochemical corrosion tests (that were repeated at least twice) and all the results were normalized by the exposed area to the corrosive media.

3.2.2. Morphological characterizations

The surface and cross-section morphology of the thin films affect their properties and behavior. Therefore, morphological characteristics are essential to interpret the corrosion behavior of the samples. In this thesis, Scanning Electron Microscopy (SEM) and Atomic Force Microscopy (AFM) are the used methods to determine the morphological characteristics of the synthesized samples.

3.2.2.1. SEM

SEM reveals microscopic information such as the size and shape of the objects in the sample under study. A monochromatic electron beam, ranging from 0.1 to 30 keV, emitted from an electron source, is focused by electromagnetic lenses on the surface of the sample under high vacuum. The interaction of the incident beam with the sample gives secondary electrons (SEs) that can reveal the sample morphology, and backscattered electrons (BSEs), which emerge from the sample after scattering and deflection that depends on the atomic weight and thus can be used for revealing the chemical composition. These electrons are measured by specific detectors [23].

In this thesis, two scanning electron microscopes (Philips XL 30 ESEM, and CARL ZEISS/Ultra 55) were used to study the surface and cross-section morphologies, respectively.

3.2.2.2. AFM

AFM allows to observe the surface at a nanometric scale. Observations can be done under ambient atmosphere on almost any type of materials (ceramics, polymers, metals, powders, and so on). In AFM, a sharp probe sweeps the surface and builds up a 2-D map of the height of the sample's surface which can be converted to a 3-D image (Figure 3- 5) [24].

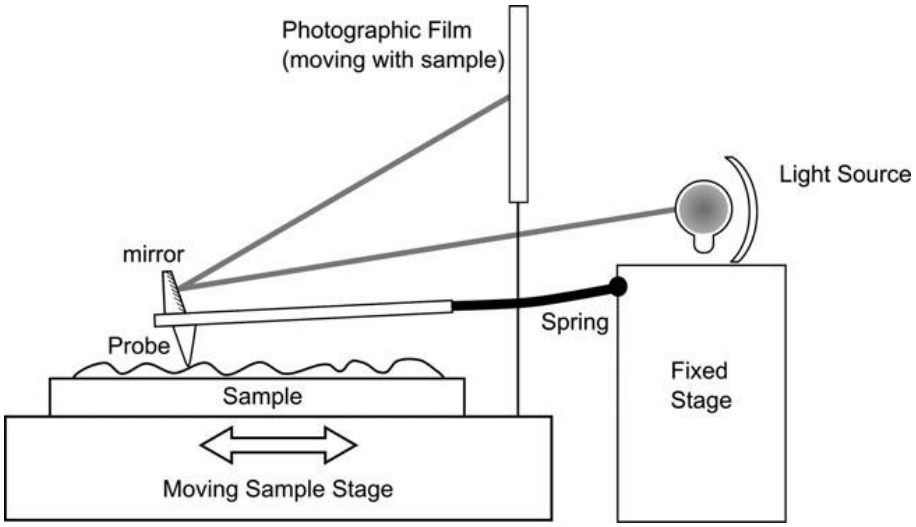

Figure 3- 5. A schematic of how a surface can be imaged by AFM *[24]*.

A Digital Instruments Dimension 3100 atomic force microscope (contactless mode) equipped with Nova software was employed in this thesis to examine the morphology and measure the roughness.

3.2.3. Physicochemical characterizations

Physical and chemical properties of the surface also play an important role in the determination of the corrosion behavior of materials, hence their evaluation is helpful to interpret the corrosion results. Energy Dispersive Spectroscopy (EDS), X-ray Fluorescence (XRF), X-ray Diffractometry (XRD), Infrared Spectroscopy (IR), and Water Contact Angle measurements

(WCA) are the main techniques used in this thesis to assess the physicochemical characteristics of the synthesized samples.

3.2.3.1. EDS

As explained in the SEM part, BSEs depend on the atomic weight of the sample atoms. The de-excitation of electrons in these atoms generates X-rays that can be detected by an EDS detector and analyzed to determine the chemical composition of the film [23]. The EDS analysis of the synthesized samples is done at the surface of the films using the same scanning electron microscope used for observing the surface morphology (Philips XL 30 ESEM).

3.2.3.2. XRF

The XRF can be used to determine the chemical composition of an unknown material or the thickness of a thin film (single or multi-layer) with a known chemical composition [25,26]. In this thesis, a Fischerscope XRAY XDV-µ is used to obtain the thickness of thin Ni films using the XRF method by comparing the experimental results to the calibrated database of standard samples.

3.2.3.3. XRD

XRD can provide details about the atomic and molecular structure of the crystalline material under study. The incident X-ray beams are diffracted in a specific direction depending on the crystalline structure (Figure 3- 6). Therefore, the intensities and angles of the diffracted beam can be used to identify the crystal structure. XRD is based on the principle of Bragg's diffraction:

$$n\lambda = 2d \times Sin\theta \qquad (3\text{-}3)$$

Where λ is the wavelength of the incident X-ray beam, n is an integer number, θ represents the angle between the incident beam and the lattice planes, and d represents the inter-planar spacing between the neighboring planes [27].

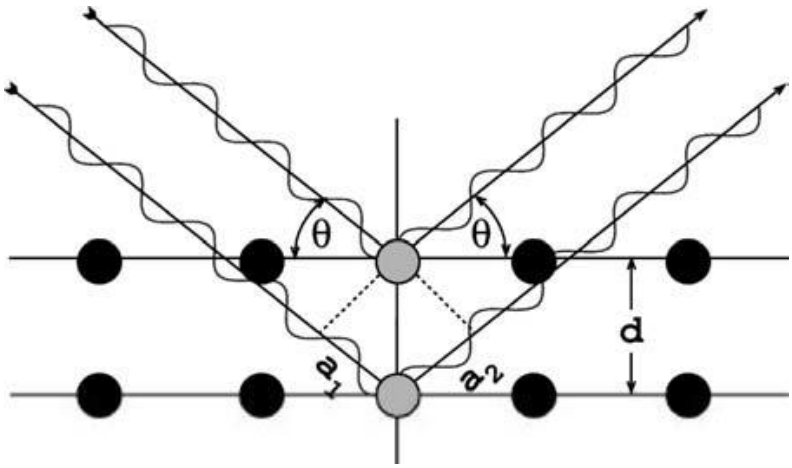

Figure 3- 6. Schematic representation of the X-ray diffraction by crystals *[27]*.

A Siemens D5000 diffractometer was employed to investigate the crystalline structure. XRD patterns are obtained with 0.04° step size by a Cu Kα radiation (λ = 0.15406 nm) generated at 40 mA and 40 kV.

3.2.3.4. IR Spectroscopy

IR spectroscopy analyzes a molecule based on the vibrations of its atoms. A sample is subjected to IR radiation over a range of frequencies while the adsorption is recorded (IR spectrum). The radiation affects the molecule electric dipoles depending on the bond strength of the molecule. Therefore, the energy at which the adsorption peak appears in the spectrum can be used as a fingerprint to identify the molecule (or a part of the molecule) by comparing it to the patterns of known molecules [28]. IR spectra, in this study, are obtained using a portable BRUKER (model ALPHA) IR spectrometer.

3.2.3.5. Water Contact Angle measurements

The surface energy of materials affects their interface with liquids and thus the occurring interactions including corrosion behavior. The contact angle between a water droplet and the material depends on the surface energy. Materials with a contact angle smaller and larger than 90º are hydrophilic and hydrophobic, respectively. The contact angle can be measured by Young's relation as [29]:

$$cos\,\theta = \frac{\gamma_{sv}-\gamma_{sl}}{\gamma_{lv}} \qquad (3\text{-}4)$$

Where γ is the interfacial tension and s, l, and v represent solid, liquid, and vapor respectively.

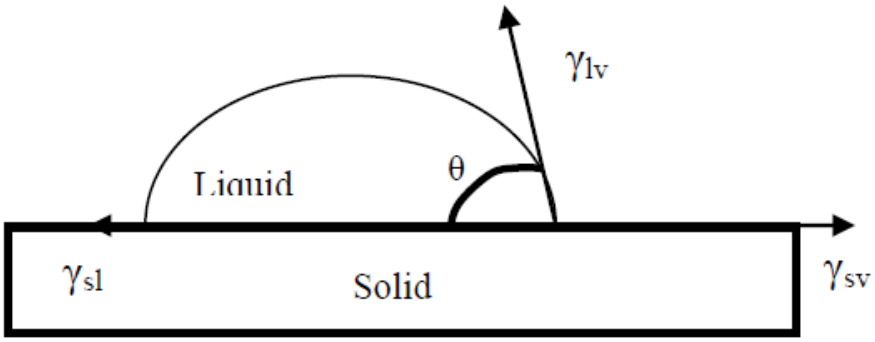

Figure 3- 7. Schematic representation of the contact angle between a liquid droplet and a solid material *[29]*.

A tensiometer (Adimec MX12P) was used to image the water droplets (2 µL) at five different locations of the samples. Drop analysis LB-ADSA plugin in ImageJ was used to measure the contact angle [30].

3.2.3.6. Other used methods

A precision scale ($\pm 10^{-4}$ g) was used to determine the mass of thin films by subtracting the mass before the synthesis from the mass after the process. The electrical resistivity of samples was measured by a precise four-probe Ohm meter (±1 mΩ).

References

[1] N. Ait Ahmed, M. Eyraud, H. Hammache, F. Vacandio, S. Sam, N. Gabouze, P. Knauth, K. Pelzer, T. Djenizian, Electrochimica Acta 94 (2013) 238–244.

[2] E. Pellicer, S. Pané, K.M. Sivaraman, O. Ergeneman, S. Suriñach, M.D. Baró, B.J. Nelson, J. Sort, Materials Chemistry and Physics 130 (2011) 1380–1386.

[3] W. Li, S. Zhang, Applied Surface Science 257 (2011) 3275–3280.

[4] R. Oriňáková, A. Turoňová, D. Kladeková, M. Gálová, R.M. Smith, Journal of Applied Electrochemistry 36 (2006) 957–972.

[5] Y.E. Sknar, O.O. Savchuk, I.V. Sknar, Applied Surface Science 423 (2017) 340–348.

[6] B.D. Falola, I.I. Suni, Current Opinion in Solid State and Materials Science 19 (2015) 77–84.

[7] R. Tarozaitė, Z. Sukackienė, A. Sudavičius, R. Juškėnas, A. Selskis, A. Jagminienė, E. Norkus, Materials Chemistry and Physics 117 (2009) 117–124.

[8] R.A. Shakoor, R. Kahraman, U. Waware, Y. Wang, W. Gao, Materials & Design 64 (2014) 127–135.

[9] A.M. Pillai, A. Rajendra, A.K. Sharma, Journal of Coatings Technology and Research 9 (2012) 785–797.

[10] O.R. Monteiro, S. Murugesan, V. Khabashesku, Surface and Coatings Technology 272 (2015) 291–297.

[11] H. Eom, B. Jeon, D. Kim, B. Yoo, Materials Transactions 51 (2010) 1842–1846.

[12] C. Shanthi, S. Barathan, R. Jaiswal, R.M. Arunachalam, S. Mohan, Materials Letters 62 (2008) 4519–4521.

[13] P.T. Kissinger, W.R. Heineman, Journal of Chemical Education 60 (1983) 5.

[14] G.D. Salian, C. Lebouin, A. Demoulin, M.S. Lepihin, S. Maria, A.K. Galeyeva, A.P. Kurbatov, T. Djenizian, Journal of Power Sources 340 (2017) 242–246.

[15] N. Plylahan, S. Maria, T.N. Phan, M. Letiche, H. Martinez, C. Courrèges, P. Knauth, T. Djenizian, Nanoscale Research Letters 9 (2014) 544.

[16] N.A. Kyerematen, F. Dumur, P. Knauth, B. Pecquenard, T. Djenizian, Comptes Rendus Chimie 16 (2013) 80–88.

[17] N. Plylahan, N.A. Kyerematen, M. Eyraud, F. Dumur, H. Martinez, L. Santinacci, P. Knauth, T. Djenizian, Nanoscale Research Letters 7 (2012) 349.

[18] N.A. Kyerematen, F. Dumur, P. Knauth, B. Pecquenard, T. Djenizian, Electrochemistry Communications 13 (2011) 894–897.

[19] M. Kemell, M. Ritala, M. Leskelä, Critical Reviews in Solid State and Materials Sciences 30 (2005) 1–31.

[20] ASTM B117-16, (2016).

[21] R. Kelly, J. Scully, D. Shoesmith, R. Buchheit, Electrochemical Techniques in Corrosion Science and Engineering, CRC Press, 2002.

[22] A. Bahramian, K. Raeissi, A. Hakimizad, Applied Surface Science 351 (2015) 13–26.

[23] J. Goldstein, Scanning Electron Microscopy and X-Ray Microanalysis, 4th edition, Springer Science+Business Media, LLC, New York, NY, 2017.

[24] P.J. Eaton, P. West, Atomic Force Microscopy, Oxford University Press, Oxford ; New York, 2010.

[25] W. BAMBYNEK, B. CRASEMANN, R.W. FINK, H.-U. FREUND, H. MARK, C.D. SWIFT, R.E. PRICE, P.V. RAO, Rev. Mod. Phys. 44 (1972) 716–813.

[26] D.K.G. de Boer, Phys. Rev. B 44 (1991) 498–511.

[27] H. Stanjek, W. Häusler, Hyperfine Interactions 154 (2004) 107–119.
[28] B. Stuart, in: Kirk-Othmer Encyclopedia of Chemical Technology, American Cancer Society, 2005.
[29] C.F. Soon, W.I.W. Omar, N. Nayan, H. Basri, M.B. Narawi, K.S. Tee, Procedia Technology 11 (2013) 487–494.
[30] A.F. Stalder, T. Melchior, M. Müller, D. Sage, T. Blu, M. Unser, Colloids and Surfaces A: Physicochemical and Engineering Aspects 364 (2010) 72–81.

Chapter 4

Aqueous Electrodeposition

This chapter is dedicated to the first part of results and discussions concerning the electrodeposition process in aqueous solution. It mainly deals with optimizing the electrodeposition electrolyte of barrier Ni alloys regarding the corrosion resistance as the key criterion.

4.1. Electrodeposition electrolyte

4.1.1. Procedure

The aqueous electrolyte of the electrodeposition of Ni and Ni-P alloys are consisted of Ni sulfate, Ni chloride, phosphorous acid, phosphoric acid, and boric acid (see 2.1 and 2.2.2.3). The first attempt was to find the optimized composition of main electrolyte regarding the corrosion behavior of the obtained Ni-P films. As a result, 150 mL of five solutions were prepared where we varied the ratio between Ni^{2+} ions sources (chloride source increasing from S1 to S5), maintaining its global concentration at 200 gr/L:

S1: 200 gr/L $NiSO_4.6H_2O$ + 5mL/L H_3PO_4 +8 gr/L H_3PO_3 + 16 gr/L H_3BO_3
S2: 190 gr/L $NiSO_4.6H_2O$ + 10 gr/ L $NiCl_2.6H_2O$ + 5m L / L H_3PO_4 +8 gr/ L H_3PO_3 + 16 gr/L H_3BO_3
S3: 175 gr/ L $NiSO_4.6H_2O$ + 25 gr/ L $NiCl_2.6H_2O$ + 5m L / L H_3PO_4 +8 gr/ L H_3PO_3 + 16 gr/L H_3BO_3
S4: 150 gr/ L $NiSO_4.6H_2O$ + 50 gr/ L $NiCl_2.6H_2O$ + 5m L / L H_3PO_4 +8 gr/ L H_3PO_3 + 16 gr/L H_3BO_3
S5: 125 gr/ L $NiSO_4.6H_2O$ + 75 gr/ L $NiCl_2.6H_2O$ + 5m L / L H_3PO_4 +8 gr/ L H_3PO_3 + 16 gr/L H_3BO_3

To evaluate the effect of agitation, S4 was also stirred at the speed of 650 rpm during the deposition process. Note that the P part of the solution (5ml/ L H_3PO_4 +8 gr/ L H_3PO_3) as well as the deposition parameters (Potential: -1 V vs. Ag/AgCl (KCl sat.), time: 7 min, and Temperature : 60 ºC) were optimized previously by another project. The pH of all the

electrolytes was 1. The counter electrode was a 36 cm^2 Pt plate maintained at 4 cm from the working electrode, and Ag/AgCl saturated with KCl (E=0,192V/SHE) is used as reference electrode in the 3-electrode setup (Figure 3-3).

The Cu lead frames, provided by the industrial partner, underwent a chemical pretreatment: 30 s in a diluted basic solution (1 mL of 30% NH_4OH solution in 200 mL of demineralized water), 30 s in demineralized water, and 30 s in a 10% H_2SO_4 solution. The aim of this pretreatment was to eliminate oxides, if there were any, and clean the sample before the deposition process.

4.1.2. Results and Discussion

Figure 4- 1 depicts the effect of the used electrolyte on the current density - deposition time curves of Ni-P films. A stable current density during the deposition process for all the solutions was observed. Increasing the Ni^{2+} chloride source enhanced the current density and subsequently the weight of the coatings in good agreement with previous results while chloride salts are known to enhance the throwing power [1–3]. Interestingly, stirring the electrolyte during the deposition process had the same effect.

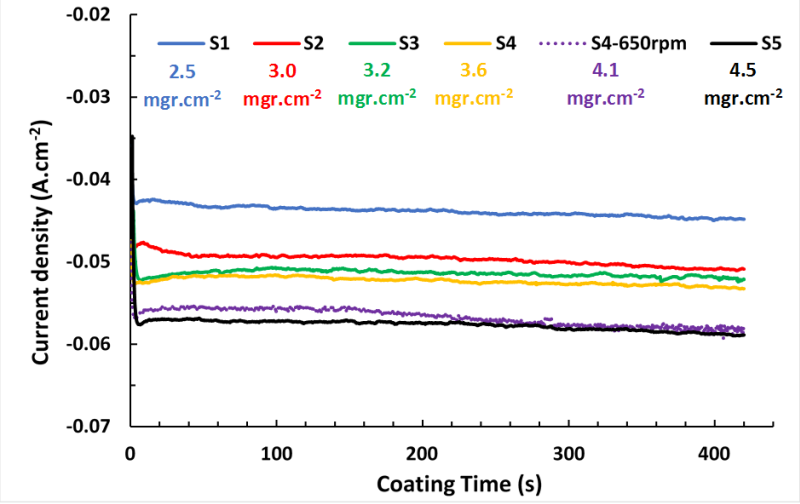

Figure 4- 1. Current density – deposition time curves of the aqueous Ni-P electrolytes under study (S1-S5).

The obtained coatings then were immerged in 3 % NaCl solution for one hour to evaluate their corrosion behavior by EIS and potentiodynamic polarization tests. Figure 4- 2 depicts the EIS results of these samples.

Similar Bode plots show that all coatings underwent the same fundamental electrochemical reaction. The presence of only one peak in the bode plots of the coatings indicates that the corrosion process involves a single time constant, which corresponds to the charge transfer reaction, meaning that the dissolution of Ni during the corrosion is the main process. The different impedance values is a representative of the different active area where this reaction occurs.

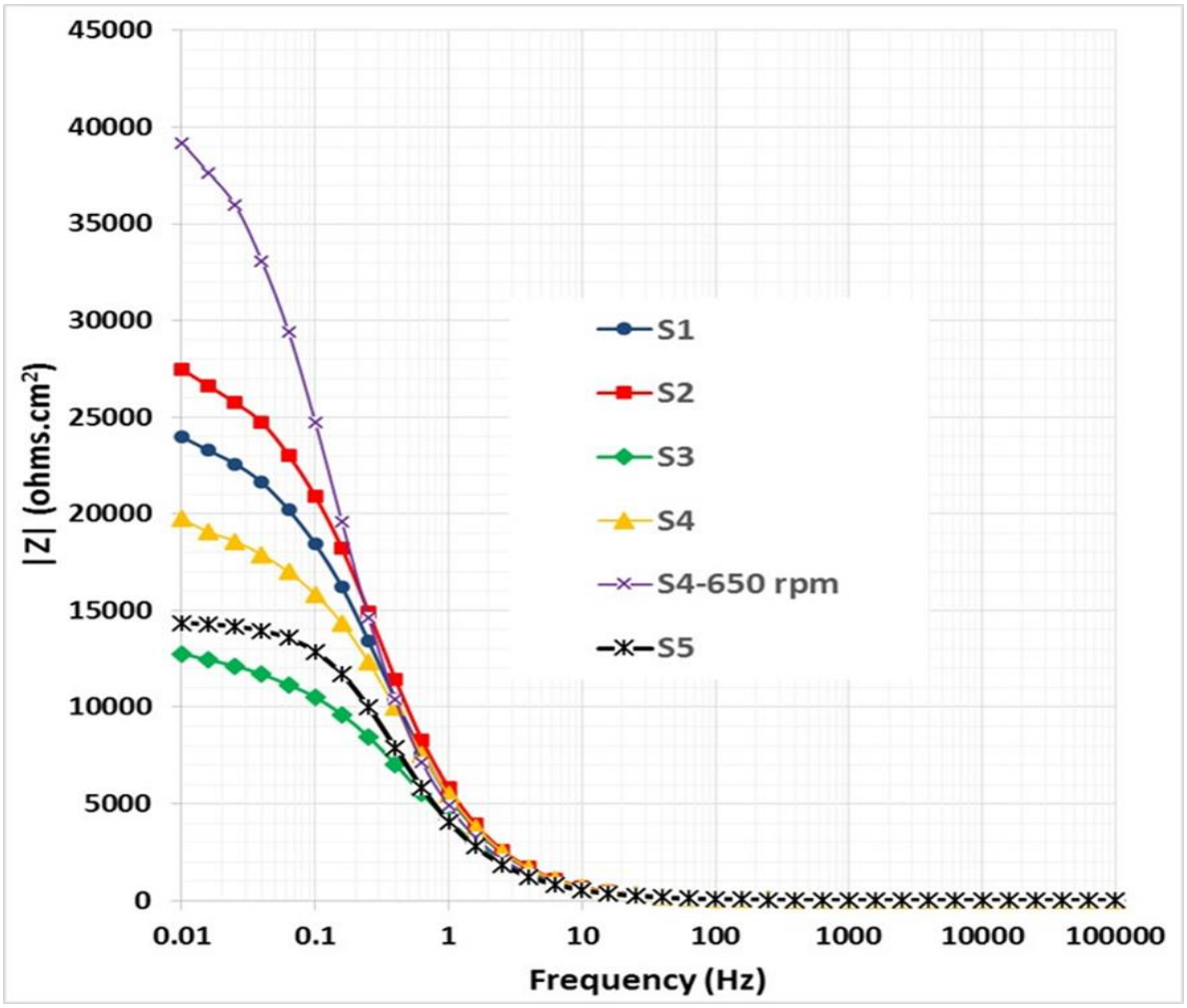

Figure 4- 2. Bode Z plots of the Ni-P films obtained from the electrolytes under study after one hour immersion in 3% NaCl solution.

Table 4- 1. The impedance values (at 0.1 Hz) of Ni-P films obtained from the electrolytes under study

Sample		|Z| at 0.01 Hz ($k\Omega.cm^2$)
Ni-P	S1	20.2
	S2	21.3
	S3	15.2
	S4	19.1
	S4-650 rpm	38.2
	S5	16.5

The impedance values can be used to compare the corrosion results. The results imply that Ni-P films improved the corrosion resistance of the substrate by reducing the charge transfer at the interface of electrolyte and electrode. It is believed that the dissolution of Ni occurs in the early stages of corrosion that leaves a P-rich film behind. This film then hinders further dissolution of Ni and decreases the corrosion rate [8].

The addition of chloride salts (S2) slightly increased the corrosion resistance, but a further increase of its concentration had a gradual negative effect (S3, S4, and S5) probably because non-homogenous films were obtained by increasing the concentration of chloride salts [1–3]. Moreover, Ni-P films with notably higher corrosion resistance were formed when the electrolyte was stirred (S4 vs. S4- 650 rpm). Stirring the solution provides fresh solution to the working electrode and ease the detachment of the formed hydrogen bubbles and thus improved the corrosion behavior.

Figure 4- 3 shows the potentiodynamic polarization results made the coatings. The extracted data by the Tafel extrapolation method, i.e. corrosion potential (E_{corr}) and corrosion current density (i_{corr}), are presented in Table 4- 2.

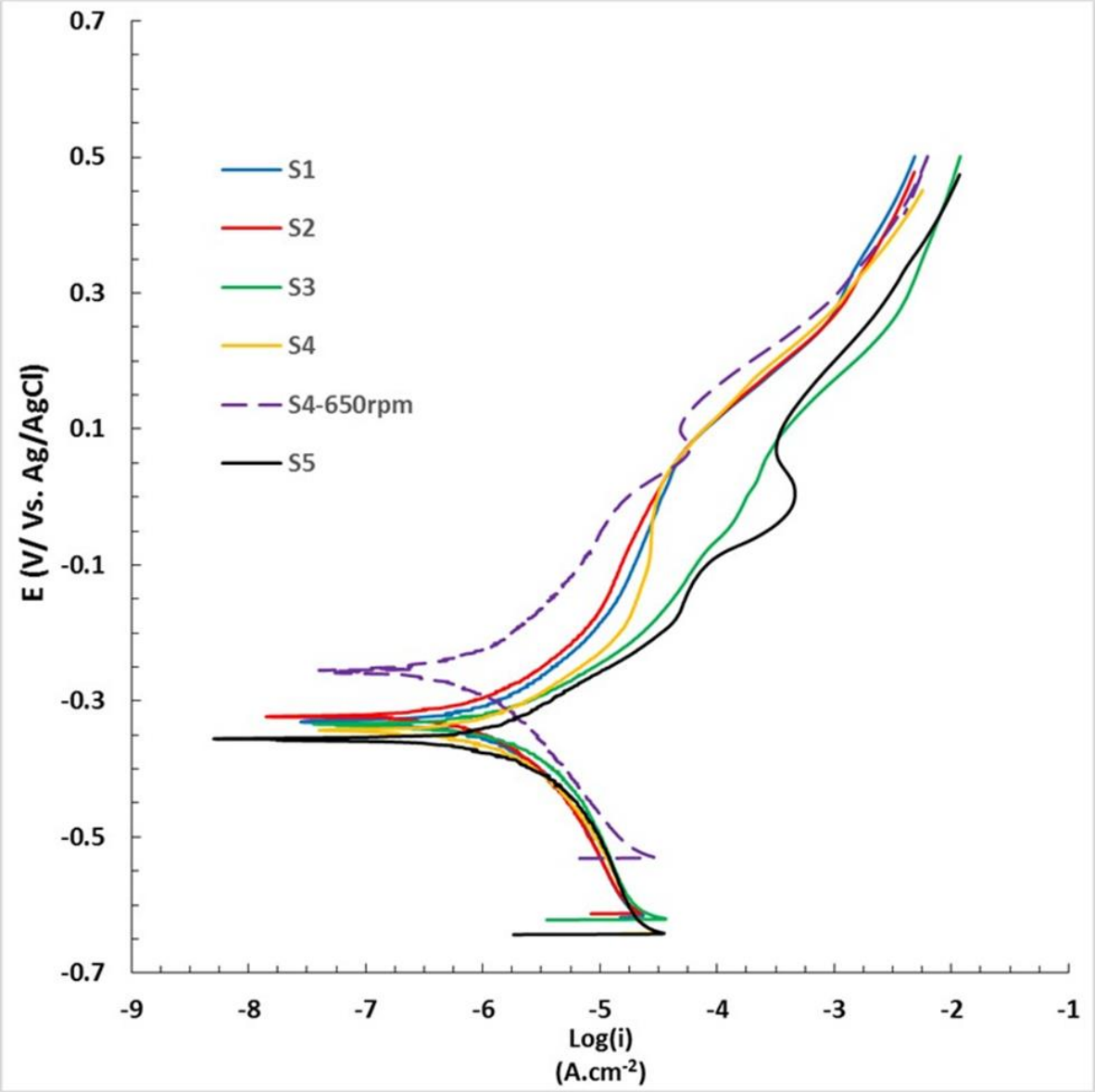

Figure 4- 3. Potentiodynamic polarization curves of the Ni-P films obtained from the electrolytes under study after one hour immersion in 3% NaCl solution.

Table 4- 2. Corrosion current density and corrosion potential of Ni-P films obtained from the electrolytes under study

Sample		i_{corr} ($\mu A.cm^{-2}$)	E_{corr} (mV) vs. Ag/AgCl
Ni-P	S1	1.49	-324
	S2	1.16	-328
	S3	1.78	-311
	S4	1.62	-324
	S4- 650 rpm	1.03	-258
	S5	1.52	-331

Based on the analyzed potentiodynamic data, it can be seen that all the presented Tafel plots have almost a similar behavior with a pseudo-passivation behavior in their anodic branch. The potentiodynamic results were in good agreement to the EIS ones, showing that the coating obtained from S2 presented the best corrosion behavior. Note that, stirring the electrolyte led to a higher corrosion resistance and a less negative corrosion potential.

As a result, S2 was chosen as the reference electrolyte and it was stirred at 650 rpm for the subsequent experiments.

4.2. Modification and optimization of NiP coatings

4.2.1. The effect of additives

The presence of additives in the electrolyte affects the properties of coatings either by adsorbing on the surface of the cathode or by forming complexes with Ni ions. Nonetheless, the use of additives, in small contents, is usually recommended to form Ni-P films. Comparing to other methods of improving the corrosion resistance of Ni-P coatings (ternary alloys and composites), additives are easier to use, more economical, and more practical since there is no concern about their precipitation or agglomeration. Therefore, the main used chemicals as additives were identified from the literatures and then were added to the main electrolyte (S2) to form Ni-P films. The additives were saccharine that is the most commonly used as carrier, brightener, and stress reducing agent; coumarin as brightener; pyridinium ions as auxiliary brightener [9]; glycine that is the smallest amino acid [10] as complexing and buffering agent [11]; sodium citrate used as complexing, buffering and leveling agent [12]; and cerium sulfate as a rare metal salt [8]. Note that the results of this part, i.e. the effect of additives on Ni-P films, has been already published in ref [13].

4.2.1.1. Procedure

Five different concentrations of additives were prepared around the concentration usually employed in literature: saccharine and glycine (0.1, 0.5, 1, 2.5, and 5 g/L), coumarin (5, 10, 50, 100, and 250 mg/L), pyridinium propyl sulfonate (0.1, 0.5, 1, 2, and 4 g/L), sodium citrate (4, 8, 12, 16, and 20 g/L), and cerium sulfate (4, 8, 12, 20, and 30 mg/L). All the samples were named using the first three letters of their respective additives and their concentration; i.e. Cou.10m represents the Ni-P coating formed in the presence of 10 mg/L of coumarin as the additive. However, a smaller counter electrode (9 cm^2) was used in this part to form the Ni-P films in the absence (the reference sample) and presence of additives.

4.2.1.2. Results and discussion

Figure 4- 4 shows the effects of the additives on current densities during NiP electrodeposition process. The current density decreases rapidly at the beginning of the coating procedure and then stays at a stationary value until the end of the process. Moreover, the addition of all chosen additives to the Ni-P electrodeposition bath led to lower current densities during the coating procedure. For example, the current is almost divided by 3 in the case of sodium citrate addition, and by 1.5 whith cerium sulfate. Therefore, even if only the water side reaction is impacted by the additives, the thickness of the Ni-P layers in presence of additives is assumed to be decreased as well. This assumption was confirmed by cross-sectional observations, gravimetric and XRF measurements that are presented in the following.

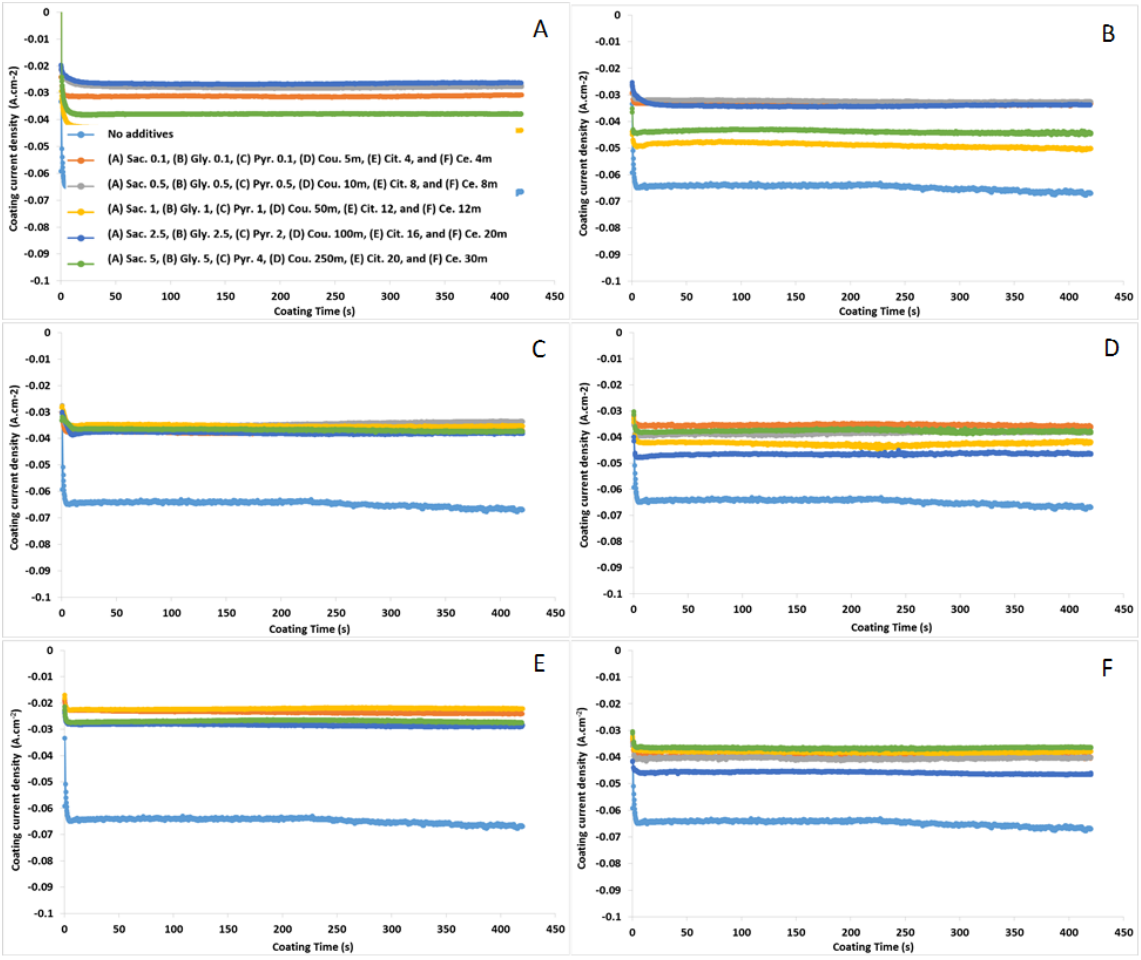

Figure 4- 4. Current density-coating time curves for Ni-P coatings in the presence of (A) saccharine, (B) glycine, (C) PPS, (D) coumarin, (E) sodium citrate, and (F) cerium sulfate as additive.

Table 4-3 and Table 4- 4 present the analyzed information from EIS and potentiodynamic polarization tests, respectively. Figure 4- 5 depicts the surface of the samples before and after the corrosion tests. The EIS and potentiodynamic polarization curves for best samples for the given additives, are depicted in Figure 4- 6 and Figure 4- 7, respectively. Based on the presented data the additives, in general, did not affect the corrosion potential but the corrosion current density and charge transfer resistance. The use of a proper amount of the tested additives improved the corrosion resistance of Ni-P films, especially at high potentials (+0.6 V vs. OCP). In the following, these results were discussed in details.

Table 4- 3. The impedance values (at 0.1 Hz) of Ni-P films obtained in the absence and presence of the additives

Sample		|Z| at 0.01 Hz ($k\Omega.cm^2$)
Ni-P		13.7
Saccharin	Sac.0.1	14.4
	Sac.0.5	21.2
	Sac.1	20.2
	Sac.2.5	44.8
	Sac.5	25.1
Glycine	Gly.0.1	40.0
	Gly.0.5	25.2
	Gly.1	23.8
	Gly.2.5	21.3
	Gly.5	20.2
PPS	Pyr.0.1	40.2
	Pyr.0.5	38.5
	Pyr.1	23.9
	Pyr.2	16.0
	Pyr.4	19.3
Coumarin	Cou.5m	38.7
	Cou.10m	27.4
	Cou.50m	36.6
	Cou.100m	43.5
	Cou.250m	27.5
Sodium Citrate	Cit.4	40.0
	Cit.8	35.3
	Cit.12	29.6
	Cit.16	32.1
	Cit.20	30.7
Cerium Sulfate	Ce.4m	38.7
	Ce.8m	46.6
	Ce.12m	31.8
	Ce.20m	36.7
	Ce.30m	33.4

i_{corr} can be used as criterion for comparing the corrosion resistance; a lower i_{corr} means a higher corrosion resistance. It is well-known that a localized corrosion process occurs on Ni-P films with a porous Au top-coat based on the high ratio of cathode area (Au) to anode area (Ni-P) that leads to a high polarization of the Ni-P film [14–16]. Therefore, the current density value at high potential (+0.6 V vs. OCP) are used to simulate the corrosion resistance of different Ni-P layers in the case of galvanic coupling with gold and thus i values measured at +0.6 V vs. OCP are reported in Table 4- 4.

Table 4- 4. Corrosion current density, corrosion potential, and current density at a high potential (+0.6 V vs. OCP) of Ni-P films obtained in the absence a presence of the additives.

Sample		i_{corr} ($\mu A.cm^{-2}$)	E_{corr} (mV) vs. Ag/AgCl	i ($mA.cm^{-2}$) at +0.6 V vs. OCP
Ni-P		1.69	-302	15.86
Saccharin	Sac.0.1	1.49	-274	7.24
	Sac.0.5	1.24	-288	3.46
	Sac.1	1.32	-256	16.92
	Sac.2.5	0.83	-246	3.32
	Sac.5	1.11	-241	13.65
Glycine	Gly.0.1	0.94	-296	0.10
	Gly.0.5	1.15	-324	0.08
	Gly.1	1.27	-302	18.85
	Gly.2.5	1.42	-284	19.73
	Gly.5	1.51	-286	15.12
PPS	Pyr.0.1	0.82	-298	0.22
	Pyr.0.5	0.84	-310	0.72
	Pyr.1	1.85	-263	1.74
	Pyr.2	2.22	-285	3.98
	Pyr.4	1.72	-266	6.05
Coumarin	Cou.5m	0.83	-310	0.68
	Cou.10m	1.51	-290	1.74
	Cou.50m	0.86	-300	0.83
	Cou.100m	0.84	-290	1.01
	Cou.250m	1.00	-303	0.35
Sodium Citrate	Cit.4	0.74	-296	0.09
	Cit.8	0.72	-309	0.05
	Cit.12	0.80	-312	0.08
	Cit.16	1.02	-295	0.19
	Cit.20	0.74	-308	0.23
Cerium Sulfate	Ce.4m	0.96	-292	1.29
	Ce.8m	0.75	-284	0.69
	Ce.12m	0.88	-300	1.58
	Ce.20m	0.82	-290	0.67
	Ce.30m	1.19	-287	1.15

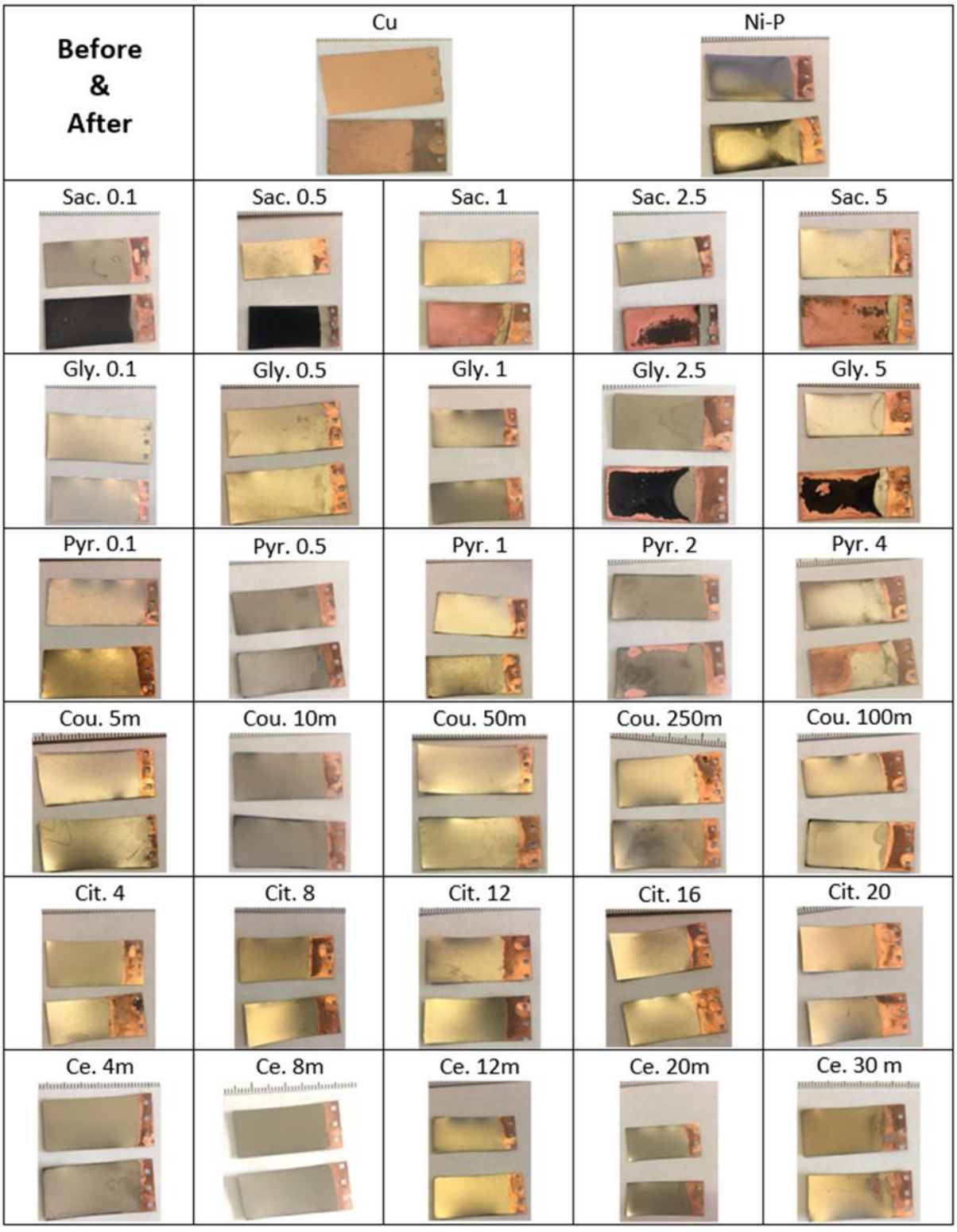

Figure 4- 5. The general look of the Cu substrate and coated samples before and after the electrochemical corrosion tests.

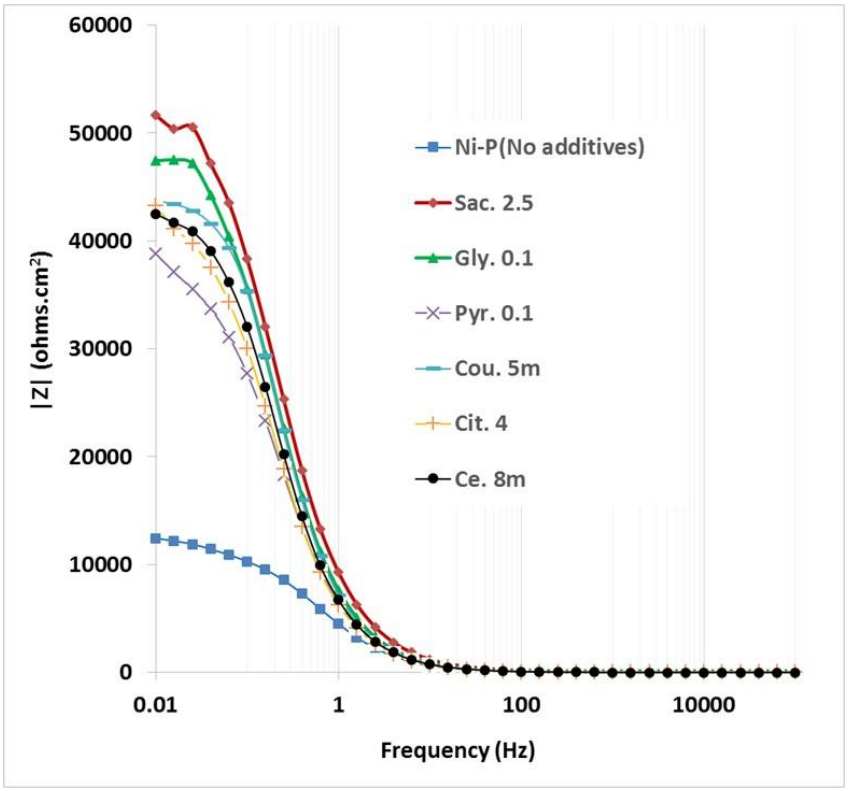

Figure 4- 6. Bode Z plots of the Ni-P films obtained in the absence and presence of the additives after one hour immersion in 3% NaCl solution.

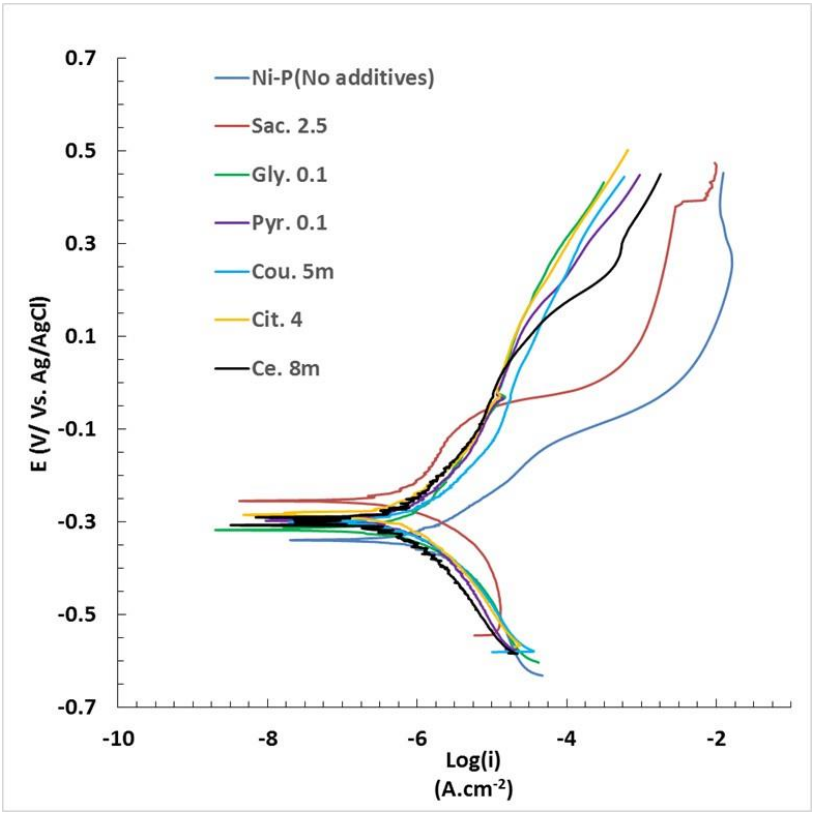

Figure 4- 7. Potentiodynamic polarization curves of the Ni-P films obtained in the absence and presence of the additives after one hour immersion in 3% NaCl solution.

Figure 4- 8 shows the X-Ray diffraction patterns of the chosen samples in each category, and Figure 4- 9 shows their surface morphology. Figure 4- 10 shows the cross-section and the surface of the Ni-P layer with no additive before and after corrosion. The chemical composition of these samples, obtained using the EDS technique, are summarized in Table 4- 5. The average thickness of the coatings with their variations determined by X-ray fluorescence on the complete surface of the samples, can be found in Table 4- 6.

The thickness of the Ni-P layer from the cross-section image was in a good agreement with the values measured by X-Ray fluorescence. Figure 4- 11 and Table 4- 8 represent the surface morphology and the average roughness values of the samples obtained by AFM.

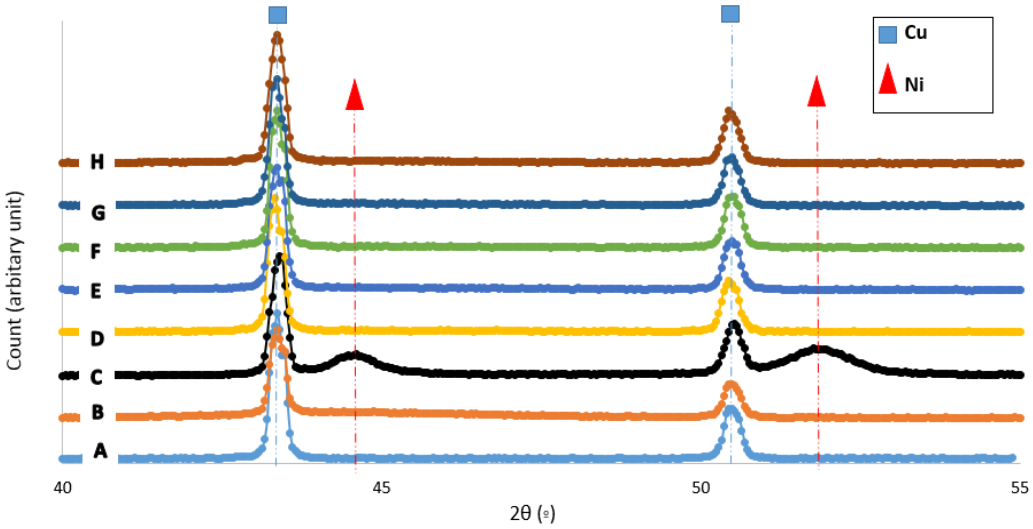

Figure 4- 8. X-Ray diffraction patterns of (A) Cu substrate, (B) Ni-P coating without additives, (C) Sac. 2.5, (D) Gly. 0.1, (E) Pyr. 0.1, (F) Cou. 5m, (G) Cit. 4, and (H) Ce. 8m.

Table 4- 5. Chemical composition of the chosen samples in each category obtained by EDS

Element / Sample	Ni (wt. %)	P (wt. %)
No additives	89.5	10.5
Sac. 2.5	98.2	1.8
Gly. 0.1	85.4	14.6
Pyr. 0.1	82.6	14.4
Cou. 5m	82.2	13.9
Cit. 4	84.7	15.3
Ce. 8m	81.2	14.6

With the exception of the sample Sac. 2.5 that had only around 2% of P, the P content was around 14% in the others. The X-ray patterns of all samples, except Sac. 2.5, is similar to the

substrate, meaning that the Ni-P layers present a completely amorphous structure. In the X-ray pattern of Sac. 2.5, on the other hand, there are two broad peaks related to the presence of crystalline Ni; its structure is a mixture of amorphous and crystalline phases. All the coated Ni-P samples, in the presence and absence of the additives, presented a similar surface morphology containing globular fungi-form features, which can be easily distinguished from the Cu substrate (Figure 4- 9). However, thinner and smoother coatings were formed in the presence of additives. The effect of these chemicals on the surface roughness is notably evident for Pyr. 0.1 and Ce. 8m where their roughness is even lower than the Cu substrate. This observation implies that the additives have a noticeable effect on the thickness and roughness of the coatings, but their surface morphology is controlled by other parameters, i.e. coating conditions.

Table 4- 6. Mass, area, thickness, and coating efficiency of the chosen samples

Sample	m (mg)	A (cm^2)	t (µm)	CE %
No additives	14.7	3.46	2.74±1.01	13.2
Sac. 2.5	5.3	4.03	1.77±0.39	9.7
Gly. 0.1	4.7	4.03	1.08±0.16	7.1
Pyr. 0.1	6.3	3.83	1.38±0.52	8.6
Cou. 5m	5.0	4.18	1.40±0.38	6.6
Cit. 4	4.0	3.85	1.54±0.42	8.9
Ce. 8m	6.3	3.92	1.64±0.45	7.5

EIS and potentiodynamic polarization curves in the absence and presence of the additives are in some extent similar, except that impedance values in bode plots were higher and the anodic branch of the Tafel plots, except for Sac. 2.5, had a non-broken pseudo-passivation behavior in the presence of additives. The passive layer was broken for Sac. 2.5 and the reference Ni-P layer (with no additives) around -0.1 V vs. Ag/AgCl, and therefore, they had an accelerated corrosion at high potentials (Figure 4- *7*). This behavior, which could be attributed to their notably lower P content (Table 4- 5), explains the appearance of these samples after corrosion (Figure 4- 5), where Ni-P and Sac.2.5 are blackened at the edges or completely dissolved,

respectively; the other samples kept their primitive shiny gray appearance after the corrosion process.

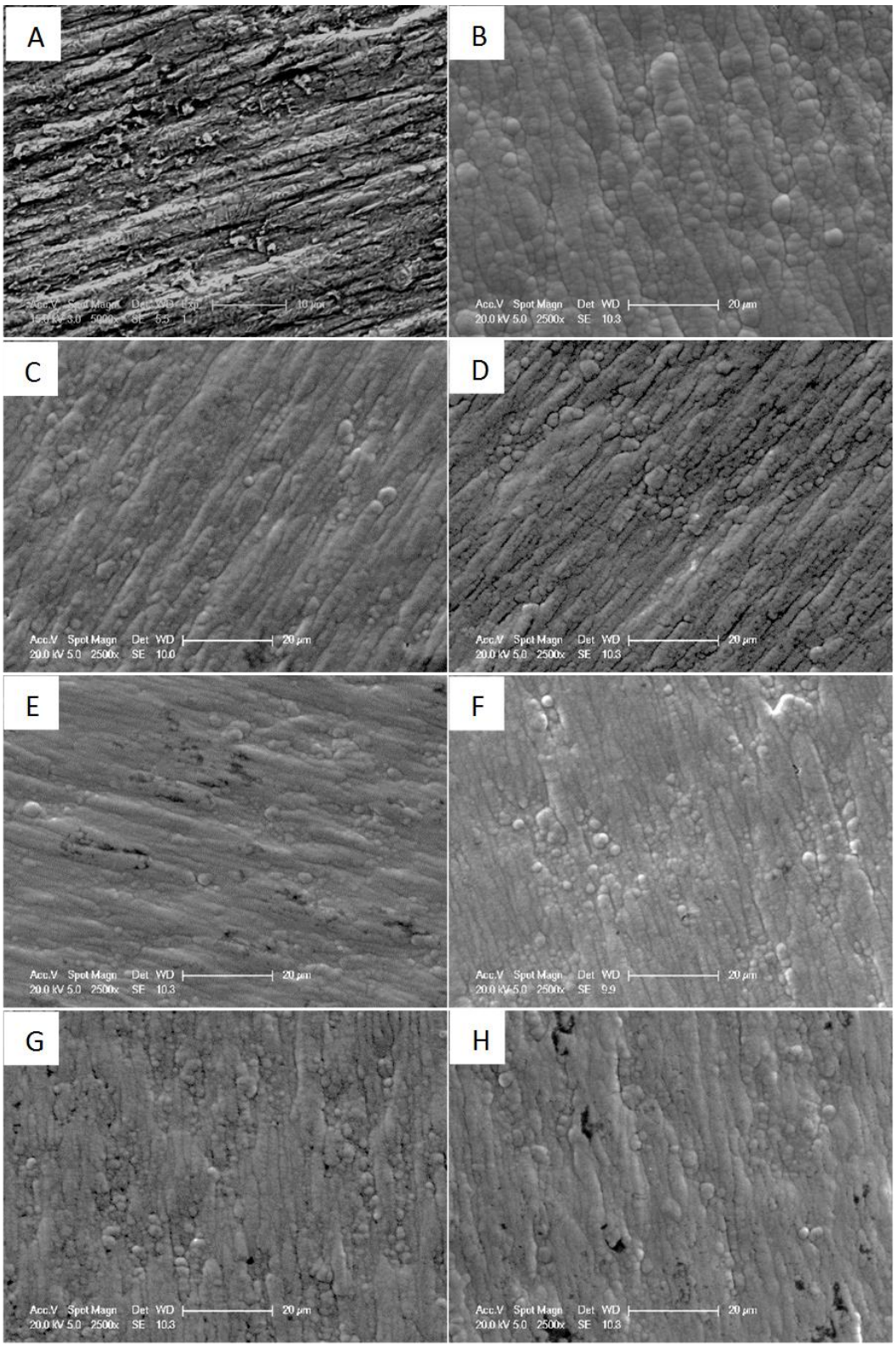

Figure 4- 9. SEM images of (A) Cu substrate, (B) Ni-P without additives, (C) Sac. 2.5, (D) Gly. 0.1, (E) Pyr. 0.1, (F) Cou. 5m, (G) Cit. 4, and (H) Ce. 8m.

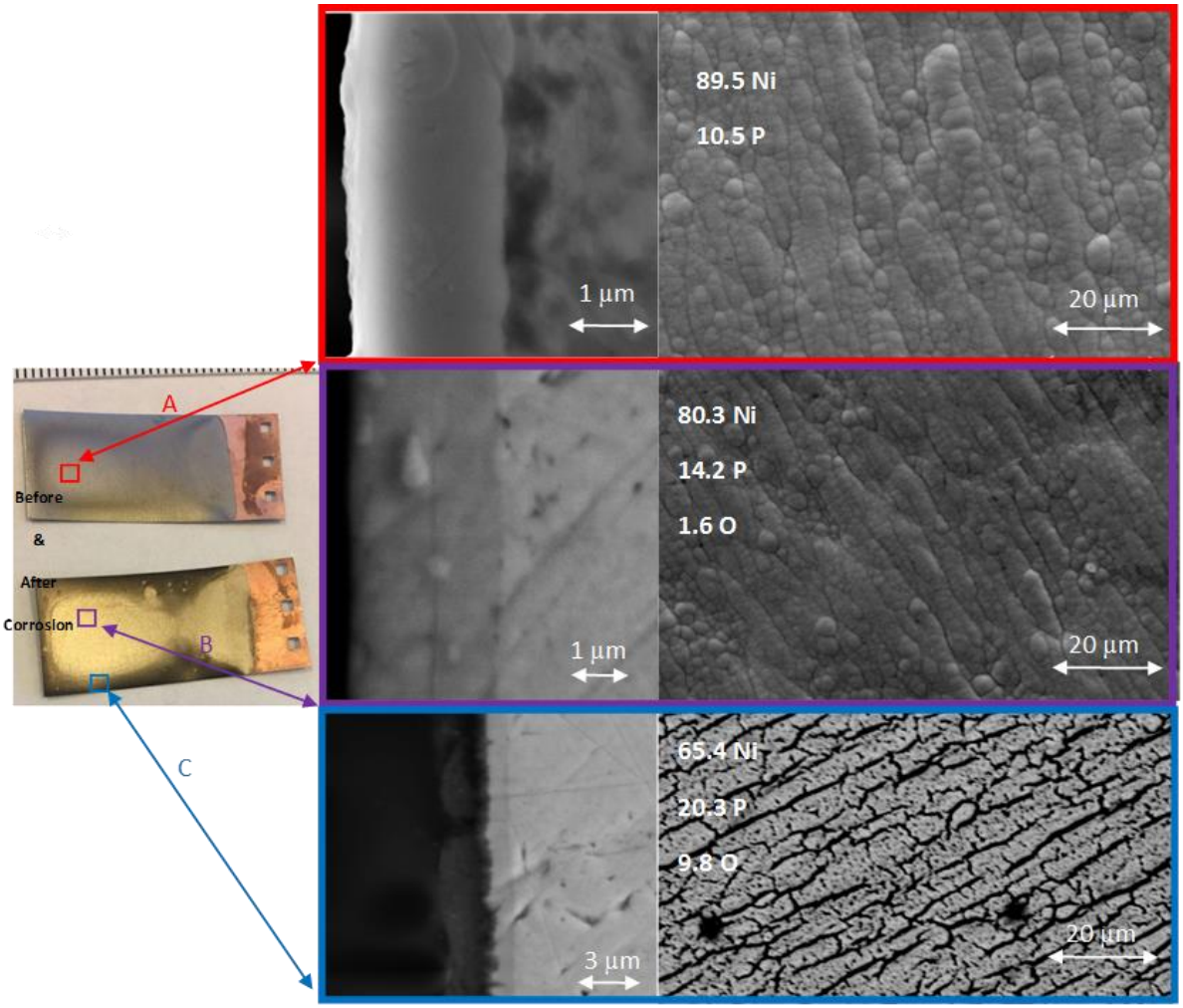

Figure 4- 10. Cross-section and surface SEM images of Ni-P without additives, (A) before corrosion, (B) shiny part after corrosion, and (C) dark region after corrosion.

Using the obtained impedance values from EIS tests, one can calculate corrosion efficiency (CorE%) and porosity index (P.I) of the electrodeposited coatings (Table 4- 7) employing the equations 4-3 [6] and 4-4 [17], respectively.

$$(CorE\%) = \left(1 - \left(\frac{R_{PS}}{R_P}\right)\right) * 100 \qquad (4\text{- }1)$$

$$P.I = \frac{R_{ps}}{R_p} \times 10^{-\left(\frac{\Delta E}{\beta a}\right)} \qquad (4\text{- }2)$$

ΔE is the difference between the corrosion potential of the coated sample and the substrate, β_a is the anodic slope of the substrate, and R_{ps} and R_p are the corrosion resistance of the substrate and the coating, respectively. Note that the Cu substrate (not presented here) had the corrosion current density of 3.32 µA.cm^{-2}, the corrosion potential of -200 mV, anodic slope of 66 mV.dec^{-}

[1], and impedance value of 6.1 kΩ.cm^2. An equation similar to (4-3) could be employed to calculate the corrosion efficiency using the current density (Table 4- 4) bearing in mind that the current density and the polarization resistance have an inverse relationship.

Table 4- 7. Corrosion efficiency and porosity density of the obtained Ni-P coatings

Sample		Corrosion efficiency (%)		Corrosion efficiency at high potentials (%)	Porosity density (%)
		Tafel	EIS		
Ni-P		63.4	55.5	-209.8	12.8
Saccharin	Sac.0.1	73.7	57.6	-41.4	3.5
	Sac.0.5	77.6	71.2	32.4	4.8
	Sac.1	72.9	69.8	-230.5	1.9
	Sac.2.5	85.5	86.4	35.2	0.7
	Sac.5	74.2	75.7	-166.1	1.1
Glycine	Gly.0.1	85.0	84.8	98.0	4.3
	Gly.0.5	80.3	75.8	98.4	14.9
	Gly.1	76.6	74.4	-268.2	8.2
	Gly.2.5	74.5	71.4	-285.4	4.8
	Gly.5	74.5	69.8	-195.3	7.8
PPS	Pyr.0.1	87.3	84.8	95.7	3.9
	Pyr.0.5	86.9	84.2	85.9	6.1
	Pyr.1	75.4	74.5	66.0	2.2
	Pyr.2	70.8	61.9	22.3	5.7
	Pyr.4	72.9	68.4	-18.2	2.7
Coumarin	Cou.5m	86.4	84.2	86.7	6.3
	Cou.10m	78.4	77.7	66.0	5.0
	Cou.50m	85.5	83.3	83.8	4.8
	Cou.100m	87.1	86.0	80.3	3.0
	Cou.250m	82.4	77.8	93.2	6.4
Sodium Citrate	Cit.4	87.6	84.8	98.2	3.5
	Cit.8	87.1	82.7	99.0	5.8
	Cit.12	85.8	79.4	98.4	7.0
	Cit.16	83.3	81.0	96.3	4.6
	Cit.20	85.2	80.1	95.5	6.4
Cerium Sulfate	Ce.4m	85.0	84.2	74.8	3.7
	Ce.8m	88.8	86.9	86.5	2.1
	Ce.12m	84.7	80.8	69.1	5.0
	Ce.20m	85.9	83.4	86.9	3.3
	Ce.30m	82.9	81.7	77.5	3.6

The Ni-P layer without additives has a 63.4/55.5 corrosion efficiency % (using Tafel/EIS test data), a really low corrosion efficiency at high potentials (-210%) and 12.8% of porosity, possibly more around the edges given that the edges blacken after the corrosion tests (Figure 4- 5). The blackened parts proved to be Nickel oxide (NiO) based on EDS analysis. The surface

and cross-section morphology of the blackened part is presented in Figure 4- 10. It can be seen that more than half of the Ni-P film is corroded and converted to NiO, leaving a cracked surface behind. The fast Ni dissolution that blackened the edge left a high P content film (20 wt. %) with a high internal stress [19], which explains the cracked surface. It should be noticed that the cross-section and surface of the shiny part is intact after corrosion while the P content has increased. Therefore, one can assume the same for other samples using additives that kept their shiny look after corrosion.

It is well known that there is a non-uniform distribution of current around the edges during the deposition that can lead to the formation of a non-uniform coating. There is a pseudo-passivation region in its anodic branch (Figure 4- 7) that ends around -0.1 V (vs. Ag/AgCl). This could be due to the localized attack of chlorine ions at the edges of the Ni-P coatings that led to a galvanic corrosion between copper and nickel, and thus, a fast oxidation of Ni that blackens the edges; which also explains the high current, and a negative corrosion efficiency at high potentials. The whole surface of the substrate got slightly tarnished and there is a passivation looking-region in its polarization curve at high potentials, possibly due to the oxidation of the surface or the formation of a chlorine film. Based on Figure 4- 5, introducing the additives has homogenized the current distribution; it can be also concluded that employing a proper content of additives can efficiently improve the corrosion efficiency, especially at high potentials, and highly decrease the porosity content (Table 4- 7). This is especially important for the microelectronic contacts, where a severe corrosion phenomenon is reported at their edges, and the presence of a gold top-coat requires a barrier film with a good corrosion resistance at high potentials due to the galvanic corrosion between gold and the Ni-P sublayer [15,16].

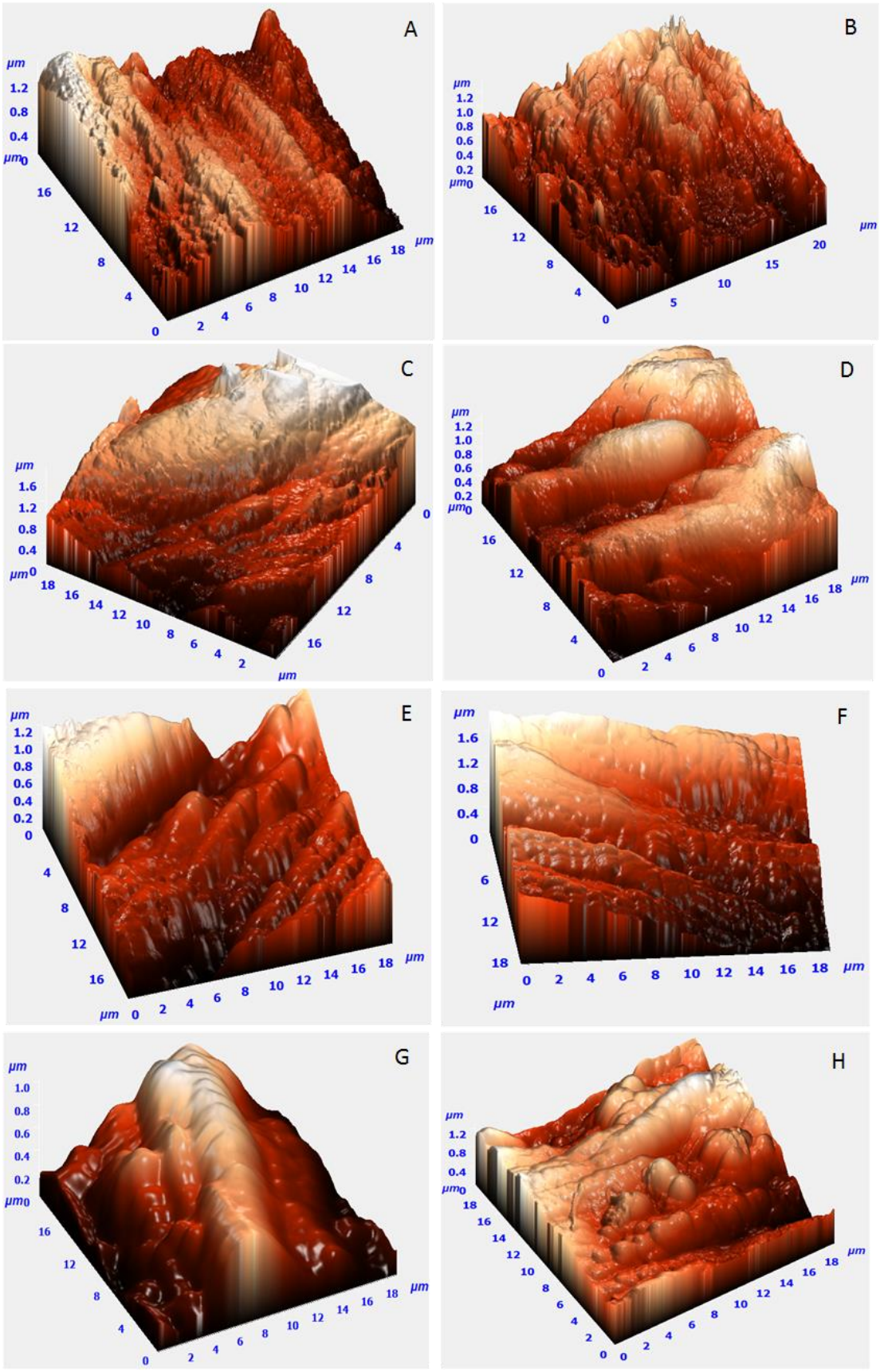

Figure 4- 11. AFM images of (A) Cu substrate, (B) Ni-P without additives, (C) Sac. 2.5, (D) Gly. 0.1, (E) Pyr. 0.1, (F) Cou. 5m, (G) Cit. 4, and (H) Ce. 8m.

Table 4- 8. Average roughness of the chosen samples obtained by AFM

Sample	Average Roughness Sa (nm)	Root mean square Sq (nm)
Cu Substrate	216	272
No additives	341	410
Sac. 2.5	343	407
Gly. 0.1	207	246
Pyr. 0.1	155	219
Cou. 5m	310	383
Cit. 4	213	249
Ce. 8m	191	238

- Effect of saccharine as an additive

The adsorption of additives on the surface of the cathode is reported to affect the activation energy, charge transfer rate in the electrochemical reactions, and electro-crystallization mechanism. Therefore, introducing additives to an electrodeposition bath affects the deposition procedure, and thus, the properties and structure of the obtained coatings [20]. Saccharine is one of the most used brightening agents in the electrodeposition of nickel. Its effect on the brightness of the coatings comes from its ability to refine the grains and increase the cathode polarization. Amorphous films with lower P content can be obtained in the presence of saccharine, because saccharine adsorbs on the cathode surface, limits the number of deposition sites and obstructs the surface diffusion of Ni. As a result, multi-phase deposits can be formed when saccharine is present in the electrolyte. Moreover, the addition of saccharine can also improve the physical properties of the coating because it can inhibit the discharge of protons on the cathode surface [21] and thus it suppresses the hydrogen evolution reaction during the deposition process [10]. It is also reported that saccharine decreases the internal stress of Ni-P coatings, however, the segregation of sulphur into the grain boundaries can increase the internal stress again in high concentrations [19].

Our results show that even though the instantaneous corrosion resistance has been improved (especially Sac. 2.5), the general corrosion behavior could not be considered appropriate due to the following reasons. The cathodic slopes are lower in the presence of saccharine meaning

a higher cathodic reaction rate. The oxidation current densities at the end of experiments are relatively high (and thus the corrosion efficiency is low at high potentials). The surface of the coatings have uniformly blackened after the corrosion process, and have completely dissolved at saccharine concentrations above 1 g/L (Figure 4- 5). In the case of Sac. 2.5, the coating has a low P content (1.8 wt. %), and a mixed crystalline-amorphous structure. The crystallinity of coatings should be enhanced with increasing saccharin concentration, since it hinders the incorporation of P. Moreover, the common defects of a polycrystalline layer, like grain boundaries, can act as high-speed pathways for the diffusion of copper to the surface during the corrosion process, especially at high potentials [15]. Therefore, a galvanic corrosion phenomenon between nickel in the crystalline state (anode) and the amorphous state (cathode) could be the reason of the blackening/dissolving of the layer in the presence of low/high concentrations of saccharine. This could be also supported by the fact that saccharine shifted the corrosion potentials compared to the Ni-P one. Moreover, Murugan et al. [16] have reported that eliminating the Ni(crystalline)/Ni-P(amorphous) interface has improved the corrosion performance of stacked layers. This could be easily extended to our results as well.

Therefore, employing saccharine as an additive, especially for microelectronics where there is a porous gold topcoat, can lead to the fast corrosion of the barrier layer, and hence its usage should be avoided for Ni-P thin films.

- Effect of glycine as an additive

Glycine is another brightener that can be introduced to the electrolyte. It can act as a buffering and complexing agent, and thus, improve the corrosion behavior, increase the brightness, and modify the structure [10,11,20]. Regarding our results, glycine as an additive efficiently improved the corrosion resistance of Ni-P thin films; however, a further increase of its concentration had a negative effect, i.e. the corrosion efficiency decreased by 10%-15% by increasing its concentration from 0.1 to 5 g/L based on the Tafel (EIS) data. In comparison to

the film with no additives, the coatings possessed a higher anodic slope (β_a) representing a slower anodic dissolution of nickel ions. However, the β_a value decreased with increasing glycine concentration, meaning a faster dissolution of Ni in the presence of more glycine. This result is in agreement with the data of Guo *et al.* [22], who used cyclic voltammetry to study the deposition of Ni-Mn films with glycine as complexing agent and showed that the dissolution of Ni occurs faster in the presence of glycine. The Ni-P coatings present lower cathodic slopes meaning a higher hydrogen evolution rate. The obtained polarization and charge transfer resistances from the corrosion tests show that glycine in low concentrations, i.e. 0.1 g/L, can improve the corrosion efficiency of Ni-P thin films. As it can be seen in Figure 4- 5, the coated samples have kept their appearance after corrosion tests up to a glycine concentration of 2.5 g/L. At higher concentrations, the surface blackened and the film dissolved mostly at the edges. The EDS analysis showed that glycine, similar to saccharine, can reduce the P content: it decreased from 14.6% at 0.1 g/L glycine to only 6.4 % at 2.5 g/L of glycine. Therefore, the same galvanic corrosion phenomenon, however in less extent compared to the saccharine samples, occurred and the surface of the samples blackened in high concentrations. By taking the corrosion efficiency at high potentials into account, it can be concluded that the coatings undergo a fast dissolution at high potentials in concentrations above 1 g/L of glycine.

- Effect of pyridinium propyl sulfonate as an additive

Pyridinium propyl sulfonate (PPS) is an active sulphur containing organic compound that is reported to have a powerful effect on the brightening of Ni deposits. It was classified as an auxiliary brightener, and it is effective when it is used in a low concentration (0.1- 4 g/L) [9]. Its usage for Ni-P coatings, however, is not reported so far. Based on the extracted data from corrosion tests, the use of PPS as an additive in low concentrations, i.e. 0.1 g/L, led to an improvement of the corrosion performance of Ni-P thin films. However, its effect was diminished by increasing the concentration; the corrosion efficiency decreased about 15% by

the increase of PPS concentration from 0.1 to 4 g/L. This is especially evident for the corrosion efficiency at high potentials, where almost a 100% drop can be seen as the concentration increased. Moreover, exfoliation of the coatings during the corrosion process occurred in concentrations above 1 g/L (Figure 4- 5). Pyridinium presents a cationic nature when it is added to acidic solutions [23,24]. Therefore, it competes with metal ions during the deposition procedure and can suppress the cation reactions. As a result, the use of high concentrations of PPS can degrade the coating quality, including an easy exfoliation by weakening the bond strength between the substrate and the coating [25].

- Effect of coumarin as an additive

Coumarin is reported to lead to coatings with a shiny look, good conductivity, and proper mechanical properties. However, it is known to highly increase the internal stress and brittleness, and hence, its concentration should be kept as low as possible (0.005 – 0.2 g/L) [9,26,27]. Moreover, its toxic nature is another reason to use it only in low concentrations [28]. The results show that coumarin even used in very small quantities has improved the corrosion behavior. The corrosion efficiency of Ni-P thin films increased by about 25% (about 300% at high potentials) by adding 5 mg/L of coumarin; the Ni-P films kept their appearance after the corrosion tests (Figure 4- 5). Meanwhile, the addition of 5 mg/L of coumarin increased the P content by 3.4% and such high P content gave Cou.5m an amorphous structure. However, no meaningful relation between the additive concentration and the corrosion resistance can be observed, possibly due to the small range of tested concentrations compared to the other additives.

- Effect of sodium citrate as an additive

Sodium citrate can act as brightening, leveling, and buffering agent in electrodeposition electrolytes, and thus, eliminates the need for other additives [12]. However, it is mainly known as a complexing agent, and thus, the deposition occurs from Ni ions in complex form, not free

ions. Higher bath stability, higher deposition rate, lower roughness, and better corrosion resistance are the reported effects of using sodium citrate as an additive for coatings [29–31]. Our results show that sodium citrate, which is relatively inexpensive, has interestingly improved the corrosion behavior of Ni-P films and their appearance was intact after the corrosion process. Moreover, 4.8% more P content was incorporated inside the Ni-P layer in its presence (4 g/L) that explains its amorphous structure. However, increasing the concentration from 4 to 20 g/L slightly decreased the corrosion efficiency.

- Effect of cerium sulfate as an additive

Finally, it has been reported that a slight addition of rare earth metals, such as Ce, Yb, and La, into deposition electrolytes refines the microstructure, decreases the grain size and improves the corrosion resistance of the obtained coatings. Rare metals tend to adsorb and form a thin film on the surface of the substrate - preferentially on crystal defects such as dislocations and grain boundaries - due to their unique 4f electron configuration, strong adsorption capacity, low electronegativity, and large atomic radius. Therefore, they decrease the amount of catalytic sites, hinder the electron transfer among ions, reduce the surface energy and increase the nucleation rate, which refines the deposited coatings. Moreover, it was demonstrated that rare metals are not incorporated inside the deposited film, and thus, they are not consumed during the process [8].

Our results show a better corrosion efficiency, both instantaneous and at high potential, and better appearance after the corrosion tests in the presence of cerium sulfate compared to its absence. The corrosion resistance notably increased by increasing its concentration to 8 mg/L; a further increase of concentration decreased the efficiency. This result is in accordance with Huang et al. [8], who suggested that a small amount of Ce ion addition decreases the defect density of coatings; however, they will also hinder the deposition of ions and lower the deposition rate. Therefore, they diminish the coating quality and corrosion resistance in high

concentrations. As conclusion, the effect of the addition of rare earth metals on the properties of the deposited coatings completely depends on their concentration.

- Comparison of the effects of each additive added in the selected concentration on the properties of thin Ni-P coatings

As a conclusion of the experiments described above, Sac. 2.5, Gly. 0.1, Pyr. 0.1, Cou. 5m, Cit. 4, and Ce. 8m were chosen as the best samples in each category with regard to the corrosion resistance.

By measuring the coating mass and its chemical composition, one can employ the following equation to calculate the coating efficiency [32]:

$$CE\ \% = \frac{mF}{It}\sum\frac{c_i}{n_i} \qquad (4\text{-}3)$$

Where m is the coating mass (g), F is Faraday's constant (96485 C/mol), I is the total current (A), t is the deposition time (s), c_i is the mass fraction of the element (Ni, and P), and n_i is the number of transferred electrons.

The measured mass, thickness, and coating efficiency of the chosen samples in each category are presented in Table 4- 6. It is obvious that introducing the additives to the electrolyte decreased the coating efficiency from 3.5% (Sac. 2.5) to 5% (Cou. 5m). Therefore, it can be concluded that employing the additives leads to coatings with higher corrosion efficiency and lower coating efficiency, respectively. Moreover, all the coatings are amorphous, except Sac. 2.5 that has a mixed crystalline-amorphous structure. Figure 4- 10 shows the cross-section of the Ni-P layer with no additive: it can be seen that a uniform compact coating has been formed. As it was suspected, the addition of these compounds have decreased the average coating thickness, i.e. from about 1 µm for Sac.2.5 to 1.7 µm for Gly.0.1 compared to the thickness of the Ni-P layer with no additives (Table 4- 6). However, the thickness variation has also decreased, meaning that a more uniform coating was formed in the presence of additives (1.01

µm for Ni-P vs. 0.16 µm for Gly.0.1). Furthermore, again except Sac. 2.5, they have higher P content, lower roughness, and better stability at high potentials compared to the Ni-P layer with no additives. Moreover, all the additives, including saccharine, decreased the porosity content, leading as the same time to an improvement of the instantaneous corrosion resistance.

Table 4- 8 shows that employing additives, except saccharine, can decrease the surface roughness from 31 nm (Cou.5m) to 186 nm (Pyr.0.1) with respect to their absence (341 nm). It is well known that coatings with higher quality and better properties form on smoother substrates, and the roughness of the substrate has an important impact on the physical properties of multilayer coatings [33,34]. Therefore, the ability of these additives to smooth the surface is especially important for electrical contacts where there is a gold top-coat. The porosity content of this top-coat is known to be the most important parameter determining the lifetime of microelectronic devices. It was reported that decreasing the substrate roughness from 0.4 µm to 0.2 µm decreased the electrographic porosity index of the gold layer by about ten times [35].

In order to investigate the relationship between the P content, the corrosion efficiency and coating efficiency of the amorphous Ni-P layers, the P content of the samples with glycine and cerium sulfate as additives was measured using the EDS technique. Figure 4- 12 depicts the P content, corrosion efficiency and coating efficiency of coatings with glycine and cerium sulfate as function of their concentration. While there is a similar trend for the corrosion efficiency and P content, there is no trend for the coating efficiency as function of the concentration of additives. Therefore, the P content definitely plays an important role in determining the corrosion behavior of amorphous Ni-P layers.

The combination of these additives, however, had a negative effect on the corrosion resistance of Ni-P films (Figure 4- 13). This limitation could be due to the synergistic effect of additives and also due to increasing the total concentration of additives inside the electrolyte.

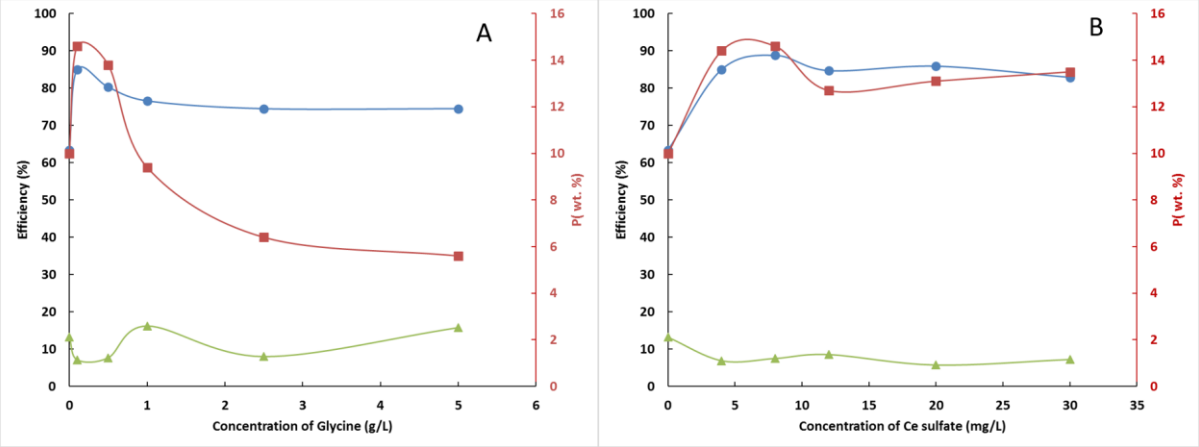

Figure 4- 12. Effects of the concentration of glycine (A) and cerium sulfate (B) as additives on the corrosion efficiency (—●—), coating efficiency (—▲—), and P content (—■—) of Ni-P layers.

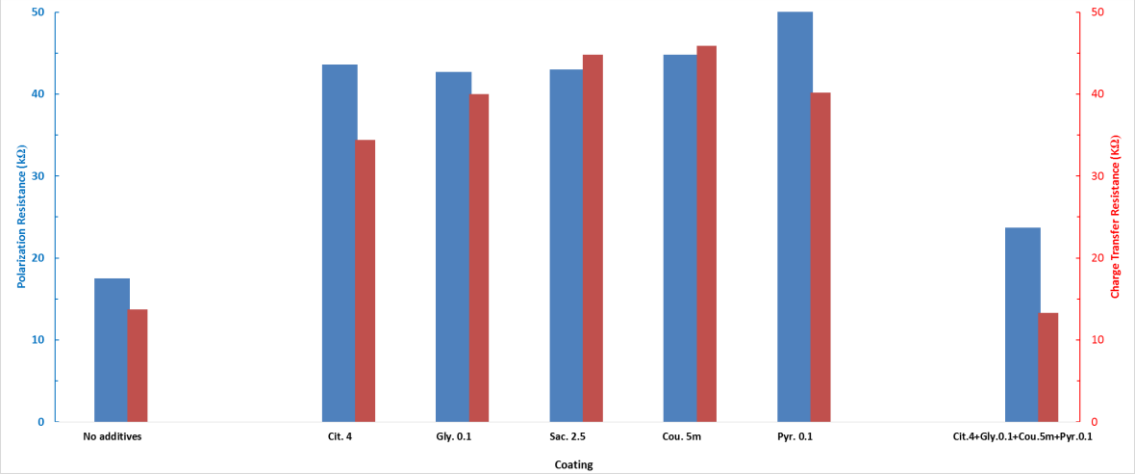

Figure 4- 13. Polarization resistance and charge transfer resistance of Ni-P films in the absence, presence of individual additives, and their combination.

4.3. An attempt to form composite Ni-P films

As explained in the chapter 2, composite films should provide higher wear and corrosion resistance. Thus, Experiments were carried out in order to form Ni-P composite films with TiO_2 nano-particles. In parallel aiming to form aesthetically pleasing blue colored filmsblue Cu pigments (Copper (II) phthalocyanine or Cu-Pc), were added in Ni bath. Note that Cu-Pc is one of the most common used pigments in painting and coating industries [36].

The main key to form composite films is to make electrolytes with stable dispersed particles. Therefore, 0.1 g/L of SDS (as an anionic surfactant), CTAB (as a cationic surfactant), and F-

27 (as a non-ionic surfactant) were added to the electrolyte to stabilize 1 g/L of TiO_2 and Cu-Pc. Figure 4- 14 shows the stability of these particles in the electrolyte after 30 minutes. TiO_2 particles were dispersed in water with a notably high stability in the presence of surfactants. However, they precipitated as soon as Ni ions were added inside the bath possibly due to the interaction between them and we chose to stop that project. Cu-Pc blue pigments, on the other hand, kept their stability even in the Ni-P deposition electrolyte.

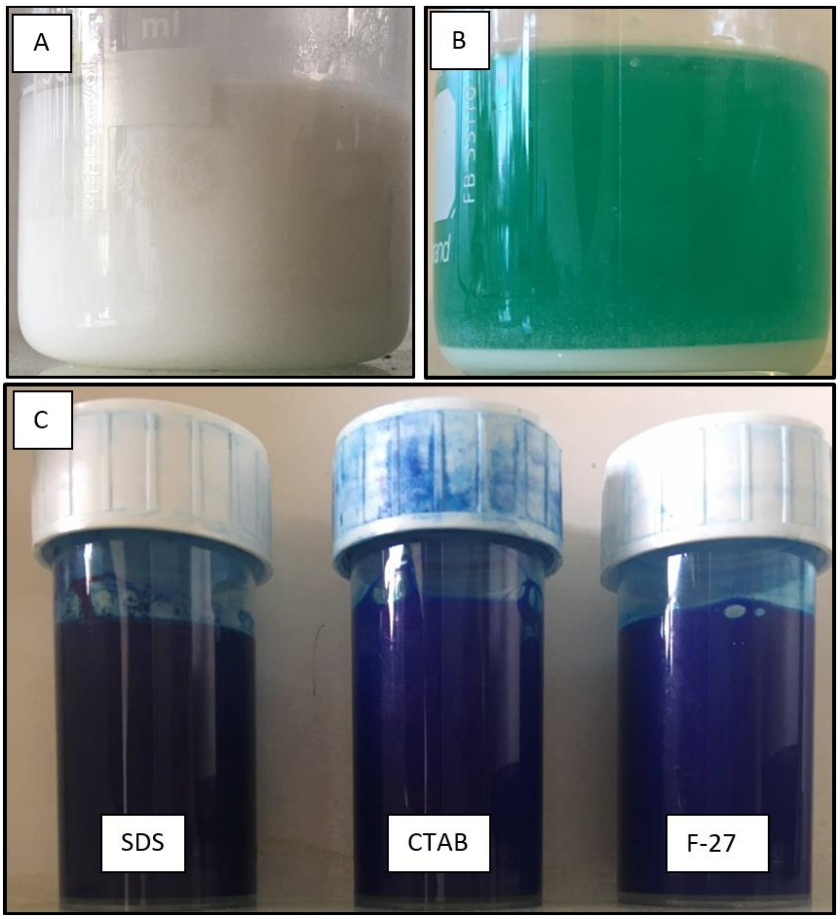

Figure 4- 14. (A) 1 g/L of TiO_2 + 0.1 g/L of surfactant in distilled water, (B) 1 g/L of TiO_2 + 0.1 g/L of surfactant in Ni-P deposition electrolyte, and (C) 1/g/L of Cu-Pc + 0.1 g/L of surfactant SDS in Ni-P deposition electrolyte after 30 minutes.

As a result, these Cu-Pc electrolytes were used to obtain colored films. The general aspect of the obtained films from the electrolytes containing Cu-Pc and surfactants are depicted in Figure 4- 15. Non-uniform blue films with notably bad qualities were obtained. To troubleshoot of this problem, the effect of surfactants on the Ni-P films was investigated.

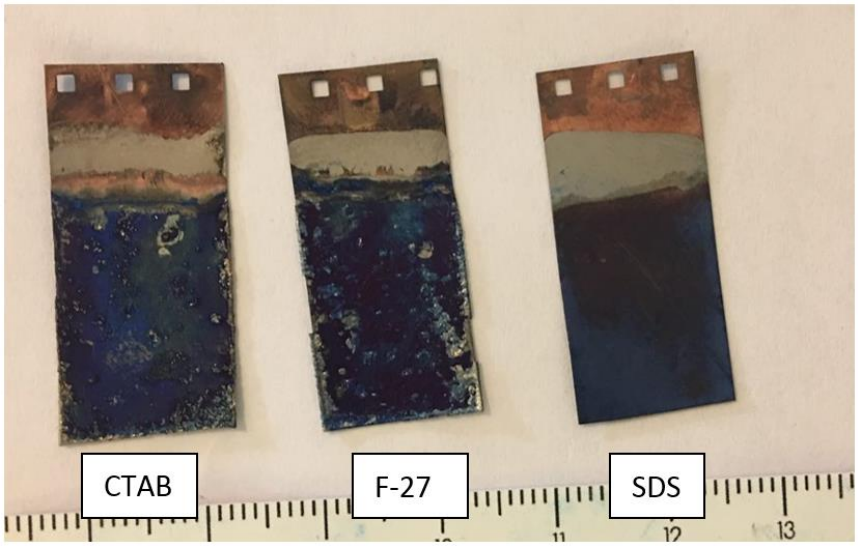

Figure 4- 15. Obtained films form the electrolytes containing Cu-Pc and surfactants.

- Effect of surfactants

The use of surfactants, as wetting agents, are claimed to improve the properties of deposited coatings due to decreasing the surface tension and hence easing the scape of hydrogen bubbles [3,21]. However, a gradual decrease in the quality of the films; i.e. general aspects (Figure 4- 16) and corrosion resistance (Figure 4- 17); was observed by the addition of surfactants and increasing their concentration.

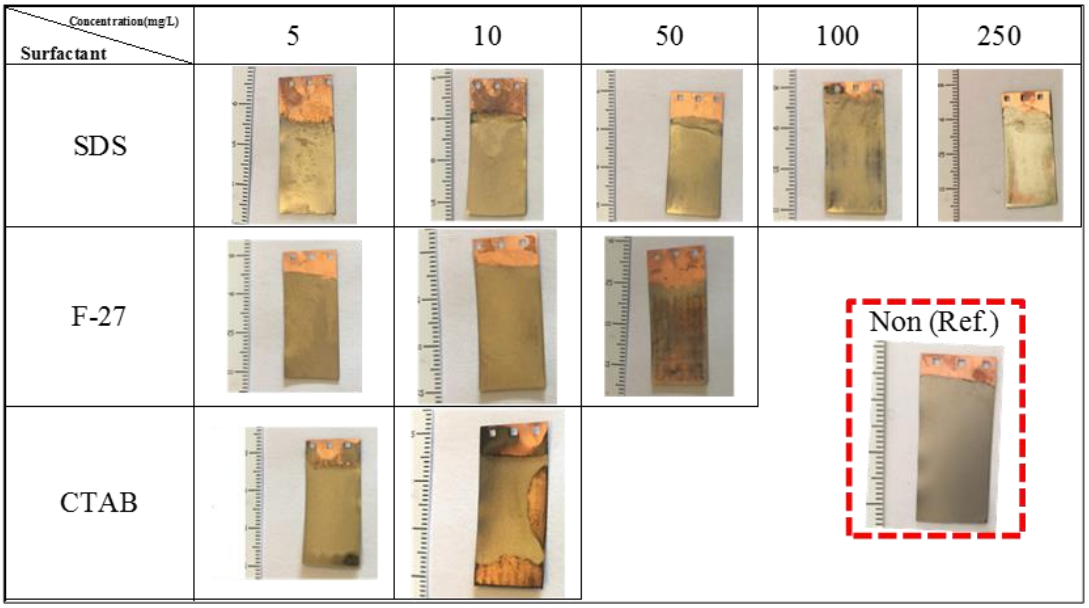

Figure 4- 16. General aspect of the obtained Ni-P films in the absence and presence of surfactants (SDS, F-27, and CTAB).

In fact, surfactants were strongly adsorbed on the surface of the working electrode and hence hindered the deposition of Ni ions. This behavior can be easily seen in formed coatings at high concentrations of surfactants. Moreover, CTAB competed with Ni ions over wining electrons [37] and thus led to a non-uniform films even at low concentrations (10 mg/L). As a result, these effects would justify the decrease of corrosion resistance and quality (also in the case of blue films) in the presence of surfactants.

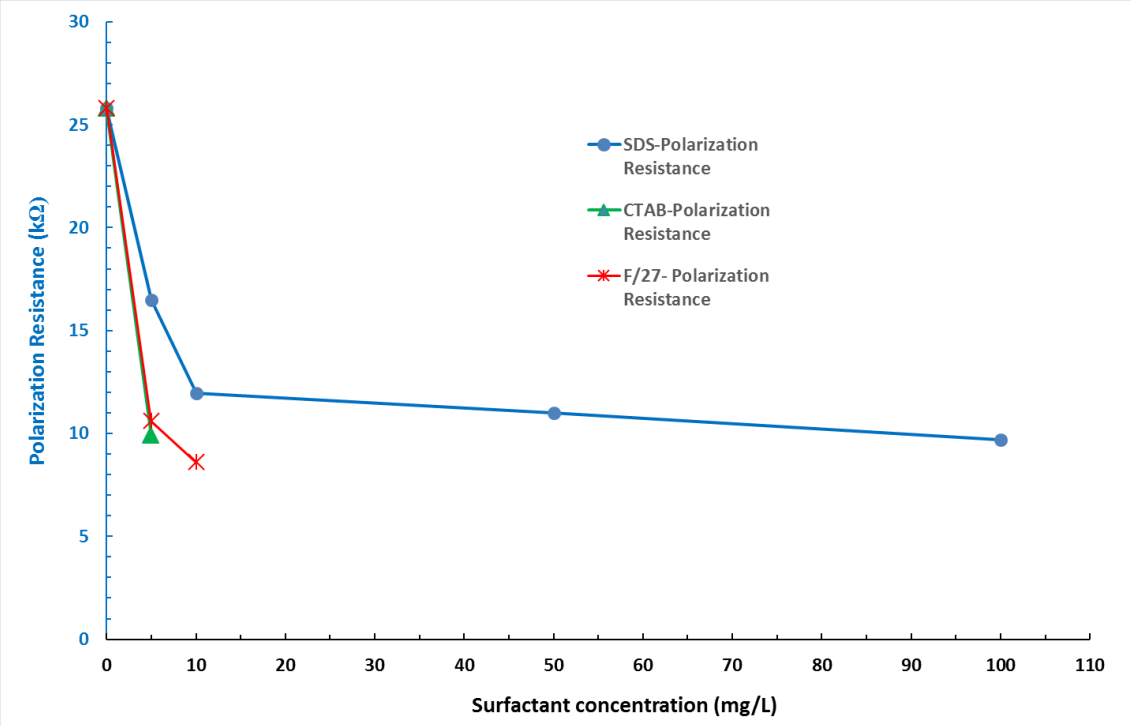

Figure 4- 17. The effect of the concentration of surfactants (SDS, F-27, and CTAB) on the polarization resistance of the obtained Ni-P films.

References

[1] R. Oriňáková, A. Turoňová, D. Kladeková, M. Gálová, R.M. Smith, Journal of Applied Electrochemistry 36 (2006) 957–972.
[2] C.A. Loto, Silicon 8 (2016) 177–186.
[3] G.A. Di Bari, Modern Electroplating 5 (2000) 79–114.
[4] Y. Yu, D. Yang, D. Zhang, Y. Wang, L. Gao, Applied Surface Science 392 (2017) 768–776.
[5] E.-S.M. Sherif, Applied Surface Science 252 (2006) 8615–8623.
[6] A.R. Madram, H. Pourfarzad, H.R. Zare, Electrochimica Acta 85 (2012) 263–267.
[7] A. Bahramian, K. Raeissi, A. Hakimizad, Applied Surface Science 351 (2015) 13–26.
[8] G. Liu, Z. Huang, L. Wang, W. Sun, S. Wang, X. Deng, Surface and Coatings Technology 222 (2013) 25–30.
[9] G.A. Di Bari, in: Modern Electroplating, John Wiley & Sons, Inc., 2010, pp. 79–114.
[10] C.D. Grill, I. Pötzelberger, J.P. Kollender, A.W. Hassel, Physica Status Solidi (A) 213 (2016) 1417–1426.
[11] R. Tarozaitė, Z. Sukackienė, A. Sudavičius, R. Juškėnas, A. Selskis, A. Jagminienė, E. Norkus, Materials Chemistry and Physics 117 (2009) 117–124.
[12] R. Oriňáková, A. Turoňová, D. Kladeková, M. Gálová, R.M. Smith, Journal of Applied Electrochemistry 36 (2006) 957–972.
[13] A. Bahramian, M. Eyraud, F. Vacandio, P. Knauth, Surface and Coatings Technology 345 (2018) 40–52.
[14] Z.H. Huang, Y.J. Zhou, W. He, Surface and Coatings Technology 320 (2017) 126–131.
[15] V.K. Murugan, Z. Jia, G.J. Syaranamual, C.L. Gan, Y. Huang, Z. Chen, Microelectronics Reliability 60 (2016) 84–92.
[16] V.K. Murugan, Z. Jia, G.J. Syaranamual, C.L. Gan, Y. Huang, Z. Chen, Surface and Coatings Technology 300 (2016) 95–103.
[17] H. Mazaheri, S.R. Allahkaram, Applied Surface Science 258 (2012) 4574–4580.
[18] J.R. Macdonald, W.R. Kenan, Impedance Spectroscopy: Emphasizing Solid Materials and Systems, Wiley, 1987.
[19] L. Chang, C.-H. Chen, H. Fang, Journal of The Electrochemical Society 155 (2008) D57.
[20] İ.H. Karahan, The Scientific World Journal 2013 (2013) 1–7.
[21] Z.H. Fang, CAS OpenIR (1997).
[22] J. Guo, X. Guo, S. Wang, Z. Zhang, J. Dong, L. Peng, W. Ding, Applied Surface Science 365 (2016) 31–37.
[23] H. Xing, T. Wang, Z. Zhou, Y. Dai, Journal of Molecular Catalysis A: Chemical 264 (2007) 53–59.
[24] X. Wang, J. Hao, Sci. Bull. 61 (2016) 1281–1295.
[25] S.W. Jiang, L. Yang, J.N. Pang, H. Lin, Z.Q. Wang, Surface and Coatings Technology 286 (2016) 197–205.
[26] Y. Li, H. Jiang, D. Wang, H. Ge, Surface and Coatings Technology 202 (2008) 4952–4956.
[27] S.T. Aruna, P.G. Lashmi, H.M. Seema, RSC Adv. 6 (2016) 11185–11192.
[28] Y. Tanaka, W. Fujii, H. Hori, Y. Kitagawa, K. Ozaki, Food and Chemical Toxicology 90 (2016) 1–9.
[29] M.S. Nur Ariffah, M.S. Nurulakmal, A.S. Anasyida, E.K. Shiu, Materials Science Forum 819 (2015) 97–102.

[30] G.-F. Huang, W.-Q. Huang, L.-L. Wang, B.-S. Zou, D.-P. Chen, D.-Y. Li, J.-M. Wei, J.-H. Zhang, Int. J. Electrochem. Sci 2 (2007) 321–328.
[31] X.-C. Wang, W.-B. Cai, W.-J. Wang, H.-T. Liu, Z.-Z. Yu, Surface and Coatings Technology 168 (2003) 300–306.
[32] X. Qiao, H. Li, W. Zhao, D. Li, Electrochimica Acta 89 (2013) 771–777.
[33] S.-H. Jeon, W.-I. Choi, G.-D. Song, Y.-H. Son, D.H. Hur, Coatings 6 (2016) 62.
[34] S. Lin, K. Zhou, M. Dai, F. Hu, Q. Shi, H. Hou, C. Wei, F. Li, X. Tong, Transactions of Nonferrous Metals Society of China 25 (2015) 451–456.
[35] M. Braunovic, N.K. Myshkin, V.V. Konchits, Electrical Contacts: Fundamentals, Applications and Technology, CRC Press, 2006.
[36] M. C. Staniford, M.M. Lezhnina, U.H. Kynast, RSC Advances 5 (2015) 3974–3977.
[37] S.W. Jiang, L. Yang, J.N. Pang, H. Lin, Z.Q. Wang, Surface and Coatings Technology 286 (2016) 197–205.

Chapter 5

Non-Aqueous Electrodeposition

This chapter is dedicated to the electrodeposition of (1) Ni barriers, (2) noble metal thin films, and (3) electropolymerization of MMA on the industrial samples (as the post-treatment) from a DMSO based electrolyte. There are three sub-chapters that deal with the mentioned subjects.

5.1. Ni barriers

As the first approach to deposit Ni alloys from DMSO, a DMSO based solution with the same chemical composition as the used aqueous electrolyte (S2) was prepared to electrodeposit Ni on a Cu substrate. The deposition parameters were the same as for the aqueous deposition, except that the deposition time was 20 minutes, the volume of the electrolyte was 50 mL and the solution was stirred at the speed of 400 rpm. However, a coating with a non-metallic black aspect was formed.

Figure 5- 1 shows the surface and cross-section morphologies of this black coating. The surface consists of several hierarchical island shape features that are regularly distributed everywhere. Such morphology (that is similar to the known lotus leave morphology [1]) highly decreases the light reflection and thus makes the surface look black. Moreover, it offers a high roughness that may increase the water contact angle. The cross-section shows several well-distributed nanometric island shape features on the surface. Moreover, the formed black film was notably adhesive since no cracks or delamination was observed at the interface of Cu and the coating.

The chemical composition of the film is summarized in Table 5- 1. The film is formed of a mixture of NiO and Ni-P. The high Cu content is due to the low thickness of the black film. DMSO can be incorporated inside the film [2] that justifies the presence of S and C.

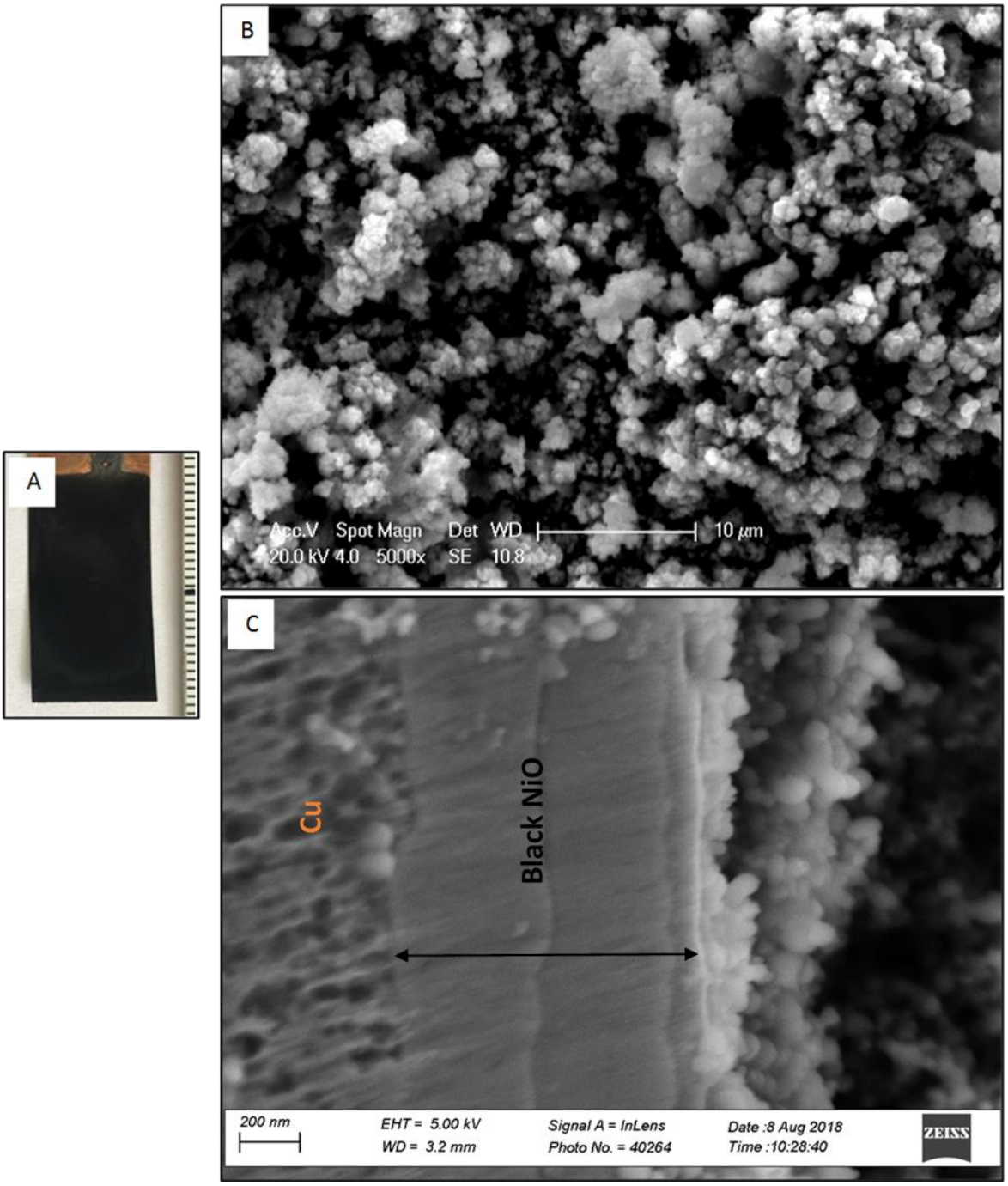

Figure 5- 1. (A) Black film formed on Cu from DMSO and its surface (B) and cross-section (C) morphology.

Table 5- 1. Chemical composition of the black coating before and after corrosion tests

Element	Before corrosion tests: Wt.%	After corrosion tests: Wt.%
C	3.6	3.2
O	11.0	13.9
P	2.6	2.8
S	7.8	8.8
Ni	61.8	56.2
Cu	13.2	15.1

The mechanism of the electrodeposition of NiO in DMSO was found to be described by the following equations in the absence (5-1) and the presence of low contents of water (5-2), respectively [2]:

$$Ni^{2+} + O^{2-} \rightarrow NiO \quad (5\text{- }1)$$

$$Ni^{2+} + 2OH^{-} \rightarrow Ni(OH)_2 \rightleftharpoons NiO + H_2O \quad (5\text{- }2)$$

Figure 5- 2 depicts the current density during the deposition of the film in DMSO. The current density for deposition from DMSO is notably lower than previously observed for Ni deposition from the aqueous bath. Therefore, it is kinetically favorable that the deposition starts from preferential sites of the substrate and continues on the same locations. Such type of 3-dimensional "island" growth (Volmer-Weber model) can lead to the formation of the rough surface.

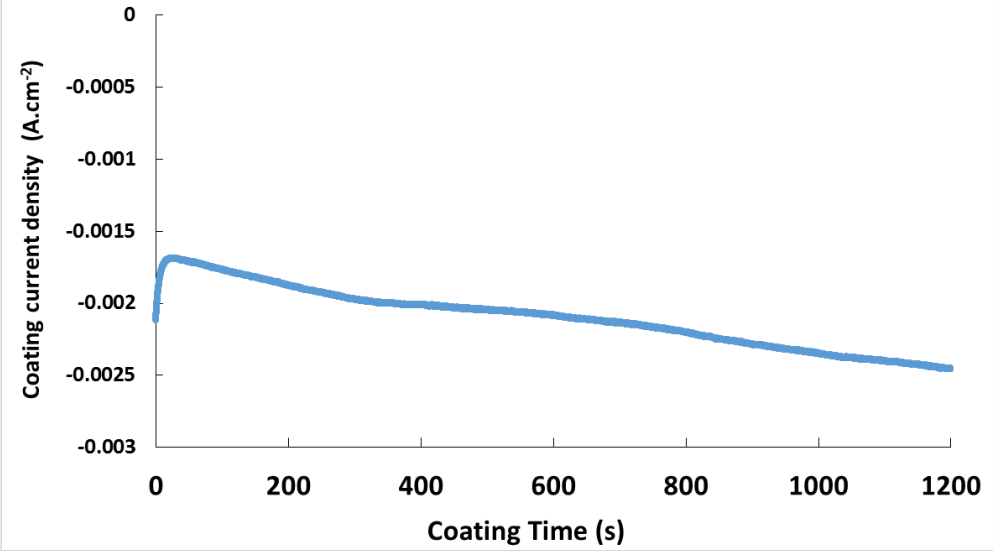

Figure 5- 2. Current density as a function of the coating time for a black film obtained in DMSO.

Figure 5- 3 shows the grazing incidence XRD pattern of the black film. A strong sharp peak at 43.5 º is attributed to the NiO (200) reflection (NiO presents a NaCl-type structure) [3,4]. The absence of any peak of Ni can be attributed to the amorphous nature of the Ni-P film. The average grain size D was estimated to be around 100 nm using Debye Scherrer's formula [3],

$$D = \frac{0.9\lambda}{\beta cos\theta} \qquad (5\text{- }3)$$

λ is the X-ray wavelength, β is the full width at half maximum of the peak, and θ is the diffraction angle. The grain size of the black film is notably bigger than the previously reported values [3–5]. The formation of bigger grains might be related to the low deposition rate from DMSO.

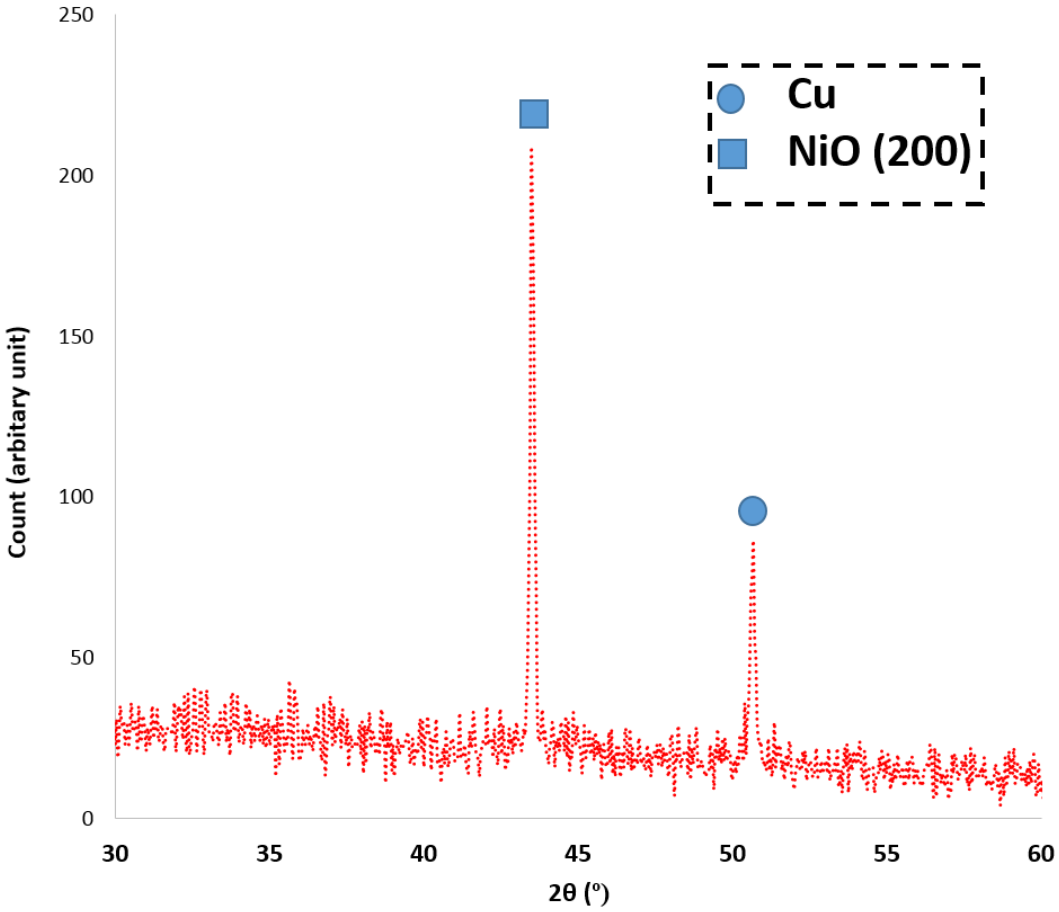

Figure 5- 3. Grazing incidence XRD pattern of the black coating.

The water contact angle of the Cu substrate and the black film are shown in Figure 5- 4. The contact angle values for the Cu substrate and the film were 83 ± 6° and 161 ± 3°, respectively. Therefore, applying the black NiO film changed the hydrophilic Cu surface to a superhydrophobic surface.

The hydrophobicity of these films was previously found to be due to the roughness of the surface [6]. The superhydrophobicity of the surface comes from the heterogeneous wetting, which means that the trapped air prevents the liquid from penetration [7]. This can be expressed by the following equation:

$$cos\,\theta^* = f(1 + cos\,\theta) - 1 \qquad (5\text{- }4)$$

Where f is the area fraction of the droplet in contact with the solid (and thus 1-f is the area fraction of the droplet in contact with the trapped air), and θ^* and θ are the contact angles of the rough coating and the substrate (or flat surface). The f value calculated for the black NiO film is 0.049: it has a very low wetting ability, notably lower than some previously reported values for superhydrophobic Ni films (0.25 [8], and 0.13 [9]).

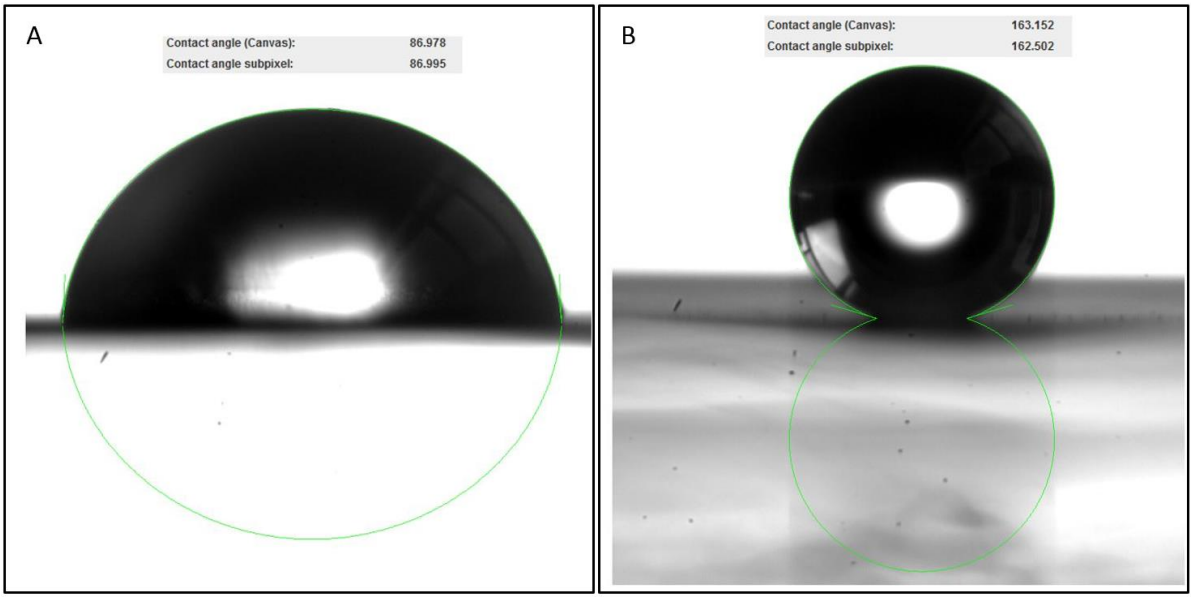

Figure 5- 4. Contact angle between a 2µL water droplet and (A) the Cu substrate, (B) the black NiO film.

The impedance spectrum of the black NiO film is depicted in Figure 5- 5. The film presents one time constant in its EIS data. The analyzed data of the black NiO film and Cu substrate are presented in Table 5- 2. The thin black NiO film increased the corrosion resistance of the substrate about two times.

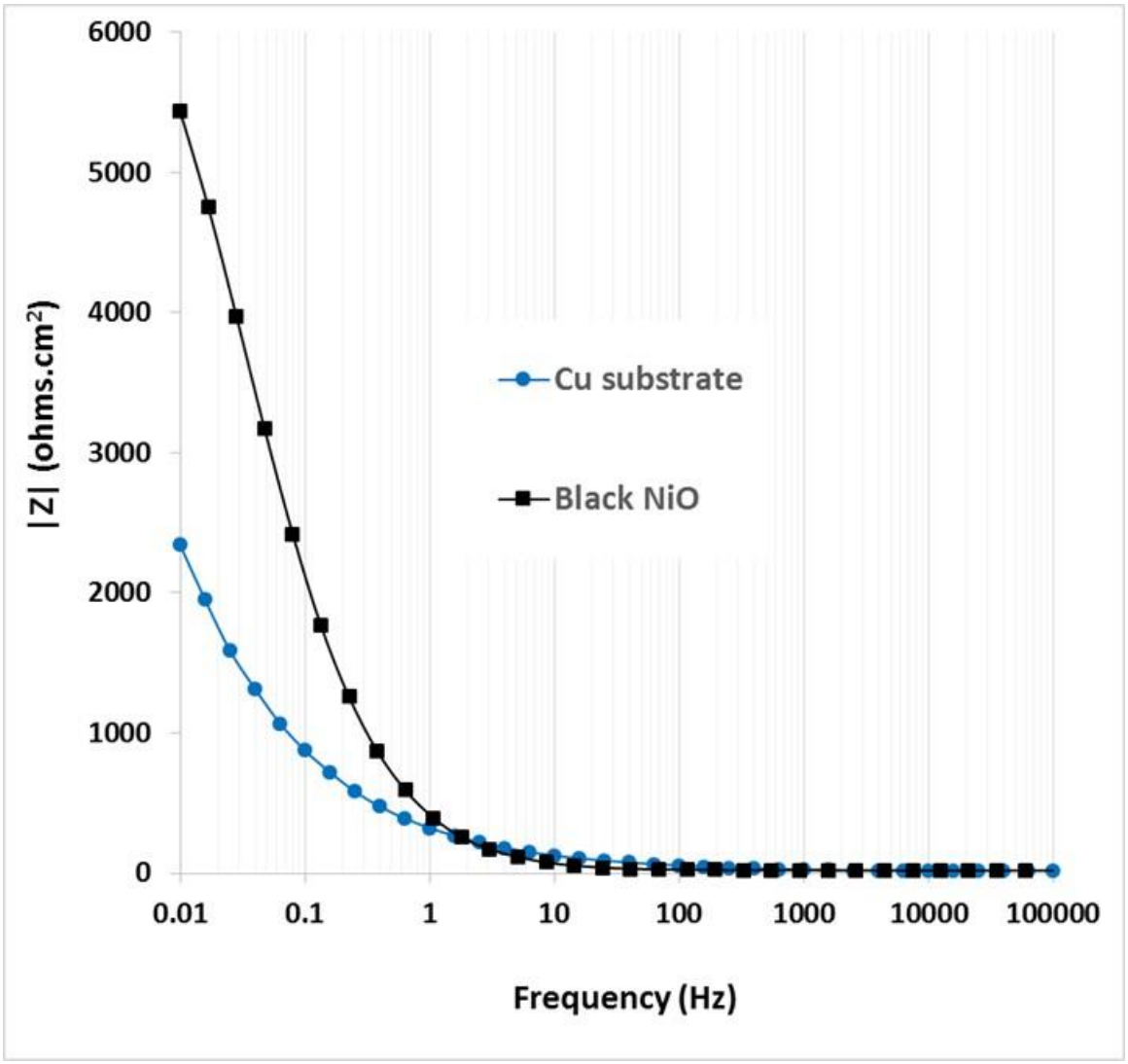

Figure 5- 5. Bode Z plots of the black NiO films and the Cu substrate.

Table 5- 2. Impedance values (at 0.1 Hz) of the black NiO film and Cu substrate

Sample	|Z| at 0.01 Hz ($k\Omega.cm^2$)
Black NiO	5.4
Cu Substrate	2.3

Figure 5- 6 shows the Tafel plots of the black NiO film and its Cu substrate. In comparison with the Cu substrate (Table 5- 3), the black NiO film notably shifted the corrosion potential (+155 mV) to more anodic regions. This means a significant decrease in corrosion inclination [10]. The corrosion current density (3.3 and 1.6 $\mu A.cm^{-2}$ for Cu and black NiO, respectively) again shows two-times increase in good agreement with EIS results. The black NiO coating

presents especially a lower current density at high potentials showing its high chemical stability.

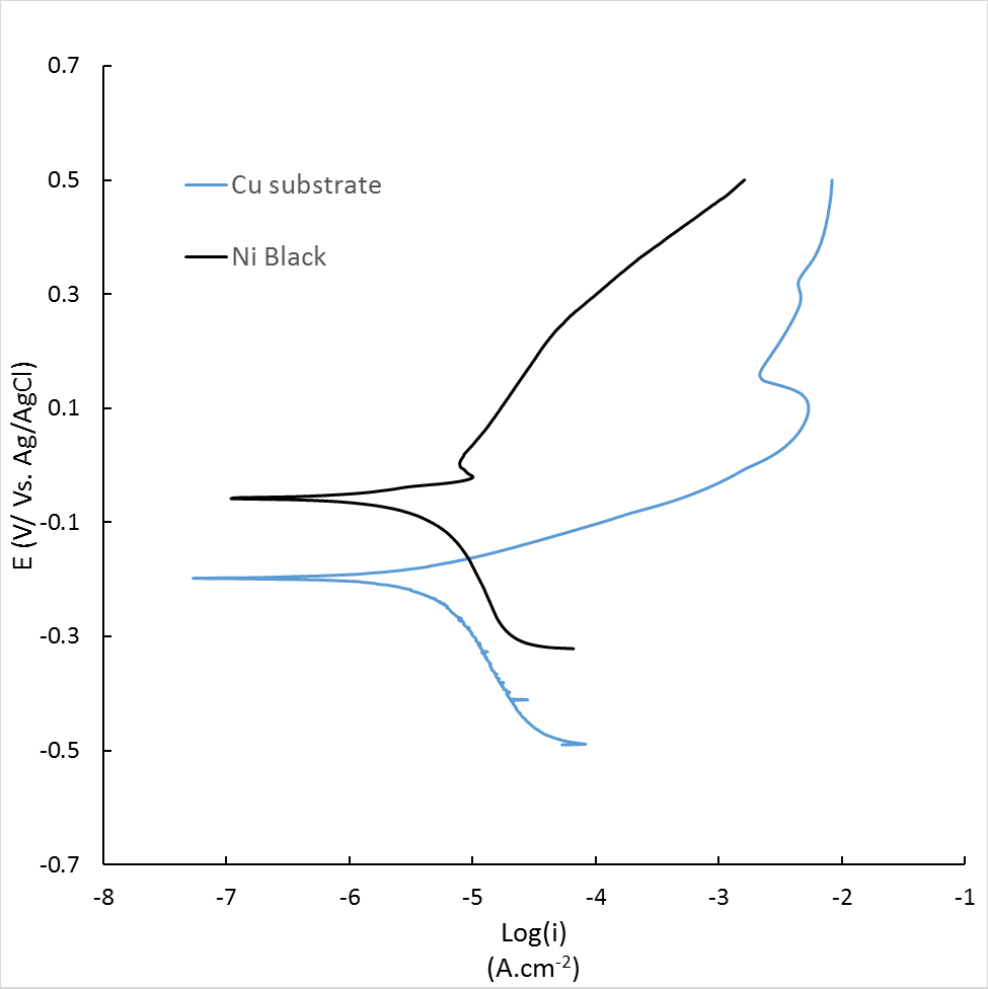

Figure 5- 6. Tafel plots of the black film and the Cu substrate.

Table 5- 3. Corrosion current density and corrosion potential of the black NiO film

Sample	i_{corr} ($\mu A.cm^{-2}$)	E_{corr} (mV) vs. Ag/AgCl
Black NiO	1.64	-45
Cu Substrate	3.32	-200

Figure 5- 7 shows the aspect and the surface morphology of the black NiO after the corrosion tests: the coating, obviously, is visually unchanged. The chemical composition of the surface after the corrosion tests is presented in Table 5- 1. Comparing the chemical composition of the black NiO film before and after the corrosion tests reveals that the amount of O increased, while the content of Ni is decreased. A part of the Ni of Ni-P was dissolved, which the surface

was enriched with other components (i.e. O and S), in agreement with the common corrosion mechanism of Ni films [10]. Therefore, the black NiO film has a high chemical stability and improved the corrosion resistance due to its superhydrophobicity. Unfortunately, this black coating had a high electrical resistance (2.8 Ω) that was notably higher than the accepted limit for electrical contacts (0.3 Ω). Moreover, the high roughness of this film would be definitely destructive if any noble metallic thin film be applied (since it will increase the porosity of the top-coat).

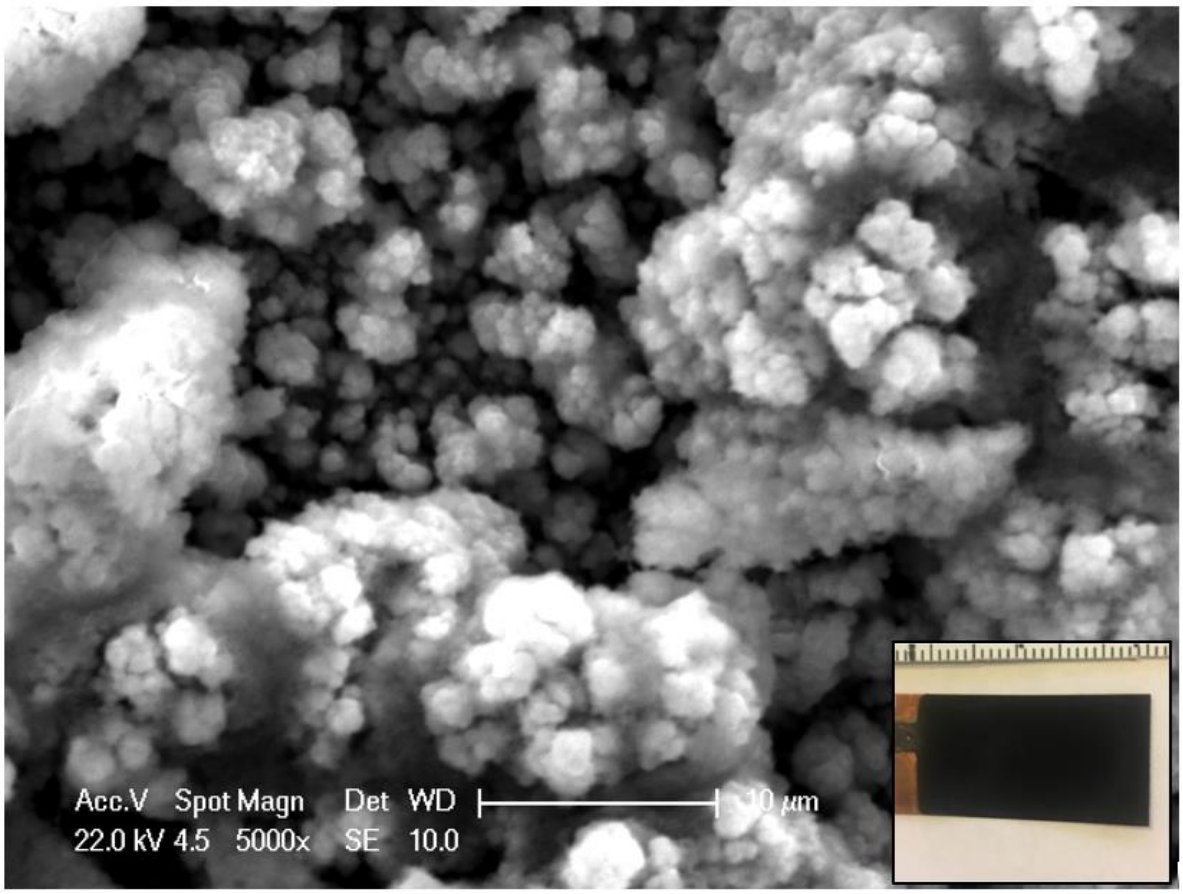

Figure 5- 7. The general aspect and surface morphology of the black film after the corrosion tests.

Ni films with metallic look was obtained only when the phosphorous acid (H_3PO_3) and phosphoric acid (H_3PO_4) in electrolyte were replaced by sodium hypophosphite ($H_2NaPO_2.xH_2O$) and sodium phosphate (Na_3PO_4), respectively. The results of the deposition of metallic Ni and Ni alloys is explained in the following.

5.1.1. Electrodeposition of Ni alloys from DMSO

A DMSO based electrolyte with the chemical composition of 190 g/L $NiSO_4.6H_2O$ + 10 g/L $NiCl_2.6H_2O$ + 8 g/L $H_2NaPO_2.xH_2O$ +8 g/L Na_3PO_4 + 16 g/L H_3BO_3 was used to deposit Ni at -1 V (vs. Ag/AgCl KCl sat.) for 1 hour, while the solution was at 60 ºC and stirred with the speed of 400 rpm. The alloys were formed by adding their salt to the introduced electrolyte; $AgNO_3$ (Ag as a more noble metal than Ni), $SnCl_2$ (Sn as a metal with similar potential to Ni), $ZnSO_4.7H_2O$ (Zn as a more cathodic metal than Ni), and $Na_2MoO_4.2H_2O$ (Mo as a metal that can be only co-deposited). The samples are named based on their alloying element and their added concentration: e.g. NiAg1 is the deposited NiAg alloy when 1 g/L of $AgNO_3$ was added to the deposition bath.

Figure 5- 8 shows the current density during the deposition of Ni, NiAg1, NiAg10, NiSn10, NiMo10, and NiZn10. Ni alloys with Ag and Sn deposited with a higher current density than Ni, but not those with Mo and Zn. This is due to the strength of ion complexes in DMSO. DMSO forms O-bonded complexes with Ni (2.11 Å), Ag (2.43 Å), Zn (2.10 Å), Mo (2.13 Å) [11], and Sn (2.17 Å) [12]. Larger complexes are easier to split and thus NiAg and NiSn alloys had higher coating current densities. All the alloys, except with Mo, had a higher mass gain. The slightly lower mass gain of NiMo could be due to the decreased deposition rate of Ni by induced co-deposition of refractory metals such as Mo [13,14]. NiZn10, on the other hand, had a lower current density but a higher mass gain than Ni. This means that Zn increased the coating current efficiency possibly due to the suppression of the hydrogen evolution reaction (HER) [15,16].

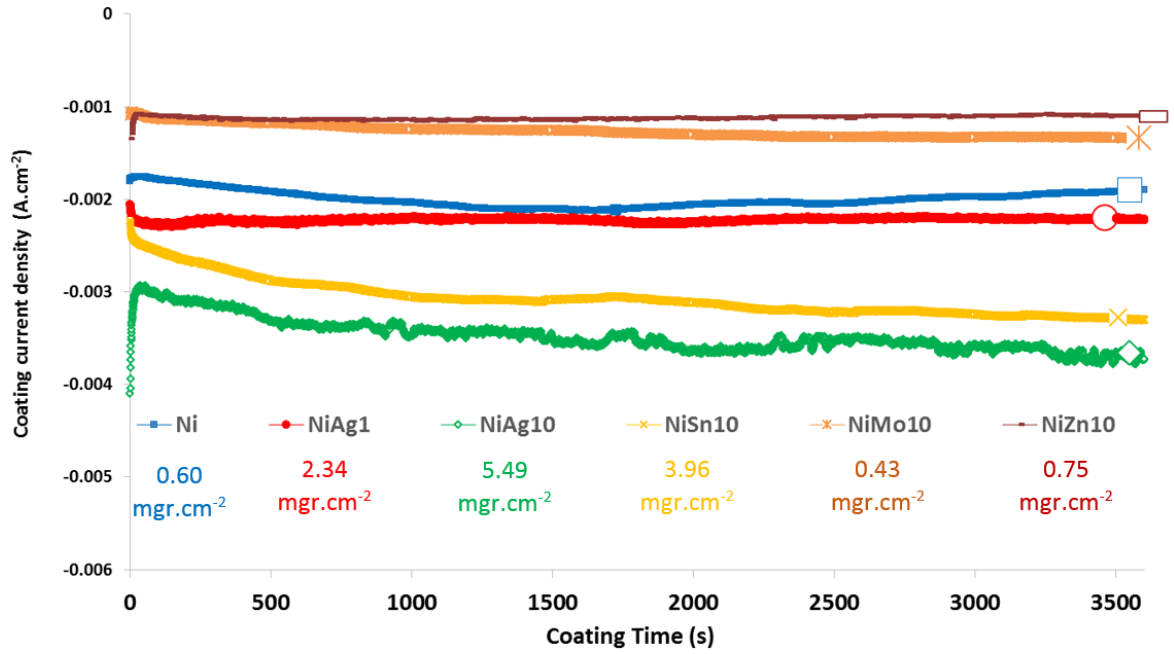

Figure 5- 8. The coating current density as a function of coating time for Ni and Ni alloy deposits from DMSO.

The surface morphology of the electrodeposited Ni and Ni alloys is presented in Figure 5- 9. Except the NiAg alloys (NiAg1 and NiAg10), all the samples had a typical morphology of Ni deposits with some pores visible on their surface that could be due to HER. NiAg1 and NiAg10, on the other hand, presented a 3D granular morphology that is typical for Ag films. There was about 4 wt.% S in the chemical composition of the Ni film showing that DMSO was trapped inside the coating. The weight percentage of alloying elements in the chemical composition of Ni alloys is depicted in Figure 5- 10. Ag and Sn had a notable presence in the deposited alloys possibly due to their nobler standard potential and more easily dissociated DMSO complexes. Possibly for the same reasons, Zn had a negligible content in the NiZn10 film. The overpotential was not high enough for the reduction of Zn ions, but these ions suppressed HER and thus NiZn10 had the lowest number of pores on its surface. It should be noted that the incorporation of P was negligible (less than 1 wt.%).

Cross-sections of the deposited films (Figure 5- 11) show that highly adhesive films were formed due to the lack of any cracks or delamination at the interface of coating/substrate. The

coatings, however, had various thicknesses: the thinnest one was Ni with about 400 nm thickness and the thickest one was NiSn10 with about 3.8 µm thickness. This observation can be attributed to the complex strength of ions in DMSO and their effect on HER. NiSn10 had a highly distributed pore network near its surface, but simultaneously the deposit was very dense near the interface with the substrate.

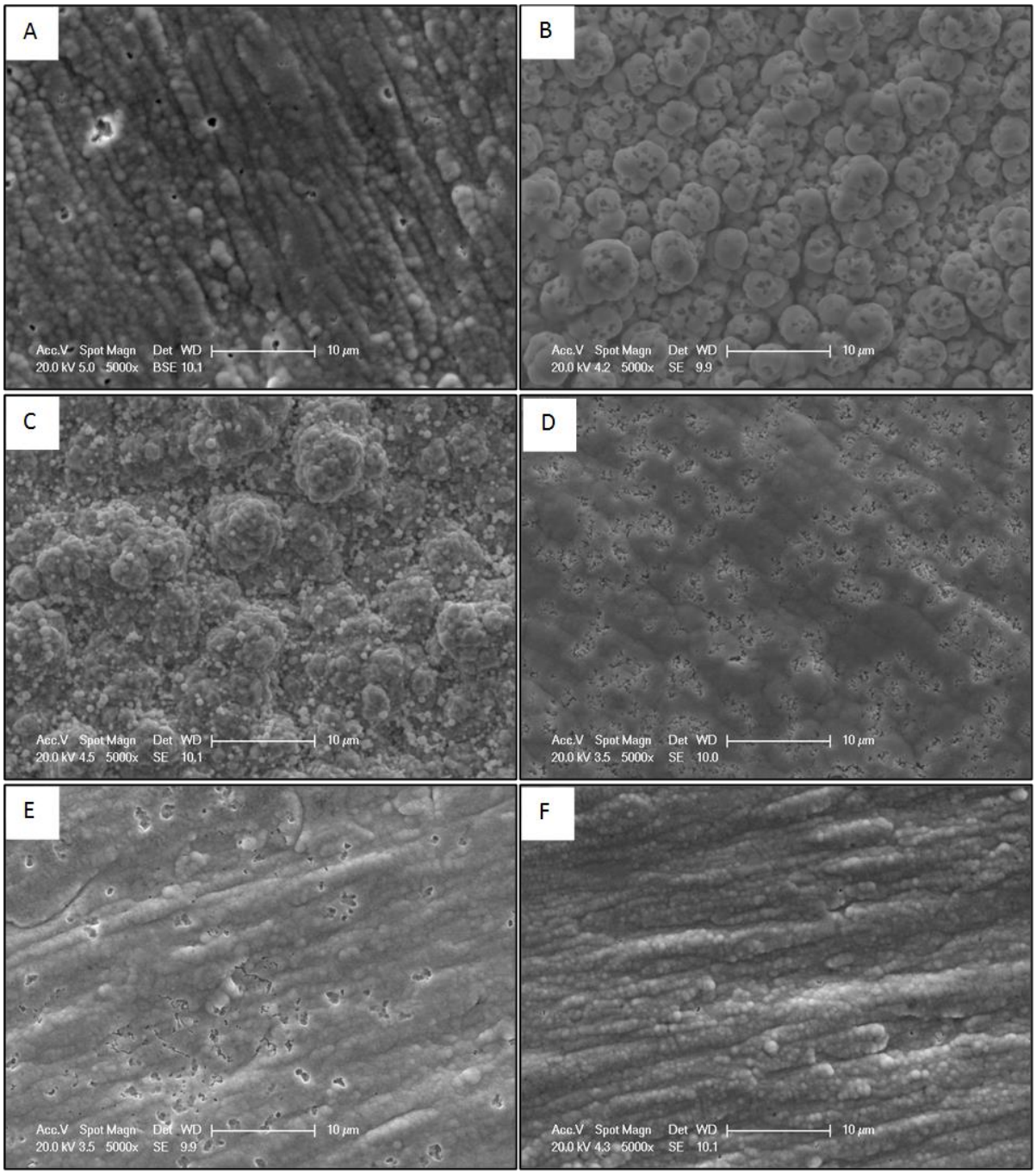

Figure 5- 9. Surface morphology of (A) Ni, (B) NiAg1, (C) NiAg10, (D) NiSn10, (E) NiMo10, and (F) NiZn10 electrodeposited films from DMSO.

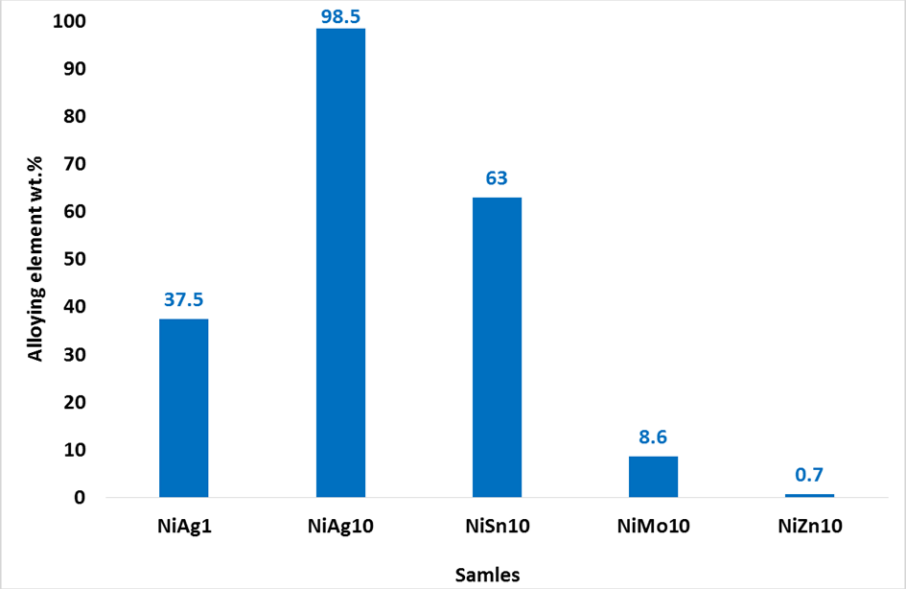

Figure 5- 10. The alloying element (wt. %) of Ni-X films obtained from DMSO.

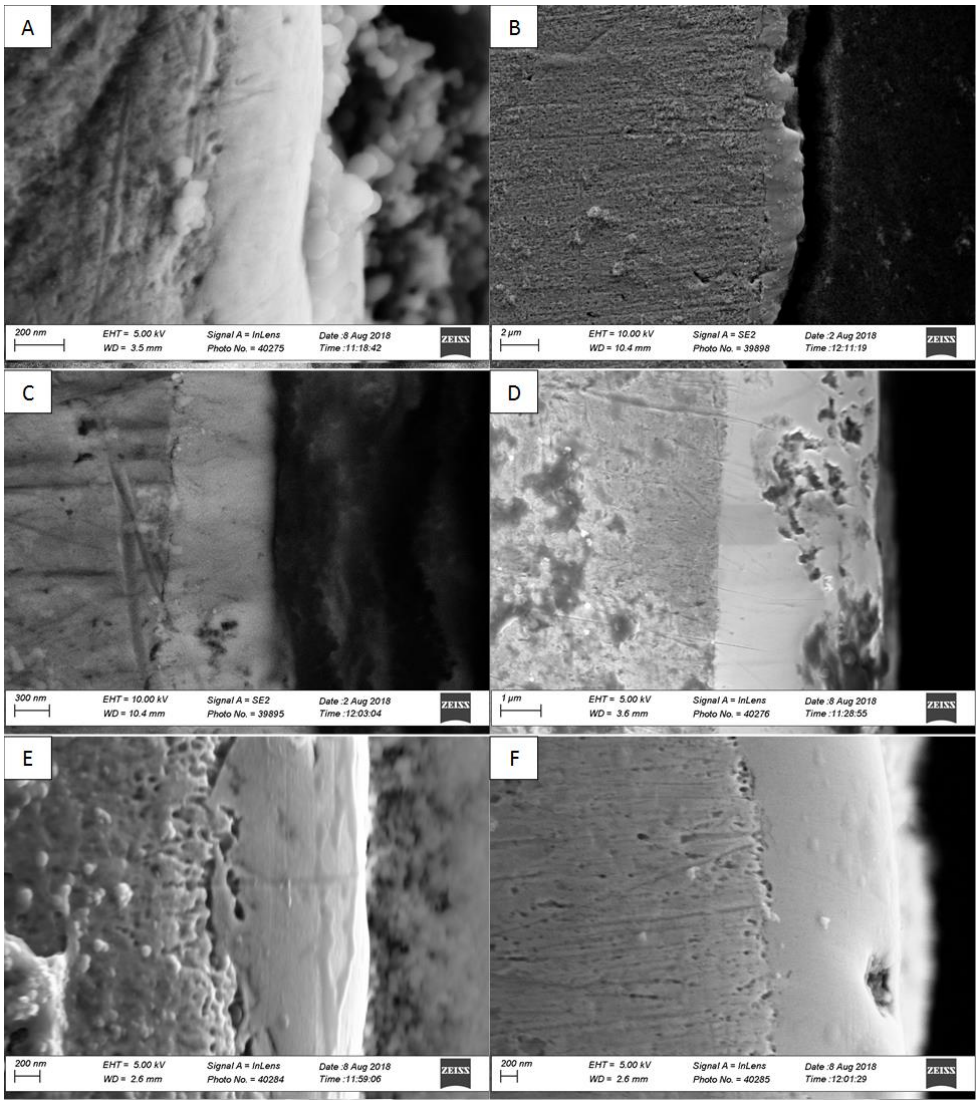

Figure 5- 11. Cross-sections of (A) Ni, (B) NiAg1, (C) NiAg10, (D) NiSn10, (E) NiMo10, and (F) NiZn10 electrodeposited films from DMSO.

Figure 5- 12 shows the grazing-angle XRD patterns of the Ni and Ni alloys deposited from DMSO. Ni, NiMo10, and NiZn10 had peaks related to Cu and Ni. Ni alloys with Ag presented peaks for Ni and Ag that are due to the formation of Ag-rich and Ni-rich zones [17]. However, NiSn10 had peaks related only to the NiSn intermetallic compound that is the common phase formed during the electrodeposition of Ni-Sn alloys [18]. Note that all the NiSn intermetallic compounds have very similar diffraction patterns [19]. The absence of Cu peaks for Ni alloys with Sn and Ag could be due to their higher thickness or higher x-ray adsorption. The crystallite size (D) of the films can be estimated by Debye-Scherrer's formula.

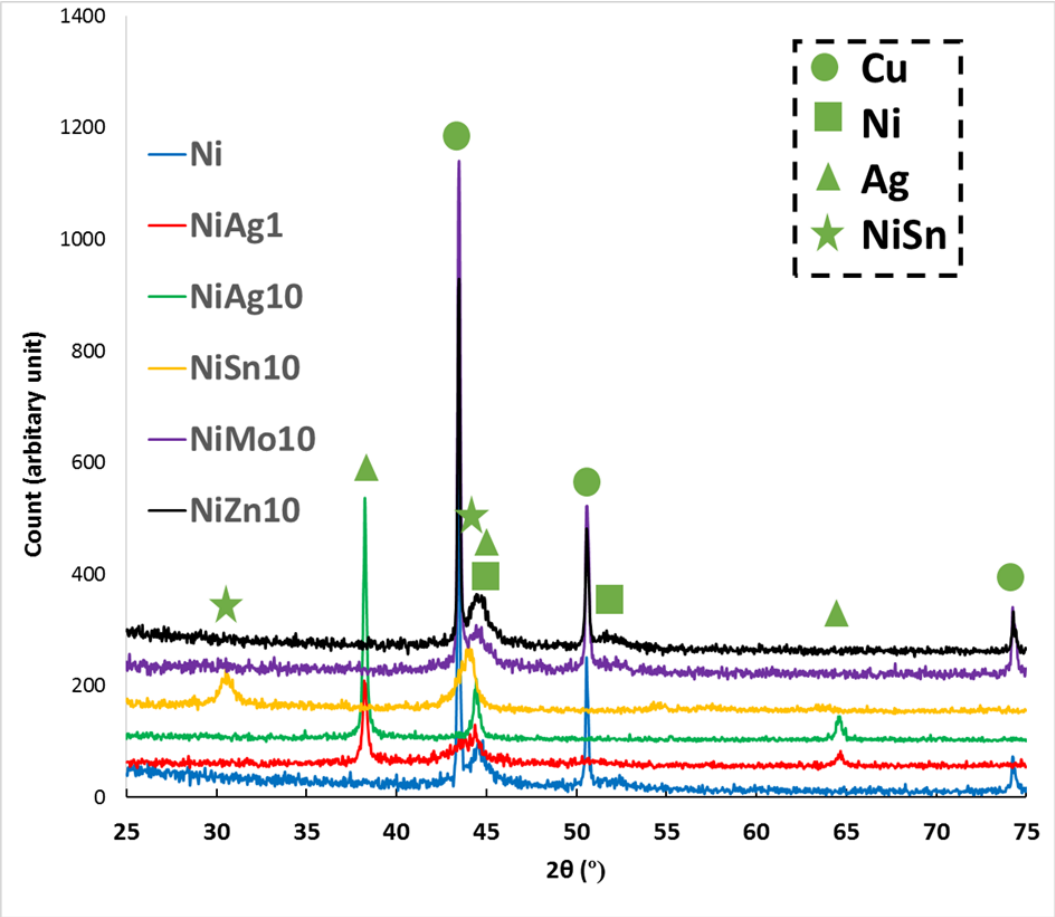

Figure 5- 12. Grazing incidence XRD patterns of Ni and Ni alloys electrodeposited from DMSO.

The Ni peak at 44.8 º for Ni (8.3 nm), NiMo10 (6.9 nm), and NiZn10 (7.4 nm) was used to determine the Ni crystallite size. Mo accumulates in the grain boundaries and decreases the

grain size of Ni deposits and even transforms its structure to amorphous at high contents [20]. The absence of any peaks for Mo or Zn could be due to their low content in the films. NiAg1, NiAg10, and NiSn10 had 30.0, 42.0, and 15.8 nm crystallite sizes, respectively, by analyzing the Ag peak (38.2 º) and NiSn peak (30.5 º). Ag and NiSn crystallites were larger possibly due to their easier reduction that favored the grain growth.

The EIS results of the Ni and Ni alloys deposited from DMSO after 60 minutes immersion in 3% NaCl are shown in Figure 5- 13. The obtained data are summarized in Table 5- 4.

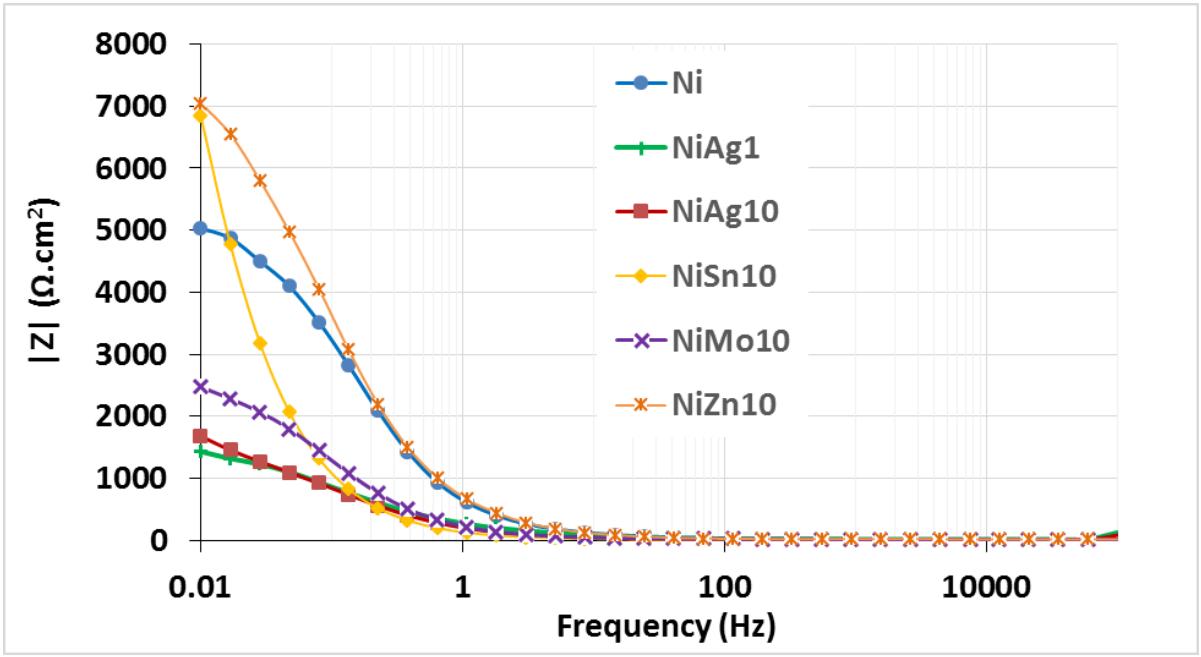

Figure 5- 13. Bode Z plots of the Ni and Ni alloys deposited from DMSO after 60 minutes immersion in 3% NaCl solution.

Table 5- 4. Impedance values (at 0.1 Hz) of the Ni and Ni alloy films obtained from DMSO

Sample	|Z| at 0.01 Hz ($k\Omega.cm^2$)
Ni	5.0
NiAg1	1.2
NiAg10	1.8
NiSn10	6.7
NiMo10	3.4
NiZn10	7.1

Considering the impedance values as the corrosion resistance, NiSn10 and NiZn10, had a higher corrosion resistance than Ni but NiAg1, NiAg10, and NiMo10 had a lower one. Ni-Sn films are known to offer a superior corrosion resistance compared to Ni [21] and thus it was expected for NiSn10 to have a higher R_{ct}. The higher R_{ct} value of NiZn10, however, is merely related to its smoother surface morphology and lower pore numbers not because of the deposition of Zn since the Zn content was negligible. Ni alloys with Ag, had a notably lower corrosion resistance probably due to the formation of galvanic coupling between Ag-rich and Ni-rich zones. NiMo10 had a slightly lower corrosion resistance than Ni. As it is mentioned above, NiMo10 had a slightly smaller grain size and thus more grain boundaries with accumulated Mo that can induce a galvanic coupling. Note that except NiZn10, all the samples had high capacitance values. This could be due to the presence of pores on the surface of Ni, NiMo10, and NiSn10 and the 3D morphology of NiAg1 and NiAg10 that offer a notably higher active surface area.

Figure 5- 14 shows the potentiodynamic curves of the Ni and Ni alloys obtained from DMSO, and all of the extracted data for the samples are presented in Table 5- 5. The polarization resistance results are in good agreement with EIS results. NiSn10 and NiZn10 coatings were superior. NiMo10 had a lower corrosion current density than Ni; however, it had also lower anodic slope and thus a faster dissolution. Mo increases the dissolution of Ni (lower anodic slope) and thus decreases the polarization resistance [20]. NiSn10, unlike other samples that were completely dissolved at high potentials (500 mV vs. Ag/AgCl), endured the corrosion tests and maintained its aspect. It showed a significantly lower current density at 500mV vs. Ag/AgCl compared to other coatings. This fact can be attributed to the formation of a dense $NiSnO_3$ oxide that gives Ni-Sn films a unique passivation even in the presence of Cl ions [21].

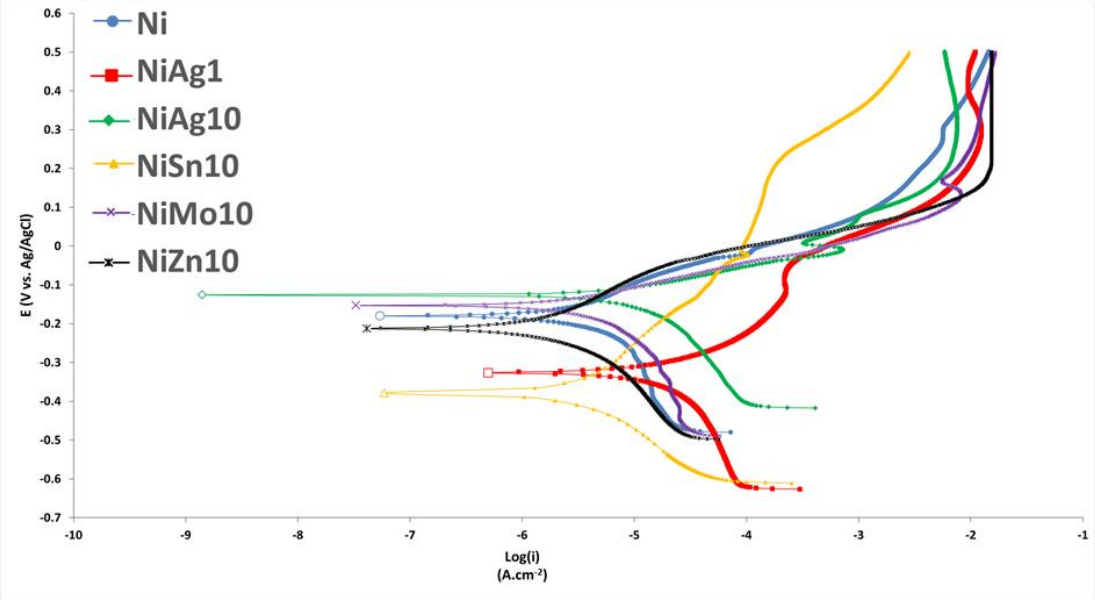

Figure 5- 14. Potentiodynamic polarization (Tafel) curves of Ni and Ni alloys deposited from DMSO after 60 minutes immersion in 3 wt% NaCl.

Table 5- 5. Corrosion current density and corrosion potential of the Ni and Ni alloys obtained from DMSO

Sample	i_{corr} ($\mu A.cm^{-2}$)	E_{corr} (mV) vs. Ag/AgCl
Ni	4.6	-153
NiAg1	23.0	-330
NiAg10	7.3	-121
NiSn10	3.1	-380
NiMo10	3.7	-172
NiZn10	2.0	-168

5.1.2. Electrodeposition of Ni composites from DMSO

We used three types of particles (see 2.4) to form composite coatings: (1) hard secondary phase particles such as TiO_2 nano-particles (NPs), (2) solid lubricating particles such as carbon nanotubes (CNTs), and (3) metallic particles such as Cu NPs. The key factor to form a composite film is to prepare a stable electrolyte with well-dispersed particles. As a result,

aqueous and DMSO-based deposition electrolytes with 5 g/L of TiO_2 NPs, CNTs, and Cu NPs were prepared and imposed to 60 minutes of ultrasonic agitation.

Figure 5- 15 shows the sediment height of the TiO_2 NPs, CNTs, and Cu NPs as a function of time for DMSO based and aqueous Ni deposition baths. CNTs had no stability in the aqueous bath, and TiO_2 NPs and Cu NPs precipitated very fast with Cu NPs being the most stable suspension. Dispersing NPs in aqueous Ni deposition electrolytes is highly challenging due to the interactions between the metallic ions and particles. The agglomeration of particles occurs even in the presence of surfactants; however, surfactants give soft agglomerated particles that can be kept in suspension using a mechanical stirrer [22]. The particles showed a high stability in the DMSO bath (less than 10% sedimentation after 24 hours). Non-aqueous electrolytes have a higher viscosity and a lower surface energy compared to water and thus they can easily wet and disperse the particles [23]. Therefore, DMSO had a good potential to be used in order to obtain composite films. Moreover, deposition of Ni-Polymer composite films is also generally limited to trapping the polymeric particles such as PTFE inside the Ni matrix [24–26]. To the best of our knowledge, the formation of these composites by simultaneous electrodeposition and electropolymerization has not been reported before. Phenol derivatives are among the most investigated insulating polymers for anti-corrosion properties [27,28]. Allyl Phenyl Ether (APhE) undergoes a monomer-isomerization polymerization at temperatures higher than 40 ºC [29]. The electropolymerization of APhE from DMSO has been recently reported for microbattery applications [30]. In this thesis, 5 g/L of APhE was added to the DMSO-based electrolyte with the purpose of forming Ni-Polymer (and also NiSn-Polymer) composite films.

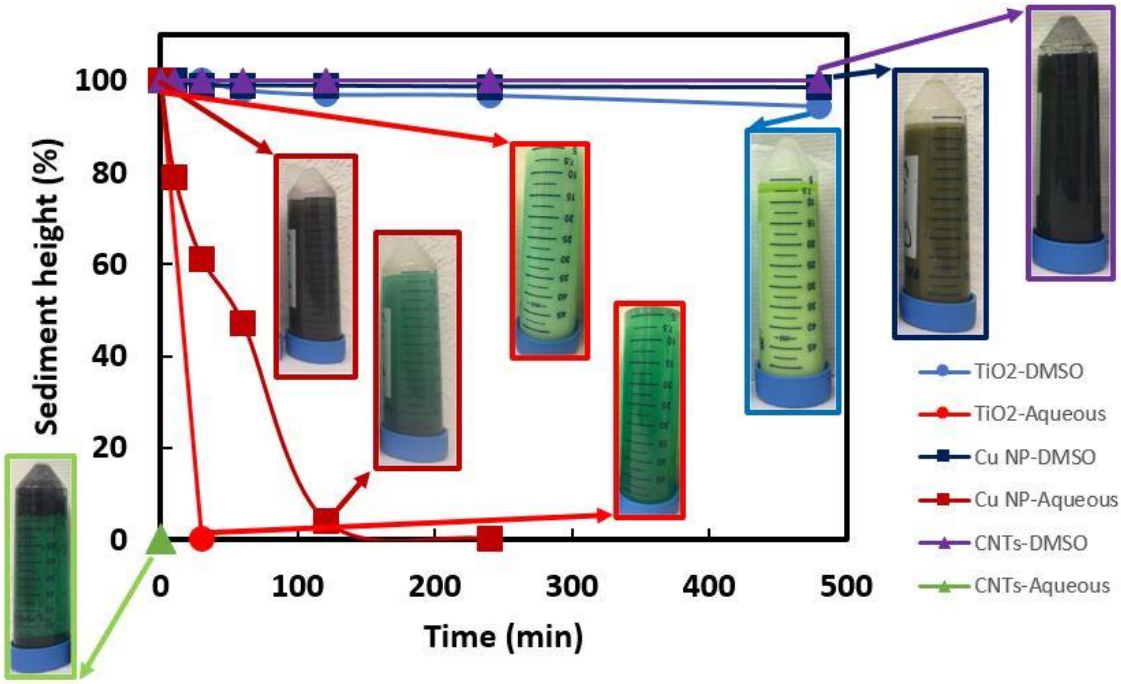

Figure 5- 15. Sediment height of TiO_2 NPs, CNTs, and Cu NPs as a function of time in DMSO based and aqueous Ni deposition baths.

The current density as a function of coating time for deposition of Ni in the presence and absence of particles is presented in Figure 5- 16. All curves are fairly similar. The mass gain (measured by reducing the mass of films before and after the deposition) of the Ni film was 0.60 $mg.cm^{-2}$ in the absence of particles but it increased between about 3 to 5 times in the presence of particles. These results suggest that particles may had a catalytic effect on the deposition and thus enhanced the deposition rate by increasing the current efficiency. The addition of APhE, however, decreased the coating current density of Ni and NiSn10. The mass gain of the composite films (0.75 and 3.79 $mg.cm^{-2}$ for Ni-5APhE and NiSn10-5APhE, respectively) were similar to deposited Ni (0.60 $mg.cm^{-2}$) and NiSn10 (3.96 $mg.cm^{-2}$).

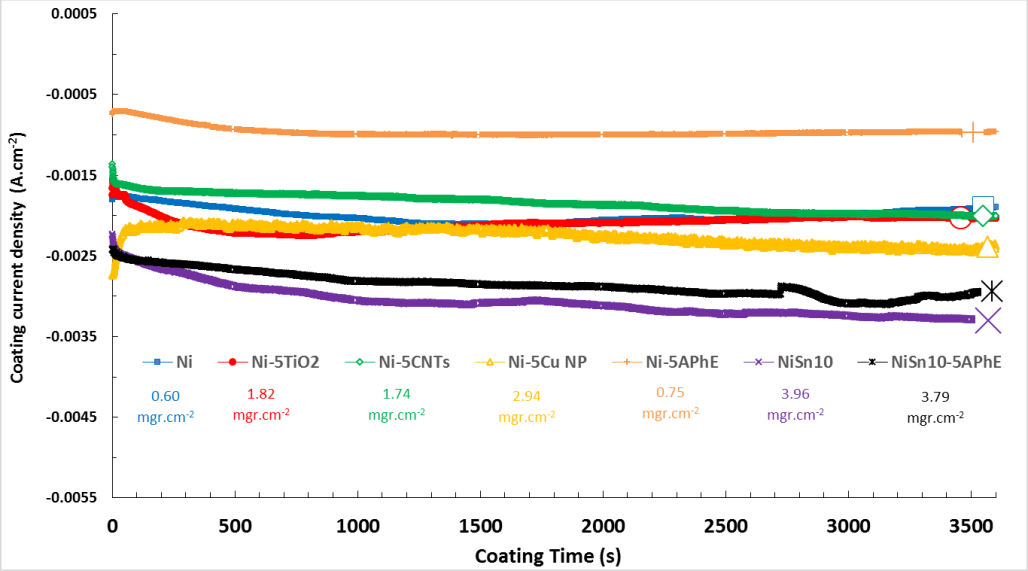

Figure 5- 16. Coating current density during the deposition of Ni in the absence and presence of particles.

The surface morphology of Ni deposits in the presence of particles is depicted in Figure 5- 17. There are a few pores visible in the absence of particles (Figure 5- 17A), but the number of pores is significantly higher and they are uniformly distributed at the surface in the presence of TiO_2 NPs and CNTs (Figure 5- 17B and C). The average size of the pores in the presence of particles was estimated to be 1.72 μm^2 by ImageJ. The coating with Cu NPs (Figure 5- 17D), on the other hand, showed a completely different morphology containing globular features. No significant effect on the surface morphology was observed in the presence of APhE for both Ni and NiSn10 samples (Figure 5- 17E and F).

The chemical composition of the Ni deposits in the presence of TiO_2 NPs and CNTs showed a negligible amount of composite elements (e.g. about 0.3 wt% of Ti). Therefore, it can be assumed that no or only few particles are embedded inside the growing film, which can be due to the low deposition rate from DMSO. Therefore, the particles cannot be trapped inside the growing deposit. These particles stay at the interface of the cathode and intensify HER as reported in [31,32] and especially for TiO_2 NPs [33–36]. Therefore, HER was intensified by TiO_2 NPs and CNTs during the deposition of Ni and led to the formation of a porous coating.

The obtained sample with Cu NPs had about 98 wt.% Cu in its chemical composition. No notable effect on the chemical composition was observed for APhE except that there was around 2 wt.% C in Ni-5APhE and NiSn10-5APhE. All the samples had S in their chemical composition showing that DMSO was trapped inside the films.

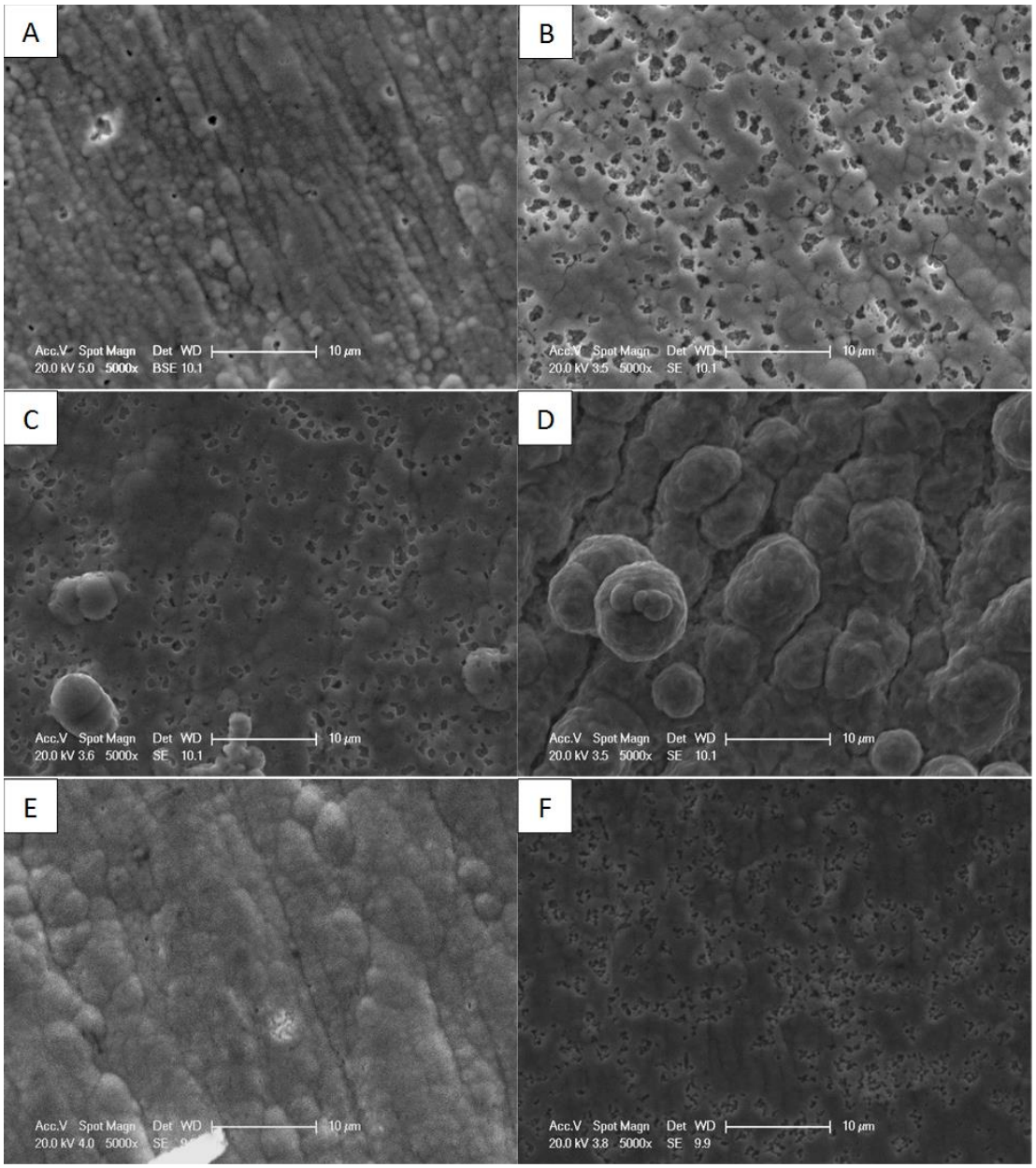

Figure 5- 17. Surface morphology of Ni deposits from DMSO in (A) absence of particles, or in presence of (B) TiO2 NPs, (C) CNTs, (D) Cu NPs, (E) APhE, and (F) NiSn10 in the presence of APhE.

The cross-section images (Figure 5- 18) shows that highly adhesive films formed on the surface of Cu. The coating in the presence of TiO_2 NPs was thicker (about 1.6 µm that is 4 times thicker than Ni films in the absence of particles), confirming the previous observation about the mass gain and the assumption that particles had catalytic effects. The addition of APhE led to the formation of thicker (almost twice) and more compact deposits. The simultaneous electropolymerization with electrodeposition can trap poly(APhE) inside the growing film and thus forms thicker and more compact films.

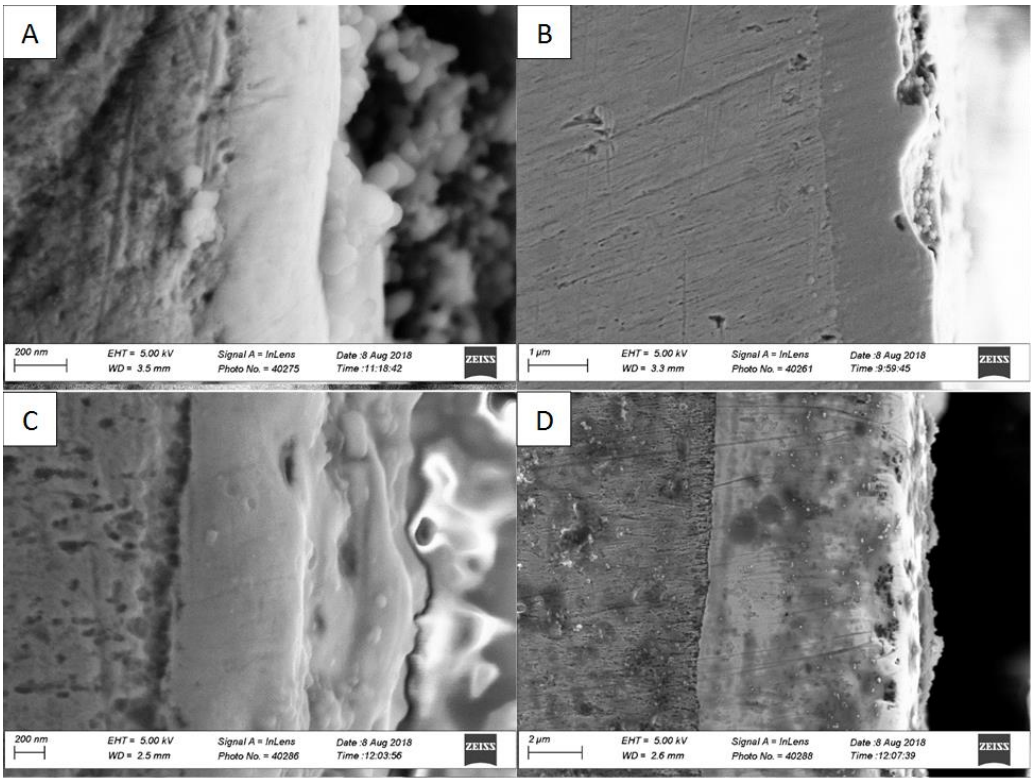

Figure 5- 18. Cross-section morphology of Ni deposits from DMSO in (A) absence of particles, or in presence of (B) TiO_2 NP, (C) APhE, and (D) NiSn10 in the presence of APhE.

To investigate the electropolymerization of APhE, a similar electrolyte to the Ni deposition but without Ni salts was prepared. IR spectroscopy was used to characterize two Cu samples, which were immersed in the electrolyte for 60 minutes, one with the similar applied potential (-1 V vs Ag/AgCl) and the other one with no potential applied. Figure 5- 19 shows the IR spectra for these two Cu substrates. The sample with applied potential showed peaks for allyl, ether, and aromatic bonds as presented in Table 5- 6. The EDS analysis of this sample showed about 3

wt% of C. The sample with no applied potential, however, presented no peaks suggesting that APhE is only polymerized by the current flow. The cathodic electropolymerization mechanism of sulfonated APhE from DMSO has been previously explained [30].-A more stable secondary radical is formed by accepting a proton from the reaction medium that leads to the formation of a linear aliphatic chain.

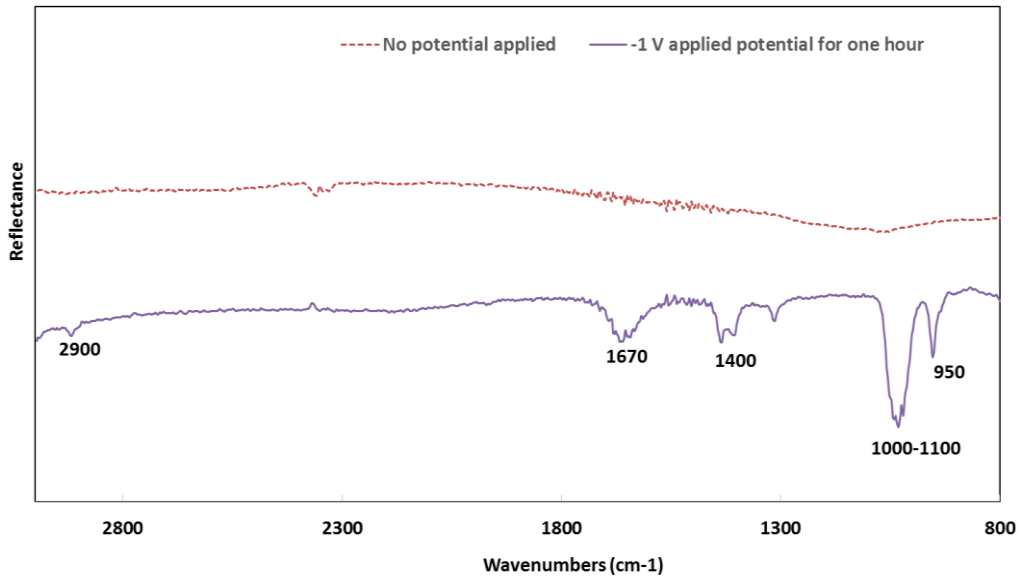

Figure 5- 19. IR spectra for Cu samples left inside the deposition electrolyte for one hour without and with applying -1 V vs. Ag/AgCl.

Table 5- 6. IR spectrum results after cathodic electropolymerization of APhE on Cu (-1V for one hour)

Wavenumbers (cm^{-1})	**Assignment**
950	R-CH=CH_2 (adsorbed monomer)
1000-1100	C-O
1400	C-C aromatic
1670	C=C aromatic

The XRD patterns of the samples in absence and presence of APhE was similar with a decrease in the intensity of peaks. Slightly smaller crystallites (7.0 , 6.3 and 12.9 nm for Ni-TiO_2 NPs, Ni-5APhE and NiSn10-5APhE, respectively) were formed suggesting that more compact coatings were obtained when APhE and TiO_2 NPs were added to the deposition bath. Note that

the XRD patterns in the absence and presence of composite element were fairly similar showing that there was no effect on the crystalline structure.

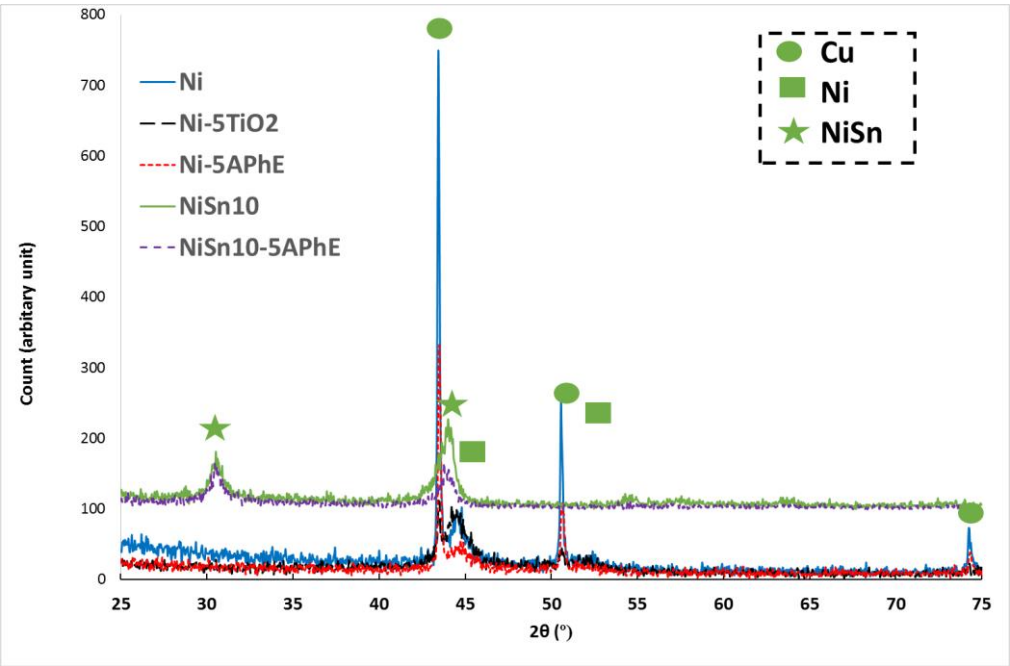

Figure 5- 20. Grazing-angle XRD patterns of Ni deposits in the absence and presence of TiO_2 NPs and APhE.

The effect of the addition of TiO_2 NPs, and APhE on the EIS and potentiodynamic polarization results of Ni and NiSn10 can be seen in Figure 5- 21 and Figure 5- 22. The obtained results are summarized in Table 5- 7 and Table 5- 8. In the case of TiO_2 NPs (and CNTs), the films had a considerably lower impedance values that suggests they can have potential applications in hydrogen production industries [37]. These films had a notably higher cathodic potential and higher corrosion current density than the Ni film in the absence of particles. This behavior is due to the formation of a highly porous surface in the presence of TiO_2 NPs and CNTs. The porosity index (Eq. 4-4) of the film increased by 6 orders of magnitude, when the film was obtained in the presence of TiO_2 NPs.

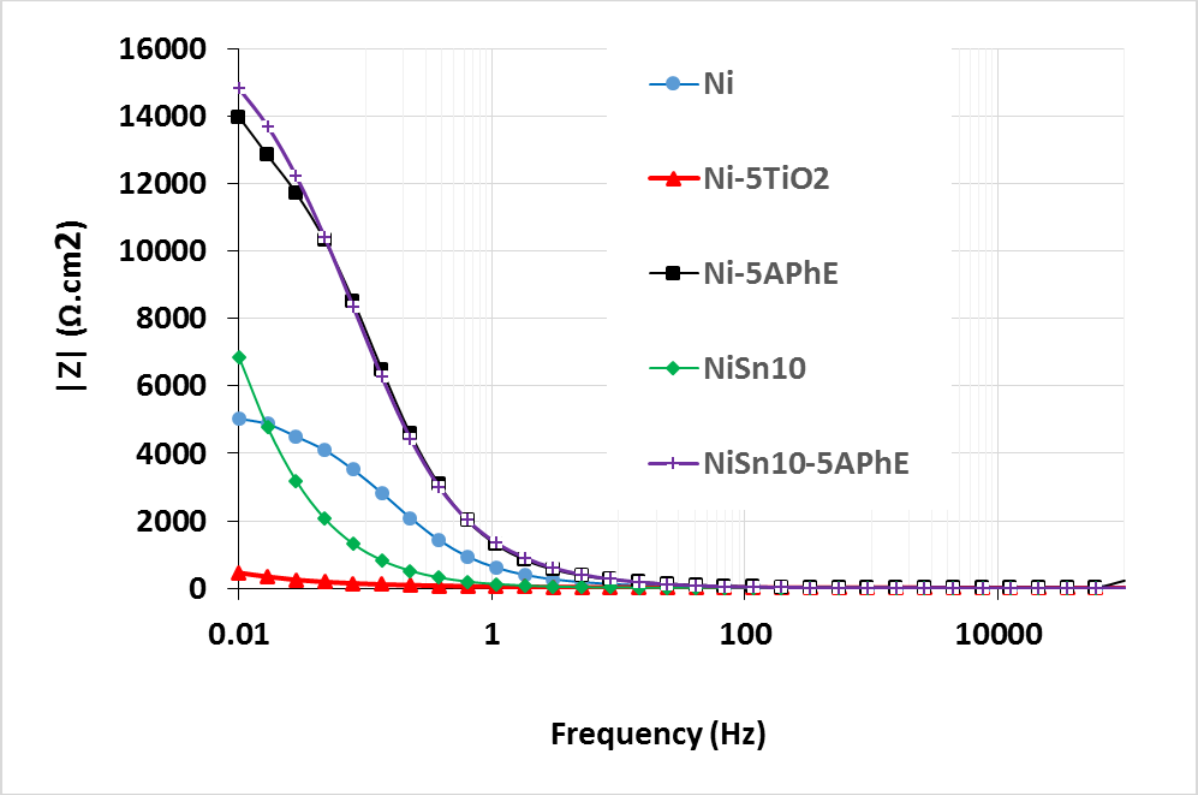

Figure 5- 21. Bode Z plots of the deposits from DMSO in the absence and presence of the composite element after 60 minutes immersion in 3% NaCl solution.

A similar shape of the curves in the presence and absence of APhE was observed. This suggests that the mechanism of corrosion is the same with and without APhE. The addition of APhE had no effect on the corrosion potential, but it notably increased the polarization and charge transfer resistances. Therefore, APhE improved the corrosion resistance by forming more compact films that enhanced the physical barrier against the corrosive media.

Table 5- 7. Impedance values (at 0.1 Hz) of the Ni-5 TiO_2 NPs, Ni-5APhE, and NiSn10-5APhE

Sample	|Z| at 0.01 Hz ($k\Omega.cm^2$)
Ni-5 TiO_2 NPs	0.5
Ni-5APhE	13.9
NiSn10-5APhE	14.8

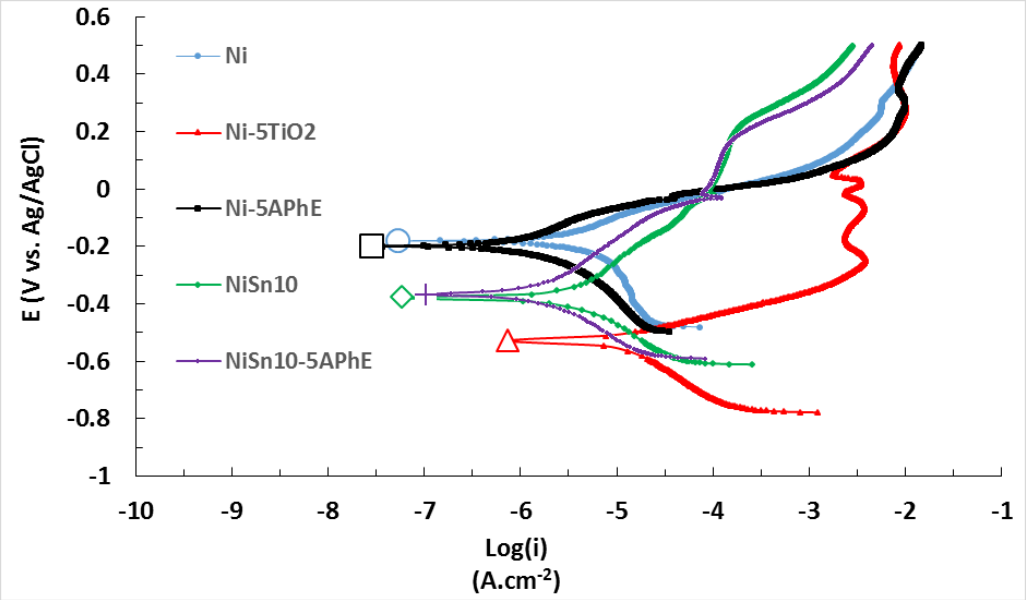

Figure 5- 22. Potentiodynamic polarization (Tafel) curves of the deposited from DMSO in the absence and presence of the composite element after 60 minutes immersion in 3wt% NaCl.

Table 5- 8. Corrosion current density and corrosion potential of Ni-5TiO_2 NPs, Ni-5APhE, and NiSn10-5APhE

Sample	i_{corr} ($\mu A.cm^{-2}$)	E_{corr} (mV) vs. Ag/AgCl	Average Tafel slope ($mV.\ dec^{-1}$)		R_p ($k\Omega.cm^2$)
			β_a	β_c	
Ni-5 TiO_2 NPs	14.88	-515	98	260	2.2
Ni-5APhE	1.02	-181	138	171	32.4
NiSn10-5APhE	1.44	-369	231	173	29.8

As conclusion, the formation of composite films from DMSO is only possible by the simultaneous electropolymerization of a monomer, here APhE. In the presence of other particles (TiO_2 NPs and CNTs), they cannot be trapped inside the film due to the low deposition rate of DMSO. These particles, however, intensify HER in the surface of the growing film and lead to formation of a porous coating with a poor corrosion behavior.

5.2. Nobel metal top-coats

NiAg and NiPd were chosen to investigate the deposition of noble metallic top-coats, as an alternative to Au, on Ni-P barrier layers. Several Ni-P coatings (Cit.4 explained in 4.2.1) on Cu

substrate were prepared. A DMSO based electrolyte (NiAg1 described in 5.1.1) was used to deposit NiAg film on Ni-P barrier layer. For NiPd, the same electrolyte was used except that $PdCl_2$ was added instead of $AgNO_3$. The electrolytes were stirred prior to the deposition for one hour at 10000 rpm using a T 18 digital ULTRA-TURRAX® IKA disperser.

Figure 5- 23 shows the surface of AgNi (Figure 5- 23A) and PdNi (Figure 5- 23B) films obtained by DC deposition at -0.8 V for 60 minutes. Several parts of the films, especially around the edges, were easily detached by washing the films with water. Therefore, the DC films obviously suffer from a poor adhesion to the Ni-P substrate. A SEM image on one edge of the AgNi coating is also shown in Figure 5- 23C. It shows similar morphologies of Ni-P (dark upper part of the image) and its thin AgNi top-coat (light lower part).

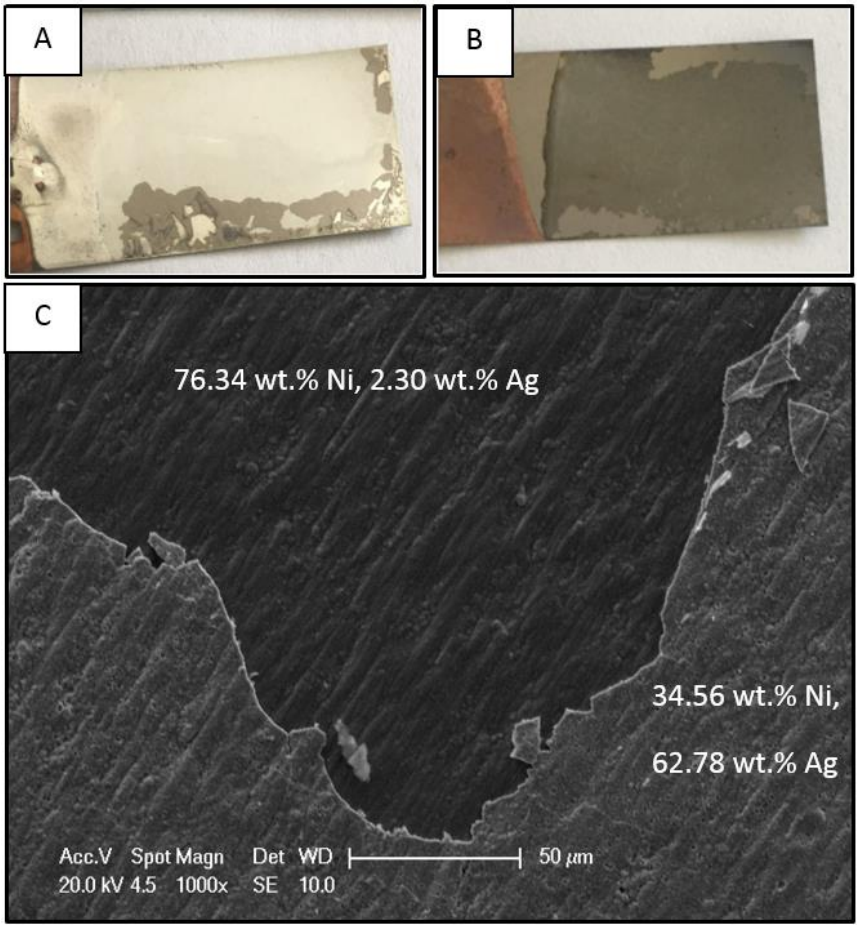

Figure 5- 23. Photographies of (A) AgNi, and (B) PdNi. (C) Surface morphology of AgNi films obtained by DC electrodeposition at -0.8 V for 60 minutes.

To understand the influence of the potential applied on the composition of the noble films, several potentials ranging from -0,6 V to -1,2 V were applied for AgNi directly on Cu. For comparison a -1 V potential was also used for PdNi deposition on Cu. The chemical composition of the noble deposits and their surface morphology were investigated. Figure 5-24 depicts the current density as function of the deposition time at these different potentials. The cathodic current density increased by applying more cathodic potentials for AgNi films. The extent of this increase is notable, except for films obtained at -1.0 and -1.2 V. The current density for PdNi (-1.0 V) was significantly lower than for AgNi (-1.0 V), and its value, in contrary to AgNi, was decreasing during the deposition. This continuous decrease in current density suggests that the deposition of PdNi is controlled by diffusion.

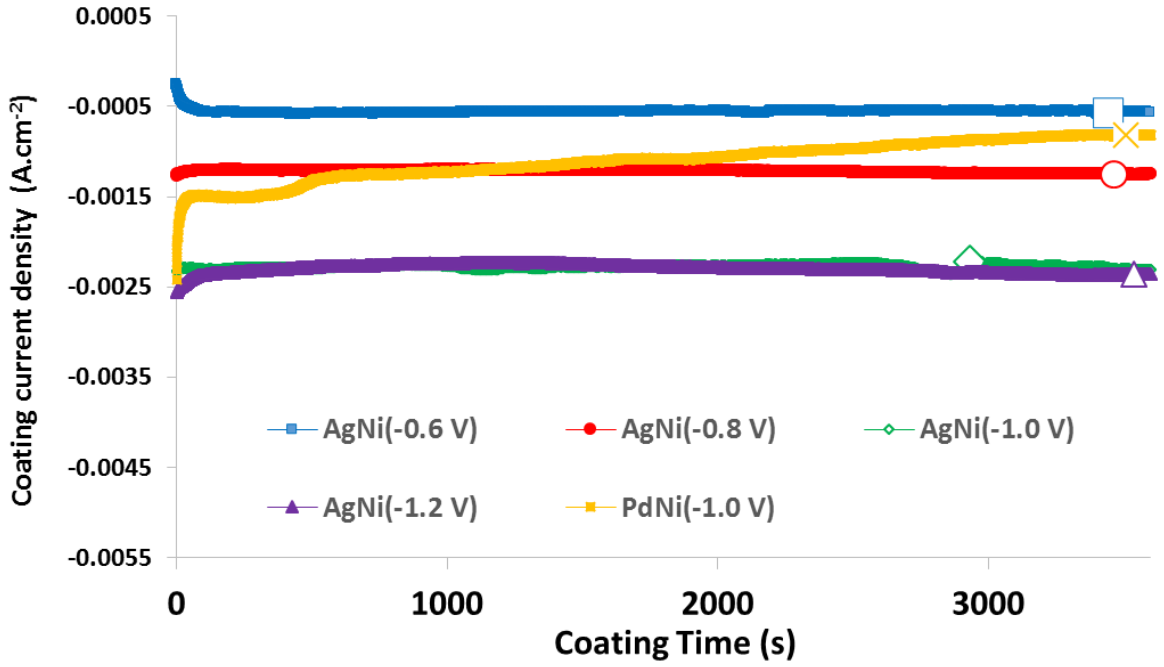

Figure 5- 24. Current density as a function of deposition time for noble thin films obtained at -0.6, -0.8, -1, and -1.2 V vs. Ag/AgCl.

Figure 5- 25 shows the surface morphology of the films obtained at different potentials. The surface morphology of AgNi films at cathodic potentials from -0.6 to -1.0 V consists of spherical features. The size of these features increased by applying more cathodic potentials.

The surface morphology of AgNi obtained at -1.2 V was highly porous, which could be due to the hydrogen evolution reaction (HER). PdNi was highly porous at -1.0 V possibly because of the catalytic effect of Pd on HER [38–40]. Note that the films became darker by applying more cathodic potentials.

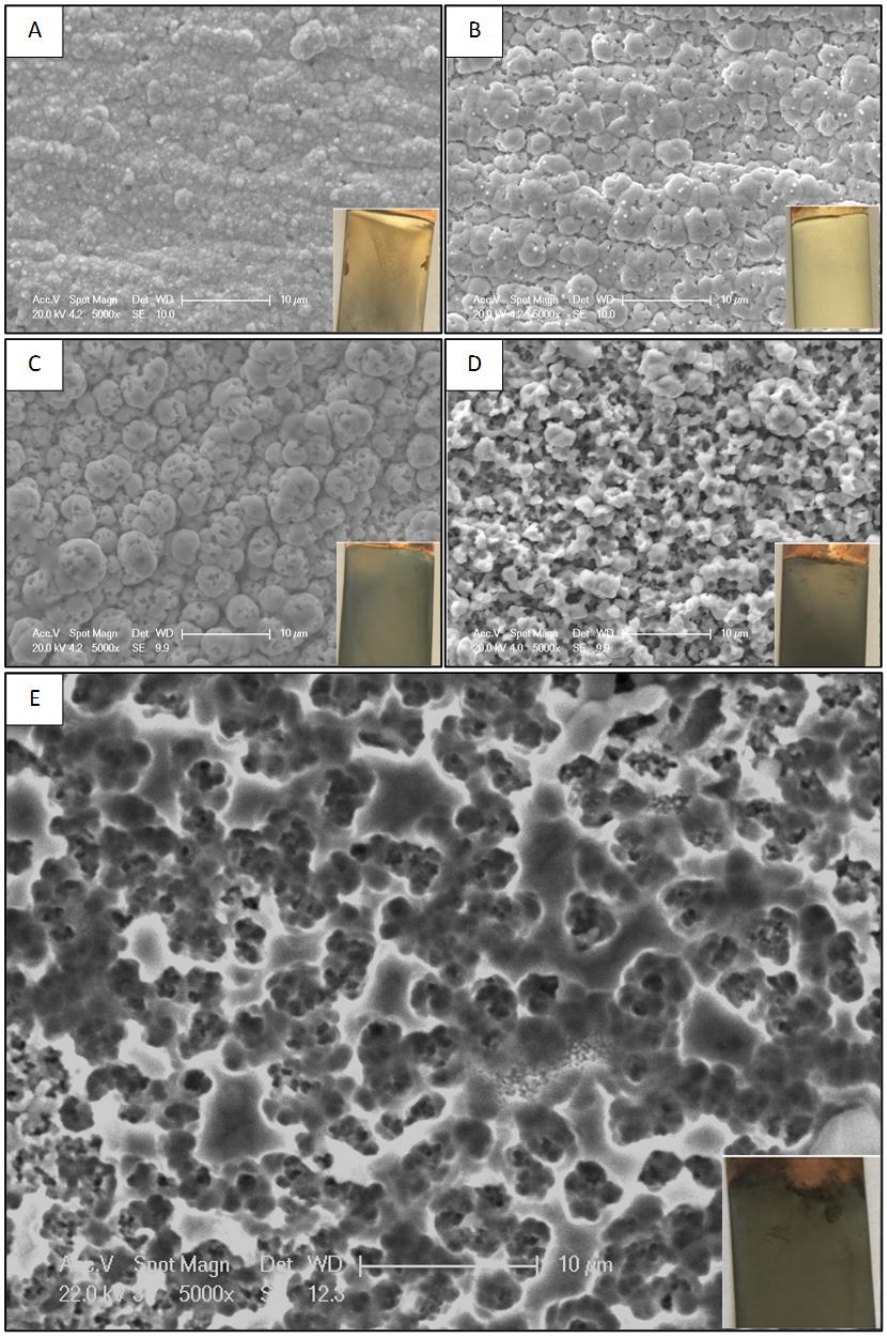

Figure 5- 25. Surface morphology of (A) AgNi (-0.6 V), (B) AgNi (-0.8 V), (C) AgNi (-1.0 V), (D) AgNi (-1.2 V), and (E) PdNi (-1.0 V) on Cu.

The chemical composition of AgNi films obtained at different potentials is shown in Figure 5-26. While the Ni content increased at more cathodic potentials, the deposition of Ag was favored at less cathodic potentials. This is in accordance to the deposition of AgNi films reported by Santhi et al. [41]. Note that the content of Ag and Pd in coatings obtained at -1.0 V was 37.5 and 3.5 wt.%, respectively (balanced with Ni).

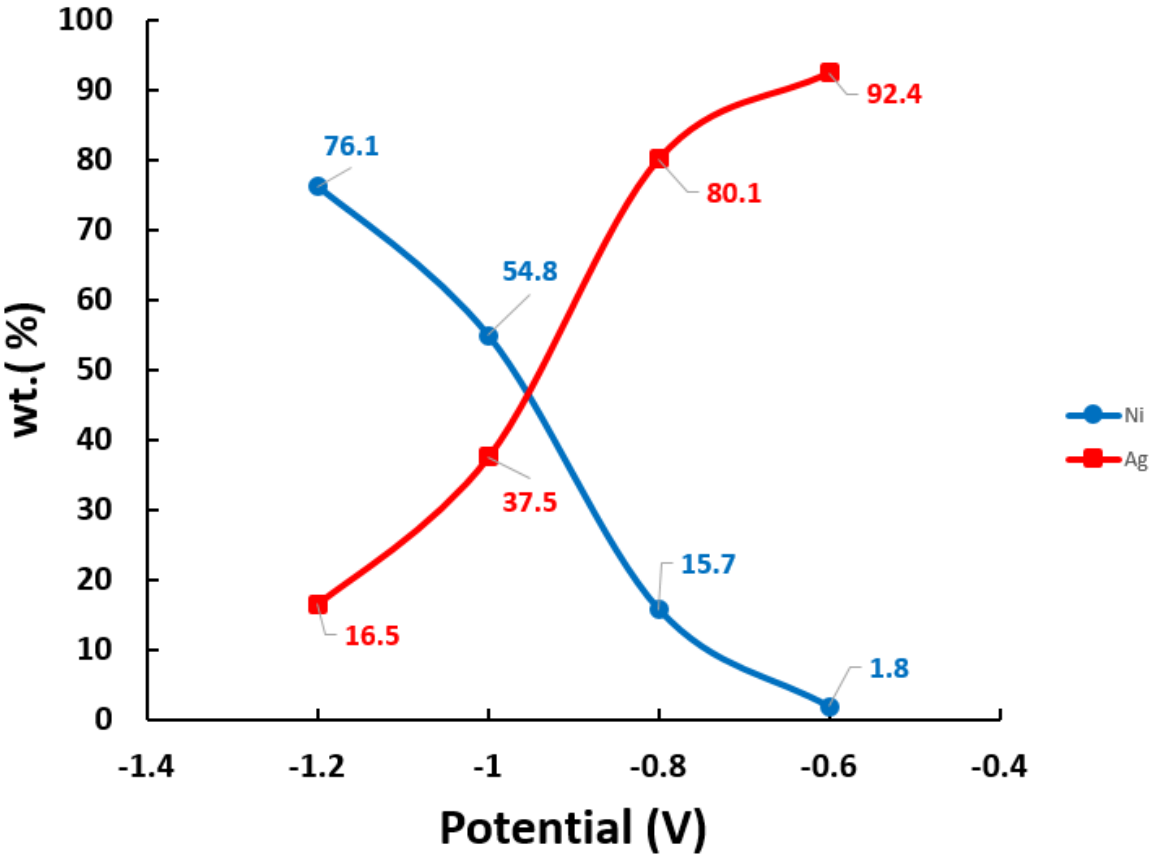

Figure 5- 26. Ni and Ag content as a function of the applied potential in DC coatings on Cu.

The low Pd content could be explained by the complexes it makes with DMSO. DMSO generally makes O-bonded complexes with metallic ions [42]. The average dimension of O-bonded DMSO complexes for Ag, Pd, and Ni is 2.43, 2.11, and 2.08 Å, respectively [11]. Larger bonds are generally easier to split, so that the deposition of Ag is easier compared to Pd. DMSO also forms an S-bonded complex with Pd [43]. Moreover, Pd was added as chloride salt that increases the overall energy barrier for electrodeposition since chlorides enhance the

strength of DMSO complexes [44,45]. As a result, Pd forms a very stable complex with DMSO, which justifies its low content in PdNi films. This can also explain the peculiar i-t behavior of PdNi during the deposition (Figure 5- 24).

To increase the adhesion of the noble coating on NiP substrate, the pulse deposition method was selected. Varying the potential during the deposition leads to the formation of a film with a chemical composition gradient. 360 pulse cycles (Figure 5- 27) were used to deposit AgNi and PdNi films on the Ni-P/Cu for the total time of 60 minutes. -1.0 (total 2 s) and -0.6 V (2 s) were used for preferential Ni and Ag deposition, respectively. The main part of the pulse was at -0.8 V (for 6 s) in order to deposit a uniform AgNi layer with an acceptable surface morphology.

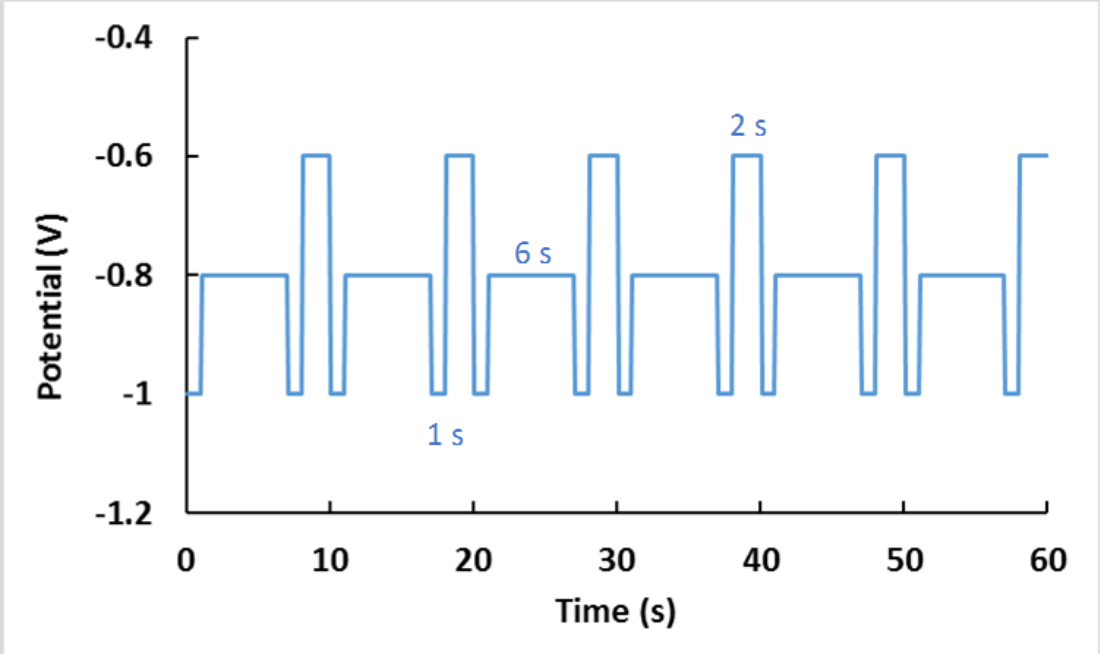

Figure 5- 27. Potential-time curve for the first 10 cycles of Ag-Ni pulse deposition.

Figure 5- 28 depicts the general aspect, surface morphology, and cross-section of AgNi and PdNi pulse-electrodeposited films on Ni-P/Cu. Uniform and adhesive films were formed by the developed pulse mode. The deposited Ni at -1.0 V could act as a bridge between the noble thin film and the Ni-P sub-layer and thus improve the adhesion to the substrate. The surface

morphology of AgNi was very similar to the DC films obtained at -0.8 V (Figure 5- 25). PdNi, however, presented the common surface morphology of electrodeposited Ni and Ni-P films. Both samples have some pores distributed in their surfaces that could be due to HER. The average pore size for AgNi was estimated to be around 1.5 μm^2 by ImageJ.

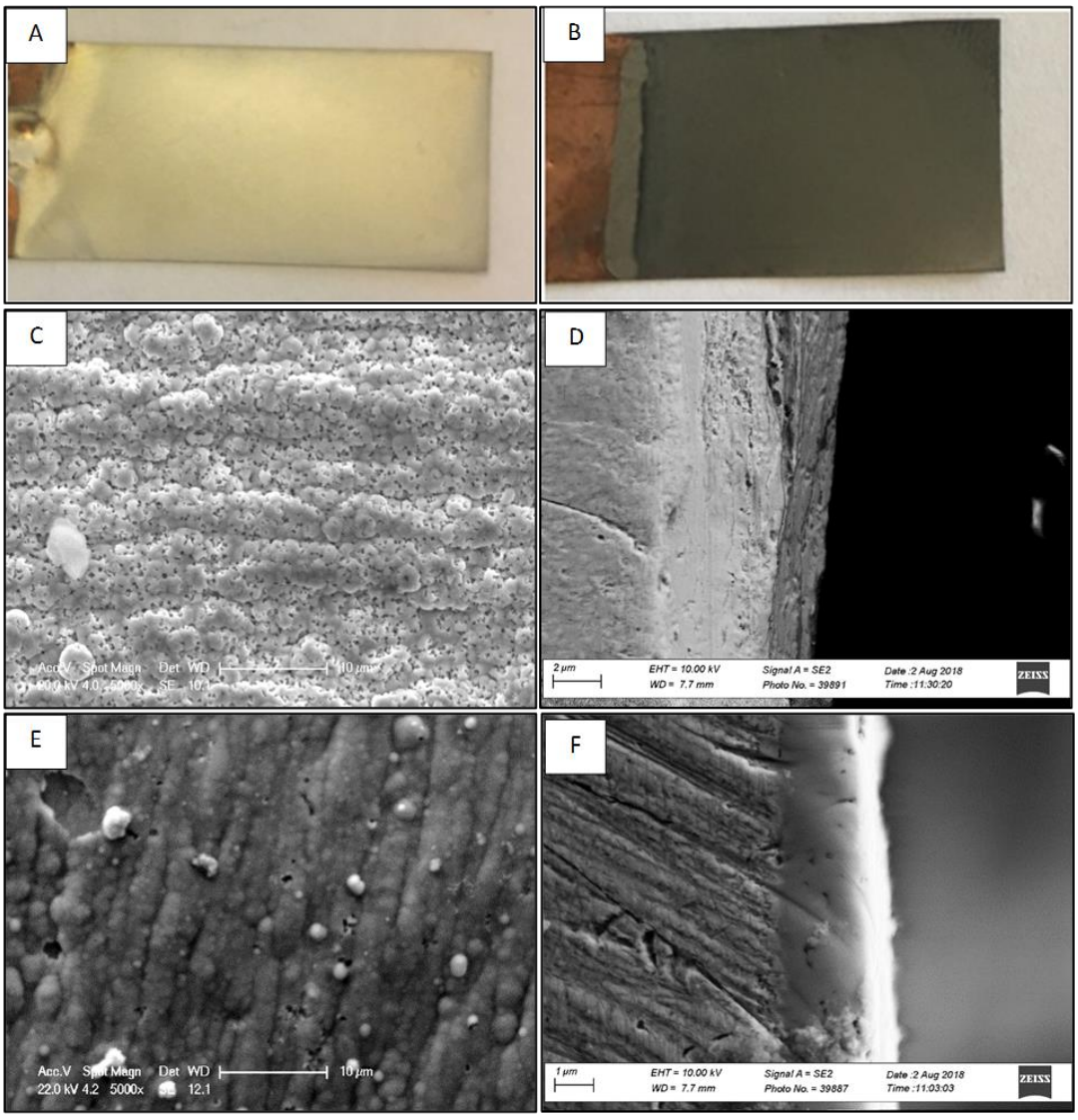

Figure 5- 28. (A) AgNi, (B) PdNi, (C) surface morphology of AgNi, (D) cross-section of AgNi, (E) surface morphology of PdNi, and (F) cross-section of PdNi pulse-electrodeposited films on Ni-P/Cu.

The chemical composition of the films is summarized in Table 5- 9. The average mass gain of AgNi and PdNi was 2.48 and 0.06 $mg.cm^{-2}$, respectively. Ag, as it was expected, had an easier deposition process and thus its content in the hard noble thin films is significantly higher than Pd (53.74 vs. 17.38 wt.%, respectively). Cross-sectional images of the films (Figure 5- 28D

and F) show that an adhesive NiAg films (about 2 µm) was formed, however, some cracks on the surface of the top-coat were visible. A thinner layer of NiPd (about 500 nm) was visible in its cross-section, which was in agreement with other observations, i.e. current density during the deposition, mass gain, and chemical composition.

Table 5- 9. Chemical composition of AgNi and PdNi pulse-electrodeposited films on Ni-P/Cu

Sample	Ni wt.%	Ag wt.%	Pd wt.%
AgNi	40.62	53.74	-
PdNi	65.47	-	17.38

The crystalline structure of the films was studied by grazing incidence XRD (Figure 5- 29). There is no peak for Pd, just a very small peak related to Ni and a strong peak attributed to Cu for PdNi. This is due to the low thickness of the film and its low Pd content. AgNi, however, has visible peaks for Ag and Ni, and no peak for Cu (due to its notably higher thickness). It has been found that electrodeposited AgNi films consist of Ag-rich and Ni-rich zones [17]. The crystalline size of Ag-rich deposits in AgNi estimated to be around 14 nm using the Debye Scherrer formula. The Ni-P barrier was completely amorphous and thus had no signature in the XRD patterns. Therefore, a nano-crystalline adhesive Ag deposit is formed on Ni-P/Cu by pulse electrodeposition.

EIS (Figure 5- 30 and Table 5- 10), and potentiodynamic polarization (Figure 5- 31 and Table 5- 11) results showed a negative effect of the applied noble metallic top-coats, i.e. NiAg1 and NiPd1, on the corrosion behavior of the Ni-P barrier layer.

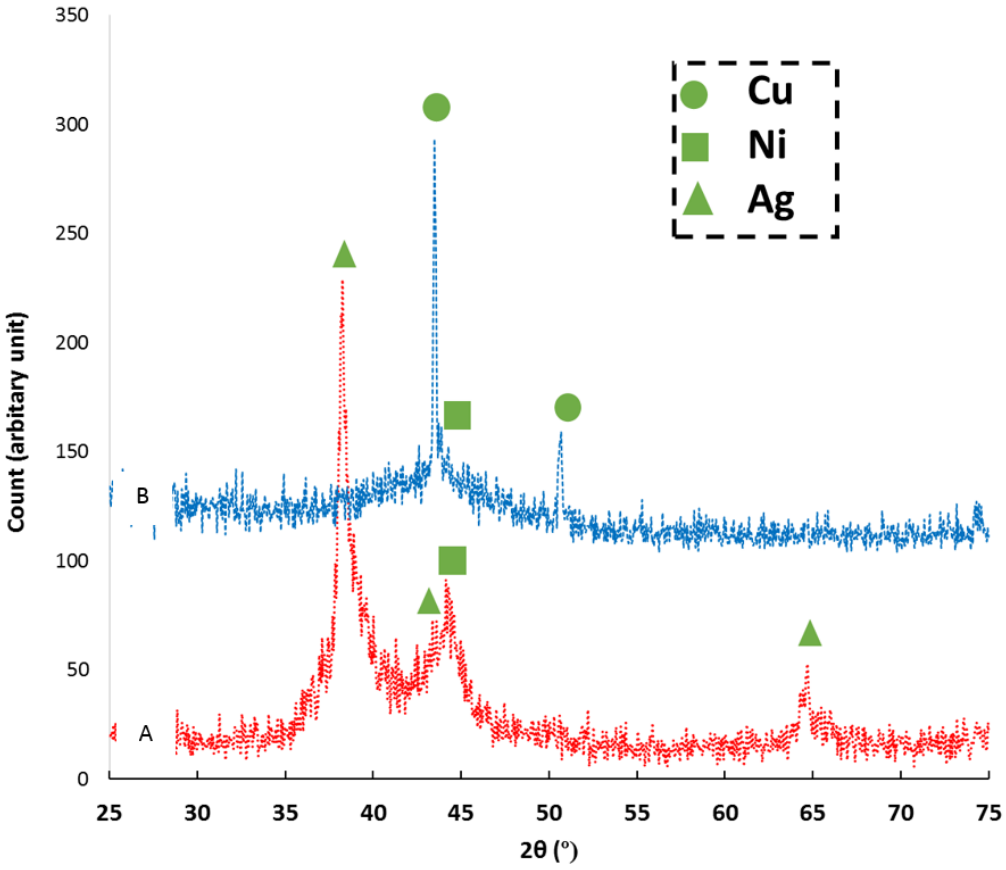

Figure 5- 29. Grazing incidence XRD patterns of (A) AgNi, and (B) PdNi pulsed-electrodeposited films on Ni-P/Cu.

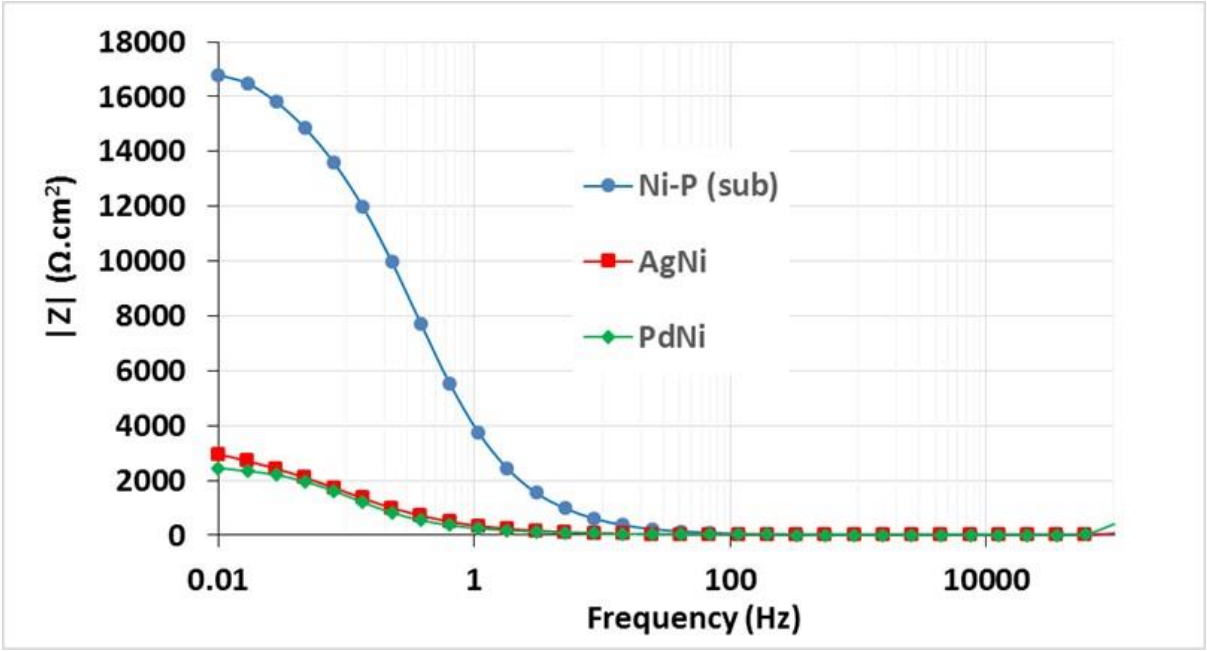

Figure 5- 30. Nyquist plots of the Ni-P barrier layer and NiAg and NiPd top-coats after 60 minutes immersion in 3% NaCl solution.

Table 5- 10. impedance values (at 0.1 Hz) of the Ni-P barrier layer and NiAg and NiPd top-coats

Sample	|Z| at 0.01 Hz ($k\Omega.cm^2$)
Ni-P barrier	16.3
NiAg	2.6
NiPd	2.2

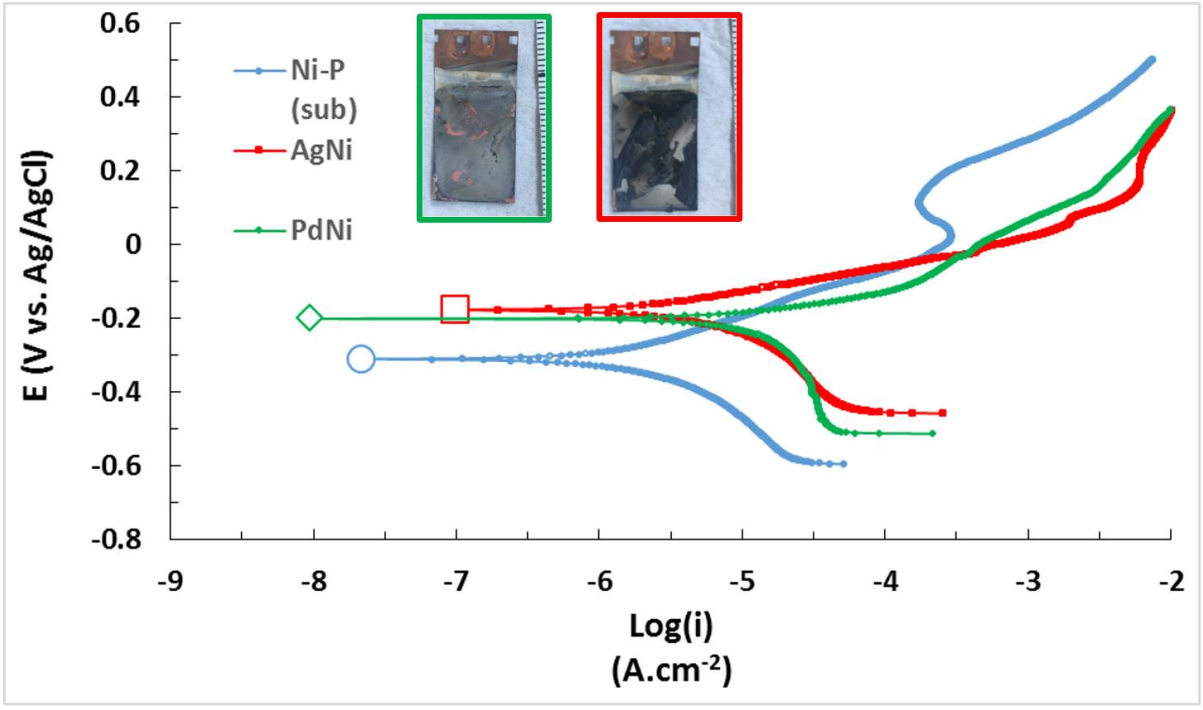

Figure 5- 31. Potentiodynamic polarization (Tafel) curves of the Ni-P barrier layer and NiAg and NiPd top-coats after 60 minutes immersion in 3wt% NaCl.

Table 5- 11. Corrosion current density and corrosion potential of the Ni-P barrier layer and NiAg and NiPd top-coats

Sample	i_{corr} ($\mu A.cm^{-2}$)	E_{corr} (mV) vs. Ag/AgCl
Ni-P barrier	1.49	-298
NiAg	4.61	-162
NiPd	10.13	-185

The poor corrosion behavior of these top-coats could be attributed to the presence of pores and cracks on their surface and the formation of galvanic coupling between Ni rich and noble metal (Ag or Pd) rich phases on the surface. The surface of NiAg turned black during the corrosion tests. Therefore, even though a highly adhesive noble top-coat was formed its corrosion behavior was not promising enough to be considered as an alternative to Au.

5.3. Post-treatment process on Cu/Ni-P/Au industrial samples

Cathodic electropolymerization of MMA (methyl methacrylate) was employed as a post-treatment process to seal the pores of the Au top-coat. A DMSO based solution containing 0.1 M KNO_3 (as supporting electrolyte) and 4 vol% MMA was used to electropolymerize MMA. KNO_3 was added to DMSO and the solution was then stirred for 60 minutes. MMA was added to the solution and the stirring continued for another 30 minutes.

Cyclic voltammetry (CV) was used in a cathodic window (-0.5 to -2.0 V) with a scan rate of 20 $mV.s^{-1}$ to polymerize MMA at room temperature. CV was used to target the polymerization on pores (due to their different surface energy), whereas applying a constant potential will thermodynamically turn the entire surface to possible nucleation sites [30]. Different numbers of cycles (5, 10, 15, 25, 50, and 100) were used to modify the Cu/ Ni-P/Au electrical contacts provided by our industrial partner. The metallic multilayers have a total thickness of about 35 µm and are deposited on an epoxy support. The samples were named after their corresponding cycle number, e.g. C0 represents the unmodified sample and C25 is the sample modified by 25 cycles of MMA polymerization. All the samples were washed with distilled water and dried with compressed air after the process.

Figure 5- 32 presents the CV curves of MMA electropolymerization in a potential range between -0.5 to -2.0 V vs. Ag/AgCl. The inlay in that figure corresponds to a smaller potential range (-0.5 to -1.5 V). The first cycle (in blue) clearly presents two reductions waves: the first one between -1.2 to -1.8 V where the reduction current is followed by a plateau, the second one below -1.8 V leading to a step rise in current.

The increase in the number of cycles, till 25 cycles, induces a rapid decrease of the cathodic current in the both regions I and II (see the inlay, for the region I). This decrease is a direct evidence of electropolymerization: the global amount of polymer grafted during each scan is

reduced because of the blocking of cathodic sites by the polymer during the previous scans. This result is in good accordance with previous works [46–48]. Another way to interpret this current decrease is that the amount of polymer at the surface increases during each cycle of polymerization increasing the electrode resistance [46,47]. Interestingly, after 50 cycles a reverse trend was observed: the cathodic current started again to increase and its value after 100 cycles was even slightly higher than after 10 cycles. The formation of a thick mechanically unstable PMMA layer can lead to a detachment from the electrode and thus exposes the metallic surface [46].

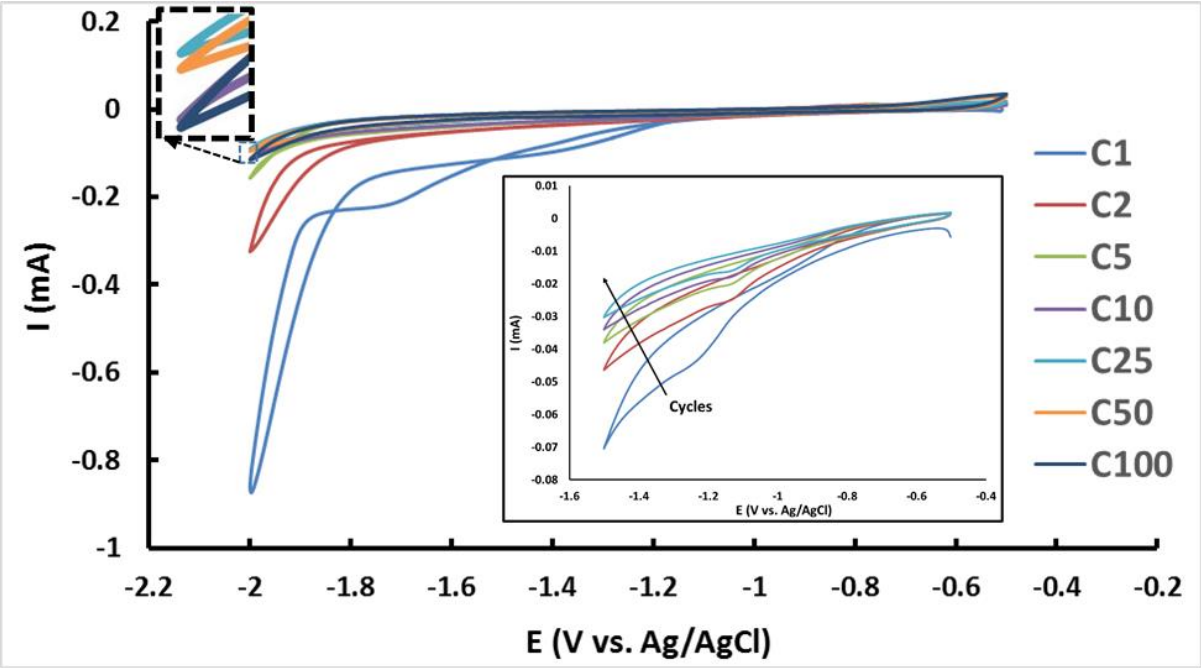

Figure 5- 32. CV curves of cathodic electropolymerization of MMA on Cu/Ni-P/Au electrical contacts from 0.1 M KNO_3 DMSO solution with a scan rate of 20 $mV.s^{-1}$.

Baute et al. [49] investigated the cathodic electropolymerization mechanism of some acrylate monomers (including MMA) from dimethylformamide (DMF). CV curves of the investigated acrylic monomers had 2 cathodic peaks. The first peak at less negative potentials was ascribed to the passivation due to the adsorption of reduced monomer. The second peak was attributed to diffusion control. The first peak (around -1.8 V) was considered the critical potential at which the reaction of electrografting happens. Note that the partial electrografting of MMA

occurs even before the first peak. This is in agreement with our results where electropolymerization was carried out from -0.5 to -1.5 V (see inlay in Figure 5- 32) and a similar decrease in current was observed.

The effect of electropolymerization cycles on the mass gain of samples is illustrated in Figure 5- 33. A strong increase of sample mass can be seen in the first 5 cycles, followed by a slow mass increase between C5 to C50 with a quasi-constant slow rate of deposition. This result is in good accordance with the small variation of the current on CV curves in Figure 5- 32 between C5 to C25. Then a drastic mass increase is observed after 50 cycles. This result could be to a non-uniform polymerization.

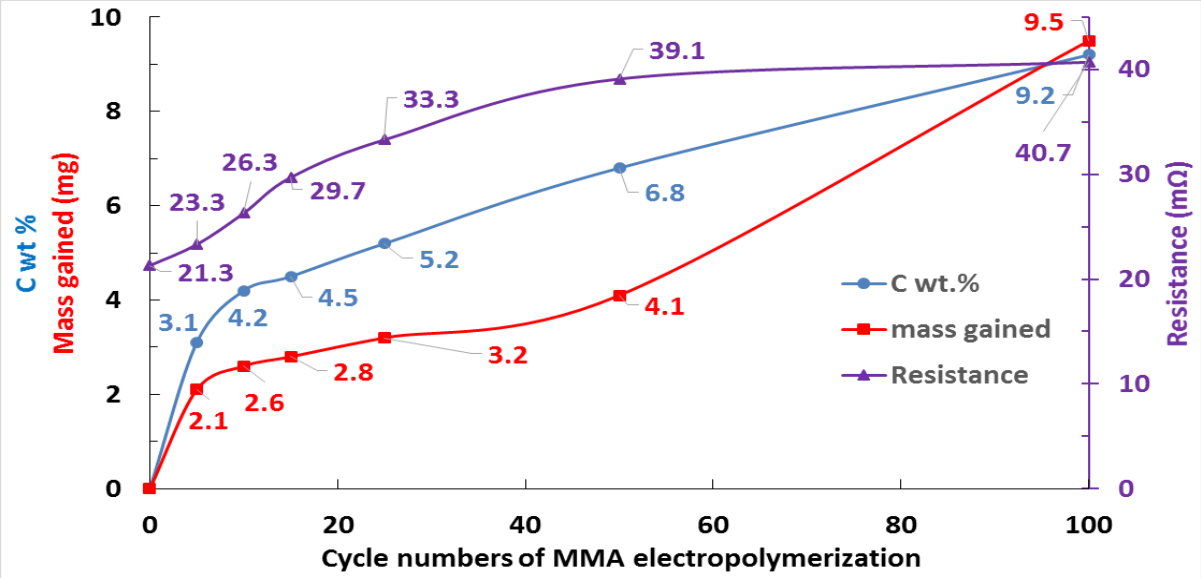

Figure 5- 33. Mass gain, C content, and resistance as a function of electropolymerization cycle number.

The EDS technique was employed to assess the amount of C (and thus polymer content) as a function of the electropolymerization cycle number (Figure 5- 33). The C content increases rapidly till C5 and then almost linearly between 5 to 100 cycles. The chemical composition of C0 was 3.3 wt% Cu, 80.6 wt% Ni, 5.7 wt% P, and 10.4 wt% Au. The EDS analysis was done at the center of each sample where a uniform distribution of current is expected. Therefore, the

inconsistency between the increase of C content and mass gained after 50 cycles could be due to a non-uniform polymerization of MMA especially at the edges of samples.

No polymer should be formed in the absence of a current flow [46]. To prove that, a sample was immersed in the electrolyte for 4 hours (that is the equivalent time of 100 cycles of electropolymerization). No supplementary amount of C was found, showing that PMMA was formed electrochemically.

To test the solubility of the formed PMMA in relation to the interaction between the polymer and the surface, C10 and C100 were immersed in tetrahydrofuran (THF) for 12 hours. The C amounts were 4.8 and 10.3 % for C10 and C100, respectively, so quite similar to the first analysis (4.2 and 9.2 % respectively). The insolubility of the formed PMMA in THF suggests a strong chemical grafting between Au and the electrodeposited polymer [46].

Figure 5- 34 shows the grazing-incidence XRD patterns of C0 and C100. The observed peaks for C0 are related to Au, Ni, and the Cu substrate. The XRD pattern intensity is related to the X-ray penetration depth [50], but pores can intensify the penetration of X-rays [51]. The strong Cu peak can be justified ((200) main orientation) by the low thickness (and the partly amorphous nature) of the Ni-P barrier layer and the Au top-coat and also the porosity of the Au film. The C100 pattern was almost similar to C0. However, it showed an increase of the intensity at low diffraction angles and a notable decrease of the peak intensity attributed to Cu and Ni. Note that the intensity for Au is almost identical. The formation of an amorphous phase, here PMMA, on the surface of metals increases the X-ray intensity at low diffraction angles [52–54]. The intensity decrease of Cu and Ni can be attributed to the PMMA-filled pores.

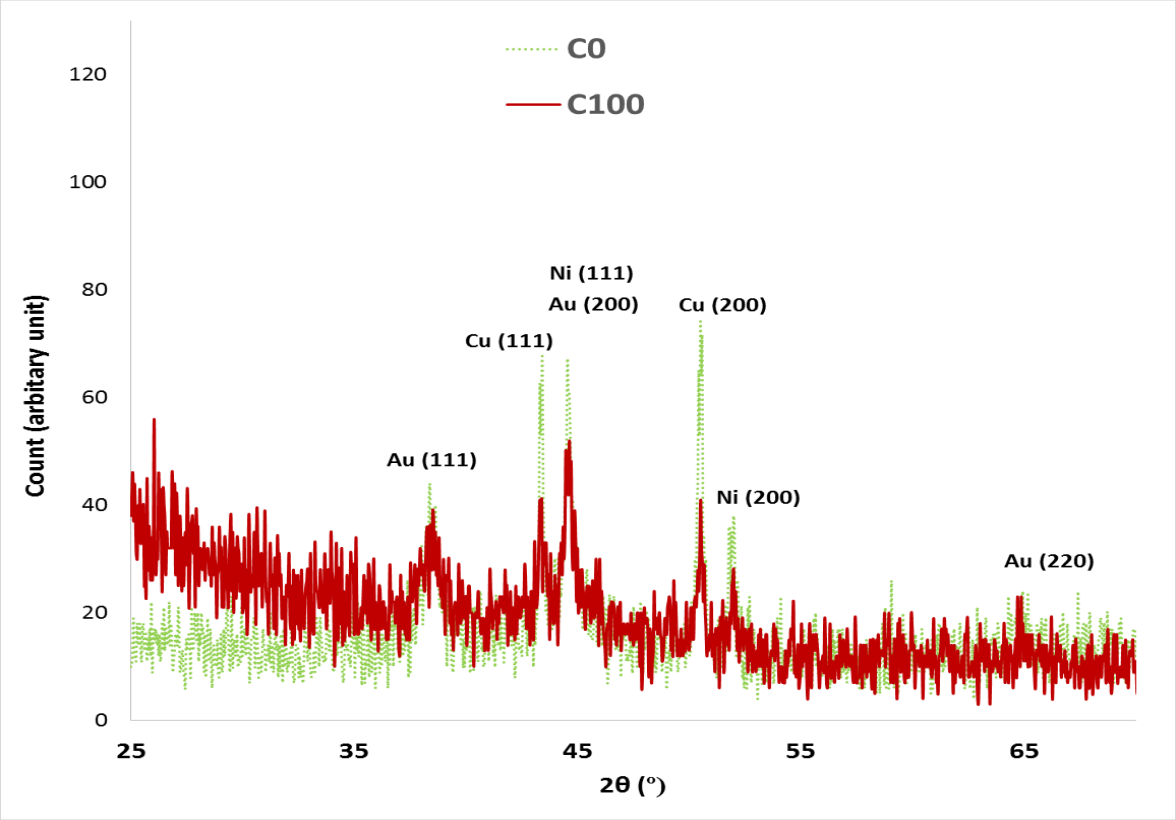

Figure 5- 34. Grazing incidence XRD patterns of C0 and C100.

Figure 5- 35 shows optical microscopy images of C0. The micrometer-sized pores are obviously distributed all over the surface. SEM observations of the surface morphology of C0 and C100 are presented in Figure 5- 36 (a and b). Both samples present a similar morphology except that C100 is slightly blurred, possibly due to the presence of an insulating PMMA deposit. At lower magnification, however, C100 has two distinct features (noted α and β in Figure 5- 36c).

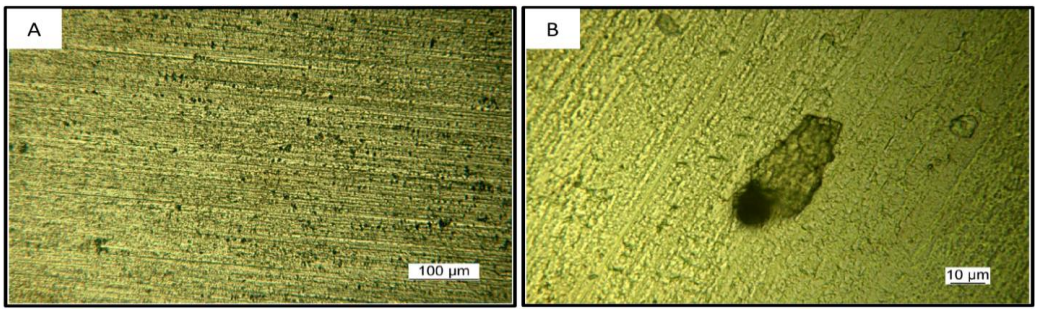

Figure 5- 35. Optical micrograph of C0 at low (a) and high (b) magnifications.

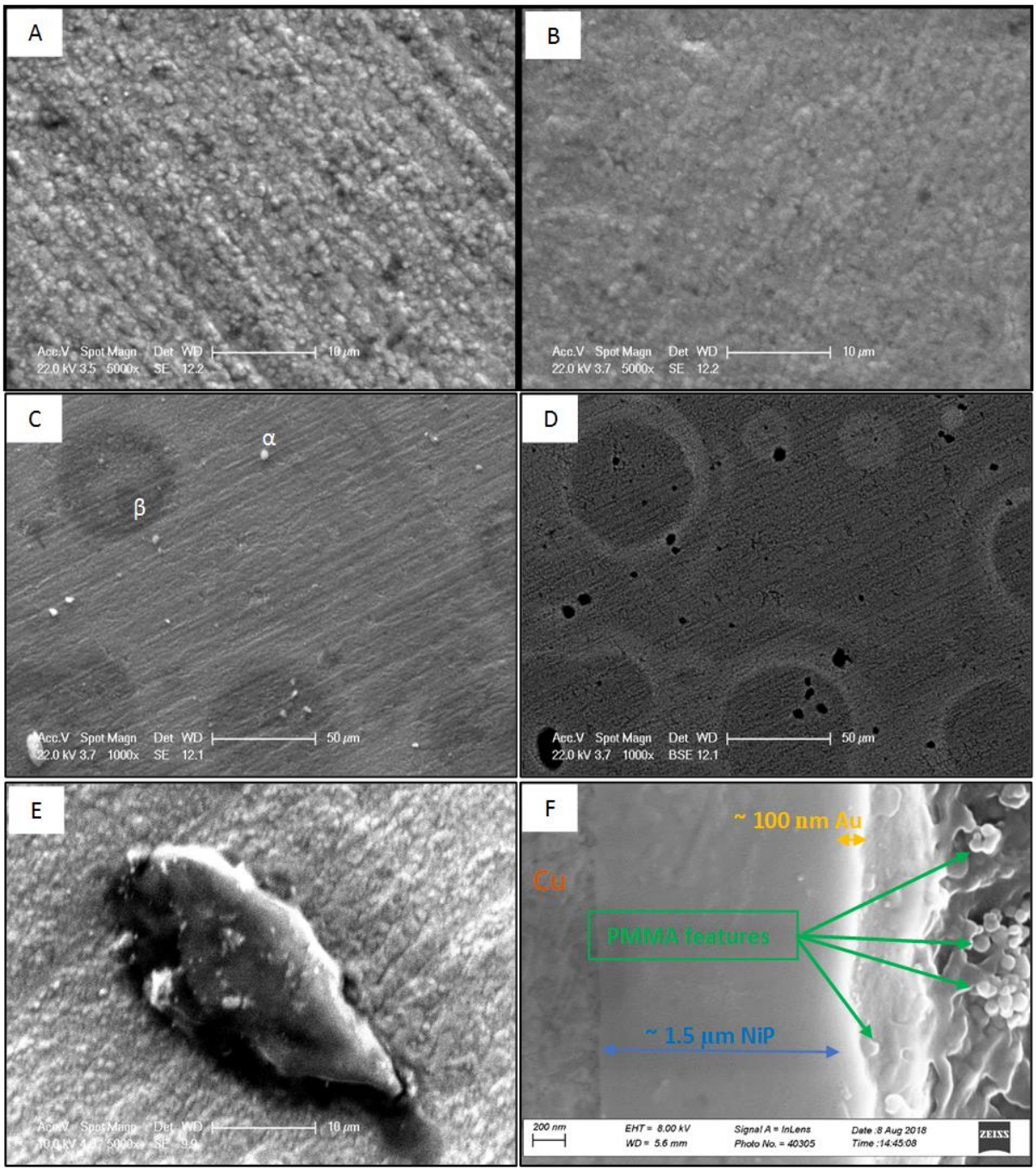

Figure 5- 36. (a) SE SEM image of C0, (b) SE SEM image of C100, (c) SE SEM image of C100, (d) BSE SEM image of C100, (e) SE SEM image of C100 (10kV electron beam power), and (f) cross-section BSE SEM image of C100 .

Figure 5- 36c-e show a non-uniform formation of polymer on the surface. This non-uniformity of PMMA has been previously reported even at higher concentrations of monomer [46]. The bright objects (marked as α) were found for all PMMA modified samples. The bright objects in SE mode are dark spots in the BSE mode, which is sensitive to the chemical composition

(i.e. average atomic number) [55] (Figure 5- 36d). This means they are composed of a material with a low atomic number. Figure 5- 36e shows one of these objects observed with a low electron beam power (to have a better resolution). Point EDS on this object showed 47.7 wt.% C that indicates it is made of PMMA. This object could have been formed in (on) the pores due to the similarities between the black spots in Figure 5- 36d and pores in Figure 5- 35a.

The halo shapes (marked as β in Figure 5- 36c) were observed only for C50 and C100. A point EDS analysis showed 16.3 wt.% C (about 7 % higher than the overall C content of C100) that suggests a localized polymerization. All the pores could be filled after a certain number of cycles. The polymerization continues on any available surface since preferential sites (as pores) are not available, leading to the formation of halo shapes in C50 and C100.

The cross-section of C100 is shown in Figure 5- 36f. The polymeric features are obvious on the surface of samples. Therefore, PMMA covered the surface and sealed the pores. The Au layer with about 100 nm thickness on about 1.5 µm thick Ni-P can be also seen in this figure.

The electrical resistance of samples as a function of the electropolymerization cycle is depicted in Figure 5- 33. C100 showed a 91% increase in the electrical resistivity. However, its resistance (40.7 mΩ) is still much lower than the resistivity limit of electrical contacts (300 mΩ) [56]. PMMA, therefore, is a potential candidate to enhance the lifetime of electrical contacts. Moreover, Figure 5- 33 supports the presence of a non-uniform polymer layer because a strong resistivity increase should be observed in the presence of a uniform polymeric film [57–59].

Figure 5- 37 shows the EIS results obtained for samples with (C5-C100) and without (C0) the presence of PMMA. The highest corrosion resistance was observed for 10 cycles of MMA electropolymerization. This maximum can be also observed in Figure 5- 38.

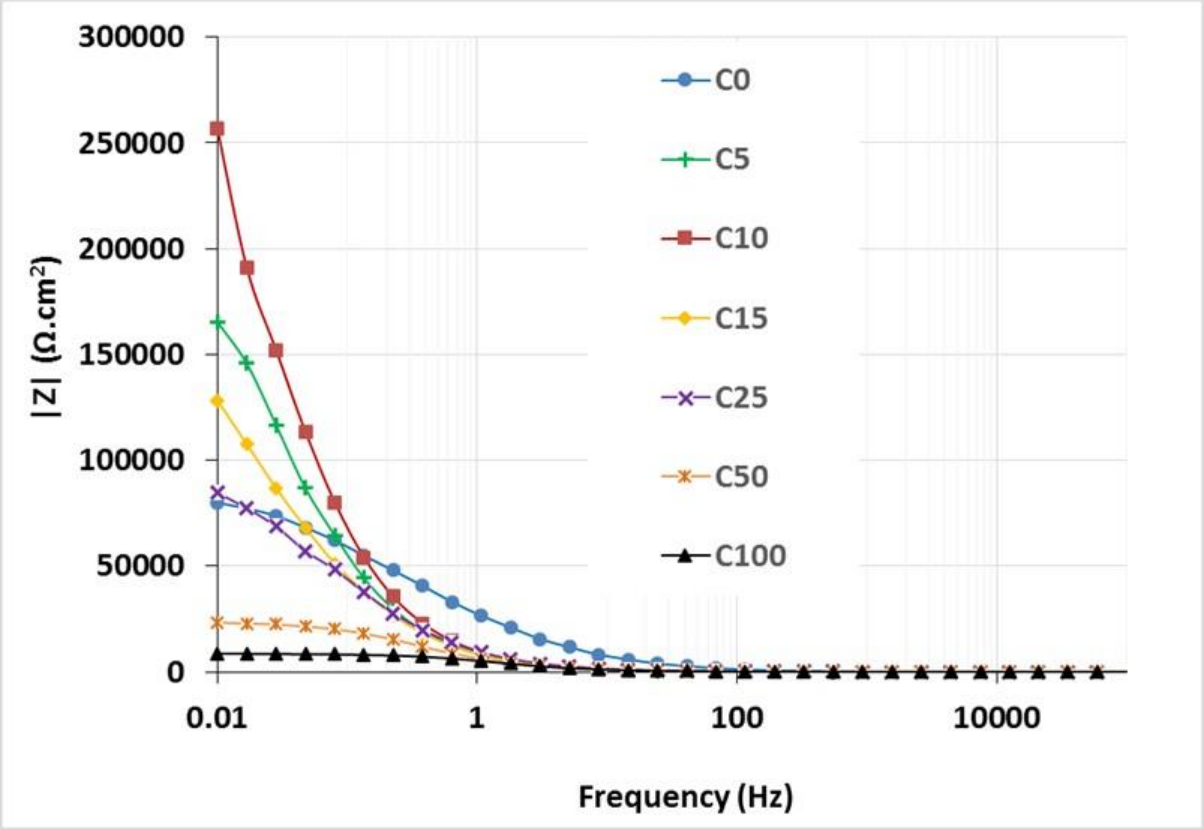

Figure 5- 37. Bode Z plots of C0-C100 after one hour immersion in 3% NaCl solution.

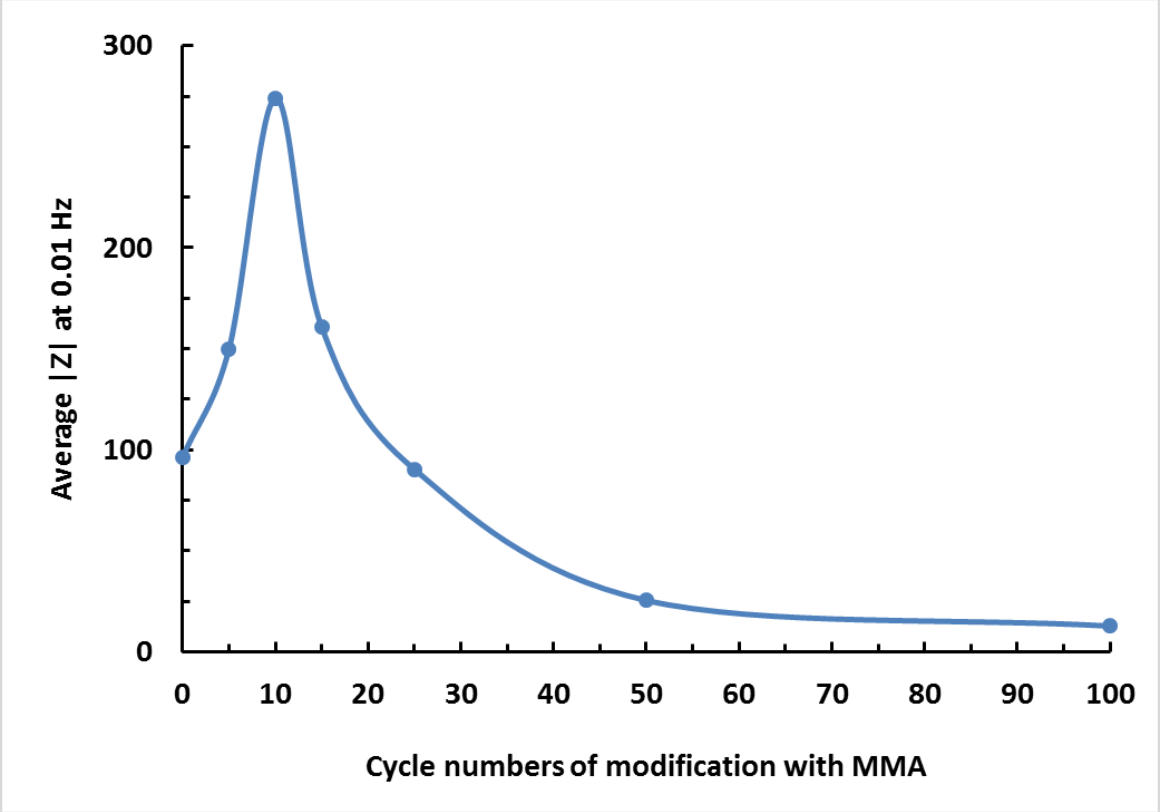

Figure 5- 38. The effect of cycle number of PMMA polymerization on the impedance value of electronic modules.

For C0, the corrosion mainly occur inside the pores. The fast dissolution of Ni in the pores occurs due to the galvanic coupling between Au (cathode) and Ni (anode). In the PMMA-modified samples, however, the pores are filled with the polymer, hence limiting the corrosion.

Assuming that the pores are filled with PMMA after polymerization, the corrosion resistance can be modeled as:

$$R_t = \frac{R_{ct} \times R_{Pol}}{R_{ct} + R_{Pol}} \qquad (5-\ 1)$$

While the metallic surface area decreases during the polymerization, the polymer surface area increases. Therefore, R_{ct} decreases after each cycle, while R_{Pol} increases.

Pores are confined spaces and an intensified corrosion process occurs inside them. Filling pores blocks these highly active corrosion sites and thus improves the overall corrosion resistance [60]. Increasing the cycle number of polymerization, however, decreases the uniformity of the surface. Therefore, the corrosion resistance decreases because a non-uniform protective layer actually promotes the corrosion by leaving a limited exposed area in the corrosive media [61].

Figure 5- 39 shows the CP curves of C0, C10, C100, and the Ni-P barrier layer and the corresponding data are summarized in Table 5- 12. A pseudo-passivation behavior in the anodic branch of the Ni-P barrier was observed. C0 showed the same behavior.

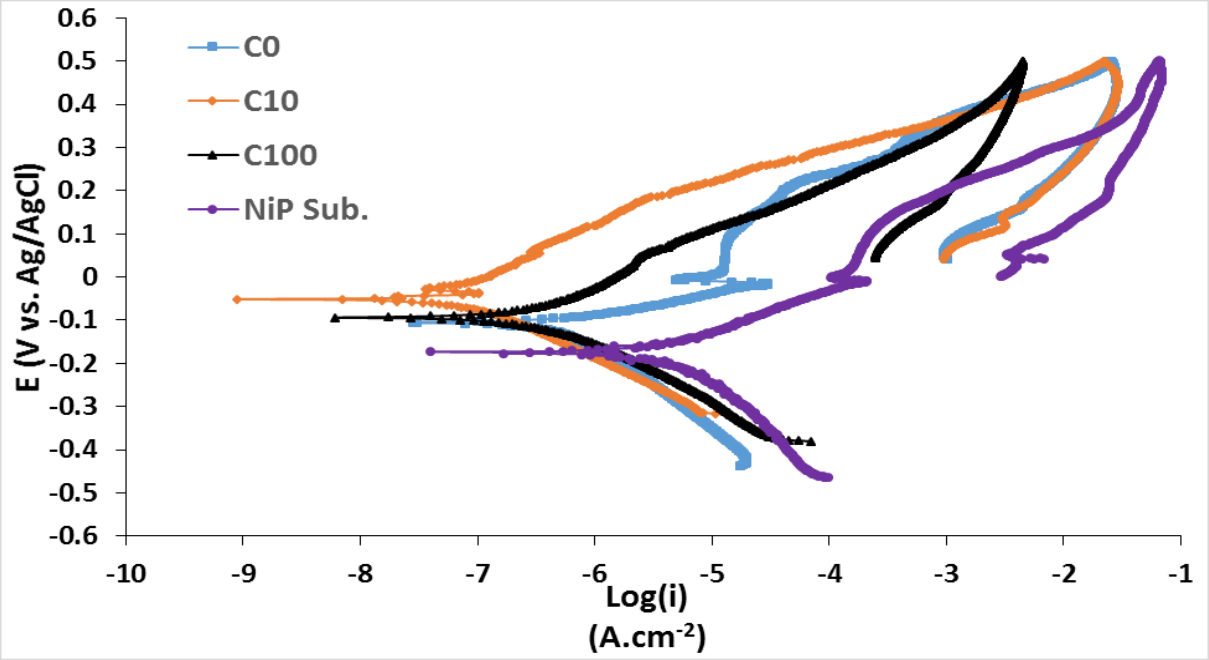

Figure 5- 39. CP curves of C0, C10, C100, and the Ni-P substrate after one hour immersion in 3% NaCl solution.

Table 5- 12. Corrosion current density and corrosion potential of Ni-P barrier layer and C0-C100

Sample	i_{corr} ($\mu A.cm^{-2}$)	E_{corr} (mV) vs. Ag/AgCl
Ni-P barrier layer	6.68 ± 0.78	-202 ± 7
C0	0.50 ± 0.10	-110 ± 7
C5	0.18 ± 0.02	-14 ± 23
C10	0.08 ± 0.01	-36 ± 3
C15	0.15 ± 0.04	4 ± 11
C25	0.24 ± 0.10	-16 ± 20
C50	1.93 ± 0.73	-33 ± 13
C100	2.68 ± 1.92	-75 ± 13

The comparison of the curves for C0 and the Ni-P barrier layer suggests a fast anodic reaction for C0. This anodic reaction could be attributed to the fast dissolution of the Ni-P under-layer due to the galvanic corrosion occurring inside the pores. The passivation behavior was not observed for PMMA modified samples, possibly due to the filled pores.

The polarization resistance values were in good agreement with those obtained from EIS tests; C10 revealed the highest resistance value. PMMA-covered samples had a nobler corrosion potential than C0. The more positive corrosion potential can be interpreted as the reduction of

the corrosion inclination [16]. Decreasing the porosity shifts the corrosion potential to less cathodic values and decreases the corrosion current density [62]. Therefore, PMMA modified samples should have a lower porosity content. The porosity index (Eq. 4-4) values for C0 and C10 were 0.0269 and 0.0008, respectively showing a 97% decrease in the porosity of the Au top-layer after 10 cycles of electropolymerization of MMA. A positive hysteresis loop was observed for all the samples showing that the occurrence of localized corrosion is inevitable. Au is generally known to be chemically inert. However, it can be corroded under anodic polarization and in the presence of chloride or bromide ions (due to the formation of Au complexes) [63]. Moreover, random pits can be always formed on the surface of metals due to their autocatalytic nature [64]. The corrosion could be even more severe for Au thin films.

Figure 5- 40 shows the surface of samples after CP tests. The surface of C0 was severely damaged and the Cu substrate can be easily seen. The corrosion on the PMMA modified samples was restricted to the formation of green spots, and C10 had the lowest number of spots. These green corrosion products are reported to be clinoatacamite ($Cu_2(OH)_3Cl$) compounds [65]. Therefore, the amount of Cu, Cl, and O after corrosion tests can demonstrate the corrosion progress (Figure 5- *41*). According to this figure, C10 presents the lowest content of Cu, O, and Cl and therefore the highest corrosion resistance. The content trend of Cu, Cl, and O (as a function of the polymerization cycle number) are in a good agreement with the respective polarization resistance and charge transfer resistance values.

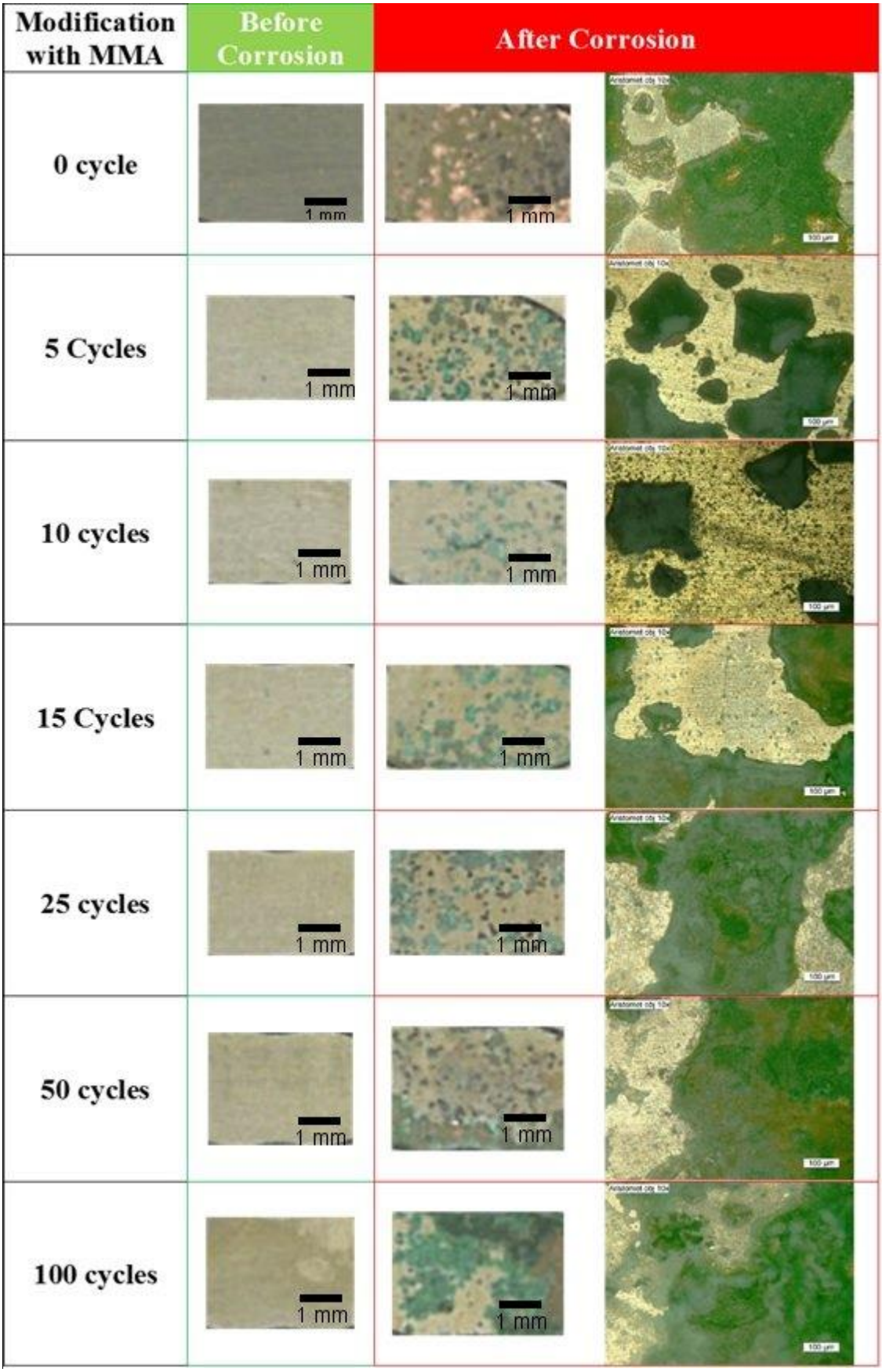

Figure 5- 40. Surface morphology of the samples before and after electrochemical corrosion tests.

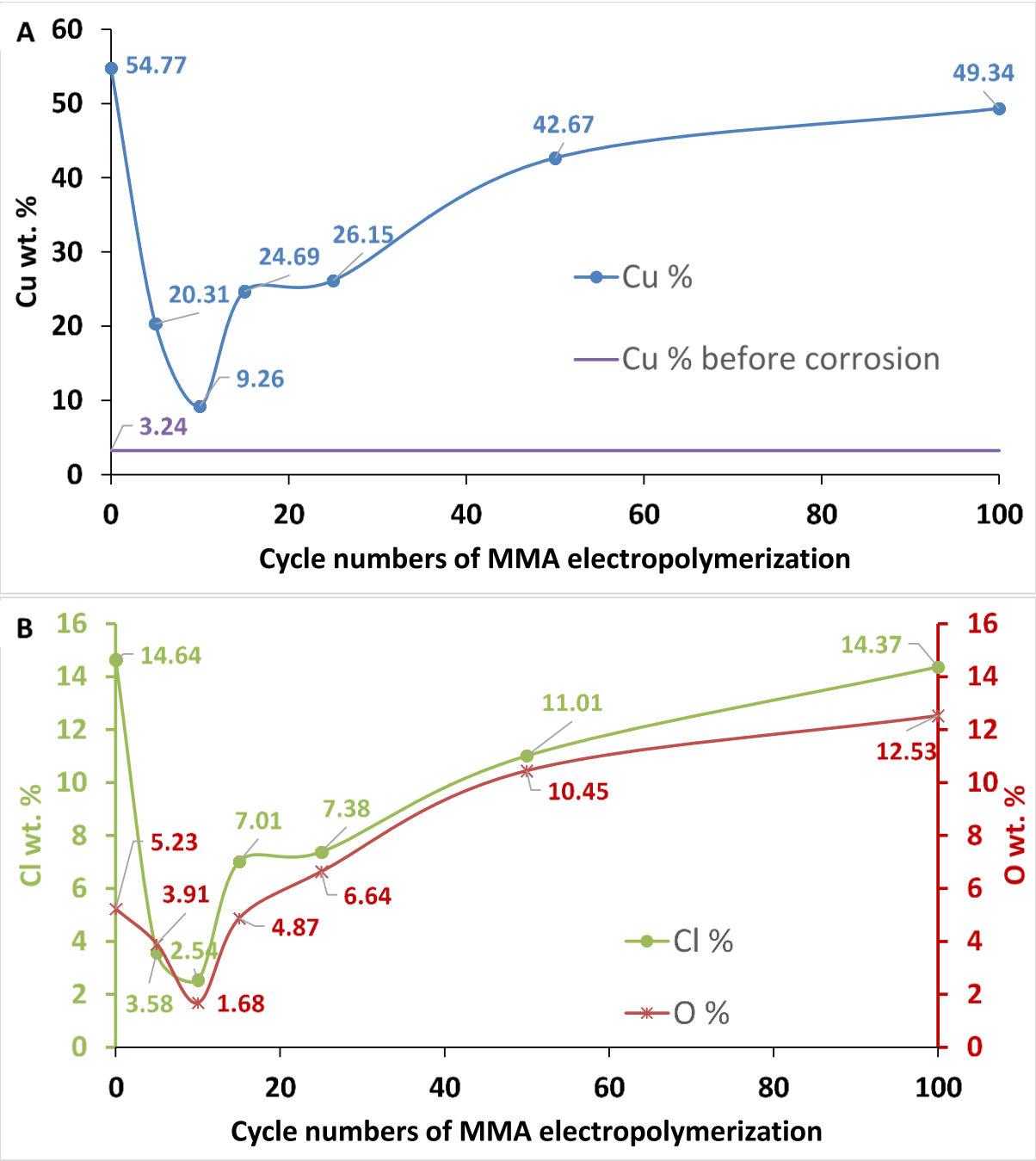

Figure 5- 41. (a) Cu wt.%, and (b) Cl wt.% and O wt.% of samples after the corrosion tests as a function of the electropolymerization cycle number.

The salt spray test, which is one of the most employed techniques to determine the atmospheric corrosion behavior of materials, was used to evaluate C0 and C10 in a long-time exposure (10 days) to corrosive media. However, the mass loss was reported to be negligible for electrical contacts during the salt spray test. As a result, weight measurement is not a suitable technique to estimate the corrosion of electrical contacts [66]. The pore size, therefore, was traced and

compared for C0 and C10 (Figure 5- 42). C0 showed a fast increase in the pore size after 48 hours and huge pores were obvious after 240 hours. On the other hand, C10 had a stable growth of pit area with an almost unchanged surface morphology after 240 hours. However, new pores were formed pointing out that the pitting corrosion is inevitable. In conclusion, all corrosion tests showed that the corrosion resistance of electrical contacts can be significantly improved by depositing PMMA using 10 electropolymerization cycles.

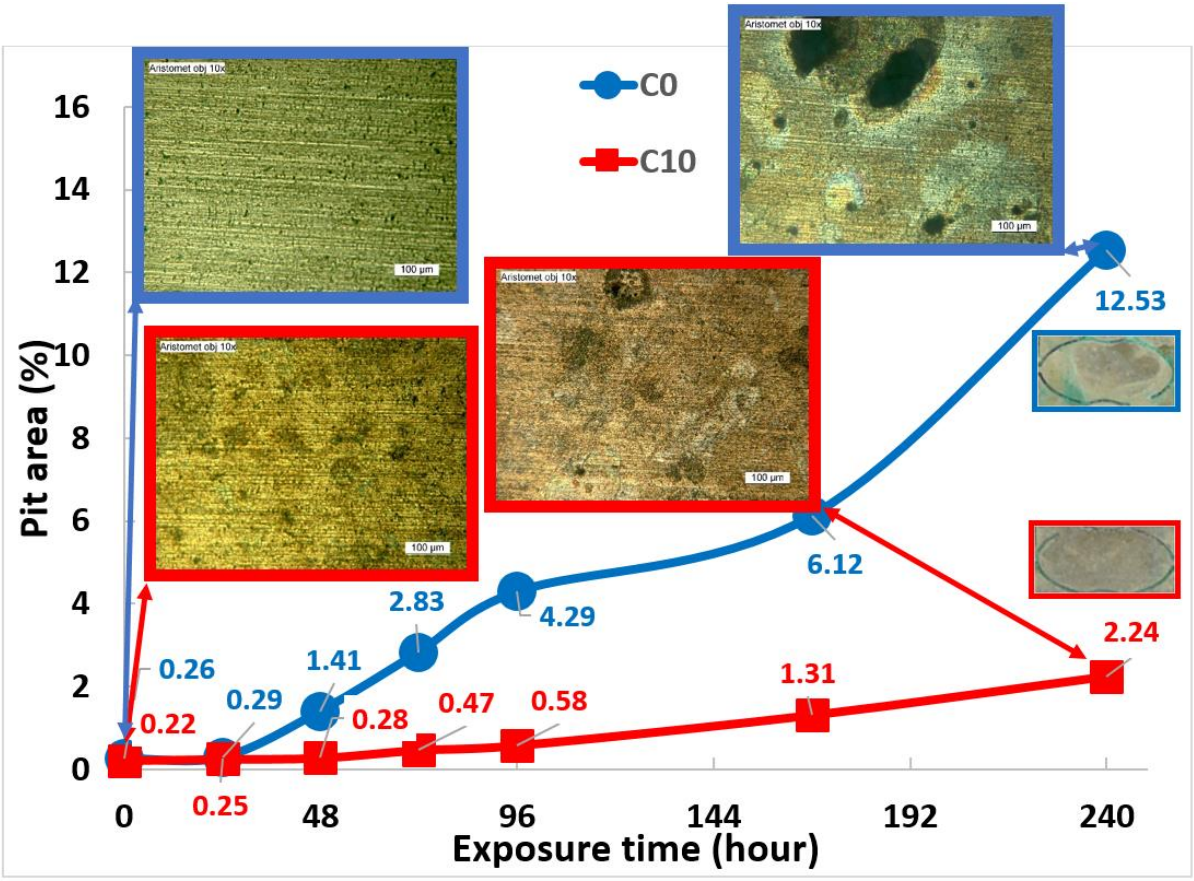

Figure 5- 42. Pit area of C0 and C10 during 240 hours of salt spray test.

The lifetime of Cu/Ni-P/Au electrical contacts can be effectively enhanced by cathodic electrodeposition of PMMA as a post-treatment process.

References

[1] Y. Liu, S. Li, J. Zhang, Y. Wang, Z. Han, L. Ren, Chemical Engineering Journal 248 (2014) 440–447.
[2] S. Koussi-Daoud, A. Planchat, A. Renaud, Y. Pellegrin, F. Odobel, T. Pauporté, ChemElectroChem 4 (2017) 2618–2625.
[3] Y. Akaltun, T. Çayır, Journal of Alloys and Compounds 625 (2015) 144–148.
[4] M.R. Das, A. Mukherjee, P. Mitra, Physica E: Low-Dimensional Systems and Nanostructures 93 (2017) 243–251.
[5] S.R. Nalage, M.A. Chougule, S. Sen, P.B. Joshi, V.B. Patil, Thin Solid Films 520 (2012) 4835–4840.
[6] M. Hashemzadeh, K. Raeissi, F. Ashrafizadeh, S. Khorsand, Surface and Coatings Technology 283 (2015) 318–328.
[7] P. Esmaeilzadeh, M.T. Sadeghi, Z. Fakhroueian, A. Bahramian, R. Norouzbeigi, Journal of Natural Gas Science and Engineering 26 (2015) 1294–1305.
[8] T. Hang, A. Hu, H. Ling, M. Li, D. Mao, Applied Surface Science 256 (2010) 2400–2404.
[9] F. Tian, A. Hu, M. Li, D. Mao, Applied Surface Science 258 (2012) 3643–3646.
[10] G. Liu, Z. Huang, L. Wang, W. Sun, S. Wang, X. Deng, Surface and Coatings Technology 222 (2013) 25–30.
[11] M. Calligaris, Coordination Chemistry Reviews 248 (2004) 351–375.
[12] M. Ozaki, Y. Katsuki, J. Liu, T. Handa, R. Nishikubo, S. Yakumaru, Y. Hashikawa, Y. Murata, T. Saito, Y. Shimakawa, Y. Kanemitsu, A. Saeki, A. Wakamiya, ACS Omega 2 (2017) 7016–7021.
[13] Y.-H. Chou, Y. Sung, Y.-M. Liu, N.-W. Pu, M.D. Ger, Surface and Coatings Technology 203 (2009) 1020–1026.
[14] D. Liu, Z. Yang, C. Zhang, Materials Science and Engineering: B 166 (2010) 67–75.
[15] J.-Y. Lee, J.-W. Kim, M.-K. Lee, H.-J. Shin, H.-T. Kim, S.-M. Park, J. Electrochem. Soc. 151 (2004) C25–C31.
[16] C.W. Lee, K. Sathiyanarayanan, S.W. Eom, M.S. Yun, Materials Science Forum 539–543 (2007) 1427–1430.
[17] Y. Raghupathy, K.A. Natarajan, C. Srivastava, Materials Science and Engineering: B 206 (2016) 1–8.
[18] U. Lačnjevac, B.M. Jović, V.D. Jović, Journal of The Electrochemical Society 159 (2012) D310.
[19] E. Rudnik, Journal of Electroanalytical Chemistry 726 (2014) 97–106.
[20] P.-C. Huang, K.-H. Hou, G.-L. Wang, M.-L. Chen, J.-R. Wang, International Journal of Electrochemical Science 10 (2015) 4972–4984.
[21] P. Møller, J.B. Rasmussen, S. Köhler, NASF SURFACE TECHNOLOGY WHITE PAPERS 78 (2013) 15–24.
[22] S.W. Jiang, L. Yang, J.N. Pang, H. Lin, Z.Q. Wang, Surface and Coatings Technology 286 (2016) 197–205.
[23] Y.-H. You, C.-D. Gu, X.-L. Wang, J.-P. Tu, Int. J. Electrochem. Sci 7 (2012) 12440–12455.
[24] D. Iacovetta, J. Tam, U. Erb, Surface and Coatings Technology 279 (2015) 134–141.
[25] S. Sangeetha, G.P. Kalaignan, J.T. Anthuvan, Applied Surface Science 359 (2015) 412–419.
[26] J. Tam, Z. Jiao, J.C.F. Lau, U. Erb, Wear 374–375 (2017) 1–4.
[27] Y. Samet, D. Kraiem, R. Abdelhédi, Progress in Organic Coatings 69 (2010) 335–343.
[28] G. Mengoli, Journal of The Electrochemical Society 134 (1987) 643C.
[29] K. Endo, T. Otsu, Polymer 32 (1991) 2856–2861.
[30] I.V. Ferrari, M. Braglia, T. Djenizian, P. Knauth, M.L. Di Vona, Journal of Power Sources 353 (2017) 95–103.
[31] J.J. Nieminen, I. Hatay, P. Ge, M.A. Méndez, L. Murtomäki, H.H. Girault, Chemical Communications 47 (2011) 5548.
[32] H. Vrubel, D. Merki, X. Hu, Energy & Environmental Science 5 (2012) 6136.

[33] D. D'Elia, C. Beauger, J.-F. Hochepied, A. Rigacci, M.-H. Berger, N. Keller, V. Keller-Spitzer, Y. Suzuki, J.-C. Valmalette, M. Benabdesselam, P. Achard, International Journal of Hydrogen Energy 36 (2011) 14360–14373.
[34] D. Chen, L. Zou, S. Li, F. Zheng, Scientific Reports 6 (2016).
[35] Y.K. Kho, A. Iwase, W.Y. Teoh, L. Mädler, A. Kudo, R. Amal, The Journal of Physical Chemistry C 114 (2010) 2821–2829.
[36] H.J. Yun, H. Lee, J.B. Joo, N.D. Kim, J. Yi, Journal of Nanoscience and Nanotechnology 11 (2011) 1688–1691.
[37] X. Yu, M. Wang, Z. Wang, X. Gong, Z. Guo, Electrochimica Acta 211 (2016) 900–910.
[38] P. Quaino, E. Santos, Langmuir 31 (2015) 858–867.
[39] M. Smiljanic, Z. Rakocevic, A. Maksic, S. Strbac, Electrochimica Acta 117 (2014) 336–343.
[40] S.-I. Pyun, T.-H. Yang, C.-S. Kim, Journal of Applied Electrochemistry 26 (1996).
[41] K. Santhi, S.N. Karthick, H.-J. Kim, M. Nidhin, V. Narayanan, A. Stephen, Applied Surface Science 258 (2012) 3126–3132.
[42] F.A. Cotton, R. Francis, Journal of the American Chemical Society 82 (1960) 2986–2991.
[43] B.B. WAYLAND', R.F. SCHRAMMZ, Inorganic Chemistry 8 (1969) 6.
[44] L.M.A. Monzon, F. Byrne, J.M.D. Coey, Journal of Electroanalytical Chemistry 657 (2011) 54–60.
[45] D.W. Meek, D.K. Straub, R.S. Drago, Journal of the American Chemical Society 82 (1960) 6013–6016.
[46] S. Cram, Electrochimica Acta 47 (2002) 1935–1948.
[47] M. Braglia, I.V. Ferrari, L. Pasquini, T. Djenizian, M. Sette, M.L. Di Vona, P. Knauth, Electrochimica Acta 265 (2018) 78–88.
[48] I.V. Ferrari, M. Braglia, T. Djenizian, P. Knauth, M.L. Di Vona, Journal of Power Sources 353 (2017) 95–103.
[49] N. Baute, L. Martinot, R. Jérôme, Journal of Electroanalytical Chemistry 472 (1999) 83–90.
[50] G. Sundararajan, L. Rama Krishna, Surface and Coatings Technology 167 (2003) 269–277.
[51] J.A. Curran, T.W. Clyne, Acta Materialia 54 (2006) 1985–1993.
[52] T. Weisemoeller, F. Bertram, S. Gevers, C. Deiter, A. Greuling, J. Wollschläger, Physical Review B 79 (2009).
[53] S.E. Fritz, S.M. Martin, C.D. Frisbie, M.D. Ward, M.F. Toney, Journal of the American Chemical Society 126 (2004) 4084–4085.
[54] H. Sirringhaus, P.J. Brown, R.H. Friend, M.M. Nielsen, K. Bechgaard, B.M.W. Langeveld-Voss, A.J.H. Spiering, R.A.J. Janssen, E.W. Meijer, P. Herwig, 401 (1999) 4.
[55] L. Reimer, in: Scanning Electron Microscopy, Springer, Berlin, Heidelberg, 1985, pp. 227–271.
[56] J. Song, C. Koch, L. Wang, Advances in Tribology 2012 (2012) 1–9.
[57] B.M. Rumyantsev, S.B. Bibikov, A.V. Bychkova, V.G. Leontiev, V.I. Berendyaev, O.N. Sorokina, A.L. Kovarskii, Russian Journal of Physical Chemistry A 90 (2016) 2426–2433.
[58] H.Q. Zhang, Y. Jin, Y. Qiu, IOP Conference Series: Materials Science and Engineering 87 (2015) 012032.
[59] A.R. Blythe, Polymer Testing 4 (1984) 195–209.
[60] G. Song, A. Atrens, M. Dargusch, Corrosion Science (n.d.) 25.
[61] J. Lee, D. Berman, Carbon 126 (2018) 225–231.
[62] W. Xu, X. Lu, B. Zhang, C. Liu, S. Lv, S. Yang, X. Qu, Metals 8 (2018) 188.
[63] M.D. Vedenyapina, V.V. Kuznetsov, D.I. Rodikova, N.N. Makhova, A.A. Vedenyapin, Mendeleev Communications 28 (2018) 181–183.
[64] G.S. Frankel, Journal of The Electrochemical Society 145 (1998) 2186.
[65] V.K. Murugan, Z. Jia, G.J. Syaranamual, C.L. Gan, Y. Huang, Z. Chen, Microelectronics Reliability 60 (2016) 84–92.
[66] V.K. Murugan, Z. Jia, G.J. Syaranamual, C.L. Gan, Y. Huang, Z. Chen, Surface and Coatings Technology 300 (2016) 95–103.

Chapter 6

Conclusions and Perspectives

6.1. Conclusions

In this study, various strategies to enhance the lifetime of Cu/Ni(Ni-P)/Au electrical contacts were identified and tested. These strategies were (1) to modify and improve the properties of Ni barrier layer, (2) to investigate the deposition of alternative top-coats of Au, and (3) to modify the porous Au top-coat with a post-treatment process.

To improve the properties of Ni-P barriers, it was found that employing an optimized concentration of certain additives (Cerium Sulfate, Coumarin, Sodium Citrate, Glycine, and Pyridinium Propyl Sulfonate) in traditional aqueous electrolytes can effectively enhance the thickness uniformity, smoothness, P content, and corrosion resistance of Ni-P films even at high potentials (500 mV vs. Ag/AgCl KCl Sat.). The effect of the concentration of additives, however, depended on the type of additive: e.g. increasing the concentration of glycine decreased the corrosion efficiency. The P content of Ni-P films played an important role in determining the overall corrosion behavior. Films with a higher P content and a higher thickness uniformity showed a higher corrosion efficiency at high potentials. Therefore, this strategy could be considered as the most economical solution to extend the lifetime of electrical modules.

To investigate the effects of alloying elements on the corrosion behavior of Ni barriers, DMSO based electrolytes were used to deposit Ni alloys containing Ag (as a nobler metal than Ni), Sn (as a metal with the similar potential range to Ni), Zn (as a metal more cathodic than Ni), and Mo (as a metal that can be only co-deposited). Ag and Mo deteriorated the corrosion resistance of Ni deposits, while the corrosion behavior was improved with Sn and Zn. The improvement

in the presence of Sn was attributed to the formation of NiSn intermetallic compound with the ability to form a stable nanometric oxide film in its surface. This alloy was the only sample that endured the corrosion tests and kept its appearance (all other samples were completely dissolved). Zn, on the other hand, did not incorporate inside the deposit but it suppressed HER during the deposition and thus led to the formation of a compacter film. Ag and Mo, however, induced galvanic corrosion and decreased the corrosion resistance of Ni deposits.

In order to form composite films and study their behavior, DMSO based electrolytes containing TiO_2 nanoparticles (NPs, as hard secondary phase particles), Carbon nanotubes (CNTs, as solid lubricant particles), Cu NPs (as metallic particles), and APhE (to form Ni-polymer composites) were prepared. The obtained Ni films in the presence of TiO_2 NPs and CNTs were highly porous with no (or a really a few) particles embedded inside. These particles intensified HER at the interface of the growing film and electrolyte and led to formation of a porous deposit that notably diminished the corrosion resistance. However, they could not be trapped inside the film due to the low deposition rate of Ni from DMSO. The film with Cu NPs were merely composed of Cu. Thicker and more compact films were obtained by the simultaneous electrodeposition of Ni and electropolymerization of APhE that formed a stronger physical barrier against the corrosion media and improved the corrosion resistance.

NiAg and NiPd noble top-coats were investigated as an economical alternative to Au thin films. Pulse electrodeposition was used to form adhesive films from a DMSO based electrolyte. Pd forms strong complexes with DMSO and thus its electrodeposition was not as easy as Ag. Therefore, NiPd was very thin (< 500 nm) and low Pd incorporation (<20 wt.%), comparing to NiAg, where a 2μm NiAg film with about 60 w.t.% Ag was formed. These films, however, were porous and thus did not offer a good corrosion resistance.

The corrosion behavior of Cu/Ni-P/Au electrical contacts can be effectively modified by cathodic electrodeposition of PMMA as a post-treatment process. A strongly electrografted PMMA was formed on top of the electrical contacts and thus sealed the pores of the thin Au top-layer. Increasing the number of polymerization cycles**,** we formed a non-uniform polymeric film on the surface. The polymerization preferentially starts at surface defects like pits and pores. Continuing the polymerization when there is no preferential site available leads to a non-uniform growth of PMMA. Therefore, a maximum of corrosion resistance is expected as a function of polymerization cycles (10 cycles in this study). The sealed pores disconnected the Ni-P barrier layer from the corrosive media and thus improved the corrosion resistance by eliminating the galvanic coupling between the Au top-coat (cathode) and the Ni-P under-layer (anode). The PMMA modified electrical contacts had a high stability against corrosion at long exposure times (10 days). Although PMMA slightly increased the resistance of samples, the resistance values were notably lower than the accepted limit for electrical contacts. As a result, electrodeposition of PMMA is an economical solution to improve the lifetime of electrical contacts.

6.2. Perspectives

The following points can be considered for future investigations:

- Investigate the effects of the mentioned additives (Cerium Sulfate, Coumarin, Sodium Citrate, Glycine, and Pyridinium Propyl Sulfonate) on the mechanical properties, i.e. hardness and wear resistance, of the electrodeposited Ni-P films from aqueous electrolytes.
- Study the effect of the mentioned additives on the porosity of the Au top-coats applied on the electrodeposited Ni-P films from aqueous electrolytes.

- Investigate the formation of Ni-Sn-P films from an aqueous bath and study its behavior in order to be used as a barrier layer.
- Investigate the possibility to enhance the deposition rate from DMSO and impede DMSO being trapped inside the deposits.
- Study the possible application of NiSn10, Black NiO, and Ni-5 TiO_2 NPs coatings in battery and supercapacitor industries due to their notable high capacitance values.
- Investigate the effect of APhE on the mechanical properties of deposited Ni films.
- Improving the properties of NiAg top-coats to be considered as a proper alternative to Au films. For example, employing a potential regime gradually decreased from a high cathodic value, which could lead to the formation of an adhesive film with a gradient in its chemical composition, i.e. richer in Ni at the interface of the barrier film and richer in Ag in the interface with the top-coat.
- Investigate the possibility of the formation of composite NiAg top-coats with the aim of improving its corrosion resistance.
- Study the effects of PMMA post-treatment on the fretting corrosion of electrical contacts, which could be improved due to the lubricating nature of polymers.

The results in thesis have been published in the papers listed below:

1. **A. Bahramian**, M. Eyraud, F. Vacandio, P. Knauth, Improving the corrosion properties of amorphous Ni-P thin films using different additives, Surface and Coating Technology, 345 (2018), 40-52.
2. **A. Bahramian**, M. Eyraud, F. Vacandio, P. Knauth, Cu/Ni/Au multilayers by electrochemistry: a crucial system in electronics - A critical review, Microelectronic Engineering, accepted.
3. **A. Bahramian**, M. Eyraud, S. Maria, F. Vacandio, T. Djenizian, P. Knauth, Enhancing the corrosion resistance of electrical contacts by electropolymerized poly(methyl methacrylate), Corrosion Science, accepted.

Conferences presentations

1. International Society of Electrochemistry (ISE) 69th annual meeting (Sep 2-7), Bologna, Italy. (Oral presentation): Electrodeposition of Ni alloys and Ni composites from DMSO.
2. International Society of Electrochemistry (ISE) 69th annual meeting (Sep 2-7), Bologna, Italy. (Poster presentation): Evaluation of the effects of varous additives on the corrosion properties of Ni-P thin films electrodeposited on Cu.
3. EuroCorr 2018 (Sep 9-13), Krakow, Poland. (Oral presentation): Comparison of additives with respect to the corrosion properties of Ni-P thin layers electrodeposited on Cu.